PROCEEDINGS OF THE XXIth ANNUAL MEETING OF THE SOCIEDADE ASTRONÔMICA BRASILEIRA (AUGUST 1995)

EDITED BY F. JABLONSKI, F. ELIZALDE, L.SODRÉ Jr. AND V. JATENCO-PEREIRA

ISSN 0104-6071

PROCEEDINGS OF THE XXIth MEETING OF THE BRAZILIAN ASTRONOMICAL SOCIETY

July 31 - August 4, 1995
Caxambu, MG, Brazil

SAB

Edited by

Francisco Jablonski,
LABORATÓRIO NACIONAL DE ASTROFÍSICA - LNA/CNPQ
C.P. 21, Itajubá, MG, 37500-970, Brazil

Flávio Elizalde,
INSTITUTO NACIONAL DE PESQUISAS ESPACIAIS - INPE/MCT
C.P. 515, São José do Campos,SP, 12201-970, Brazil

Laerte Sodré Jr. and **Vera Jatenco-Pereira.**
INSTITUTO ASTRONÔMICO E GEOFÍSICO - USP
C.P. 9638, São Paulo, SP, 01065-970, Brazil

Ficha catalográfica:

Sociedade Astronômica Brasileira
Proceedings of the XXIth Meeting of the Brazilian Astronomical Society
205 páginas.

Contribuições de conferencistas. 1996.
I. Título: Proceedings of the XXIth Meeting of the Brazilian Astronomical Society

ISSN: 0104-607I

Distribuição:

Instituto Astronômico e Geofísico - USP
Av. Miguel Stéfano, 4200 - Parque do Estado
04301-904 - São Paulo - SP

XXIth MEETING OF THE BRAZILIAN ASTRONOMICAL SOCIETY

July 31 - August 4, 1995
Hotel Glória, Caxambu, MG, Brazil

TABLE OF CONTENTS

Section 4: Galactic Astronomy and Interstellar Medium

Section 5: Stellar Astrophysics

Section 6: Solar System and Astrometry

FOREWORD

This volume contains the proceedings of the XXIth Meeting of the Brazilian Astronomical Society ("Sociedade Astronômica Brasileira" - SAB), held at *Hotel Glória*, Caxambu, MG, Brazil, on July 31 - August 4, 1995.

Only the invited talks given at the conference are included, but the meeting also had a large number of poster presentations, whose abstracts, as usual, have been published in a special number of the Bulletin of the Brazilian Astronomical Society (vol. 15, no. 1, 1995).

We had all the contributed papers in the form of posters, so the authors had enough time to explain their work, while the talks with duration of 40 minutes covered broad subjects and reached most of the audience.

The meeting was very fruitful owing to the excellent contributions of many invited speakers and to the large number of poster presentations.

We are very grateful to Fundação de Amparo à Pesquisa do Estado de São Paulo (FAPESP), Conselho Nacional de Desenvolvimento Científico e Tecnológico (CNPq), Coordenadoria e Aperfeiçoamento de Pessoal de Nível Superior (CAPES), Fundação de Amparo à Pesquisa do Estado do Rio de Janeiro (FAPERJ) and Fundação de Amparo à Pesquisa do Estado do Rio Grande do Sul (FAPERGS) for the meeting financial support.

FAPESP
Fundação de Amparo à Pesquisa do Estado de São Paulo

We are also grateful to FAPESP for financing this volume of the proceedings.

Francisco Jablonski
Flávio Elizalde
Laerte Sodré Jr.
Vera Jatenco-Pereira

Section 1

Extragalactic Astronomy and Cosmology

WHAT CAN WE LEARN FROM NEAR-INFRARED COLOURS OF SPIRAL GALAXIES?

R. F. Peletier[1] and M. Balcells[2]

(1) - Kapteyn Astronomical Institute
Postbus 800, 9700 AV Groningen, Netherlands and
Instituto de Astrofísica de Canarias
Via Lactea s/n, 38200 La Laguna,
Tenerife, Spain.
(2) - Kapteyn Astronomical Institute
Postbus 800, 9700 AV Groningen, Netherlands.

Abstract

Colours of spiral galaxies generally are affected by the underlying old stellar population, younger stars, and extinction by dust. Old and young populations generally can be disentangled using a combination of blue and near-infrared colours. Extinction effects are very hard to take into account, except for galaxies with special orientations. In this paper we give some results of one of the first modern studies of galactic bulges and disks in various optical and near-infrared bands, and its implications for the stellar populations of spirals.

1 Introduction

When one compares spiral galaxies with ellipticals, one can notice that much less is known about the stellar populations of the former than of the latter, When one then looks at a grand-design spiral, one immediately understands the reason for this. Spirals not only seem to have an old, underlying population, but many times they also contain young stars, as well as dust between the stars. For ellipticals one can in general get a good idea of the metallicity, just from an optical colour like $B-V$. For spirals with a combination of young and old stellar populations one colour is not sufficient to be able to separate them. Even a combination of several optical colours (e.g. $U-V$ and $B-V$) is generally not sufficient, since one cannot distinguish between a lower metallicity of the old population, and a larger fraction of young stars. To overcome this problem one has to go to the near-infrared. Tully *et al.* (1982) and especially Frogel (1985) has shown that the $U-V$ vs. $V-K$ diagram is a very useful tool for detecting young stellar populations in spirals. Since $V-K$ is a very red colour, it happens that young stars do not contribute as much in $V-K$ as in $U-V$, and that for a given $V-K$ the $U-V$ of an old population is very different from the $U-V$ of a combination of old and young stars. On the other hand Frogel noticed that there is a considerable scatter in the $U-V$ vs. $V-K$ diagram for spirals, much larger than for ellipticals, and that many spirals were redder than the reddest ellipticals.

These two effects very likely are due to extinction by dust. Images of edge-on galaxies, like NGC 891, show many magnitudes of extinction by dust in the central regions of the

disk. Because of this, the integrated colours of this galaxy are very red (Wirth & Shaw 1983). In Balcells & Peletier (1994,hereinafter called Paper I) we have shown that the colours of the stellar populations themselves in these objects are not red, in general even bluer than those of ellipticals of the same size.

Since that paper only discusses data in the optical, the information presented about stellar populations in bulges was limited. For that reason we have obtained images in J and K for the sample, with a new two-dimensional detector with a resolution that is sufficient to spatially select regions that are not or almost not affected by extinction. The colours (optical and optical-infrared) of these regions have been analyzed in the way described by Frogel (1985), and in this paper we discuss the implications for stellar populations in spiral galaxies. In particular, we discuss the differences between bulges and disks.

2 Sample and observations

We have investigated a sample of early-type spiral galaxies, ranging from S0's to Sbc. These galaxies generally have bulges that can be separated rather easily from their surrounding disk. Furthermore, except for the latest type, the amount of extinction by dust in these galaxies is limited, so that the colours will still be able to contain information about the stellar populations. The galaxies have inclinations larger than 50°, and are the brightest galaxies in a certain part of the sky. These two properties enable us to also on the basis of their morphology, and not just on their surface brightness profiles, separate disk and bulge.

The sample that we observed were are galaxies of Table 1 of Paper I, except for 2, which had declinations larger than 60°, and so could not be observed at UKIRT. Optical data (presented in that paper) were obtained for all galaxies. All galaxies of the *dustfree* subsample were observed both in J and K. The other galaxies were all observed in K, but not necessarily in J.

The optical data consist of U, B, R and I surface photometry, obtained in June, 1990, on the 2.5m INT telescope at La Palma. The data have been described in Paper I. The pixelsize of the data was 0.549", and the effective seeing on the images lies between 1.2" and 1.6". The images were taken under photometric conditions.

The near-infrared data were observed in June, 1994, at the 4m United Kingdom Infrared Telescope at Hawaii, using IRCAM3 (Puxley & Aspin 1994), an infrared camera equipped with a 256 × 256 InSb array. The observations will be described in detail in a subsequent paper (Peletier & Balcells, in preparation). The array has a pixelsize of 0.291", as measured on the images, so that the field is about 75" on the side. Cosmetically, the array is very clean, with less than 1% bad pixels. For every object we took images in 10 positions, which each consisted of several readouts, making up a total integration time of 100s per position. The object was moved around on the chip on 6 of these exposures, while 4 consisted of blank sky, about 10' from the galaxy. The data were flatfielded using median sky flat fields, and a final mosaic was made aligning the individual frames. The

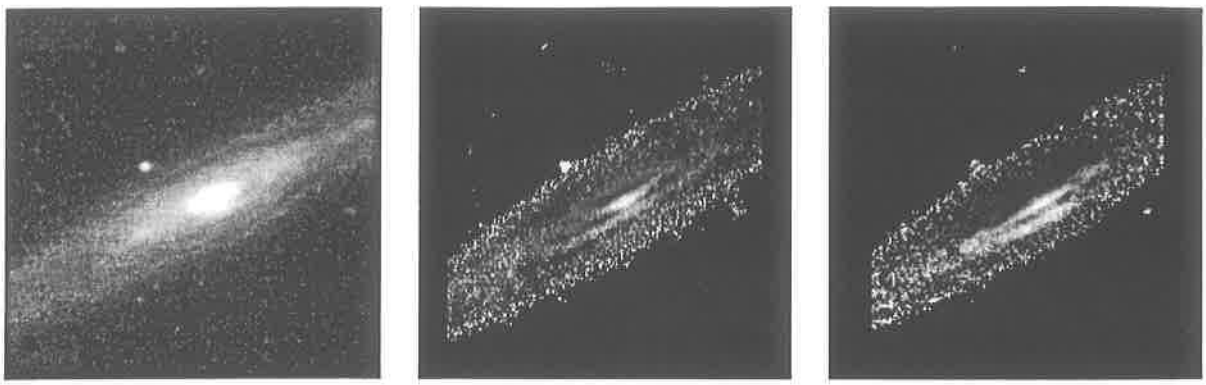

Figure 1: Greyscale image and two colour maps of IC 1029, showing the geometry and position of the dustlanes in a typical galaxy (a) and the lack of colour differences between bulges and disks (b and c).

effective seeing on the final frames was between 0.8" and 1.0". Here also the frames were taken under photometric conditions, with maximum zero point errors of 0.1 mag in J and K.

In Fig. 1 we show for a typical galaxy a composite $U-R-K$ map, and two colour maps. These show the bulge and disks, and the regions with the largest extinction and star formation. In Fig. 2 we show a cut along the minor axis in the $U-R$ vs. $R-K$ diagram. One side of the galaxy is well behaved, and $U-R$ is increasing for increasing $R-K$, but on the other side the combination of extinction, scattering and star formation makes this diagram very hard to interpret.

3 Dust in spiral galaxies

Colours contain useful information about stellar populations only when they have been corrected for extinction. Since the effects of extinction can be severe, the errors introduced by correcting for it are often so large that it is better to choose regions of the galaxy that are not, or very little, affected by extinction. In paper I we describe the procedure we employ to find extinction-free regions of bulges. For disks the situation is more complicated. Since dust and stars here are mixed almost everywhere, one cannot find dustfree regions. From a colour map (e.g. Fig. 1) one can see that the extinction in these early-type spirals is almost all concentrated on one side of the galaxy. This is the case for all galaxies that are not seen close to edge-on. One minimizes the extinction if one measures the disk colours on the other side. Since we are interested in radial and not vertical disk profiles we have measured the colours in wedges, at 15° from the major axis, with a width of 10°.

For this procedure to work the disk itself should contain relatively little extinction,

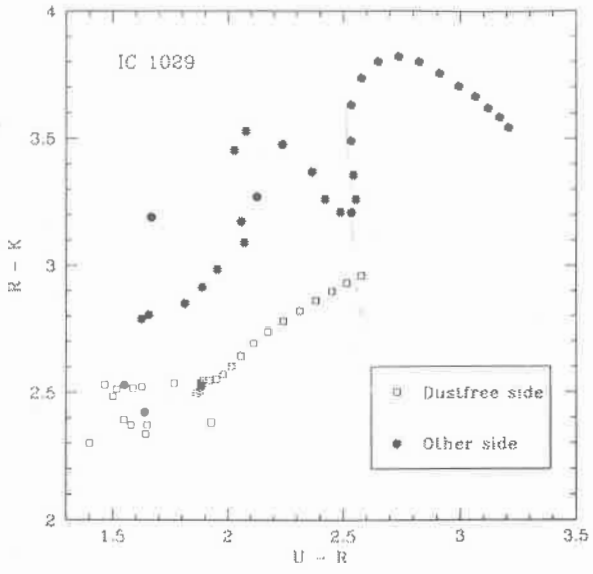

Figure 2: Color-color diagram of a minor axis cut of IC 1029. Both sides are indicated by different symbols.

since otherwise both sides are severely affected. A way to measure the extinction in the disk is to measure its radial colour gradient between a band that is affected by extinction and one that is not, e.g. B and K (Peletier *et al.* 1995). If the density ratio of dust and stars is more or less constant the central extinction will be much larger than the extinction in the outer parts, purely because of the difference in stellar density. In dusty galaxies this will cause the scale lengths in B to be much larger than those in K. In Fig. 3 we plot scale length ratios between B and K as a function of galaxy type. The open squares are points from Peletier *et al.* (1994). In that paper also details are given about how the radial scale lengths have been determined. Fig. 3 is very instructive. One can see that the scale length ratios for galaxy types up to 2 (Sab) are almost never larger than 1.4. Scale length ratios for galaxies of type 6 and larger also are small. Only galaxies of type 3-5 are sometimes very dusty. This is in good agreement with the surface-brightness vs. inclination test (Valentijn 1990). An independent estimate for the scale length ratios due to stellar population gradients is 1.1 – 1.2 (Peletier *et al.* 1995). This means that disks of galaxies of type 2 or smaller are likely not to be very dusty, and so the effects of dust in this paper will in general not be very large. We may be reasonably confident to use the colours for stellar population measurements.

4 Stellar populations from dustfree colours

In Paper I a discussion is given of optical ($U-R$, $B-R$ and $R-I$) colours and colour gradients as a function of other parameters like bulge luminosity. It was found that about half the bulges have the same colour as elliptical galaxies of the same luminosity, and that the other half is bluer in $U-R$ and $B-R$. This was interpreted as a sign of the

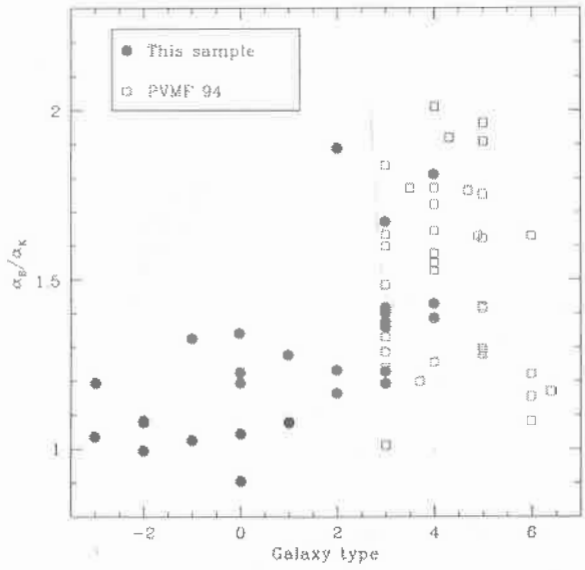

Figure 3: Scale length ratios between B and K of galaxy disks as a function of galaxy type.

presence of younger stars, under the assumption that all ellipticals are old (15 – 17 Gyr). Now, with the combination of optical and near-infrared colours, we don't have to make that assumption any more and can directly determine the average age of the stars.

First we present, in Fig. 4, some colour-colour diagrams for the bulges. 30 galaxies are plotted, at $r_{eff}/2$, or 5", if $r_{eff} < 10$", but only 20 in the diagram in which J is included, since 10 galaxies were not observed in J. Also included are lines of single burst models of constant age, with metallicity varying. These models are from Vazdekis *et al.* (1995) described elsewhere in these proceedings. The models are made by converting theoretical parameters like effective temperature and gravity to colours, choosing an initial mass function and integrating along a theoretical HR diagram, similar to Peletier (1989) and Worthey (1994). In this case however, we have taken a lot of care with the temperature–metallicity–colour calibration that the integrated models fit the data for giant elliptical galaxies. For example, for a given $B-V$ the $V-K$ given by Worthey (1994) is much too red to fit the giant elliptical galaxies. In Fig. 4 models are plotted for ages of 17, 12, 8, 4 and 1 Gyr. Along the lines metallicity ranges from Z=0.05 to Z=0.0004. One can see that only the diagrams that contain optical and optical-infrared colours can separate age and metallicity. $R-K$ and $J-K$ are both sensitive to more or less the same kind of stars, so in this diagram metallicity and age cannot be separated. The same holds for the $U-R$ vs. $B-R$ diagram. The systematic error in the model colours, due to uncertainties in the stellar evolution theory, or lack of template stars, seems to be on the order of 0.1 or 0.2 mag, although this value can be smaller, since the reddest bulges not necessarily have to be 17 Gyrs old. Despite these errors some galaxies in the $U-R$ vs. $R-K$ diagram cannot be fitted by a model of 17 Gyr, and for some the best fitting model only has an age of 1 Gyr. This does not mean that there is no underlying old stellar population present,

but just that a much younger stellar population is dominant.

We see that most of the reddest, and also largest (Paper I) bulges are old, and that some have to be younger. It is also noteworthy that all bulges here are redder than $R-K$ = 2.4. This means that the metallicity of all these bulges is larger than about 0.3 $Z_{\odot}$. This is probably due to the way the sample was chosen - bright nearby galaxies, automatically excluding all dwarfs, and galaxies with low metallicities.

We now compare the colours of bulges with those of disks. Even though both bulges and disks are generally bluer with increasing radius (de Jong 1995; Paper I), the gradients are small enough that we can assign representative values for the colour of each component. For bulges, we have taken the colour at 0.5 r_{eff} or at 5 arcsec, whichever is larger. For disks we use the colours at 2 major axis scale lengths. We find that disk colours, while somewhat bluer, are very similar to bulge colours for all the galaxies (see Fig. 5). Here the diagonal line indicates the locus where both colours are equal. The average differences between disk and bulge and bulge colours are 0.126 $\pm$ 0.165 for $U-R$, 0.045 $\pm$ 0.097 for $B-R$, 0.078 $\pm$ 0.165 for $R-K$ and 0.016 $\pm$ 0.087 for $J-K$. Unless there is a conspiracy between metallicity and age, this diagram implies that age differences between bulges and disks are small. Our result is in disagreement with Bothun & Gregg (1990) who for a sample of S0 galaxies, using near-infrared aperture photometry, found that for a given J-K disks were on the average 0.4 - 0.5 mag bluer in $B-H$ than bulges. We claim that the errors in their measurements are much larger than they claim. In our data, the range in colours between the galaxies is much larger than the average colour difference between bulge and disk of the same galaxy. According to the models a bulge is at most 30% older than its disk, or much less, if metallicity gradients are taken into account.

What can we learn from this about the formation of spiral galaxies? The data of this paper put the strong constraint that disks of early-type spirals must have been formed together with, or just after the bulge. It does not endanger the traditional model of Eggen, Lynden-Bell & Sandage (1962) of galaxy formation, but on the other hand implies that it is very unlikely that there were three discrete events of massive star formation: for the bulge, the disk, and the thick disk. The properties of bulge and inner disk seem to merge smoothly in terms of for example kinematical properties and kind of stars. The continuous infall model of Gunn (1982), where the age of the stars is determined by the free-fall collapse time of the infalling gas, would produce such a system, since these time scales will be similar for bulge and inner disk.

An alternative way of forming bulges has been proposed by Combes *et al.* (1990) and others. They form a bulge through the formation, and later desctruction of a bar due to dynamical instabillities. This method does not predict any age differences, and is in good agreement with our results here. However, galaxies with large bulges like the Sombrero cannot be formed in this way, and also one would not expect a continuous change in colours, colour gradient and surface brightness profile shape from large bulges of S0's to small Sb bulges (Andredakis *et al.* 1995).

Apart from the colours themselves we also have measured some colour gradients. In Fig. 6 a plot is given of $R-K$ colour gradients in the bulges as a function of total K-band magnitude. Since $R-K$ is an indicator of old stellar populations measuring the bulge

gradients in this colour is a good way to measure the metallicity gradients in bulges. Two different symbols are used for our galaxies. The filled circles indicate the galaxies of the dustfree sample of Paper I. The filed squares are those that may contain some dust. There are no significant differences to be seen between the $R-K$ gradients of both groups, showing that dust extinction is not a major factor influencing the gradients. The gradients are somewhat larger than the visual-infrared gradients of elliptical galaxies (Peletier *et al.* 1990, Silva & Elston 1994). Our average $R-K$ gradient is $\Delta(R-K)/\Delta(\log r) = -0.232$, and for $U-R$ -0.399. For ellipticals average values are -0.14 for $R-K$ and -0.20 for $U-R$, although not much data are available for $R-K$. In Paper I we concluded from the similarity between gradients in the optical between bulges and disks that this is a strong argument to show that bulges and ellipticals formed in the same way, and that the subsequent disk-formation did not substantially affect the bulge. We can say the same now using the $R-K$ colour. A recent review by Minniti *et al.* (1995) shows that possibly also the bulge of our own galaxy has a similarly small colour/metallicity gradient, even though earlier measurements by Terndrup (1988) were indicating large values. Fisher *et al.* (1996) find that for a sample of S0 galaxies the vertical gradients in the bulge in $B-R$ and in absorption line strength are much larger than the radial gradients. Although we don't have many galaxies in our sample that are really edge-on we also see hints for the same effect, and this might be the reason of Terndrup (1988)'s large metallicity gradient in our Bulge. Using colour - metallicity conversions by Vazdekis *et al.* (1995) we have converted our average $R-K$ and $U-R$ gradients to metallicity gradients, assuming constant age. From $R-K$ we find that on the average $\Delta(\log Z) = -0.41$ per dex in radius, and from $U-R$ we find a value of -0.42.

Also plotted in Fig. 6 is the sample of Terndrup *et al.* (1994) of similar kinds of galaxies. Even though almost all $R-K$ gradients of our sample are negative, those of Terndrup *et al.* can be both positive and negative. We presume that the errors in that sample are larger than indicated by the errorbars, something which is possible, since they used a small detector covering a small field.

As a final point we would like to talk a bit about colours of disks as a function of galaxy type. Here the colours are the ones that have been determined in such a way as to minimize the effects of extinction (see above). 4 different colours are plotted in Fig. 7. The $J-K$ and $R-K$ colours here are indicators of the old underlying stellar population that constitutes most of the mass. $B-R$ and $U-R$ also depend on additional young stars. Noteworthy is the fact that there is not much change in the colour, when varying galaxy type. One can say that ellipticals, S0's and spirals up to type 2 (Sab's) have more or less the same colours, indicating few young stars and similar metallicities. Some galaxies of type 3 obviously suffer from extinction effects, while in all colours, but especially in $U-R$ galaxies of type 4 (Sbc's) are bluer than the others. This figure shows again that a considerable fraction of the stars in Sbc's and probably also later type spirals is young.

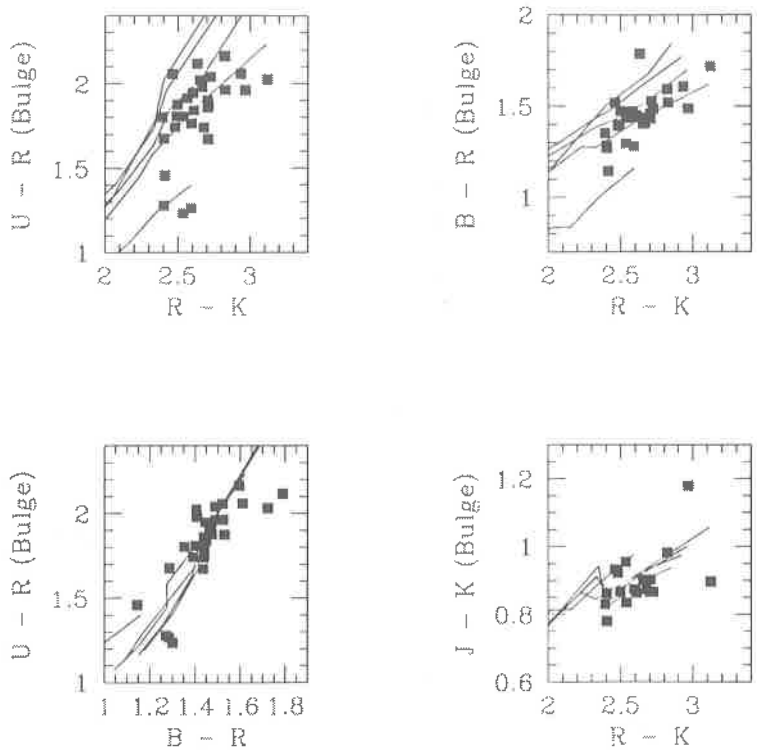

Figure 4: Colour-colour relations for the bulges. Also drawn are lines of constant age by Vazdekis *et al.* (1995). Plotted are ages 17, 12, 8, 4 and 1 Gyr.

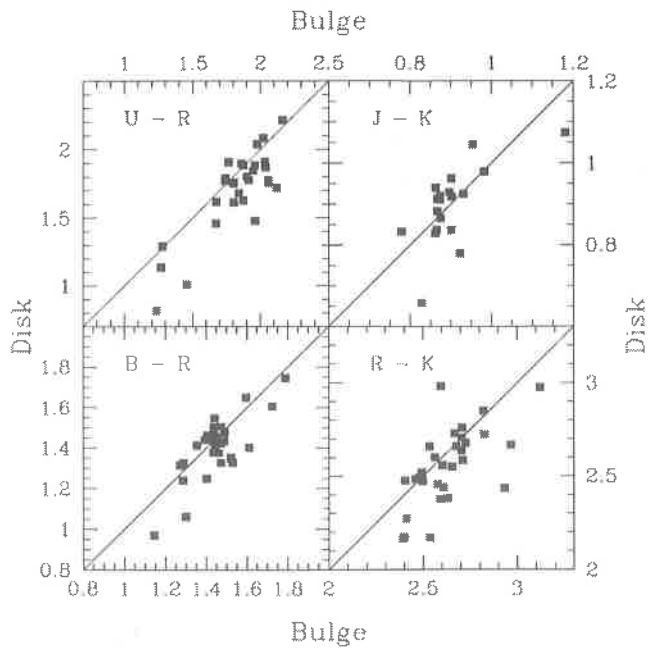

Figure 5: Disk colours as a function of bulge colours

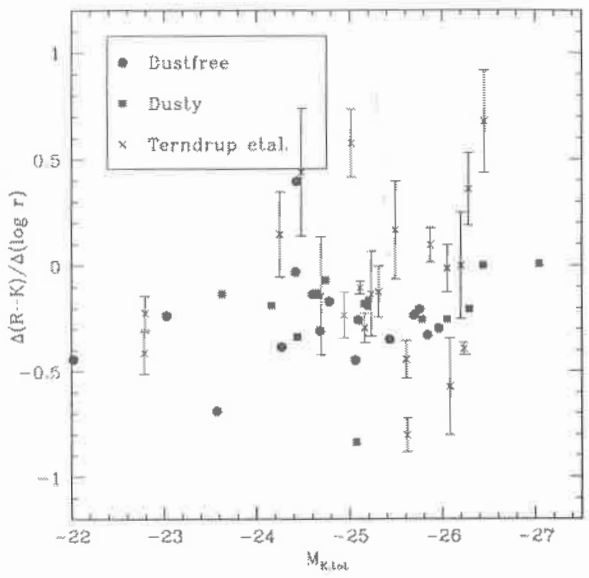

Figure 6: $R-K$ gradients for the bulges. Also plotted are the data of Terndrup *et al.* (1994)

5 Conclusions

The most important results that have been discussed in this paper are:

- By investigating colour gradients in disks between B and K for a sample of 70 galaxies we find that galaxies of type 3-5 are much more affected by extinction than are others. In the galaxies of other types, it is possible to find regions that are only slightly affected by extinction, and for which the colours can be used to study stellar populations.

- Using colour-colour diagrams of optical and optical-infrared colours, and comparing them with single age, single metallicity stellar population models, we find that a considerable fraction of the bulges in the sample has to be younger than elliptical galaxies, or contain a large fraction of stars that are younger than those in elliptical galaxies. The differences in colour from one galaxy to another can be much larger than the colour difference between the bulge and disk of the same galaxy. For that reason the inner disks of these galaxies cannot be more than 2-4 Gyrs younger than their bulges.

- Radial $R-K$ colour gradients of bulges are negative and small. Bulges generally are redder in the center than in their outer parts, and the average colour gradient is about 0.2 mag per dex. These values are due to metallicity, or possibly age gradients, but not due to extinction by dust. Metallicity gradients inferred from $R-K$ gradients are very similar to those calculated from $U-R$, indicating that the contribution from very young stars in these galaxies is small.

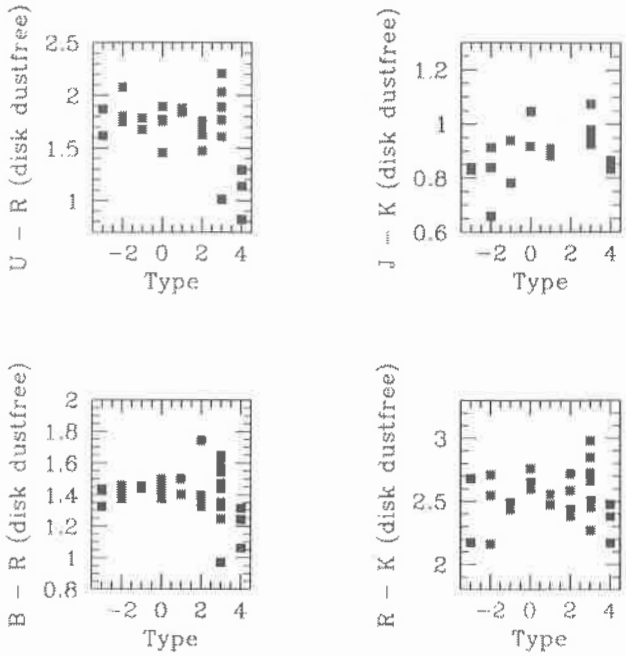

Figure 7: Disk colours as a function of galaxy type.

- Dustfree colours in disks are remarkably constant. Only for galaxies of type 3 and later disks are significantly bluer than those of S0's.

Acknowledgments

We acknowledge the help Massimo Stiavelli for help with observations and Alejandro Vazdekis making available his stellar population models before publication.

References

Andredakis, Y.C., Peletier, R.F. & Balcells, M., 1995, MNRAS 275, 874
Balcells, M. & Peletier, R.F., 1994, AJ 107, 135 (**Paper I**)
Bothun, G.D. & Gregg, M., 1990, ApJ 350, 73
Combes, F., Debbasch, F., Friedli, D. & Pfenniger, D., 1990, A&A 233, 82
de Jong, R.S., 1995, Ph.D. Thesis, Univ. of Groningen
Eggen, O., Lynden-Bell, D. & Sandage, A.R., 1962, ApJ 136, 748
Fisher, D., Franx, M. & Illingworth, G., 1996, ApJ, in press.
Frogel, J.A., 1985, ApJ 298, 528
Gunn, J.E., 1982, in *Astrophysical Cosmology*, ed. H.A. Brück, G.V. Coyne, and M.S. Longair; Vatican City: Pontifica Academia Scientiarum, p. 233

Minitti, D., Olszewski, E., Liebert, J., White, S.D.M., Hill, J.M. & Irwin, M.J., 1995, ESO preprint 1088
Peletier, R.F., 1989, Ph.D. Thesis, Univ. of Groningen
Peletier, R.F., Valentijn, E.A. & Jameson, R.F, 1990, A&A 233, 62
Peletier, R.F., Valentijn, E.A., Moorwood, A.F.M. & Freudling, W., 1994, A&A Suppl. 108, 621.
Peletier, R.F., Valentijn, E.A., Moorwood, A. & Freudling, W., Knapen, J.H. & Beckman, J.E., 1995, A&A 300, L1
Puxley, P. & Aspin, C., 1994, Spectrum 2, 4
Silva, D,R. & Elston, R., 1994, APJ 428, 511
Terndrup, D.M., 1988, AJ 96, 886
Terndrup, D.M., Davies, R.L., Frogel, J.A., Depoy, D.L. & Wells, L.A., 1994, ApJ 432, 518
Tully, R.B., Mould, J.R. & Aaronson, M., 1982, ApJ 257, 527.
Valentijn, E.A., 1990, Nature 346, 153
Vazdekis, A., Casuso, E., Peletier, R.F. & Beckman, J.E., 1995, in preparation
Wirth, A. & Shaw, R., 1983, AJ 88, 171
Worthey, G., 1994, ApJ Suppl 95, 107

UV SPECTRA OF EARLY-TYPE GALAXIES[1]

Charles J. Bonatto*, Eduardo Bica*, Miriani G. Pastoriza*
and Danielle Alloin**

(*) - Departamento de Astronomia, IF-UFRGS, CP 15051,
Porto Alegre 91501-970, RS, Brazil
(**) - Observatoire de Paris/Meudon, URA 173 CNRS,
F-92195 Meudon Principal Cedex, France

Abstract

We analyze the UV spectra of the early-type galaxies in the IUE library, including both normal and active nuclei. We coadded them into groups of similar spectral properties in the UV, also taking into account those in the visible/near-infrared ranges. This procedure provided spectra with a much higher signal/noise ratio than in previous studies, which as a rule were based on individual spectra and therefrom derived colour indices. As a consequence of the coadding procedure, information on spectral features can be accessed and analyzed. We obtained several spectral groups of galaxies characterized by red and blue stellar populations. The red stellar population groups present a far-UV flux with varying intensities. It was possible to infer on the extinction law affecting some internally reddened galaxies; there are cases in which the presence of the $\lambda 2200$ Å absorption feature suggests reddening similar to the Galactic law, and others without the $\lambda 2200$ Å feature, suggesting the SMC law.

1 Introduction

The International Ultraviolet Explorer (IUE) Satellite has been collecting fundamental data on a wide variety of astronomical objects since 1978. Recently we have used the IUE library to study the spectral properties of a large sample of star cluster spectra with an unprecedented signal to noise (S/N) ratio by coadding them into groups. The grouping procedure allowed us to analyze in detail the far-UV properties of star clusters, with reliable information on absorption features. The results of this analysis are presented in Bonatto et al. (1995, hereafter Paper I).

In what concerns galaxies, several studies of IUE spectra by object class have already been carried out, e.g. the spectral atlases of Kinney et al. (1993) for star-forming galaxies, and of Rosa et al. (1984) for H II complexes.

In this work we gather the spectra of the early-type galaxies stored in the IUE database and analyze together the ensembles of normal and active early-type galaxies, in view of better understanding their far-UV spectral properties. We also use in the interpretation single-aged UV templates of stellar populations, *i.e.* the star cluster spectral groups from Paper I, which considerably constrain the conclusions.

[1]Based upon data collected with the International Ultraviolet Explorer (IUE) Satellite, supported by NASA, SERC and ESA

Some early-type galaxies (in this work, ellipticals and S0's) are known to emit considerable amounts of energy in the far-UV, producing the so-called UV turnup (e.g. Bertola et al. 1980; Oke et al. 1981). However, the origin and characteristics of this emission are not yet quite well understood. So far, studies of these objects have employed individual IUE spectra which usually have a rather low (S/N) ratio, or are based on colour indices (Burstein et al. 1988; Longo et al. 1991). Bica & Alloin (1988) have used interpolated continuum distribution. The different spectra of early-type galaxies, in addition to the red stellar populations with varying amounts of UV turnup, also present evidence of bursts of star formation (e.g. Burstein et al. 1988).

The analyses of IUE spectra of Active Galactic Nuclei (**AGN**s) in early-type galaxies have been mostly focussed on variability, e.g. NGC 3516 (Wanders et al. 1993) and Mk 279 (Stirpe et al. 1994). Our goal here is to study average properties by coadding spectra of a given **AGN**, then classifying and coadding them into groups of comparable spectral characteristics. So we work with a time average of the activity states in which the nuclei were observed.

2 Star clusters spectra

In order to interpret composite stellar populations, and in particular galaxies at high redshift, it is necessary to consider both age and metallicity as essential parameters. Observationally, one should cover a spectral range as wide as possible: young populations will show up better in the ultraviolet (UV) whereas old components are conspicuous in the visible and infrared (IR) ranges. Galaxies present indeed a wide variety of stellar populations, ranging from those dominated by old components to those with recent star formation events (see for a review *e.g.* Bica 1992).

The IUE library contains a wealth of information on different classes of objects. In the present study we use all the available integrated spectra in the IUE library of star clusters in the Galaxy, LMC, SMC and Fornax, as well as H II regions in M 101, M 33, LMC and SMC, for a comprehensive analysis of their ultraviolet spectral properties as a function of age and metallicity. The approach is similar to previous analyses in the near-UV, visible and near-IR ranges (Bica, Alloin & Schmitt 1994, and Bica & Alloin 1987), *i.e.* by defining spectral windows and continuum tracings for equivalent widths (W) measurements. As the signal to noise ratio (S/N) in individual spectra is in general moderate we decided to group them according to similarities in the object class, age and metallicity after information in the literature and, as the ultimate criterion, the UV spectral properties given the available S/N ratio.

The following steps were taken to build the final spectral groups: (*i*) we averaged individual spectra of a given object working separately in the short (SWP) and long (LWP and LWR) wavelength ranges. A few spectra were eliminated at this stage because they presented problems such as instrumental defects, discordant continuum distribution and/or spectral features; (*ii*) using the information on the object class, age and metallicity, we averaged the spectra of different objects — the ultimate criterion being the spectral

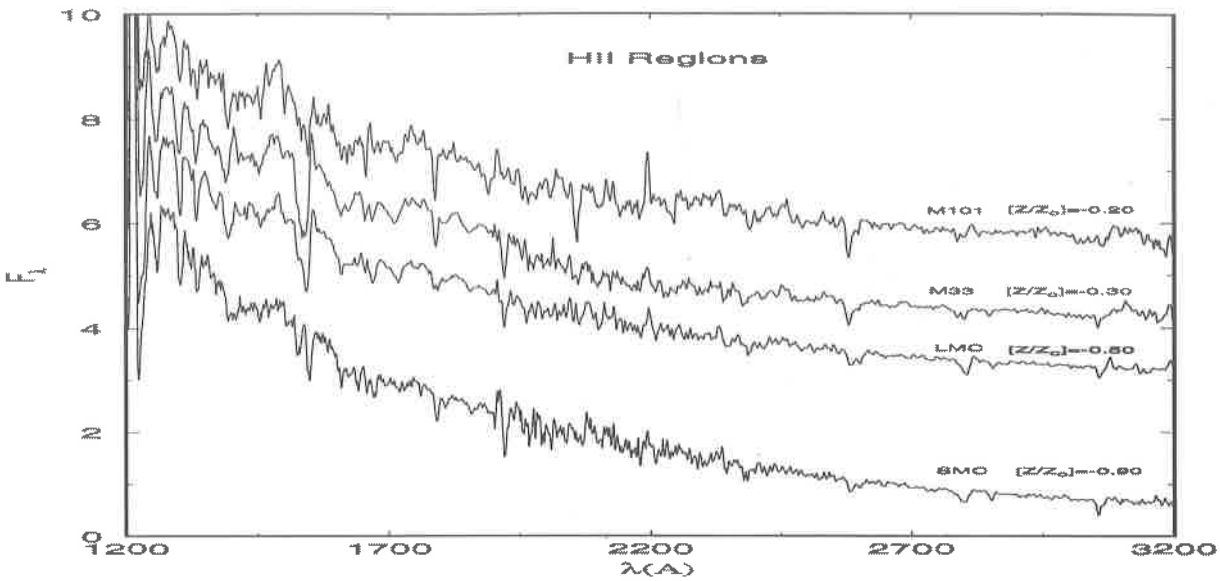

Figure 1: M 101, M 33, SMC and LMC H II region spectral groups; metallicities are indicated; Flux in F_λ units normalized at λ2646Å, while constants have been added to the spectra for clarity purposes

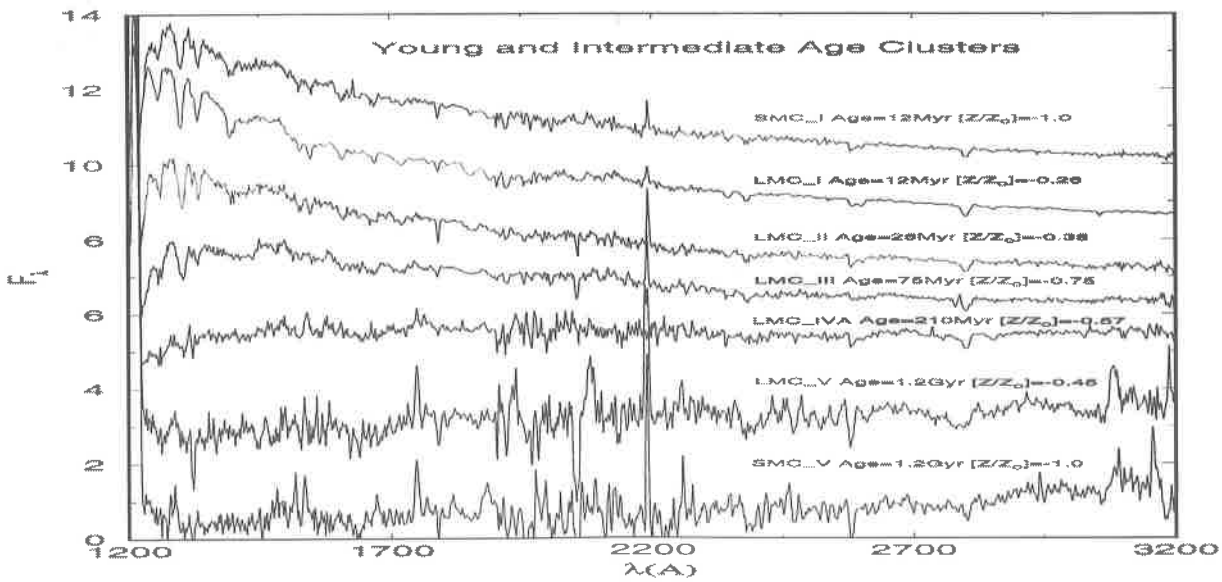

Figure 2: LMC and SMC young and intermediate age star cluster spectral groups; ages and metallicities are indicated; units as in Fig. 1

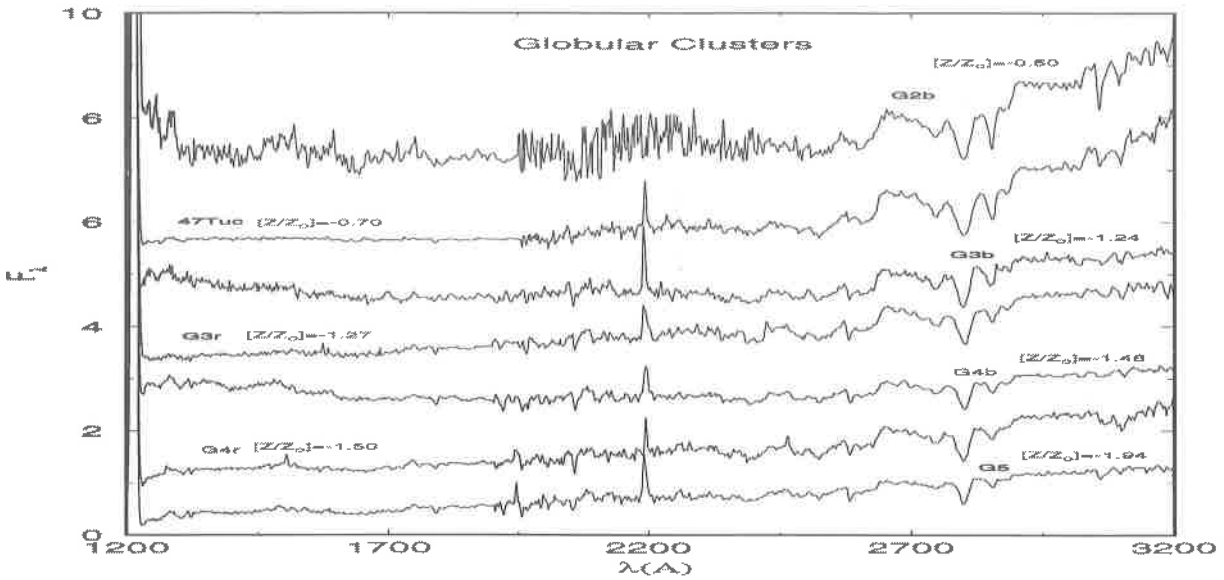

Figure 3: Globular cluster spectral groups; ages are $> 10\,Gyr$ and metallicities are indicated; units as in Fig. 1

similarity; and (*iii*) the short and long wavelength domains were finally connected. The weights in the averages were given according to the square of the S/N ratio.

We show in Figure 1 the H II region spectra of the four groups; the young and intermediate age cluster groups are in Figure 2; and in Figure 3 we show the globular clusters groups.

3 Early-type galaxies

The spectra have been extracted from the IUE database as stored at the Instituto Astronômico e Geofísico of the Universidade de São Paulo (IAG–USP). We have selected the available SWP, LWP and LWR spectra of early-type galaxies obtained with the large aperture ($10'' \times 20''$) mode.

Galaxies present a wide range of spectral properties, but those presenting similarities can be grouped, a procedure which allows one to study their average properties in more detail with better (S/N) ratio data. In order to study the UV spectral lines in detail it is necessary first to coadd the available IUE spectra of an individual object, and subsequently coadd into spectral groups those of different objects which result similar. For the present grouping procedure the ultimate criterion is similarity of UV spectra within the available (S/N) ratio, but we also considered their spectral properties in the visible and near-IR ranges found in the literature, together with their classifications as **AGN**, H II galaxy, Starburst, as well as usual normal stellar population types. The spectral groups were built in a similar way as the star cluster groups. We ended up with 8 groups characterized by a red stellar population (Figure 4) and 5 groups with an **AGN** or a blue stellar population (Figure 5).

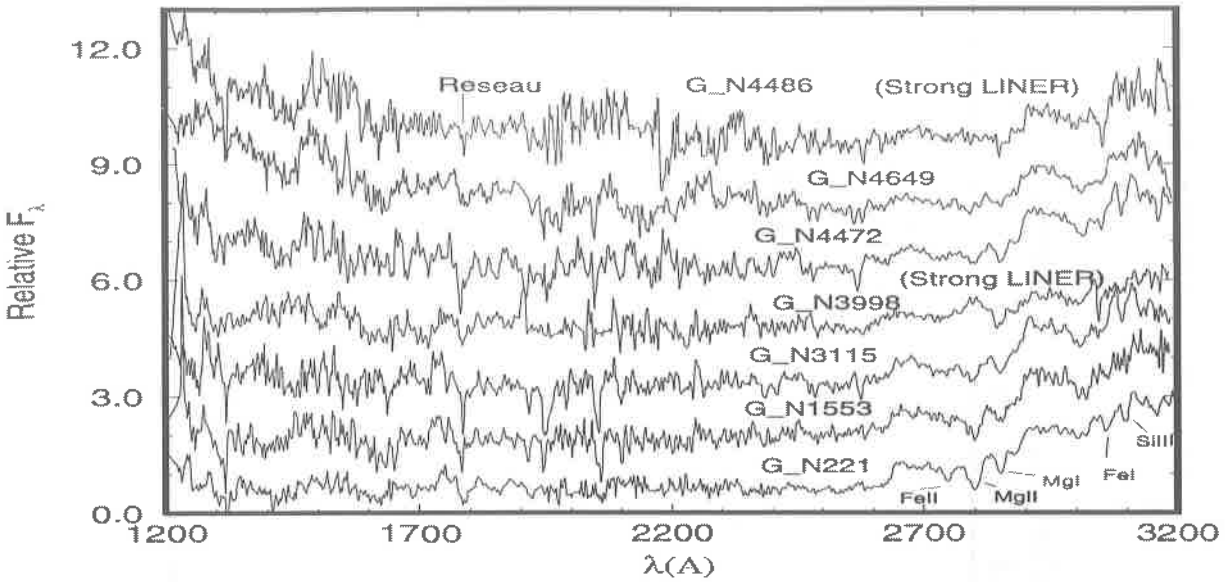

Figure 4: Groups for red stellar populations in early-type galaxies with varying contribution from the UV turnup. Flux in F_λ units normalized at λ2646 Å, while constants have been added to the spectra for clarity purposes, except for the lowest one

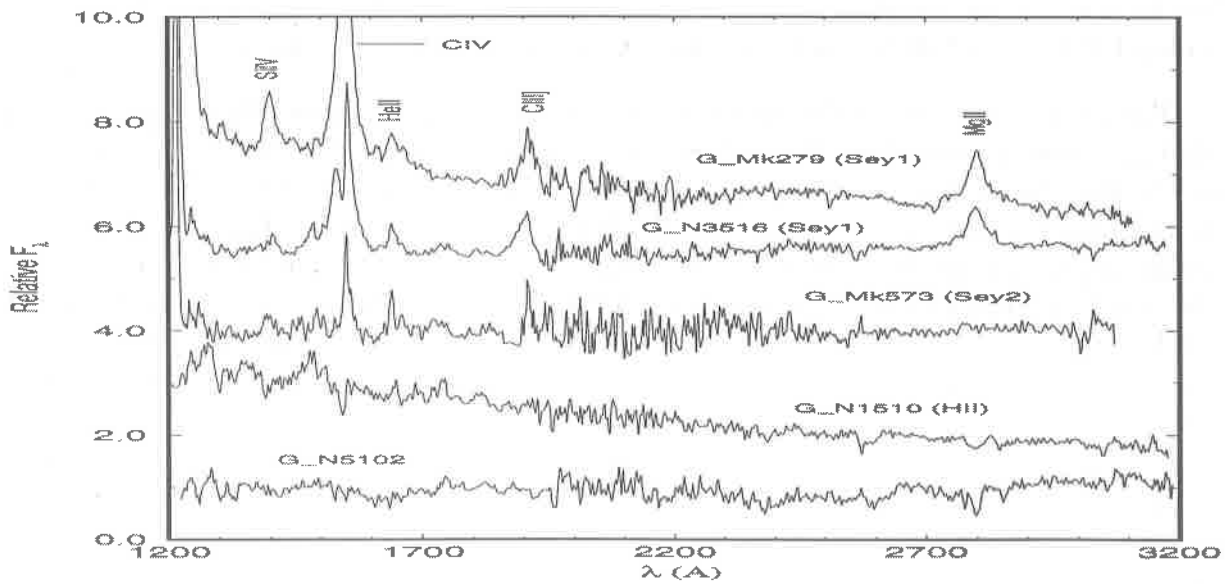

Figure 5: Groups for active nuclei together with those for blue stellar populations in early-type galaxies. Notice how the two groups of Seyfert 1s have similar emission lines but differ in the continuum slope. Flux in F_λ units normalized at λ2646 Å, while constants have been added to the spectra for clarity purposes, except for the lowest one

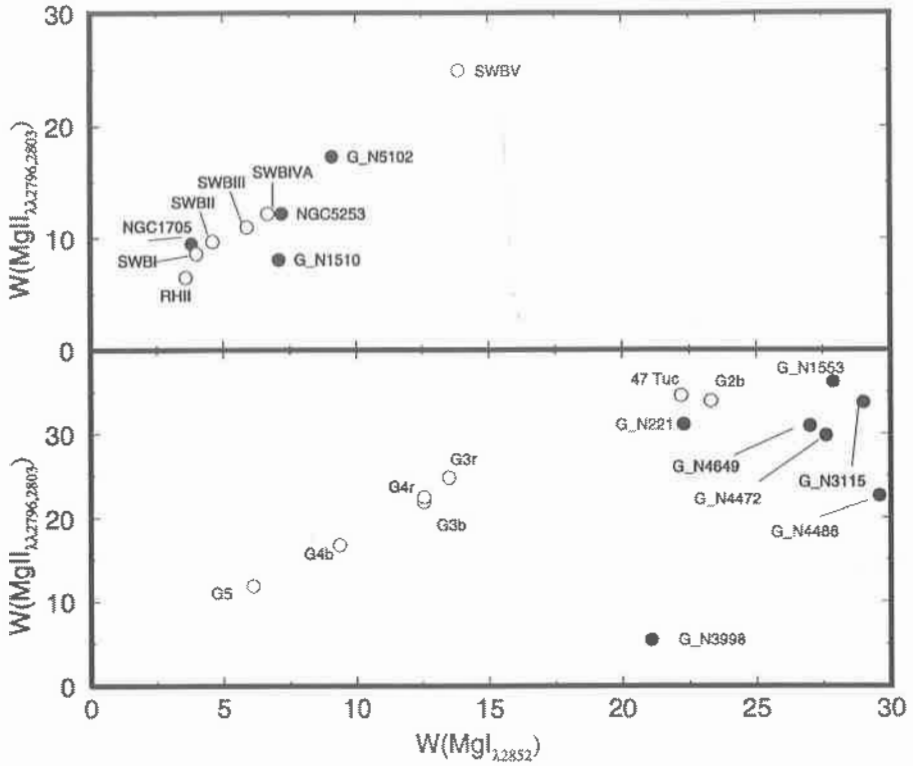

Figure 6: Equivalent widths of Mg I and Mg II for galaxy and/or groups (filled symbols). Upper panel: blue stellar population groups; lower panel: red stellar population groups. Ws for star cluster templates (open symbols) are also plotted as comparison. Groups of strong LINERs, G_N3998 and G_N4486, have W(Mg II) diluted by emission

We selected two strong absorption features in the LWP/R range (Mg II$_{\lambda\lambda 2796,2803}$ and Mg I$_{\lambda 2852}$) and plotted their Ws in Figure 6, in order to investigate the basic properties of UV lines for galaxies and to compare them to the Ws for star clusters from Paper I. In the upper panel of Fig. 6 we show W(Mg II$_{\lambda\lambda 2796,2803}$)$\times$ W(Mg I$_{\lambda 2852}$) for the blue stellar population groups and individual galaxies. They occupy similar loci as the blue star clusters SWB I (age $\approx$ 10 Myr) to SWB IVA (age $\approx$ 200 Myr), and the template RH II which is an average of H II regions in M 101, M 33, LMC and SMC. The loci of the H II/amorphous galaxies NGC 1705, NGC 5253 and the group G_N1510 suggest that they are not pure H II regions, but contain a range in age. The Ws for the red stellar population galaxy groups are compared to those of the globular cluster templates in the lower panel. For the globular clusters, the sequence from G 5 to G 2b (and 47 Tuc) increases in metallicity up to $[Z/Z_{\odot}] \approx -0.5$ (Paper I). As expected, the galaxy groups are close to the metal-rich globular clusters. In Mg I they present larger Ws indicating higher metallicity, but in Mg II Ws are comparable, which might be related to a saturation effect in the galaxies, the presence of some emission and/or some interstellar absorption excess in the line of sight to the globular clusters. Notice that the groups G_N3998 and G_N4486, which are strong LINERS, have significantly smaller W(Mg II$_{\lambda\lambda 2796,2803}$) with respect to the other galaxy groups. This is certainly caused by a contribution of Mg II$_{\lambda\lambda 2796,2803}$ in emission.

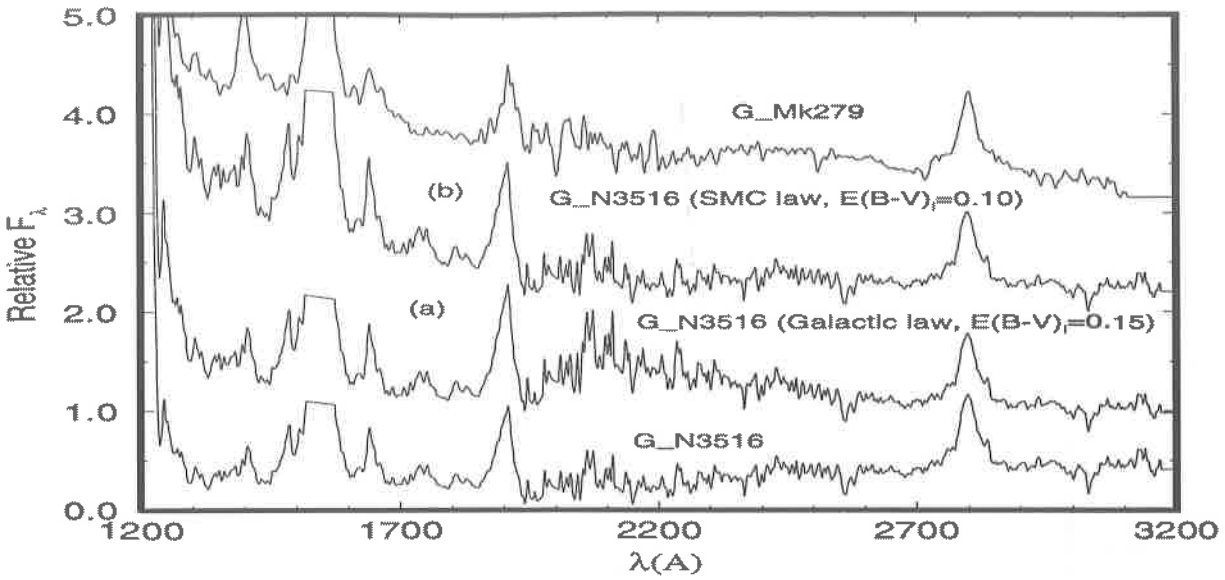

Figure 7: The redder Seyfert 1 group G_N3516 has been reddening corrected using (a) a Galactic extinction law with E(B−V)=0.15, and (b) the SMC law with E(B−V)=0.10. As compared to the bluer Seyfert 1 group G_Mk279, the Galactic law underestimates the far-UV flux and overestimates the λ2200 Å correction, whereas the SMC law produces a very similar spectrum. Fluxes are in F_λ units normalized at λ2646 Å, while constants have been added to the spectra for clarity purposes, except for the lowest one. The strong C IV emission has been clipped for clarity

4 Seyfert galaxies

We obtained two groups of Seyfert 1 galaxies: the spectrum of G_Mk279 is considerably bluer than that of G_N3516. Otherwise, equivalent widths and FWHM of the emission lines do not present systematic differences. In principle, three possibilities might explain the continuum difference between both groups: *(i)* reddening difference; *(ii)* the galaxies in the two groups would be in different average activity states; and *(iii)* the G_Mk279 group might contain a starburst component. We applied several tests in order to constrain these possibilities. If differential internal reddening is responsible for the effect, the reddening law must not contain a strong λ2200 Å bump. This can be seen in Fig. 7 since the SMC extinction law (Prévot et al. 1984) with E(B−V)=0.10 applied to the G_N3516 spectrum reproduces quite well that of G_Mk279, whereas Seaton's (1979) law with E(B−V)=0.15 already overestimates the λ2200 Å correction while, at the same time, it underestimates the far-UV flux.

Assuming that emission lines are comparable in both groups of Seyfert 1 galaxies, we normalized the spectra to equal Mg II$_{\lambda\lambda 2796,2803}$ and obtained the difference spectrum G_Mk279 − G_N3516. In Fig. 8 we compare the resulting spectrum to that of the typical nuclear starburst NGC 5236, and also to the power-law $F_\lambda \propto \lambda^{-1.8}$, which provides the

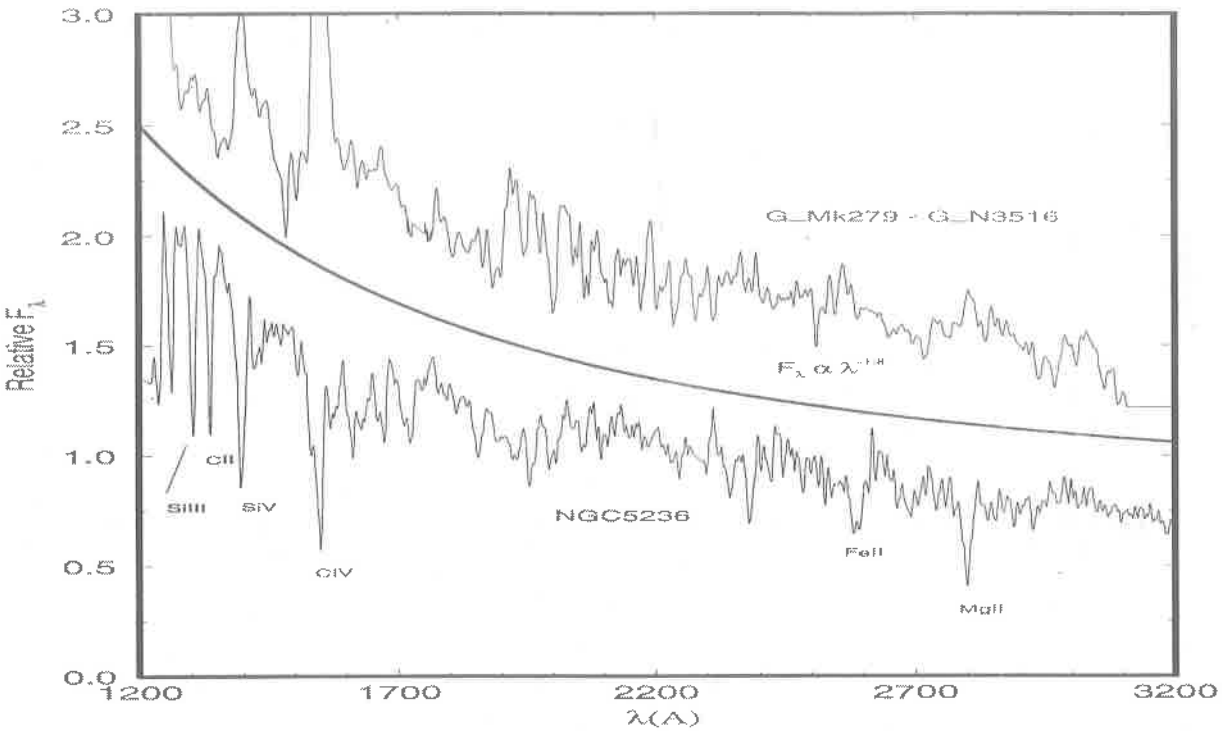

Figure 8: The difference spectrum between the bluer (G_Mk279) and redder (G_N3516) Seyfert 1 groups is compared to a power-law continuum and to the nuclear starburst NGC 5236. Fluxes are in F_λ units normalized at $\lambda 2646$ Å, while constants have been added to the spectra for clarity purposes, except for the lowest one

best fit to the continuum of the difference spectrum. The power-law fits well the difference continuum, as also does the starburst continuum. In the latter case, however, the starburst absorption lines are not conclusively present in the difference spectrum. On the other hand, both a power-law and a starburst continuum with such steep slope would cause a considerable dilution in the equivalent widths of the emission lines of G_Mk279 with respect to those of G_N3516, which is not the case.

We conclude that internal reddening appears to be the cause of the continuum difference between the two Seyfert 1 groups. Within the scenario of the *Unified Model of AGNs* the nuclei of the galaxies in the group G_N3516 would be seen at lines of sight which cross larger amounts of the dusty torus (Antonucci 1993). If this is the case, our results from Fig. 7 would suggest that the extinction law in the dusty tori does not have a conspicuous $\lambda 2200$ Å bump, resembling more that of the SMC.

In Fig. 9 we compare the SWP region of the Seyfert 2 group G_Mk573 with that of the Seyfert 2 prototype NGC 1068. It is worth noting that individual IUE spectra in the G_Mk573 group are very noisy and do not contain much information. We assumed that they were Seyfert 2 galaxies relying on visible spectra. The resulting UV spectrum of the group confirms the Seyfert 2 nature of its members because of the similarity to the spectrum of NGC 1068. The FWHM for the ensemble of the emission lines reinforces this

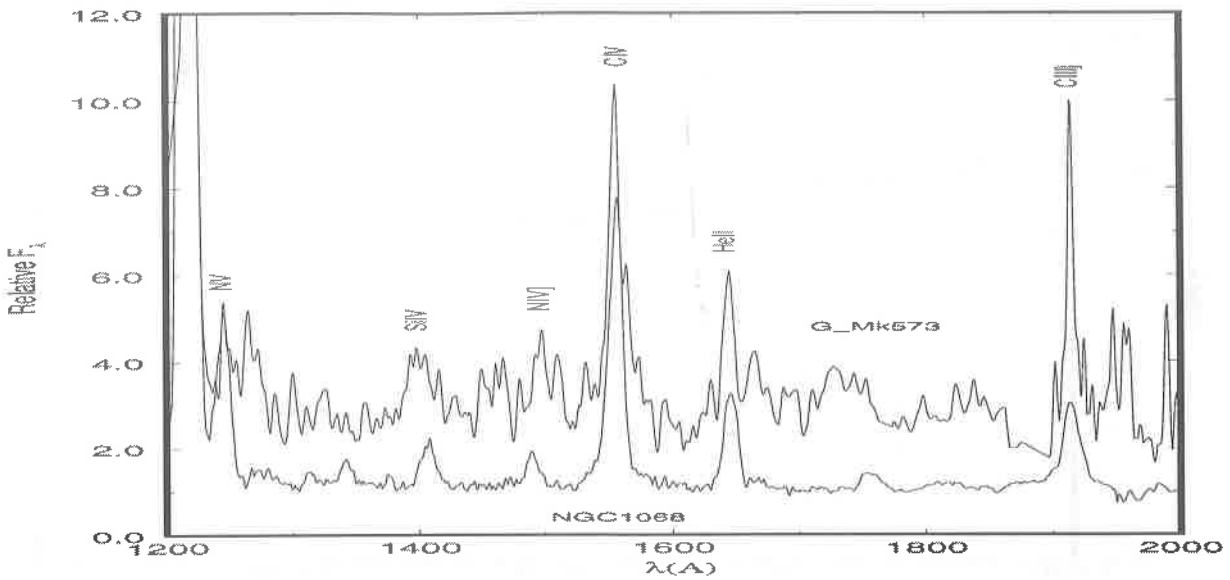

Figure 9: The SWP region of the Seyfert 2 group G_Mk573 is compared to that of NGC 1068; emission lines in G_Mk573 have similar width and relative intensities as in NGC 1068. Fluxes are in F_λ units normalized at λ2646 Å, while a constant was added to the upper spectrum for clarity purposes

conclusion. In terms of the equivalent width, those of the group G_Mk573 are systematically larger than those of NGC 1068, which suggests a higher excitation and/or less contamination by a stellar continuum component in the former.

5 Blue groups

We compare in Fig. 10 the spectrum of the group G_N1510 (average of H II and/or amorphous galaxies) with that of NGC 5253. As expected, the spectra are very similar. Emission lines are not characteristic features of the UV spectrum of H II galaxies. We also show in Fig. 10 the H II region template from Paper I (including SMC, LMC, M 33 and M 101 H II regions), the star cluster templates SWB I (age $\approx$10 Myr) and SWB II (age $\approx$25 Myr). Thus, the presence of strong emission lines in the UV spectra of galaxies, e.g. Mg II$_{\lambda\lambda 2796,2803}$, such as in those of Seyfert nuclei is not related to conventional star-formation, indicating the presence of activity. The different slope between the H II region template and both H II galaxy spectra might be explained by more internal reddening in the latter two. If this is the case, the extinction law would necessarily be similar to that of the SMC because of the absence of the λ2200 Å absorption in the H II galaxies. Alternatively, the slope can also be changed by a combination of the H II template with other recent star formation templates, e.g. SWB II. In the latter case, such galaxies would have been forming stars in the last $\approx$50 Myr.

We compare in Fig. 11 the spectrum of the group G_N5102 with those of the star

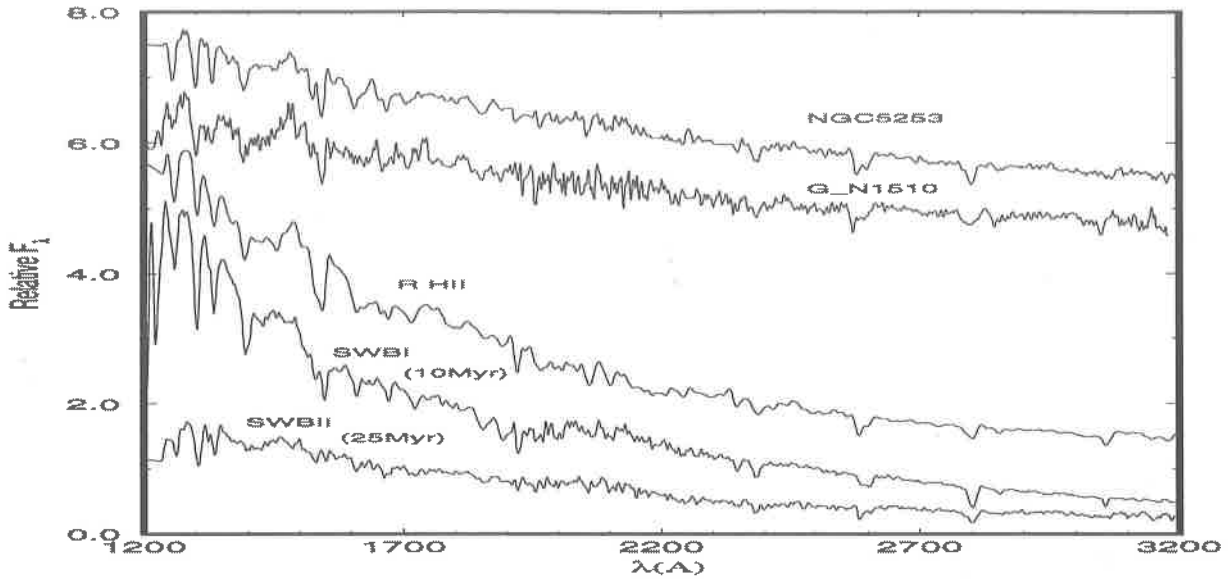

Figure 10: The spectrum of the group G_N1510 is compared to that of NGC 5253 and to those of H II region and star cluster templates of different ages. Fluxes are in F_λ units normalized at $\lambda 2646$ Å, while constants have been added to the spectra for clarity purposes, except for the lowest one

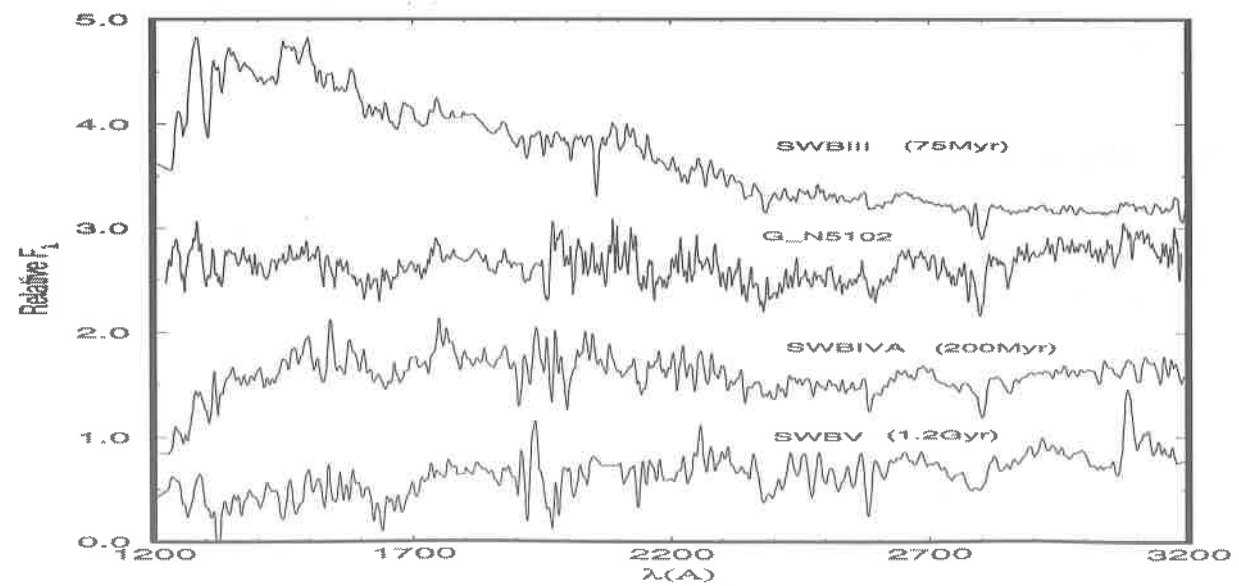

Figure 11: The spectrum of the blue population group G_N5102 is compared to those of star cluster templates at different ages. Fluxes are in F_λ units, normalised at $\lambda 2646$ Å. Constants have been added to the spectra for clarity purposes, except for the bottom one

cluster templates SWB III (age ≈ 75 Myr), SWB IVA (age ≈ 200 Myr) and SWB V (age ≈ 1.2 Gyr). Two members of this galaxy group, NGC 5102 and the M 31 companion NGC 205, were population-synthesized in the visible and near-IR ranges with a star cluster base in Bica (1988, NGC 5102 therein referred to as the template E 8) and Bica et al. (1990), respectively. They concluded that these galaxies had a strong burst of star formation at ages $t \approx 100 - 500$ Myr. In the UV (Fig. 11) it is confirmed that the cluster template SWB IVA (≈ 200 Myr) must be a major contributor to the G.N5102 group.

6 Red groups

At this moment we are working on the groups characterized by the red stellar population. We hope that the resulting (S/N) ratio is enough to allow us to find the origin of the UV turnup observed in some spectra of early-type galaxies.

Acknowledgments

We thank CNPq and FINEP for partially supporting this work; C.B. thanks FAPERGS for covering travel expenses to the XXI SAB meeting.

References

Antonucci, R.R.J., 1993, *ARA&A*, **31**, 473.

Bertola, F., Capaccioli, M., Holm, A.V. & Oke, J.B., 1980, *ApJL*, **237**, L65.

Bica, E., Alloin, D., 1987, *A&A*, **186**, 49.

Bica, E. & Alloin, D., 1988, *A&A*, **192**, 98.

Bica, E., Alloin, D. & Schmidt, A.A., 1990, *A&A*, **228**, 23.

Bica, E., 1992, *in "The Stellar Populations of Galaxies", eds. B. Barbuy , A. Renzini*, **IAU Symp. 149**, p.215.

Bica, E., Alloin, D., Schmitt, H.R., 1994, *A&A*, **283**, 805.

Bonatto, C., Bica, E. & Alloin, D., 1995, *A&ASS*, **112**, 71.

Burstein, D., Bertola, F., Buson, L.M., Faber, S.M. & Lauer, T.R., 1988, *ApJ*, **328**, 440.

Kinney, A.L., Bohlin, R.C., Calzetti, D., Panagia, N., Wyse, R.F.G., 1993, *ApJS*, **86**, 5.

Longo, G., Capaccioli, M. & Ceriello, A., 1991, *A&AS*, **90**, 375.

Oke, J.B., Bertola, F. & Capaccioli, M., 1981, *ApJ*, **243**, 453.

Rosa, M., Joubert, M. & Benvenutti, P., 1984. *A&AS*, **57**, 361.

Seaton, M.J., 1979. *MNRAS*, **187**, 73p.

Stirpe, G.M. et al. , 1994. *A&A*, **285**, 857.

Wanders, I. et al. , 1993. *A&A*, **269**, 39.

REDSHIFT SURVEYS OF FIELD GALAXIES

Christopher N.A. Willmer

CNPq/Observatório Nacional,
Rua General José Cristino 77,
Rio de Janeiro, RJ, 20921-030, Brazil
e-mail: cnaw@on.br

1 Introduction

In this contribution I will present some of the main results obtained from redshift surveys of galaxies. Because of space constraints, the coverage will be at best superficial, and omissions, inevitable. For more complete reviews the reader is refered to works by Sandage (1988) for an overview of observational tests of world models; Hubble (1936), Mihalas & Binney (1981) for reviews of the early work; Giovanelli & Haynes (1991), where many of the main results of redshift surveys are reviewed; Koo & Kron (1992) who deal with the evolution of faint galaxies and Peebles (1993), who shows the inter-relation between theory and observations.

A few definitions should be explained before proceeding further. The first refers to *field galaxies*. As noted by Koo & Kron (1992), these are objects which are selected without regard to their environment (*e.g.*, galaxies in clusters), or to some special characteristics (*e.g.*, X-ray emission). In general, the samples of field galaxies are selected through criteria such as the observed flux in a given wavelength domain, for which a selection function can be easily calculated.

Redshift surveys of field galaxies aim at measuring galaxies in a volume that constitutes a *fair sample*, such that its statistical properties may be considered as representative of the properties of the Universe as a whole (Peebles 1980). The surveys can be carried out using either *full* or *sparse sampling*. Fully sampled surveys aim at observing all galaxies to a given limit, while sparse samples use a random sub-sample of the catalogue of objects. The latter allows probing a larger volume of space for the same amount of telescope time when compared to fully sampled surveys. Another advantage of sparse sampling is that it can reduce the noise due to the discrete nature of the galaxy distribution when measuring statistics such as the spatial two-point correlation function (Kaiser 1986). On the other hand, one loses information of certain higher order characteristics of the distribution, even when using an optimal sparse sampling rate (Szapudi & Szalay 1995).

2 First results

Both counts of galaxies and redshift surveys had an imense boost in the beginning of this century with the use of photographic plates, and in the 1970's and 1980's, with the development of solid-state detectors. Of the ealier work, we will concentrate on two results.

The first is the demonstration by Hubble (1926) that the number counts of galaxies in the magnitude range $m_{pg} = 8.5 - 16.7$, obeyed the following power-law

$$Log(N(m)) = 0.6m + constant \quad (1)$$

when averaged over many directions. This value is also quite close to what would be expected in the case of a Euclidean Universe, and suggested that averaged over very large scales, the distribution of galaxies is homogeneous. This also meant that different from stars, there was no "edge" in the distribution of galaxies, so that these objects could be used to trace properties of the Universe. The second was the demonstration by Hubble (1929) of the tight correlation between the radial velocity and distance, the latter measured using distance estimators such as cepheids and brightest galaxies in clusters. This relation provided observational evidence supportive of Friedmann's (1922) solution for the field equations of General Relativity Theory, where an expanding Universe was predicted.

In the 1930's galaxy counts were carried out covering large extents of the sky in both hemispheres, and in smaller regions, but to much fainter magnitudes using the largest available telescopes (*e.g.*, Hubble 1936). Another important effort was the systematic coverage of the sky made in the 1950's through the Palomar Observatory–National Geographic Society Sky Survey (POSS I), which had plates taken in blue (O) and red (E) colours, while analogous efforts in the southern hemisphere were carried out in the late 1970's and early 1980's, using the Schmidt telescopes in Siding Spring (UKST) and the European Southern Observatory (ESO). The POSS I database was visually inspected by Abell (1958) who presented a list of rich clusters, and by Zwicky and collaborators (1961-1968, hereafter CGCG), who produced a catalogue of galaxies and clusters of galaxies. These works showed that even though on large scales the number counts suggest that the distribution of galaxies is fairly homogeneous, on short scales galaxies have a tendency to cluster. This behaviour is particularly striking when examining the map made by Seldner *et al.* (1977) of the counts down $m_{pg}\sim19$ carried out by Shane & Wirtanen (1967) of plates obtained with the Carnegie astrograph at Lick Observatory. Both the CGCG and the Shane & Wirtanen (1967) counts were used by Groth and Peebles (1977) to study the two-point angular correlation function, and provided some of the first estimates of the clustering of galaxies. The scale length found by Groth & Peebles (1977) corresponds to r_0=4.7 h^{-1} Mpc for the de-projected spatial correlation function.

3 The first complete redshift surveys

In spite of the limitations of photographic plates, the catalogue of bright galaxies covering both celestial hemispheres compiled by Shapley and Ames (1932) was systematically used to measure redshifts and the complete sample was finally published by Sandage and Tammann (1981, RSA). Because this sample is dominated by galaxies belonging to the Local Supercluster, its use for the characterization of large-scale properties of the galaxy distribution is somewhat restricted. For instance, the first determinations of the redshift-

space two-point correlation function by Davis, Geller & Huchra (1978) using a catalogue with a similar depth as the RSA, produced a correlation length of r_0=2.4 h^{-1} Mpc for the galaxies in the north galactic hemisphere and r_0=3.6 h^{-1} Mpc in the southern galactic hemisphere (Peebles 1980).

The first survey to probe beyond the Local Supercluster was the CfA1 by Davis *et al.* (1982), who used a sample of 2401 galaxies derived from the CGCG, and showed that galaxies form a complex distribution where an alternation between regions almost devoid of galaxies and clusters and lower density filaments was clearly seen. However, because the Local supercluster and galaxies belonging to Coma are contained within this sample, it was possible that some physical parameters that were estimated using this sample, such as the mean volume density of galaxies, could be biased. This prompted the realization of surveys in other directions of the sky. The southern counterpart of the CfA1, the SSRS1 (da Costa *et al.* 1988), probed a region of the sky were few nearby (and rich) clusters of galaxies were found, and thus was more representative of what a typical "field" sample would be. Other important surveys using other wavelength bands are those using the catalogue of sources detected by the IRAS satellite to define galaxy samples (Strauss *et al.* 1990; Fisher *et al.* 1995; Saunders *et al.* 1991) and the surveys which measure the the neutral hydrogen emission at 21 cm (*e.g.*, Giovanelli & Haynes 1991; Maia 1993).

Because most of these surveys presented structures with scale sizes of the same order as the survey depth, it was possible that these still did not constitute fair samples. Thus, it would be necessary to explore even larger volumes, using samples with fainter limiting magnitudes (*e.g.*, CfA2, de Lapparent *et al.* 1986; Geller & Huchra 1989; SSRS2, da Costa *et al.* 1994). The combined CfA2 and SSRS2 surveys, both limited at B(0)=15.5, constitute the largest fully sampled optical surveys of nearby galaxies (da Costa 1995). These provide the most detailed maps of the quasi-three dimensional distribution of galaxies, where a complex of interconnecting "voids" are delineated by thin, almost flat, structures where galaxies are preferentially distributed. The characteristc size of these "voids" ranges from about 20 h^{-1} up to 50 h^{-1} Mpc. However, the presence of structures such as the "Great Wall" (Geller & Huchra 1989), with sizes comparable to the survey depth ($\sim$ 150 h^{-1} Mpc), suggests that even these surveys may not have attained a fair sample of the Universe. On the other hand, the statistical analyses carried out using these samples have produced fairly consistent results. The two-point correlation function, which is defined by the excess probability of finding two galaxies at a given separation, has been found to obey a power-law of the form

$$\xi(r) = (r_0/r)^{\gamma} \qquad (2)$$

with $r_0 \sim 5$ h^{-1} Mpc and $\gamma \sim 1.8$, when calculated for all the nearby galaxy samples. The CfA2 and SSRS2 are deep enough that a meaningful estimate of the three-dimensional power-spectrum can be made. If galaxies are good tracers of the matter distribution, the power spectrum should in principle provide information on the fluctuations of the distribution of mass, which can be directly compared with model predictions. For the combined CfA2-SSRS2 it is found that the power-spectrum rises monotonically from small scales up to $\sim$ 200 h^{-1} Mpc, showing only weak signs for a turnover beyond that distance

(da Costa 1995).

Another important statistic is the luminosity function, which may be parameterized using the Schechter (1976) form:

$$\phi(L)dL = \phi^* e^{-L/L^*}(L/L^*)^{-\alpha} d(L/L^*) \tag{3}$$

which, when expressed in magnitudes becomes:

$$\phi(M)dM = -0.4 Log_e(10)\phi^* 10^{0.4(M^*-M)(\alpha+1)} exp[-10^{0.4(M^*-M)}]dM \tag{4}$$

The luminosity function has been investigated for both the CfA2 (Marzke *et al.* 1994) and SSRS2 (da Costa *et al.* 1994). The Schechter parameters differ between both works, while the SSRS2 parameters are consistent with those measured by deeper surveys (Loveday *et al.* 1992; Vettolani *et al.* 1994). The inconsistencies found for the CfA2 sample can be due to a variety of reasons, which could be either systematic errors in the CGCG magnitudes or even incompleteness in the CGCG.

The luminosity function when calculated for different morphological types shows that the Schechter parameters are generally similar, except in the case of irregular galaxies whose faint-end slope is much steeper (Marzke *et al.* 1994). The SSRS2 database was combined with the ESO Surface Photometry Catalogue (Lauberts & Valentijn 1989) to study the behaviour of the luminosity function with colour. A preliminary analysis carried out by da Costa *et al.* (1995) has shown that blue galaxies tend to have a faint-end slope similar to that detected for Irregular galaxies, suggesting that a nearby population of blue galaxies is a possible contributor to the faint galaxy counts (da Costa 1995).

An issue which is still not well quantified, refers to the frequency of Active Galactic Nuclei, and how the presence of this phenomenon could be related to local environment. The frequency of AGNs has been estimated to be $\sim$ 2% by Maia *et al.* (1995), who inspected spectra belonging to the combined SSRS1 and SSRS2 database.

4 Redshift surveys using sparse sampling

While the ESO/SRC survey plates were being taken, much effort was placed on developing fast plate measuring machines that could handle the large amount of data generated from such scans. The UKST plates were digitized and analysed using objective methods by two independent machines, the APM (Kibblewhite *et al.* 1984) and COSMOS (MacGillivray & Stobie 1984). The APM survey (Maddox *et al.* 1990) contains galaxies down to b_J=20 for the region $\delta \leq$17.5° and b$\leq$-40° . A total of about 2 million galaxies were detected and provided a sample with angular coverage and depth similar to the galaxy counts of Shane and Wirtanen (1967).

A bright ($b_J \leq$17.15) subsample of 1769 galaxies was selected to carry out a redshift survey using a 1 in 20 sampling rate, which constitutes the Stromlo-APM survey (Loveday *et al.* 1992). The galaxies were visually inspected and had their morphological types classified. The characteristic depth of this survey is about 12000 kms^{-1} (the CfA2 and SSRS2

have a characteristic depth of $\sim$ 7000 kms^{-1}). The luminosity function for this sample, presents the following Schechter parameters: α=$-$0.97$\pm$0.15; M*=$-$19.50$\pm$0.13 and ϕ^*=1.40$\pm$0.17$\times10^{-2}$ h^{-3} Mpc^3, and in this calculation the k-corrections of Efstathiou, Ellis & Peterson (1988) were taken into account. Although these results were not confirmed by Marzke *et al.* (1994) for the CfA2, both the shallower SSRS2 (da Costa *et al.* 1994) and the deeper ESO Slice Project (Vettolani *et al.* 1994) present a similar determination as Loveday *et al.* (1992). These authors also found that the luminosity parameters for early and late type galaxies are different. Other results from this survey refer to the clustering properties of galaxies when selected by morphology and luminosity, using the two-point correlation function both in real and redshift-space (Loveday *et al.* 1994). The correlation function is quite different when calculated in real and redshift space, the latter usually being flatter. These authors confirm earlier findings by Davis & Geller (1976) and Giovanelli, Haynes & Chincarini (1986) that early type galaxies present a stronger correlation than later types when calculated in real space. On the other hand, in redshift space, the correlation of early types is much flatter, even when compared to late-type galaxies, indicating that "early-type galaxies suffer from enhanced space distortions". They also find that lower-luminosity galaxies (L<L*) are more weakly correlated than galaxies with L$\sim$L* on scales larger than 1 h^{-1} Mpc, while the clustering properties of brighter (L>L*) is similar to those of L$\sim$ L*. This effect is seen both in real and in redshift space. Loveday *et al.* (1994) conclude that the luminosity segregation could be a primordial effect, "due to a lower bias factor for low-luminosity galaxies", while the segregation by morphological type could be enhanced by environmental effects.

5 Surveys of faint galaxies

Several small areas on the sky were explored using plates taken at the prime-focus of 4m-class telescopes at the AAT, KPNO and CTIO, and used to make number counts to very faint limiting magnitudes (B$\sim$22). At the faint end the number counts are above the expected value for no-evolution (NE) models, the discrepancy being usually larger in the blue counts. This result implied that significant evolution could have occurred at low redshift, such that faint galaxies were more luminous and bluer due to a higher stellar formation rate. To address this question, Broadhurst, Ellis & Shanks (1988, BES) designed a redshift survey of galaxies selected in the magnitude interval and band where the greatest discrepancies between the observed and predicted NE counts were found. About 230 galaxies with 20.0$\leq$b$_J\leq$21.5 were observed. The redshift distribution however, is very close to what would be expected for NE models, while a large fraction of the spectra show evidence of star formation for z>0.1. In order to conciliate the excess in number counts with the behaviour close to NE shown by the redshift distribution, BES proposed a model where the excess number counts is due to low-luminosity objects, but which at z$\sim$0.2 presented bursts of star formation, and which have undergone significant evolution in the recent past.

A similar effort was carried out by Koo, Kron and Szalay (*e.g.*, Szalay 1987) in three

other directions of the sky, down to a limiting magnitude of b_j=21. The redshift distribution of these samples showed large regions of about 200 h^{-1} Mpc that were devoid of galaxies. One of these directions was almost opposite to the survey of BES, and in Broadhurst *et al.* (1990, BEKS), both samples in the direction of the galactic poles were combined to quantify the properties of the large-scale structures to z~0.5. The combined sample covered a baseline of about 2000 h^{-1} Mpc in comoving coordinates. By calculating the pair separations along the line of sight, a significant peak was detected at separations of the order of 130 h^{-1} Mpc, which was also detected by the one-dimensional power-spectrum. This peak also presented a fairly low probability of being due to noise, and the most likely interpretation was that this could be the signature of the characteristic size of voids which would be delineated by large low-density structures analogous to the Great Wall. In order to verify whether such periodic pattern occurred in other directions of the sky, new surveys were carried out, some a few degrees away from the main probe at the north galactic pole (NGP) (Ellman 1994), others along the SA68-Anti-SA68, and Hercules-Anti-Hercules direction (Koo *et al.* 1993). These works showed that the repetition pattern detected by BEKS was not found in the other axes, while the survey close to the NGP showed that probes separated from the main survey by a few degrees (corresponding to several tens of Mpc in projected distances), presented peaks at the same redshifts, suggesting structures with scale sizes comparable to the Great Wall could be causing the redshift peaks.

A survey designed to characterize the properties of the structures causing the first peaks in the BEKS northern sample, was carried out by Willmer *et al.* (1994) who measured redshifts for more than 300 galaxies in a 4° by 49′ slice close to the NGP. This survey showed that the BEKS peaks were in fact caused by large coherent structures showing a variety of inclinations relative to the line of sight, and whose physical properties (velocity dispersion, projected surface density) were similar to what had been measured for the Great Wall by de Lapparent, Geller and Huchra (1991) and Ramella, Geller & Huchra (1992).

To determine what population of galaxies causes the excess counts relative to NE models, several surveys deeper than BES for blue-selected samples were carried out by Colless *et al.* (1990, 1991, 1993). The galaxies measured in these surveys all had z<1, implying that the excess counts could not be due to luminosity evolution of higher-redshift galaxies. A deeper survey was carried out by Glazebrook *et al.* (1995a), which, although detecting galaxies beyond z=1. still showed that most of the objects were at smaller redshifts, suggesting that simple luminosity evolution could not account for the observed discrepancy between the number counts and the redshift distribution. In order to reconcile these results, one possible model would be number density evolution through the merging of galaxies. In a survey of K-band selected galaxies. Glazebrook *et al.* (1995b) showed that the K-band luminosity functions does not present evidence of evolution for z<0.5, while for z>0.5 there is evidence of luminosity evolution, but such that there could not have been any density evolution.

Finally, a survey carried out with the Canada-France-Hawaii Telescope (Lilly *et al.* 1995, and references therein) has produced results regarding the properties of the lu-

minosity function to z$\sim$1 for a sample of galaxies selected in the range 17.5$\leq$I$\leq$22.5 in five different areas of the sky. Lilly *et al.* (1995) present a luminosity-colour diagram for different redshift intervals, and show that the "luminosity function of red galaxies shows very little change in either number density or luminosity over the entire redshift range 0<z<1", while blue galaxies show "substantial evolution at redshifts z>0.5". In this work, red galaxies are defined as objects which are redder than typical present-day Sbc galaxies. These authors find a significant excess of galaxies relative to the local luminosity function as measured by Loveday *et al.* (1992) for redshifts below 0.2 and galaxies with M_{AB}(B)$\sim$–18, similar to the what was found by Marzke *et al.* (1994), which could "represent the descendants of the evolving blue population seen at higher redshifts after modest luminosity evolution".

6 Works in progress

A follow-up of the CfA2 is being carried out by Geller *et al.* (1995), which will measure redshifts for all galaxies in a 100° × 1° slice centered at δ=29° . The sample was defined from photographic photometry of POSS I E plates down to a limiting magnitude of R=16.4. This work shows a distribution where the repetition of structures is clearly seen, there being no structures larger than the characteristic depth of the survey.

Kirshner, Oemler, Schechter and Shectman (1987) had carried out several pencil-beam surveys close to the galactic poles using sparse sampling through which they discovered a large underdense region, originally estimated to have a size of $\sim$ 80 h^{-1} Mpc in the Boötes constellation. More recently, these authors designed a survey, again using sparse sampling, in the southern sky, using a sample defined from CCD photometry, where slabs of 1.5° by 1.5° are observed through drift scans (*i.e.*, the CCD is read at the same rate as the earth's rotation) and used to derive a specroscopic sample, which is observed using a multi-fibre system installed on the 2.5 m telescope at the Las Campanas Observatory. This survey aims measuring redshifts for about 30000 galaxies within the magnitude range of 16.0 $\leq$ r $\leq$ 17.5. The sampling rate is 6 galaxies out of 10, and due to the cut in surface brightness, the efficiency (*i.e.*, gathering a measurable spectrum) is $\sim$ 90%. The distribution of galaxies shows many structures with scales $\leq$ 50 h^{-1} Mpc and preliminary results from this survey show that about 20% of the galaxies present emission lines. The two-point correlation function measured in this survey shows results similar to those detected in shallower surveys. However, when separated between spectral characteristics (presence or not of emission lines) they find that at small separations galaxies with emission lines tend to have a lower correlation than galaxies without emission lines (Shectman *et al.* 1992), suggesting that galaxies in denser environments could have undergone gas depletion.

A survey attaining a similar depth as KOSS is the ESO Slice Project (Vettolani *et al.* 1994), probing a 22° × 1° slice, limited at b_J=19.4, at δ=–40° . This survey uses a sample of galaxies originated from the Edinburgh-Durham COSMOS catalogue (Heydon-Dumbleton *et al.* 1989). Preliminary results from this survey indicate that the luminosity function parameters agree with those measured by Loveday *et al.* 1992. They also detect

some of the southern peaks of BEKS, though the periodicity is not as strong.

A somewhat deeper work is the ESO-Sculptor survey of de Lapparent and collaborators (Bellanger *et al.* 1995; Arnouts *et al.* 1995) with the aim of characterizing the large-scale properties of the galaxy distribution out to depth of z∼0.5. The catalogue of this survey is derived from CCD photometry obtained in B,V and R in a slice of $1.75° \times 0.2°$. The number counts in the three colours show evidence of evolution, while the galaxy colours in B–R and B–V show a blueing trend of ~ 0.5 magnitudes for $21.0 \leq R \leq 23.5$ (Arnouts *et al.* 1995). The spectroscopic sample contains ~ 1000 galaxies brighter than R=20.5, and is expected to be completed in 1995.

7 Concluding remarks

Redshift surveys have been the one of the most important means of characterizing the statistical properties of galaxies in the nearby Universe. Not only have they have allowed a quasi-three-dimensional view of the distribution of galaxies, but more importantly, from the statistical analyses it becomes possible to place observational constraints which must be satisfied by successful models for the formation and evolution of galaxies and large-scale structures. We could thus summarize some of the main results from these works that we have presented above:

1. Galaxies tend to concentrate on low-projected density structures which surround large (≤ 50 h^{-1} Mpc) regions within which few bright galaxies are found.
2. The two-point correlation function presents discrepancies when measured in real and redshift space.
3. The scale size where the correlation function becomes 1 is roughly the same both from optical as well as infrared samples, and corresponds to ~ 5 h^{-1} Mpc.
4. The two-point correlation function presents slight differences depending on what kind of sample is used, *i.e.*, different values are measured when galaxies are divided between morphological types, luminosity classes, colours or presence of emission lines.
5. The luminosity function parameters measured for the nearby samples (z<0.1) present similar values. When calculated for different types and morphologies it is found that the Schechter parameters are fairly similar for all morphologies except for irregular galaxies and blue galaxies which present steeper slopes.
6. The deeper surveys show that redder galaxies present almost no evidence for evolution since $z \sim 1$, while blue galaxies present evidence of significant evolution since z> 0.5.

8 References

- Abell, G.O. 1958, ApJS, 3, 211
- Arnouts, S., de Lapparent, V., Mathez, G., Mazure, A., Mellier, Y., Bertin, E., & Kruszewski, A. 1995, AA, submitted
- Bellanger, C., de Lapparent, V., Arnouts, S., Mathez, G., Mazure, A., & Mellier, Y. 1995, AASS, 110, 159

- Broadhurst, T.J., Ellis, R.S., & Shanks, T. 1988, MNRAS, 235, 827 (BES)
- Broadhurst, T.C., Ellis, R.S., Koo, D.C., & Szalay. A.S. 1990, Nature, 343, 726 (BEKS)
- Colless, M., Ellis R.S., Taylor, K., & Hook, R. 1990, MNRAS, 244, 408
- Colless, M., Ellis R.S., Taylor, K., & Shaw, G. 1991, 253, 686
- Colless, M., Ellis R.S., Taylor, K., Broadhurst, T.J., & Peterson, B.A. 1993, MNRAS, 261, 19
- da Costa, L.N., Marzke, R.O., Pellegrini, P.S., & Santarosa, G. 1995, in preparation
- da Costa, L.N., Pellegrini, P.S., Sargent, W.L.W, Tonry, J., Davis, M., Meiksin A., Latham, D.W., Menzies, J.W., and Coulson, I. A. 1988, ApJ 327, 544
- da Costa, L.N., Geller, M.J., Pellegrini, P.S., Latham, D.W., Fairall, A.P., Marzke, R.O., Willmer, C.N.A., Huchra, J.P., Calderon, J.H., Ramella, M., & Kurtz, M.J. 1994, ApJ, 424, L1
- da Costa, L.N., 1995, to appear in "Clustering in the Universe", Proc, of XXXth Moriond Conference, Les Arcs"
- de Lapparent, V., Geller, M.J., and Huchra, J.P. 1986, ApJ 302, L1
- de Lapparent, V., Geller, M.J., & Huchra, J.P, 1991, ApJ, 369, 273
- Davis, M., & Geller, M.J. 1976, ApJ, 208, 13
- Davis, M., Geller, M.J., & Huchra,J.P. 1978, ApJ, 221, 1
- Davis, M., Huchra, J.P., Latham, D.W., & Tonry, J. 1982, ApJ, 253, 423
- Efstathiou, G., Ellis, R.S., & Peterson, B.A. 1988, MNRAS, 232, 431
- Ellman, N. 1994, Ph.D. Thesis, University of California at Santa Cruz
- Friedmann, A. 1922, Z. Phys., 10, 337,
- Fisher, K.B., Huchra, J.P., Strauss, M.A., Davis, M., Yahil, A. & Schlegel, D. 1995, ApjS, in press
- Geller, M.J., & Huchra, J.P. 1989, Science, 246, 897
- Geller, M.J., et al. 1995, in preparation
- Glazebrook, K., Ellis, R.S., Colless, M., Broadhurst, T.C., Allington-Smith, J., & Tanvir, N. 1995a, MNRAS, 273, 157
- Glazebrook, K., Peacock, J.A., Miller, L., & Collins, C.A. 1995b, MNRAS, in press
- Giovanelli, R., Haynes, M.P. 1991, ARAA, 29, 499
- Giovanelli, R., Haynes, M.P., & Chincarini, G. 1986, ApJ, 300, 77
- Groth, E.J., and Peebles, P.J.E. 1977, ApJ 217, 385
- Heydon-Dumbleton, Collins, C.A., & MacGillivray, H.T. 1989, MNRAS, 238, 379
- Hubble, E. 1926, ApJ, 64, 321
- Hubble, E. 1929, Proc. Nat. Acad. 15, 168
- Hubble, E. 1936, "The Realm of the Nebulae", (New Haven: Yale University Press)
- Kaiser, N. 1986, MNRAS, 219, 785
- Kibblewhite, E.J., Bridgeland, M.T., Bunclark, P. & Irwin, M.J. 1984, in Astronomical Microdensitometry Conference, NASA CP 2317, 277
- Kirshner, R.P., Oemler, Jr., A., Schechter, P.L., and Schectman, S.A. 1987, ApJ 314, 493
- Koo, D.C., Ellman, N., Kron, R.G., Munn, J.A., Szalay, A.S., Broadhurst, T.J., & Ellis, R.S. 1993, ASP Conf. Ser. Vol. 51, Observational Cosmology Symposium, ed. G.

Chincarini, A. Iovino, T. Maccacaro, & D. Maccagni (San Francisco: ASP), 112
- Koo, D.C., & Kron, R. 1992, ARAA, 30, 613
- Lauberts, A., and Valentijn, E.A. 1989, "The Surface Photometry Catalogue of the ESO-Uppsala Galaxies", (Garching-bei-München:European Southern Observatory)
- Lilly, S.J., Tresse, L., Hammer, F., Crampton, D., & Le Fèvre, O. 1995, preprint
- Loveday, J., Peterson, B.A., Efstathiou, G., & Maddox, S.J. 1992, ApJ, 390, 338
- Loveday, J., Maddox, S.J., Efstathiou, G., & Peterson, B.A. 1994, Preprint
- MacGillivray, H.T., & Stobie, 1984, Vistas Astr., 27, 433
- Maddox, S.J., Sutherland, W.J., Efstathiou, G., & Loveday, J. 1990, MNRAS, 243, 692
- Maia, M.A.G. 1993, Proc. of the XIXth SAB Meeting, ed. J. Braga, B. Barbuy, N.V. Leister, p. 157
- Maia, M.A.G., Suzuki, J.A., da Costa, L.N., Willmer, C.N.A., & Rité, C. 1995, AASS, submitted
- Marzke, R.O., Geller, M.J., Huchra, J.P., & Corwin, H.G. 1994, AJ, 108, 437
- Metcalfe, N., Shanks, T., Fong, R., & Roche, N. 1995, MNRAS, 273, 257
- Mihalas, D. & Binney, J. 1991, "Galactic Astronomy", (New York: W.H. Freeman and Company)
- Peebles, P.J.E. 1980, "The Large-Scale Structure of the Universe", (Princeton: Princeton University Press)
- Peebles, P.J.E. 1993, "Principles of Physical Cosmology", (Princeton: Princeton University Press)
- Ramella, M., Geller, M.J., & Huchra, J.P. 1992, ApJ, 384, 396
- Sandage, A. 1988, ARAA, 26, 561
- Sandage, A., & Tammann, G.A. 1981, "A Revised Shapley-Ames Catalog of Bright Galaxies", (Washington: Carnegie Institution of Washington, Publ. 635) (RSA)
- Saunders, W., *et al.* 1991, Nature, 349, 32
- Schechter, P. 1976, ApJ, 203, 297
- Seldner, M., Siebers, B., Groth, E.J., & Peebles, P.J.E. 1977, AJ, 82, 249
- Shane, C.D., Wirtanen, C.A., 1967, Publ. Lick Obs., XXII, Part 1
- Shapley, H., and Ames, A.A. 1932, Harvard Ann., 88, N° 2
- Shectman, S. *et al.* 1992, Clusters and Superclusters of Galaxies, ed. A. C. Fabian (Dordrecht: Kluwer)
- Strauss, M.A., Davis, M., Yahil, A., and Huchra, J.P. 1990, ApJ 361, 49
- Szalay, A.S. 1987, in "Large Scale Structures in the Universe", ed. L. Martinet, M. Mayor, (Sauverny: Geneva Observatory)
- Szapudi, I., & Szalay, A.S. 1995, preprint
- Vettolani, G., *et al.* 1994, to apppear in "Wide Field Spectroscopy and the Distant Universe", ed. S.J. Maddox, A. Aragon-Salamanca, (Singapore: World Scientific)
- Willmer, C.N.A., Koo, D.C., Szalay, A.S., & Kurtz, M.J. 1994, ApJ, 437, 560
- Zwicky, F., Herzog, E., Karpowicz, M., and Kowal, C. 1961-1968, Catalog of Galaxies and Clusters of Galaxies, (Pasadena: California Institute of Technology), 6 vols (CGCG)

MAGNETIC RECONNECTION WITHIN GALACTIC AND EXTRAGALACTIC STAR FORMING REGIONS

Luiz Carlos Jafelice

Departamento de Física Teórica e Experimental
UFRN - CCE - Campus Universitário
C.P.: 1641 - CEP 59072-970 Natal, RN - BRAZIL
PHONE: 55-84-231 95 86 branch: 27 - FAX: 55-84-231 97 49
email: lcj@ncc.ufrn.br

Abstract

We discuss the relevance of the mechanism of magnetic reconnection within star forming regions. The role played by such a mechanism in the process of star formation and the observational consequences are briefly discussed for both interstellar and intracluster environments.

1 Magnetic reconnection

Magnetic reconnection (MR) is a well known process of conversion of magnetic energy into other forms of energy (e.g. kinetic, thermal, of plasma waves, etc) (Biskamp 1994). What characterizes the process of MR is the topological change it causes in the magnetic field. This aspect is very important in the treatment of transport processes in magnetized plasmas, particularly for collisionless plasmas as those observed in the interstellar medium and the intracluster medium of galaxies.

Although such a process is well known in laboratory and astrophysical plasmas, recent theoretical and experimental results involving tridimensional treatment of the problem (Biskamp 1994) have revealed that the previous knowledge is still quite incipient. Such results, however, clearly indicate that magnetic energy dissipation rates (or MR rates) are independent of the value of the collisional resistivity and are basically associated with the typical Alfvén time scale. Contrary to the first 1D and 2D studies on MR, the main different and relevant results obtained recently come from the use of numerical simulations (Biskamp 1994 and references therein) and on the realization of the importance of taking adequately into account the boundary conditions when dealing with the MR physics (Priest & Forbes 1992).

The results of the works by Costa & Jafelice 1995, Friaça & Jafelice 1995, Jafelice & Friaça 1995a and Jafelice & Friaça 1995b are briefly commented on below.

2 Star formation and magnetic fields

The process of star formation is intimately dependent on the presence of magnetic fields. That process will proceed differently in what concerns, e.g., its rate and the shape of the initial mass function, whether the magnetic field is present or not.

In the scenario of star formation process usually adopted, one can point out the following relevances of magnetic field features:

1. Magnetic fields, in general, are important in defining (Mestel 1990; Rees 1994):
   (a) The Jeans mass; and
   (b) The efficiency of angular momentum transfer.
2. Magnetic reconnection, in particular, is important to account for (McKee et al. 1992):
   (a) Topological changes in the magnetic field;
   (b) Magnetic field annihilation; and
   (c) The internal structure of molecular clouds.

Topological change is essential for star formation. A molecular cloud forms out of diffuse interstellar medium with a magnetic field which is well connected to the field of that medium. Nevertheless, when the star forms out of the molecular cloud it has a field essentially detached from the interstellar field (McKee et al. 1992).

Interstellar protostars condense with too much initial magnetic flux (Rees 1994). Magnetic fields are expected to increase the value of the Jean's mass and to make it more difficult for the protostar to contract. Furthermore, flux freezing conditions, even if just approximately valid, would imply in an excess of magnetic flux as the protostar contracts gravitationally. Protostars must get rid of such an excessive flux, and magnetic reconnection is a source of magnetic annihilation.

Molecular clouds are clumpy instead of homogeneous. Values for the magnetic field of giant molecular clouds lower than the equipartition values added to not so small clumps will imply in inevitable tangled magnetic fields within the cloud because of the motions of the gas, which favours the reconnection, gradually detaching the clumps from the interclump medium. Magnetic braking is expected to make an important contribution in transferring angular momentum from the forming star to the surrounding medium. However, such a process may be greatly modified in clumps where the field connection with the rest of the cloud is much more weak because of the ocurrence of reconnection (McKee et al. 1992).

3 MR within the interstellar medium

Costa & Jafelice 1995 study the role played by the MR process in the evolution of magnetic fields within galactic star forming regions. In a first approximation they propose a simple model to treat the temporal evolution of the MR process in that context. The model consists of considering that the electric current layer whose rearrangement will imply in the tearing and reconnection of the magnetic field lines associated to it, is plane and

infinite, and has its fragments (after the tearing) moving away from one another according to a quadratic law in time. Comparisons are made with other propositions for dynamic evolution in systems involving reconnection (in other astrophysical contexts) found in the literature.

The authors compare the time scale, t_{lc}, typical for topological changes in the magnetic field due to the reconnection, with time scales relevant to the star formation. The results indicate that for conditions observed within star forming regions, t_{lc} is quite small compared to time scales associated, for example, to the free fall or to the ambipolar diffusion. Such results quantify and reinforce the relevance of MR during the formation of stars.

In a second approach of that model they adopt a geometry with cylindrical symmetry and study the efficiency and energetic contents involved when the magnetic field lines which have been just reconnected are freed and retreat (due to the own field lines tension), dragging and accelerating the material wraped by them during such a contraction. They solve numerically the nonlinear acceleration equation associated to that material for the geometry considered and the conditions observed within star forming regions. This part of the work is being carried out in this moment and there is not yet any conclusive result about it.

4 Condensations within cooling flows

X-ray observations of clusters of galaxies have revealed that the gas in the core of several clusters has a cooling time shorter than a Hubble time, thus allowing to infer a cooling flow towards the center of cluster, where, interestingly, there is always a dominant galaxy (for reviews, see Fabian 1991). Additionally, in some cooling flows, optical emission line filaments are seen around the central galaxy. These filaments are thought to be a phase of evolution of thermal instabilities arising in the cooling flows. The optical filaments are the most outstanding optical signature of cooling flows.

Several models, considering different mechanisms of ionization and heating of the gas – shocks, thermal conduction, and photoionization by soft X-rays produced in the cooling gas – have met problems in explaining the observed line ratios and luminosities (see Jafelice & Friaça 1995a for further discussion and references).

The possibility of MR as a source of excitation for such filaments have been generically suggested by some authors (Johnstone & Fabian 1988; Soker & Sarazin 1990; Tribble 1991). Jafelice & Friaça 1995a treat the process of MR in those filaments in greater detail through a quantitative approach and the results are compared with the observations. In Friaça & Jafelice 1995 we consider anomalous effects associated with MR in such flows, as we summarize below.

4.1 MR in the Intracluster Plasma

The plasma of the intracluster medium of galaxies is collisionless, magnetized and has, in general, a value of $\beta_{pl} >> 1$ (where the ratio between the plasma kinetic energy density

and the magnetic energy density $\beta_{pl} = 8\pi n_e k_B T_e / B^2$, with n_e being the electron number density, T_e the electron temperature, B the ambient magnetic field, and k_B the Boltzmann constant). When we talk below of low- and high-β regions we are referring, respectively, to values of $\beta_{pl} < 1$ and $\beta_{pl} \geq 1$ within such regions. This dimensionless parameter allows to distinguish between those regions where the plasma dynamics is determined mainly by magnetic forces (i.e., where $\beta_{pl} << 1$) and those where the dynamics is governed by hydrodynamic forces (i.e., where $\beta_{pl} >> 1$).

Filaments with optical emission are observed basically in the inner parts of the clusters. In these inner parts, corresponding to distances from the cluster centre of up to ~ 20 kpc, one expects to have $\beta_{pl} \sim 1$. Such a reduction of β_{pl} from values $>> 1$ for the outer regions to values ~ 1 for the inner ones, is mainly because of the increase in the value of the magnetic field which, frozen-in to the ambient plasma, is dragged by the plasma in its process of contraction towards the centre of the cluster (Soker & Sarazin 1990).

In the subsequent process of condensation and formation of the filaments β_{pl} gets even smaller, and can reach, in principle, values quite smaller than 1. The filaments are expected to be sites of low-β on the grounds of: 1) the amplification of the magnetic field due to the compression of the magnetic field frozen-in to the plasma as the gas condenses to form the filament; and 2) the decrease of the thermal energy density due to the radiative losses taking place in the denser medium of the forming filament. In the phase of filament formation, the gas evolution is nearly isochoric and the latter reason is the most relevant for the reduction of β_{pl}. Anyway, the final result is that both processes contribute to make an ambient ICM plasma in which $\beta_{pl} \sim 1$ (for distances to the cluster centre, say, ≤ 20 kpc) easily achieve values of $\beta_{pl} << 1$ within the filaments.

Observational backing to the above scenario comes from the study by Ge (1991) on magnetic fields in clusters of galaxies with intense cooling flows that clearly indicates that optical line emitting nebulae are magnetically dominated, in some cases with β_{pl} as low as $\sim 10^{-2}$ within the filaments (as, for example, for the cluster A1795).

The MR process taking place within intracluster emitting nebulae is a collisionless one. We define, as usual, the Alfvénic Mach number $M_e \equiv V_e / V_{Ae} \simeq 1/\ln R_{me}$, which gives the reconnection rate of the MR process (where R_{me} is the magnetic Reynolds number). For typical filament conditions one obtains $R_{me} \simeq 1.3 \times 10^{19} M_e$, which gives us for the conditions within intracluster filaments the value $M_e \simeq 0.02$, which is in very good agreement with usual values for the reconnection rate expected to be found in astrophysical plasmas (Priest 1982).

In Jafelice & Friaça 1995a the evolution of the cooling filaments is obtained by solving the hydrodynamical equations of mass, momentum and energy conservation (see Friaça 1993). The cooling function and the coefficients of collisional ionization, recombination and charge exchange of the ionization equations were all calculated with the atomic database of the photoionization code AANGABA (Gruenwald & Viegas 1992).

It seems that MR cannot be the dominant mechanism powering line emission in cooling flows, as it underproduces Hα and [NII]λ6583. However, it could be an important ingredient to explain the emission coming from low ionization lines, such as [OI]λ6300, constituting an additional component acting together with other mechanisms producing

most of the emission in Hα and higher ionization lines (such as [NII]λ6583). On the other hand, the study of MR-based models demonstrates that MR heating constitutes an alternative to shocks as a source of $[OI]$ emission for moderately bright filament systems. MR, however, is not sufficient to power not even the $[OI]\lambda6300$ emission in the most luminous systems, like Perseus. In this case, the shock model represents a best candidate to explain the optical emission.

In a consistent picture of the evolution of condensates in the intracluster medium, MR, allowing the condensates to lose magnetic field, is a necessary link in the formation of cold, dense clouds that are needed to account for the excess X-ray absorption, star formation and presence of dust in cooling flows. As suggested above, it is likely that other processes are corroborating with MR in the energization of intracluster filaments. In this sense we are beginning to study quantitatively the possible relevance of Alfvén waves in such an energization (Friaça et al. 1995). The idea is to compare numerical calculations with observations considering three general situations: cases in which reconnection acts alone, those in which Alfvén waves act alone, and those in which both processes are acting at the same time.

A general conclusion from the study in Jafelice & Friaça 1995a is that in the formation of condensates out of the cooling flow, large amounts of energy are locked in magnetic fields, and, as the MR is needed to get rid of surplus magnetic pressure, it has a role to play in the energetics of cooling flows.

Furthermore, estimates made in that work strongly suggest that the physical scenario for MR in intracluster nebulae is expected to be very rich in plasma effects, where a wealth of plasma instabilities may be ruling important physical processes. In particular, plasma effects may be governing the magnetic energy consumption, heat conduction and the resulting emission signature emerging from these nebulae. The physics and efficiency of the MR process as well as observational consequences in this case can not be properly studied from a magnetohydrodynamic approach. A specific theoretical approach to treat collisionless reconnection in the presence of plasma instabilities will be done elsewhere.

4.2 Other Consequences of MR in Cooling Flows

Friaça & Jafelice 1995 treat, on the one hand, anomalous effects (following Jafelice 1992) in processes involving the formation and energization of filaments within cooling flows and, on the other hand, the effect of energetic electrons accelerated due to the reconnection process.

Those electrons, with energies in the range 1 to 10 keV, may play an important role in the production of forbidden emission lines for ions like $OIII$ and heavier. In that study the authors compare line ratios (like, e.g., $[OIII]/[OII]$ *versus* $[OIII]/H\beta$) with the cases they calculate in which energetic electrons generated by the reconnection are absent and those in which they are present. At the moment there is not yet any conclusive result; the expectation is to obtain some signature and observational predictions from that kind of study.

Anomalous effects are studied aiming to address the fate of the mass which is removed

(i.e., which condenses) from cooling flows. The flow rate can be very high (up to some hundreds of solar masses per year), nevertheless the last destiny of the removed mass is not known (Fabian 1994). On the one hand plasma instabilities have a great influence in the process of MR which occurs in the collisionless plasmas within those flows (as shown by Jafelice & Friaça 1995a), and such plasma effects may have important implications also at a macroscopic level (as shown in Jafelice 1992). On the other hand, the reconnection process is expected to have a fundamental importance in the star formation process (McKee et al. 1992; also the first results in Costa & Jafelice 1995). Therefore, the interrelationship between those processes is expected to have important implication in the formation of stars within the intracluster medium. In that work the authors address the study of stellar formation in that medium which, in many aspects, have quite different physical conditions from those found in star forming regions within galactic interstellar media (which increases the interest in that kind of study).

In Jafelice & Friaça 1995b the authors discuss the possible relationship between the optical signature of the cooling flows and the cluster evolutionary history. They also propose a scenario to take into account the destiny of the mass removed from the cooling flow and they make some observational predictions.

It follows from such a scenario that one must expect that much more filaments are present within the flows than those observed, even for cooling flows where optical filaments have already been detected. In their model the association between the evolutionaries histories of the cluster as a whole and of the cluster magnetic field topology is crucial to explain the presence or absence of optical filaments.

Their analysis indicate that the anti-correlation between the rotation measure decrement and the optical emission observed in clusters with high cooling flow rates suggests that the presence of faded (i.e., "invisible") filaments shoud be searched through rotation measure observations.

The scenario proposed lead to a consistent picture to the fate of the mass removed from the cooling flow. The final destiny of that mass is naturally either faded filaments (which may abound in most cooling flows) or a cooling flow population of mainly low-mass dim objects. MR, allowing the condensates to lose magnetic field, is a necessary link in the formation of cold, dense clouds that are needed to account for the excess of X-ray absorption, star formation and the presence of dust in cooling flows.

5 Final comments on magnetic fields in astrophysics

There is an important point to be emphasized which the recent research on astrophysics is making clearer in the last years: The magnetic field importance in many astrophysical phenomena is **not** necessarily because of its intensity.

Originally, mainly because of the lack of observational data concerning magnetic fields, the natural difficulty to deal with magnetic fields in analytical studies, and because in several situations the magnetic field was not dynamically relevant, its influences were underestimated and the magnetic field was simply excluded from the calculations. (Note,

however, that those were not the only real motives for that posture; some prejudice or overlooking was present in some cases.)

That procedure is not else justifiable in a plenty of astrophysical contexts. In many cases the magnetic field is stronger than initially assumed, but that is not the more unexpected new result. Even dynamically weak magnetic fields revealed to be significant because of their influence on microscopic processes, like thermal conductivity and other transport processes (Jafelice 1992; Rees 1994).

Magnetic reconnection is particularly important in this latter aspect because it naturally implies unexpected interrelationships (and many yet unpredictable ones!) between:

1. Local and global features of a given system through topological changes associated with the reconnection; and between

2. Microscopic and macroscopic features of the system through the effects of the reconnection on transport and energetic processes.

Transport properties, like thermal and electrical conductions, proceed much more efficiently along magnetic field lines than across them. This is particularly conspicuous for collisionless plasmas as those present in interstellar and intracluster media. On the one hand, reconnection can make regions with quite different physical conditions (like, e.g., temperature, density, chemical composition, etc.), which were initially separated, to be connected; on the other hand it can make a condensation which was cooling, for example, through the conduction along magnetic field lines to become substancially thermally insulated from the surrounding medium. In either case the evolutionary implications for the whole system may be quite different than if reconnection was not taking place. (Some implications of this scenario for the formation of condensations and stars in the intracluster medium of galaxies is discussed in Jafelice & Friaça 1995b.)

As one can see, the future work involving magnetized astrophysical media is very stimulating and has many important open questions to be tackled. Magnetic fields may be directly relevant, through their dynamic contribution, or indirectly because they affect transport processes, energy input (through MR) and/or topological changes.

In short, **magnetic fields can establish unexpected connections between local processes and global phenomena in a given system which are widely unknown and unexplored yet**. That constitutes a rich and challenging research field for young (as well as old!) astrophysicists. What are you waiting to set to work, then? Good luck!

Acknowledgements

The author would like to thank the organizers for the invitation to present this lecture during the XXI Annual Meeting of the *Sociedade Astronômica Brasileira*, held in Caxambu, MG (Brazil; in August 1995) and the Brazilian agency CNPq for partial support.

References

Biskamp D., 1994, Phys. Rep., 237, 179
Costa, J.R.V., Jafelice, L.C., 1995, work in preparation
Fabian A.C., 1994, ARAA, 32, 377
Friaça, A.C.S., 1993, A&A, 269, 145
Friaça, A.C.S., Jafelice, L.C., 1995, to be submitted for publication
Friaça, A.C.S., Gonçalves, D.R., Jafelice, L.C., Jatenco-Pereira, V., Opher, R., 1995, work in preparation
Ge J.P., 1991, PhD. Thesis, New Mexico Institute of Mining and Technology, New Mexico
Gruenwald, R.B., Viegas, S.M., 1992, ApJS, 78, 153
Jafelice L.C., 1992, AJ, 104, 1279
Jafelice L.C., Friaça A. C. S. 1995a, submitted for publication
Jafelice L.C., Friaça A. C. S. 1995b, to be submitted for publication
Johnstone R.M., Fabian A.C., 1988, MNRAS, 233, 581
McKee C. F., 1992, in M. Matthews and E. Levy, eds., Protostars and Planets III. University of Arizona, Tucson
Mestel L., 1990, in R. Beck, P.P. Kronberg, R. Wielebinski, eds, Proc. IAU Symp. No. 140, Galactic and Intergalactic Magnetic Fields. Kluwer, Dordrecht, p. 259
Priest E.R., 1982, Solar Magnetohydrodynamics. Reidel, Dordrecht
Priest E.R., Forbes T.G., 1992, J. Geophys. Res., 97, 16757
Rees M. J., 1994, in D. Lynden-Bell, ed., Cosmical Magnetism. Kluwer, Dordrecht, p. 155
Soker N., Sarazin C.L., 1990, ApJ, 348, 73
Tribble P.C., 1991, MNRAS, 248, 741

GAMMA–RAY BURSTS: A COSMOLOGICAL SETTLING

Gustavo A. Medina Tanco
Instituto Astronômico e Geofísico, USP

Abstract

A brief introductory review is given on the state of the art of gamma-ray burst (GRB) research, and a model (due to Medina Tanco, Steiner and Terlevich 1995) is presented relating their sources with a possible evolving cosmological scenario. We assume that the mechanism of GRB generation is related to binary interactions of compact remnants (white dwarfs, neutron stars or black holes) and show that the dense cores of elliptical galaxies are observationally acceptable sites for GRB production. We use the elliptical galaxy core luminosity function of Terlevich and Boyle (1994) with power law luminosity evolution to calculate theoretical $\log N$ vs. $\log S$ curves which we fit to the observations of BATSE. We show that for a universe with $L = 0$, deceleration parameter $q_0 = 0.5$ and core formation beginning at $z_1 = 4$, BATSE data can be acceptably fit by GRBs of luminosity L_{GRB} 1.2×10^{51} erg/sec, and local GRB generation rate of 0.8 events/Mpc^3/Gyr. We also calculate that the maximum depth reached by BATSE is z_{max} $2.8 - 2.9$, and predict an apparent repetition periodicity versus observed flux relationship (inside the 4^o diameter error box of BATSE) which has a minimum of ≈ 2 yr for the faintest bursts and which increases strongly with flux for brighter GRB.

1 Introduction

The existence of the γ-ray bursts (GRB) was suggested for the first time by Colgate (1968). He speculated the possibility that supernova remnant shock waves in distant galaxies could produce a flash of γ-rays when hitting stellar surfaces. Klesbesadel, Strong and Olsen (1973) discovered the GRB testing this conjecture. However, they did not discovered the GRB in connection with extragalactic supernovas. A new puzzle was born that, even now, more than 2500 publications (Hurley, 1995) and 140 different theoretical models later (Nemiroff, 1994), still remains mostly unsolved.

Basically, the GRB are a burst of γ photons with approximately daily frequency and energies varying between a few keV and some MeV (but three events are known with energies in the GeV band).

The duration of the burst is very variable, covering 5 orders of magnitude from some few msec to 5 minutes. Their temporal structure is fragmentary and complicated, which has suggested to some authors that something is being broken, or coming out into pieces, during the process.

Two basic different types of GRB can be distinguished, the classical GRB and the soft gamma repeaters (SGR). The SGR, as their name proclaims, are softer than the classical ones (with energies of only a few keV) and, principally, they repeat. Three such bursts are known, two in the general direction of the galactic center and one in the direction of the

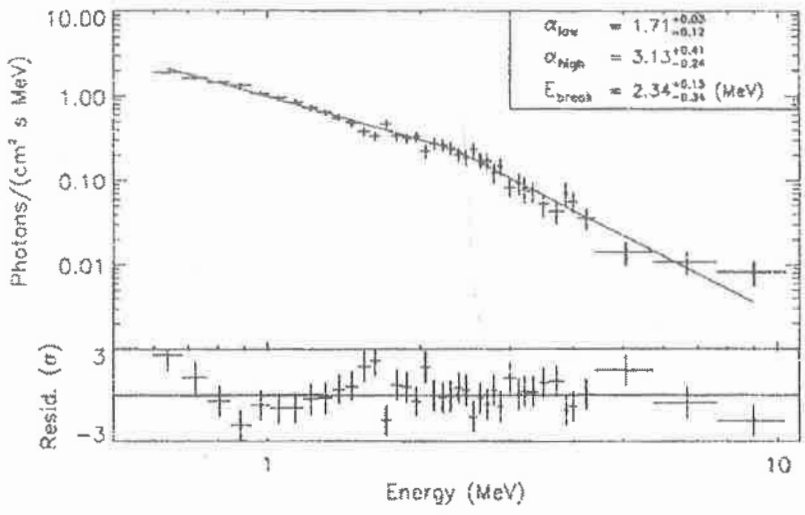

Figure 1: typical GRB spectrum

LMC. Two of this repeaters are associated with young ($\geq 10^4$ yr) supernova remnants, and the most accepted model for their energy source is magnetic reconnection near the surface of highly magnetized neutron stars, with $B_{surfase} \cong 10^{14}$ Gauss, called magnetars (Duncan and Thompson 1994).

We are interested, however, on the classical GRB. They are harder than the SGR and, apparently, they do not repeat on scales of $\cong$ 1 yr. They are characterized by the lack of X-ray emission. Their spectra are increasing in the hard X-ray region, with a turn-over in the soft γ-rays and a power law extending up to a cut-off in the γ-ray region (see Figure 1). There is no observationally favored model for them.

The ideas about the nature of the classical GRB have been strongly influenced by the BATSE (Burst And Transient Source Experiment) experiment on board the CGRO (Compton Gamma Ray Observatory) satellite. During the first few years after the discovery of the GRB the largest variety of theoretical models was published, including both, galactic and extragalactic astrophysical objects (comets, white dwarfs, neutron stars, black holes, AGNs, ultra-relativistic iron dust grains, etc.). Nevertheless, by the end of the 70's and along the 80's, and for reasons that will explain bellow, an implicit consensus was reached about galactic neutron stars (thick disk population). This consensus was so strong that, by the end of the decade, the models were mostly refinements of this general idea.

In April 1991 BATSE was launched and, in September of the same year, its first results were released to the public. Whatever the consensus at that time, it finished on the light of the BATSE data. This was due to the fact that, contrary to any expectation, no sign of the galactic disk was found in the observed angular distribution, which was remarkably isotropic (see, Figure 2). Furthermore, the brightness distribution ($\log N$ vs. $\log S$ curve) showed a decreased of the density of burst at the larger distances (Figure 3). That is, the GRB distribution has an edge. Both factors combined almost rule out models which

comprise only a disk population. In the search for more isotropic distributions inside the Galaxy, two must be mentioned: (a) a nearby heliocentric distribution, like the Oort's cometary cloud and, (b) a halo distribution.

The last option, a natural extension of the neutron star hypothesis, counts the off-center position of the Sun inside the Galaxy as one of its most mortal enemies. The more isotropic the GRB distribution observed, the larger the halo. Up to the present, compatibility with the observations requires a halo of more than 300 kpc in size, which implies not few problems. For example, the Maguellanic Clouds would be completely inside the halo, which should produce some observable anisotropy. Moreover, if our Galaxy has a huge GRB-producing halo, it is difficult to avoid such halos around nearby galaxies. In particular, M31 should have a halo twice as large as ours, and it should be certainly observable by BATSE. It must be noted that this arguments, if not strong enough to completely rule out the halo models, make them each time more difficult to fit into the observational constraints.

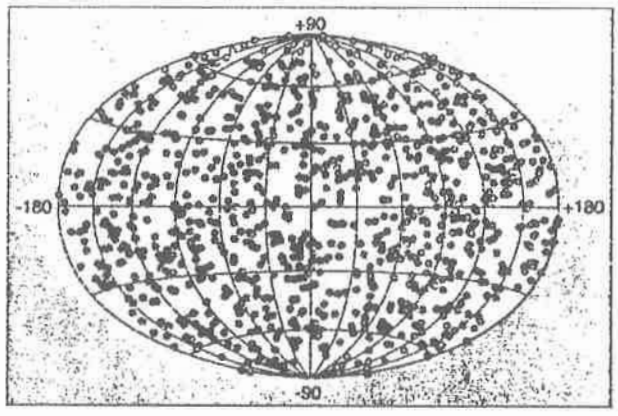

Figure 2: angular distribution of GRB seen by BATSE

Oort's cloud models, on the other hand, have problems of their own. Due to the off-center position of the Earth in the Solar System, the minimum size of the source region should be $\approx 5 \times 10^4$ A.U.. Among the various problems, we can mention: (a) the lack of a certain granularity in the angular distribution that should be observable (Eichler 1994) but it is not; (b) nearby stars should produce some observable anisotropy due to their own Oort's clouds; (c) the $\log N$ vs. $\log S$ curve deduced from known distributions, like the distribution of the comets, does not agree with the observed one for GRB.

In summary, even if none of the above distributions can still be discarded, the cosmological hypothesis is gaining strength as the observations proceed. Note, nevertheless, that a combination of different populations of sources is always possible, as already proposed by some authors, however logically difficult to justify this strategy may be. In this way not even a disk population can be completely ruled out.

A key question concerning classical GRB is if they repeat on scales of few months to one year. The answer is, to say the least, tricky. This is due, mainly, to the large error box in angular positions (whose diameter can be estimated as $\approx 4^{o}$) inherent to BATSE detections. Consequently, repetition is practically translated into clustering on scales of $\approx 4_{o}$. Moreover, different types of repetition produce different signatures in the data (it is not the same, for example, to have 499 sources that not repeat and one that repeats 501 times in a sample of 1000 events, than 500 sources that repeat once in the same sample). The problem is more severe when the low number of available events is taken into account.

But, what is the importance of the existence of repetition ? Basically, the fact that it helps to distinguish between large groups of models. For example, galactic disk models require, in general, repetition to match the GRB detection rate due to the small number of nearby sources. Cosmological models, on the other hand, are originated at so large distances that the extremely high energies involved need the complete destruction of the production region during the emission process. Clearly, no repetition is possible in the latter case. True repetition, at least, since gravitational lensing and missassociation of angularly close events (specially in a small-number- statistics context), could emulate repeaters in various time scales.

BATSE data are released as discrete packages or catalogs. The first catalog, BATSE 1B, contained 260 events, the second, BATSE 2B, 471 events and, the third catalog (still unreleased, despite already in use by the BATSE team), BATSE 3B (?), should include $\approx$ 1000 triggers. BATSE 1B generated not few discussion regarding repetition, since it showed (a dubious) clustering on scales $< 4_{o}$. BATSE 2B did not solved the problem, but increased the number of adherents to the no-repetition main stream. At present, the BATSE team, working with data from the still unavailable 3B catalog, claims that $< 20\%$ of the GRB repeat on scales of $\approx$ 1 yr with 99 % confidence. The most appropriate answer seems to be that, apparently, classical GRB do not repeat on time scales spanning from few months to $\approx$ 1 yr. Note, however, that repetition on scales of seconds to minutes is not ruled out.

Another question of fundamental importance says about the intrinsic luminosity interval observed. Are GRB approximate standard candles or not ? The brightness distribution observed by BATSE extends over nearly 2.5 dex and, schematically, is formed by two branches with slopes $\approx 3/2$ and ≈ 0.8 respectively. The transition between both regimes is rather abrupt (< 1 dex), which seems to suggest a limited intinsic luminosity interval. In fact, a study of the integral moments of the observed differential brightness distribution (Horack and Emslie 1994, Wald 1939) in Euclidean space show that 80% of the observed GRB are drawn from a population of sources with luminosities varying by less than a factor 6 (Horack, Emslie e Meegan, 1994). This would mean, in practice, that GRB can be regarded as standard candles !

Finally, another problem of relevance is whether lines actually exist in GRB spectra. Two GRB, among 23 GRB observed by the Japanese satellite Ginga, presented absorption lines in the $\approx 15 - 75$ keV range (Murakami et al.1988; Graziani et al. 1992). In one of the events, the lines constitute a harmonically separated pair: 19.3 and 38.6 keV respectively. In the other event, only one line at 21.1 eV is observed. This spectral features were

interpreted as cyclotron lines produced in magnetic fields of the order of $\approx 10^{12}$ Gauss, which was interpreted as a strong indication of a neutron star involved in the emission process. This lines, however, are not observed by BATSE. This discrepancy is, still now, matter of intense debate due to the fact that, even if BATSE spectra rarely extend to low enough energies to detect the 20 keV line, the 40 keV line should be clearly visible in principle. However, once instrumental differences between both experiments and the pertinent statistical factors are taken into account, it is not easy to conclude whether a discrepancy actually exist. Finally, lines with energies slightly below 511 keV were reported in the past, and interpreted as electron-positron annihilation lines, gravitationally redshifted while escaping from the neighborhood of a neutron star. They are not observed by BATSE either, and a consensus exist that they are actually absent in GRB spectra.

The general picture is that there is still considerable room for speculation in the field. This is due, principally, to the fact that the available statistics are rather poor at present and the situation will not change in the near future as the gathering information rate is low (one event per day). Even the isotropy, certainly high, is not known yet with precision enough to completely rule out halo or heliocentric models of the Oort's cloud type, despite the increasing popularity of cosmological models. It is not even clear whether mixed models, including disk and/or halo galactic populations are a plausible way out. Consequently, it must be admited that, at present, the uncertainty in the location of the sources spans 10 orders of magnitude, ranging from some tens of thousands of A.U. to some few Gpc. To this it must be added the uncertainty about the temporal repetition scales (seconds to years - if they repeat at all); the significance of the taxonomic distinction of two classes of bursts, with duration above and below ≈ 2 sec; the uncertain existence of cyclotron lines in the spectrum that could point to a particular astrophysical object; the fact that galactic models can reproduce the observed spectra rather easily but not the spatial distribution of the burst, while exactly the opposite is true for the cosmological models; etc..

2 GRB in a cosmological environment

We can take three facts as an starting point: (a) that the angular distribution of GRB is highly isotropic, (b) that the distribution of sources, as indicated by the brightness distribution function, seems to be inhogeneous, and, (c) that 70 % of the published theoretical models involve neutron stars as the main object associated with the generation mechanism of the burst, while 15 % include black holes or white dwarfs, that is, 85 % of the models comprise compact objects which we could call generically as ashes of stellar evolution. With this in mind, the most appropriate sites to look for the sources of the GRB seem to be those located at cosmological distances where intense star formation process took place and a high density of compact objects can be found. A class of astrophysical environments that fulfill these requirements are the nucleus of elliptical galaxies that underwent a star burst phase at some moment of their history.

Two questions appear immediately: (a) why the preference for compact objects and,

(b) why a star burst region, and not nuclear region of steady star formation ?

The preference for compact objects has basically two contributions, one historic, the other energetic. Historically, the detection of possible cyclotron lines by Ginga consistent with TGauss magnetic fields, characteristic of the surface of neutron stars, and of possible electron-positron annihilation lines redshifted by an amount equivalent to the gravitational redshift resulting from the escape off the surface of a neutron star, had initially a great influence on the theoretical modeling of the physical processes behind the emission mechanism. On the other hand, in case that the sources were effectively located at cosmological distances, the total energy released in a GRB episode must be of the order of $L_{GRB} \times \Delta\tau_{GRB} \approx 10^{51}$ erg/sec $\times 30$ sec $\approx 1\%$ of the gravitational binding energy of a canonical neutron star, or $\approx 0.2\%$ of its rest mass. This, together with the fact that all that energy is packed in a relatively small region of space from which it can be promptly freed under appropriate circumstances, makes of neutron stars favorite candidates to GRB progenitors [1] .

It seems to be an observational fact the lack of spatial correlation between the galaxies that are undergoing a star burst phase, and the angular positions of the GRB. Therefore, even if the star bursts are favorable events in the sense that they are able to build up a large density of compact remnants in a short time interval (e.g., $\approx 10^6$ objects in a region with a diameter of only ≈ 1 pc in a sound crossing time ≈ 60 Myr), the GRB production process must be decoupled from them. A natural way to accomplish such a decoupling is to admit that the GRB are originated by the compact remnants of stellar evolution on a much longer time scale than that of the star burst which originated them. That would be the case, for example, if the GRB were produced by the collision of compact objects, or the merging of binary systems. Then, there would be two relevant time scales: (i) the characteristic time scale of the star burst (i.e., of the formation of the compact objects) tstar burst ≈ 60 Myr and, (ii) the characteristic (interaction, merging, etc.) time associated with the physical mechanism responsible for the GRB, $\tau_{GRB} \approx$ few Gyr, i.e., perhaps comparable with the lifetime of the host galaxies.

3 Analytical modeling and numerical comparison with the observations

Following Medina Tanco, Steiner and Terlevich (1995), if n'_{GRB} is the number of GRB produced per proper volume per proper unit time, and n_{SBC} is the proper density of galactic cores that experienced a starburst phase at some time in the past (SBC), we can write:

$$n'_{GRB} = \left(a \times n_{CR}^{b}\right) \times n_{SBC} \qquad (1)$$

[1] It must be noted that, in the case of galactic origin, the temporal variability of the flux is not a strong criteria for restricting the size of the related astronomical object, but only of the emission region instead. Hence, for example, the energy could be released in a stellar flare, in which case the emission region is compact (the magnetic loop) but not the associated astronomical object (the star).

where, n_{CR} is the density of compact remnants (CR) in the nuclear region after the star burst, and a and b are constants that take into account the physics of the specific mechanism through which the burst energy is released.

In this context, the evolution of the luminosity function of the cores of elliptical galaxies in which the star burst is taking place should be related to the evolution of the rate of GRB per unit proper volume, since the mass processed during the star burst gives the total mass in compact leftovers after the AGN phase.

Following Terlevich & Boyle (1993) we assume that the luminosity function of young cores of ellipticals undergoes strong evolution between $z = 2$ and the present epoch, and that its redshift dependence is well represented by a power law,

$$\phi(z) \propto (1+z)^k \tag{2}$$

where k lie in the range $3.1 < k < 3.6$ and adopt here $k = 3.3$. At a given redshift z, the density of galactic core that went through a starburst phase, n_{SBC}, is built up from the integration from $z = z_1$ to z of the rate of star bursts, $n_t(z)$, which we assume evolves in the same way as the luminosity function of SBCs. That is,

$$\begin{aligned} n_t(z) &= \text{const} && \text{for } 2 < z < z_1 \\ n_t(z) &= (1+z)^k && \text{for } 0 < z < 2 \end{aligned} \tag{3}$$

The density of galactic nuclei is given by:

$$n_{SBC}(z) = \int_{z_1}^{z} n_t(z) \times \frac{\partial t(z)}{\partial z} \times dz \tag{4}$$

where $t(z)$ is the proper time. In addition, in the present approximation the rate of GRBs per unit proper time, per unit volume is proportional to the proper number density of galactic nuclei that underwent a star burst event at some time in their history,

$$n'_{GRB} = \xi \times n_{SBC} \tag{5}$$

Hence, the number of GRBs observed per unit time with flux larger than a certain value F is:

$$N_t(>F) = \int_0^z \frac{\xi n_{SBC}}{(1+z)} \times 4\pi \times r^2(z) \times \frac{\partial r(z)}{\partial z} \times dz \tag{6}$$

where $r(z)$ is the proper distance to a redshift z, and z is obtained by inverting the equation:

$$F(z) = \frac{H_0^2 L_{GRB}^{ph}}{4\pi c^2 Z_q^2(z)(1+z)^2} \tag{7}$$

which gives the flux observed from an event of luminosity L_{GRB}^{ph} photons per unit proper time at redshift z, where

$$Z_q(z) = \frac{\{q_0 z + (q_0 - 1)[(1 + 2q_0 z)^{1/2} - 1]\}}{q_0^2 (1 + z)} \tag{8}$$

Note that equation (6) assumes that the GRB's spectrum is flat. However, if we consider a power law spectrum, $L_\nu \propto \nu^\alpha$, an expression equivalent to (7) can be written for the ratio C_{max}/C_{min}, the peak count rate in units of the threshold count rate:

$$\frac{C_{max}}{C_{min}} = \left(\frac{1+z}{1+z_{min}}\right)^{1+\alpha} \times \frac{Z_q^2(z_{min})}{Z_q^2(z)} \tag{9}$$

where z_{min} is the maximum depth at which BATSE can see a GRB.

Depending on the desired approximation, either (6) and (7) or (6) and (9) can be used as the parametrical form of the $\log N$ vs. $\log S$ curve.

Figures 4 and 5 show the fitting of equations (6) and (7) to the $\log N$ vs. $\log S$ curve observed by BATSE for more than 687 GRBs as given by Horack (1994). Different values of q_0 and z_1 are used, and it can be seen that, despite some freedom in the adjustment is allowed, a good fitting is obtained for $q_0 = 0.5$ and $z_1 = 4$. If these values are used for normalization of the curves, then the resultant intrinsic luminosity of the GRBs (flat spectrum) in 50-300 keV is $L_{GRB} \approx 10^{51}$ erg/sec $\approx 1\%$ of the rest mass of a neutron star when integrated over a characteristic time scale ($T90$) ≈ 30 sec), while the local rate of GRBs production per unit volume is $n'_{GRB} \approx 0.8$ Mpc^{-3} Gyr^{-1}, or one event each $\approx 10^5$ yr in the local group. It seems also that BATSE is reaching as deep as $z_{depth} \approx 2.8 - 2.9$.

In Figure 6 we show the $\log N$ vs. $\log S$ observed curve superimposed to the calculated curves for a power law GRBs energy spectra (eqs. (6) and (9)) of index $\alpha = 0.5, 1.0, 1.5, 2.0$ and 2.5, and the same parameters used to fit figures 1.a-b, and $z_{min} = 4$. It can be seen that an average spectral index $\alpha \approx 1.5$ can fit the data despite some dispersion. This result agrees well with fittings to the actually observed GRB's spectra in the 50-300 keV band by Pendelton et al. (1994) (see also, Fig 9 of Meegan et al. 1994).

The luminosity obtained in the case of a power law spectrum with $\alpha = 2$ is $L_{GRB} \approx 1.2 \times 10^{51}$ erg/sec in the 50-300 keV.

In the model presented here, galactic cores inside a given solid angle with the aperture of the error box but at different redshifts could give place to the identification of apparent repeaters when working with small number statistics. The importance of this effect may be easily estimated. If GRB can be considered as standard candles, we could expect that different events of the same repeater should be observed with similar brightness. Hence, the period between events observed inside an error box of aperture $\Delta\Omega$ with flux in the interval $(F, F + DF)$ can be approximated by:

$$\tau_r ep = \left[\frac{\delta\Omega}{4\pi} \times n'_{GRB}(z) \times 4\pi \times r^2(z) \times \frac{\partial r(z)}{\partial z} \times \frac{F(z)\Delta F_{rel}}{\partial F(z)/\partial z}\right]^{-1} \tag{10}$$

where $\Delta Frel = \Delta F/F$. It can be seen that, for ΔF_{rel} as high as 100 % for the previous fitting, the period of the apparent repeaters can vary between ≈ 2 and 40 yr for the faintest bursts, depending on how much restrictive is our definition of repeating events.

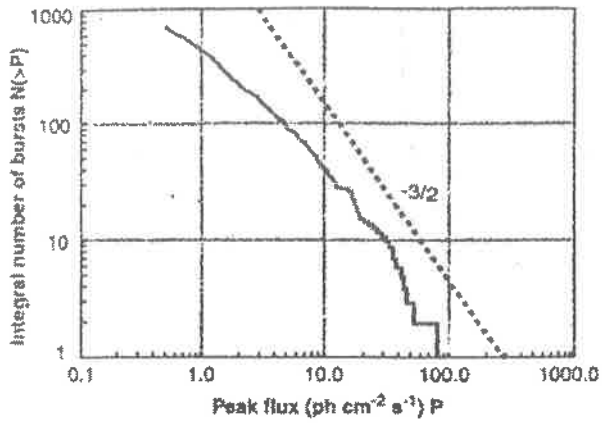

Figure 3: GRB's brightness seen by BATSE

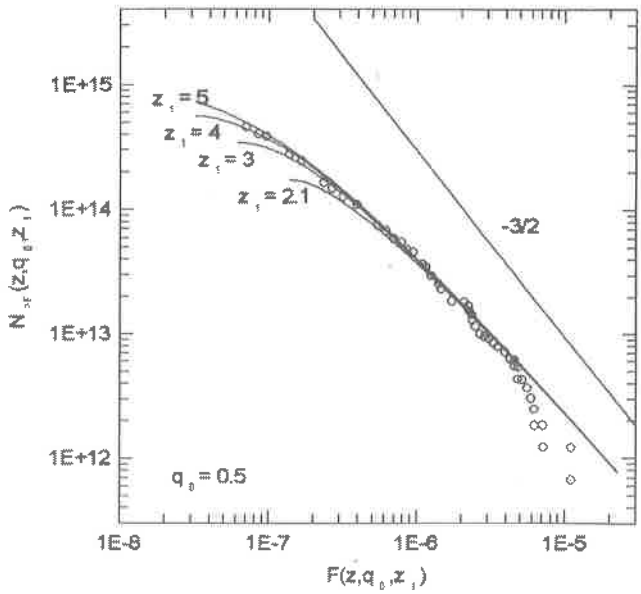

Figure 4:

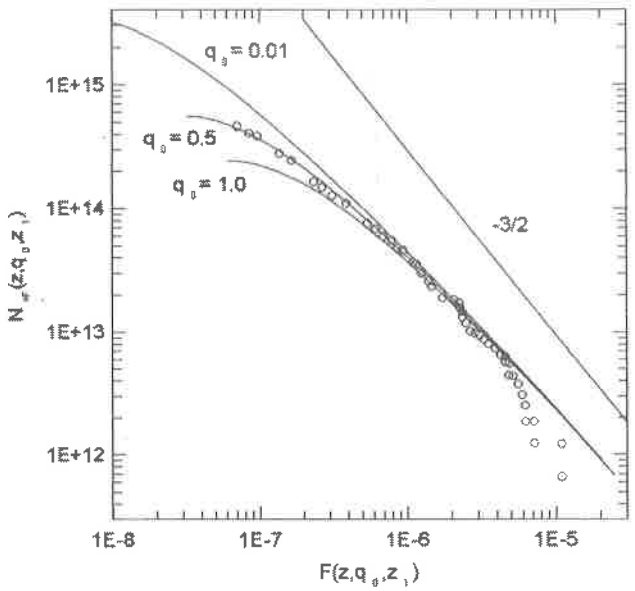

Figure 5:

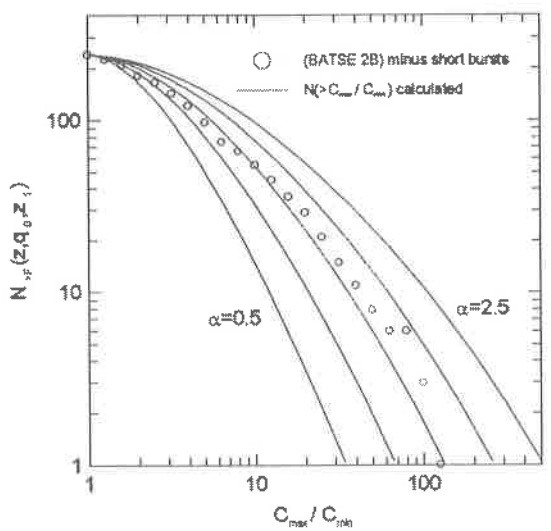

Figure 6: power law spectrum at the source.

Nevertheless, this values are consistent with the present lack of small scale clustering or repetition.

4 Conclusions

There is still considerable room for speculation in the field of GRB. This is due, principally, to the fact that the available statistics are rather poor at present and the situation will not change in the near future as the gathering information rate is low. However, if the GRBs sources are located at cosmological distances, as growing evidence from BATSE seems to point, then the total energy channeled into γ-rays by the mechanism powering GRBs amounts to a considerable fraction of the rest mass or gravitational energy of a solar mass compact body. This makes appealing catastrophic processes involving compact objects like white dwarfs, neutron stars, or black holes. Therefore, the natural places to look for the GRB sources are those where it is likely to find a high density of these compact objects. One such place is the core of an elliptical galaxy that, at some time in its early history, underwent a violent star burst phase. The evolution of these starbursts can be tracked as a function of redshift by following the evolution of the SBC's luminosity function. By doing this it is possible to demonstrate that GRB production in these cores is compatible with BATSE observations for at least $q_0 = 0.5$, and starburst turning on at $z_1 = 4$.

References

[1] Cohen E. and Piran T., 1995, A & A, in press.

[2] Fishman G. J., Brainerd J. J. and Hurley K. (eds), 1994, Gamma-ray Burst 2nd Workshop, Huntsvile 1993, AIP Conf. Proc. 307, American Institute of Physics, Ney York.

[3] Graziani C. et al., in Gamma-Ray Bursts, C. Ho, E. Fenimore and R. Epstein (eds.), Cambridge Univ. Press., p 407,1992.

[4] Hartwick F. D. A.and Shade D., 1990, Ann. Rev. Astron. Astrophys., 28, 437.

[5] Horack J. M., 1994, Science, 265, 1186.

[6] Horack J. M., Emslie A. G. and Meegan C. A., 1994, Ap. J., **426**, L5.

[7] Hurley K., 1994, GRBs 2nd Workshop, Huntsville, AIP Conference Proc. 307, G.J. Fishman, J.J. Brainerd and K. Hurley (eds.), pp. 726-729.

[8] Kouveliotou et al, 1993, ApJ Lett, 413, 101L.

[9] Mao S., Narayan R. and Piran T., 1994, ApJ, 420, 171.

[10] Medina Tanco G. A., Steiner J. E. and Terlevich J. R., in preparation.

[11] Meegan C. A., Fishman G. J., Wilson R. B., Paciesas W. S., Pendleton G. N.,Horack J. M., Brock M. N., Kouveliotou C., 1992, Nature, 355, 143.

[12] Meegan C. A., Fishman G. J., Wilson R., Brock M., Horack J., Paciesas W., Pendleton G., Briggs M., Koshut T., Kouveliotou C., Teegarden B., Matteson J. and Hakkila J., 1994, GRBs 2nd Workshop, Huntsville, AIP Conference Proc. 307, G. J. Fishman

[13] Murakami T. et al, Nature 335,234,1988

[14] Nemiroff R. J., 1994, Comments Astrophys., 17, 189.

[15] Pendelton et al., 1994, in preparation.

[16] Terlevich, R., 1992 in: Relationship Between Active Galactic Nuclei and Starburst Galaxies, ed. Filippenko, A.V. Pub. Astron. Soc. Pacific, San Francisco, p. 253.

[17] Terlevich R. and Boyle B. J., 1993, MNRAS, 262, 491.

BLACK HOLES: FROM GALACTIC NUCLEI TO ELEMENTARY PARTICLES

José P. S. Lemos

Departamento de Astrofísica, Observatório Nacional-CNPq, Rua General José Cristino77, 20921 Rio de Janeiro, Brazil, E-mail:lemos@on.br.

Abstract

We present a broad review on black holes. We analyse some of the fundamental concepts in black hole theory, the observational and theoretical status of stellar and galactic black holes, and their appearance as quantum objects.

1 What is a black hole?

One of the basic ingredients of a physical theory is its set of fundamental constants. Thus, for instance, classical mechanics has no fundamental constants. The Newtonian theory of gravitation contains one constant alone, the universal constant of gravitation, G. The electromagnetism of Maxwell contains the velocity of light c, which in vacuum is a fundamental constant. Planck's constant h, which appeared directly from an experimental result (the black body spectrum), was immediately taken as the fundamental constant of quantum mechanics, developed among others by Bohr, Heisenberg and Schrödinger. Thermodynamics yields the Boltzmann constant k_B which arguably can be considered fundamental. These theories and their constants can then be combined to yield unified theories. If one tries to unite classical mechanics and electromagnetism one obtains the theory of special relativity which has c as a fundamental constant. The electric charge e is a constant of nature. If we join e and c one obtains classical electrodynamics of Thomson and Lorentz, which is of course related to special relativity. If one further joins h one obtains quantum electrodynamics due to Dirac and developed by others, afterwards. The unification of the electromagnetic and the weak forces by Weinberg and Salam as well as the inclusion of the strong force in the grand unified theories by Glashow and others also mix the fundamental constants of each separate theory. Finally, if one combines G and c one obtains the theory of general relativity of Einstein. On further joining Planck's constant h one should obtain quantum gravity, a theory which is still eluding the realm of physics, although there are some hints as to what it should be.

Black holes (BHs) are objects which belong to the theory of general relativity, and can be used to explain many powerful phenomena observed in the celestial sphere. On the other hand, their (quantum) effects and the singularities they hide yield an excellent framework to probe into the nature of quantum gravity.

A simple Newtonian argument can lead us to the concept of dark star, the Newtonian closest relative to the black hole (BH) of general relativity. The escape velocity v_e of an object ejected from the surface of a body, such as a star, of mass M and radius R, is given by $\frac{1}{2}v_e^2 = \frac{GM}{R}$. The escape velocity on Earth is 11 km/s, on a white dwarf it is around 6000 Km/s. A dark star is defined as a star for which the escape velocity is greater

or equal to the velocity of light, i.e., for which the following relation holds $\frac{1}{2}c^2 \leq \frac{2GM}{R}$. However, such a star is not a black hole for two reasons. First, the velocity of light is not a fundamental constant (i.e., it has no fundamental meaning) in Newtonian gravity, and thus other objects thrown with tachyonic velocities can escape and be detected at infinity. Second, the dark star is only dark for distant observers, near its surface the star is still bright since it emits light, although it cannot escape to infinity.

The correct theory to explain the BH phenomenon is general relativity. The BH is a "state of the gravitational field", different from the state of the gravitational field of a star. We can understand BHs most easily through the collapse of a star (see e.g. [1] [2] [3] [4] [5]). As the star collapses, its own radius shrinks. From Newtonian gravity we know that the force the star exerts on an object goes as r^{-2}. Thus, a contraction by a factor two increases the force by a factor four. In addition, if the star collapses to a point, the force becomes infinite at $r = 0$. General Relativity yields a different result, the gravitational force increases more rapidly than r^{-2}. The force is then infinite when the radius of the star is $R = \frac{2GM}{c^2}$, the Schwarzschild radius. The spherical surface formed at this radius is called the event horizon. When a star of fixed mass M attains this radius, a BH is formed. The difference between Newtonian gravity and general relativity is of importance only when the star gets closer to its Schwarzschild radius, where the gravitational field is strong. Time near a strong gravitational field goes more slowly than time far away, and space is highly curved. BHs are holes in spacetime, caused by a strong space curvature and by drastic changes in the flow of time.

When the BH forms there are two regions connected to each other, the inside and the outside of the event horizon. As the matter of the star continues to collapse inside the event horizon it will form a singularity where curvatures and densities of infinite strength are formed. Inside the event horizon light is trapped. Light not only does not escape to infinity, it cannot escape to the outside of the BH. However, to an outside observer the story is different. As the BH is being formed, the luminosity of the original star decays exponentially, $L = L_o e^{-\frac{t}{\tau}}$ where the characteristic time is very short, $\tau = 3\sqrt{3}\frac{GM}{c^3} = 2.6\text{x}10^{-5}\frac{\text{M}}{\text{M}_\odot}\text{s}$. In a few millionths of a second the star turns totally black. Another important feature is that the collapse of the star results in a BH whose properties are characterized by three parameters only: mass, charge and angular momentum. One then says that BHs have no hair (in fact, they have three hairs). All the other properties, or "hair", of the matter of the star that formed the BH disappear. No observation can reveal the nature of the original star, whether it had a magnetic field, or possessed anti-matter, or was made of fermions, or bosons, or it had any other hairs.

2 Stellar black holes

BHs with stellar masses can form through the collapse of the iron cores of massive stars after they have reached the end of their thermonuclear evolution. The outer layers of the star explode in a supernova leaving at its center, depending on the core's mass, a neutron star or a BH. The maximum mass for a neutron star is still a matter of debate, since it

depends strongly on the equation of state of the constitutive matter. Rhoades and Ruffini [6] found a maximum mass of $3.2M_\odot$, while Hartle [7] can put an upper limit of $5M_\odot$, (see also [8]). However, Bachall et al. [9] argued that one can construct a $100M_\odot$ star made of other types of matter at nuclear densities which they called Q-stars (related in some sense to Witten's strange stars [10]). Thus the limit of the maximum mass 3.2 or $5M_\odot$ is still uncertain, although probably correct. The sizes of a BH and a neutron star do not differ much. For a $1M_\odot$ object, the neutron star has 10 Km of radius, whereas the BH has 3 Km.

An isolated stellar BH cannot be seen. A BH can only be observed if it belongs to a binary system [11], and is detected through spectroscopic observations of the bright optical companion. The main problem is that the unseen body can also be a neutron star, and to distinguish between both possibilities one has to follow a complicated list of steps. A binary system can evolve in the following way: first, two massive stars, with masses of the order of $20M_\odot$ form a binary system. Then, in a second stage, the more massive star evolves more rapidly and soon becomes a compact body with a few $M_\odot$ after having exploded in a supernova. Finally, the other star also evolves to become a similar compact star. One thus has a binary system of two compact stars, of which the most famous example is the binary pulsar of Hulse and Taylor [12]. During the second stage, when the binary is composed of one compact and one giant star there is the production of spectacular phenomena visible in the X-ray band. The binary systems in this stage are called X-ray binaries.

X-ray binaries have a very short orbital period which by Kepler's third law implies the objects are very close. Since the Roche lobe of the binary system (the surface of gravitational neutrality) can be filled in part by the massive companion, the outer layers of the massive star are captured by the compact star. The captured gas then forms an accretion disk. The emission of X-rays can happen through several processes. If the compact star is a neutron star then the gas, through a magnetic field mechanism, hits the crust of the neutron star regularly with the consequent emission of X-rays. The neutron star is then called an X-ray pulsar, with luminosities of the order $10^4 L_\odot$. If, instead of regular, the X-ray emission is sporadic, then the source is called a burster. Bursters are usually produced through an explosion of the surface of the neutron star, but can also appear by eruption of a very hot region of the accretion disk [13] [14]. In this last case the matter from the luminous companion spirals towards the unseen compact object and emits X-rays with temperatures of $10^8 - 10^9$K. These temperatures are generated through dissipation by viscous processes of the gravitational energy of the infalling matter accelerated to high velocities.

BHs do not have a hard solid surface, the explosion happens in the disk. Is there any way to distinguish between BH and neutron stars bursts? One could think that variability would give some clues. If a source (disk, in the case) changes shape, the speed of change cannot exceed the speed of light. If one detects variability in a time Δt, the size of the source is at most $l \lesssim c\Delta t$. If the source changes in $\Delta t \sim 10^{-3}$s, then its linear size is $l \sim 300$ Km. For a stellar BH, its inner edge (defined as the last stable orbit, see e.g. [15]), is of the order of 30 Km in radius say, so its circumference is around 200 Km. A rotating

hot bubble emitting X-rays would have a varability in the milisecond range, as observed. This could be a signature for a BH. However, Circinus X-1 also shows fluctuation of this order, and it was shown that it also has periodic bursts which characterizes a neutron star [16]. The identification of a black hole through radiation processes is not yet well developed, although it is a field advancing quickly. The best criterion to identify a BH is to find its mass through dynamical studies of the X-ray binaries. The weighing of stars in binaries is a technique fully understood nowadays.

Knowing the orbital period of the binary and the projected mean speed of the optical star, one can using Kepler's law to deduce the mass function defined by [17], $f(M) \equiv \frac{(M_x \sin i)^3}{(M_x+M_c)^2} = \frac{P(V_c \sin i)^3}{2\pi G}$, where M_x and M_c are the masses of the X-ray source and the companion respectively, i is the orbital inclination angle, P is the orbital period and $V_c \sin i$ is the projected velocity semiamplitude of the optical companion. If one puts $M_c = 0$ and $i = 90^0$ one gets the mimimum possible value for M_x which in this case is equal to $f(M)$. What one would really like to obtain is an $f(M)$ greater than $5M_\odot$. However, following the theory, a value close to $3.2M_\odot$ yields already a good BH candidate.

There are three very strong candidates, two good candidates and a list of possible candidates. We start here giving some properties of the three very strong candidates. **(1a) Cygnus X-1** – It was discovered in 1971 [18] and it is a persistent source with $L_x \sim 2\text{x}10^{37}$erg/s. It is a high mass X-ray binary. The orbital period is 5.6 days and $V_c \sin i \simeq 76$Km/s which yields a low $f(M) = 0.35M_\odot$. Now, one has to derive a reliable lower limit for the mass, which is a difficult task. The optical companion is a blue giant with mass $M_c \sim 30M_\odot$. The inclination angle is supposed to be $i \sim 30^0$ (there are no eclipses). This gives a mass of $M_x \sim 16M_\odot$ [19]. The most conservative assumptions lead to $M > 3M_\odot$. **(1b) LMC X-3** – It was discovered in 1983 [20]. It is a persistent source and a high mass X-ray binary with $L_x \sim 3\text{x}10^{38}$erg/s. $P = 1.7$ days and $V_c \sin i \simeq 235$Km/s. This gives $f(M) = 2.3M_\odot$. The mass of the companion is estimated to be $M_c \sim 6M_\odot$ which then yields $M_x \sim 6M_\odot$. Since the distance to the Magellanic cloud is known one can use Paczyński method [21] to infer $M_x \gtrsim 4M_\odot$. **(1c) 0620-00** – It was discovered in 1986 [22]. Contray to the other two, it is a transient source. It is a low mass X-ray binary with $L_x \sim 1\text{x}10^{38}$erg/s. $P = 0.32$ days and $V_c \sin i \simeq 467$ Km/s yielding $f(M) = 3.18M_\odot$. Based solely on the value of the mass function, the minimum mass is already equal to the BH threshold mass. It is considered the strongest of the very strong candidates. $M_c \sim 0.7M_\odot$ which is low, and yields the following lower limit $M_x \sim 4M_\odot$.

There are two other candidates which have been weighed, although the uncertainties are greater than the sources mentioned above. **(2a) CAL87** – One has $L_x \sim 1\text{x}10^{36}$erg/s. It is an interesting system since it undergoes eclipses. If $M_c > 0.4M_\odot$ it was found that $M_x \gtrsim 4M_\odot$ [23]. **(2b) LMC X-1** – $L_x \sim 2\text{x}10^{38}$erg/s. The optical companion is still not identified conclusively. However, there are hints that $M_x \gtrsim 3M_\odot$. There are a number of other candidates which have been selected because they show X-ray behavior similar to Cygnus X-1, of which the prime example is GX239-4, and others which show transient behavior similar to 0620-00, such as GS2000+25, GS2023+33, GS1124-68, 4U1543-47, 4U1630-47, H1705-250 [24]. Further dynamical studies are needed to obtain the masses of these sources . The spectacular source SS433 which shows emission of jets was recently

discarded as a black hole, since its mass was shown to be $M \sim 1.4 M_\odot$ [25].

What are then the features that allow us to identify a BH candidate? The classical steps are: 1) The luminosity of the X-ray source has to be high $L_x > 10^{36}$erg/s and of rapid variability < 1s. This implies that the binary system must contain an accreting compact object. 2) The optical companion is identified and allows to measure the orbital period and the projected orbital velocity, to yield $f(M)$. 3) The mass of the optical companion and the inclination of the orbit are inferred or limited, based on the distance, optical spectrum, L_o, and eclipes. Then using $f(M)$ one deduces M_x. 4) If the mass of the object is $M_x \gtrsim 3.2 M_\odot$ then it is considered a BH candidate. There are now three other criteria which can help in identifying a BH candidate: (i) the source has a spectrum with soft X-rays, $\sim$ 1Kev. (ii) Fe emission lines very near the compact object (will) allow one to measure the velocity of the rotating disk. This then implies a dynamical measure of M_x [26]. (iii) Hard X-rays $\sim$ 100Kev are a signature of BHs, since neutron stars have a hard surface whose radiated photons cool the accretion disk through Compton cooling [27]. These last too criteria are very recent [28], and it is expected the situation will improve with work on some other half-dozen sources.

One drawback is that all these criteria are indirect. One really wants to come close to the collapsed object. In the long run, one is after clear evidence for the existence of an event horizon [29] [30]. This might be possible after the gravitational antennas are fully operating, to detect unambiguously the formation of a BH. If the BH is in a binary one expects subsequent X-ray emission. How many BHs there are in the Galaxy? The last estimates give 1000-3000 BHs, of the same order as the number of neutron stars [24].

3 Black holes in galactic nuclei

We have seen that in the complete gravitational collapse of a star a BH can form with mass in the range $3 - 20 M_\odot$. Yet, the theory of gravitational collapse allows for the formation of BHs with much greater masses, masses that can be in the range $10^3 - 10^9 M_\odot$. These BHs may appear in the core of clusters of stars or in the center of galactic nuclei. If the mass of the original system is very large, there is no uncertainty in the equation of state of the collapsing matter when it crosses the event horizon. Indeed, at $R = \frac{2GM}{c^2}$, the density of the matter is $\rho = \frac{3c^6}{32\pi G^3} \frac{1}{M}^2 \simeq 1.3\text{x}10^{16} (\frac{M_\odot}{M})^2 \text{g/cm}^3$. For a $\sim 1 M_\odot$ BH the density is very high, above the nuclear density. However, for a $\sim 10^8 M_\odot$ object one has $\rho \sim 1\text{gm/cm}^3$. In this case one has $\frac{R^3}{R_\odot{}^3} \sim 10^8$. This roughly means that for a cluster composed of 10^8 suns, the cluster crosses its own Schwarzschild radius when the suns, uniformly distributed over the volume, are touching each other. For a $\sim 10^{10} M_\odot$ object one has $\rho \sim 10^{-4}\text{gm/cm}^3$. In this case, $\frac{R^2}{R_\odot{}^2} \sim 10^{10}$, which roughly means that for a cluster made of 10^{10} suns, it crosses its Schwarzschild radius when the suns, distributed uniformly over a spherical layer of thickness of one sun diameter, are touching each other. In all these latter cases the physics when the matter crosses the horizon is well known.

Theory and numerical simulations favor the appearance of a binary system in the

center of globular clusters. The compact binary scatters any incoming star. There is, in principle no formation of a BH in the core of the cluster. This is supported by observation. However, central BHs are not totally excluded [13].

There is controversy about the existence of a central BH in our Galaxy since it was first proposed in 1971 [31]. The Galactic center has the following features: (1) a disk of gas with inner and outer radii given by $5 - 30$ light years (ly); (2) a cavity interior to the disk with $2\text{x}10^6$ stars; (3) a possible BH with $2\text{x}10^6\text{Km} \sim 2\text{x}10^{-7}$ly accreting matter slowly. The evidence for a central compact source comes from the radio emission of a region as small as the orbit of saturn around the Sun [32]. This source is called Sgr A* and has $L \sim 10^{34}\text{erg/s} \sim 10L_\odot$ ($\sim 10^4$ times the luminosity of a single radio pulsar). From the disk of gas, one can infer (if it is in a Keplerian orbit) a central mass of $5 - 8\text{x}10^6 M_\odot$. Subtracting the mass in the red giants one obtains $3 - 6\text{x}10^6 M_\odot$. The evidence favors the existence of a central BH, although it is not absolutely convincing [33] [34]. Evidence against the existence of a central BH has appeared after observations from the Sigma/GRANAT telescope led to the conclusion that, contrary to expectations, there is no X-ray source coincident with Sgr A* [35]. However, there are now models which can explain the phenomenon in a natural way in which the matter is swallowed before it has time to radiate [36].

There is also dynamical evidence that M31 (Andromeda) has a compact massive source at its center with $M \sim 3\text{x}10^7 M_\odot$ which favors the existence of a BH [37]. M32 also harbors a central dark object of $M \sim 5\text{x}10^6$. There is evidence for very massive nuclei in other nearby galaxies, in NGC 4594 (the Sombrero galaxy) [38] and in NGC 3115 [39].

The nuclei of most galaxies are inactive, in the sense that $L \sim 10^{-4} L_{\text{galaxy}}$. There are active galactic nuclei (AGN) which can shine more than the entire galaxy. Galaxies that have AGN are 1% of all the galaxies. Examples of AGN are the quasars (of which 3C273 has a luminosity equivalent to 10^3 galaxies), blazars, Seyferts, radio galaxies and other objects. In a spectrocospic classification these AGN are divided in AGN type 1 which show broad and narrow emission lines and AGN type 2 which show only narrow emission lines. They have some common features: (1) non-thermal radiation, (2) high concentration of mass in a small region, (3) variability in luminosity, (4) ejection of jets at great distances and (5) similarities with normal galaxies.

The idea is to explain generically all different objects and phenomena with one model. The most favored model invokes accretion onto central supermassive BHs as the ultimate power source for these luminous objects which radiate at the Eddingtom limit. Even, if one invokes other central objects, such as spinars (yielding their rotational energy) or a cluster of packed stars (supplying nuclear energy through supernova explosion), the emission of so much energy from such a small volume (which is measured through variability) leads inevitably to the collapse to a BH [40]. There is also the possibility that some galactic nuclei may contain two massive BHs in orbit around each other [41]. Further out from the central object, there is a dusty accretion torus which provides a mechanism to understand AGN 1 and 2 [42]. The jets, when they exist, point from the central region into two opposite directions aligned with the rotation axis of the torus. The blazars are thought to be quasars with one jet pointing towards us. The spectroscopic differences in AGN are

also due to different orientations of the torus with respect to the Earth. If one can see the inner edge of the torus one observes both the broad lines emitted in the inner region by high speed clouds and the narrow lines emitted in the outer edge. If the torus is seen edge-on only the narrow lines are observable.

The evidence to detect the central mass, both in AGN and normal galaxies, is based in most cases on the increase of mass-to-light ratio in the central region. Only in two cases, M87 and NGC4258, is the value for the central mass based on gas dynamics rotating around the central mass. By using the Hubble Space Telescope it was possible to measure the Doppler shift of emission lines from doubly ionized oxygen around $R \sim 60$ly from the center of M87 [43]. This implies a rotation velocity of $v \sim 550$Km/s for the gas in orbit which then gives $M = \frac{v^2 R}{2G} \sim 2 - 3\text{x}10^9 M_\odot$. The mass is so great in such a small region that is difficult to think of any other explanation than a supermassive black hole inhabiting the center of the galaxy. If, for instance, the mass were contained in solar type stars in a dense cluster, they would be packed 100 thousand more times closely than in the solar neighborhood. However, this is discarded, since there is not enough light comimg from this region. In the case of NGC4258, recent work [44] [45] has also pointed to the confirmation of two things: 1. Keplerian velocities of ~ 1000Km/s in an inner orbit of very small radius, $R \sim 0.4$ly, around the central mass have been measured which imply a mass of $M \sim 2\text{x}10^7 M_\odot$. This work is considered to provide the strongest case for a supermassive BH in the center confirming the predictions of Lynden-Bell [46]. 2. The velocities are measured through water masers which are found to come from a torus-like region confirming the unifying model of Antonucci and Miller [42]. It has been suggested [47] that the best one can do for the black hole case is to refute the other models on physical grounds. For NGC4258 this has been undertaken [48].

One can thus have a model in which all galactic phenomena are unified, not only within AGN themselves, but also relating normal galaxies and AGN. In AGN, part of the potential energy is released when matter approaches the event horizon and the energy escapes as radiation providing the mechanism to power the emission. An accretion rate of a few tens of $M_\odot$ per year, which can be supplied by surrounding gas and by stars tidally disrupted in the gravitational field, will provide a power greater than 10^{47} erg/s which would explain even the highest quasar luminosities [49]. In normal galaxies there is no matter to be accreted. The real difference then between the nuclei of normal galaxies and AGN is, in this model, not the mass of the BH, but the phase of the cycle of accretion. The quiescent nuclei would be BHs starved of fuel, i.e., dead quasars.

4 Quantum black holes and elementary particles

We have described in the previous sections stellar BHs with masses $3 - 20 M_\odot$ (and $10 - 60$Km), and galactic BHs with $10^6 - 10^9 M_\odot$. But there also exists the possibility of having BHs with much smaller masses. For instance, if the Earth with mass $\sim 10^{27}$gm $\sim 10^{-6} M_\odot$ was compressed to a radius of 1cm it would turn into a BH. There is the possibility that primordial BHs with mountain masses, 10^{14}gm $\sim 10^{-19} M_\odot$, and a radius similar to the

proton radius 10^{-13}cm could be formed in the early universe [50]. The smallest possible BH would have a mass of 10^{-5}gm and a radius equal to 10^{-33}cm, the Planck radius, which is thought to be the minimum possible radius that occurs in nature. Smaller masses would have a Schwarzschild radius smaller than the Planck radius, and thus if compressed into a BH, these masses would be snatched by the Planck regime, (i.e., by the spactime foam [51] [52]), before they had turned into a BH.

Of course, these BHs have a totally different interest from the macroscopic and giant BHs. Their physical effects are of a different kind. Let us take the mountain mass BH, $M \sim 10^{-19} M_{\odot}$ and $R \sim 10^{-13}$cm. Its gravitational attraction at a distance of 10m would be relatively small ($\sim 0.1\text{m/s}^2$). Its tidal force on a 1cm tight object of 1gm would barely be felt at a distance of 10cm. Such a black hole could cause some damage on nearby objects, but not a lot. For a Planckian 10^{-5}gm BH its gravitational atraction would give an acceleration of 10^{-6}cm/s^2 at a distance of 10^{-5}m, roughly the size of a living cell. On this basis, even if one of these BHs enters our body we would live without noticing it, the accretion onto it would be vanishingly small. However, there are other proceses that would made the BH noticeable, and these could cause damage in our body.

There was a great turn in BH theory after Hawking found in 1974 that BHs can radiate through quantum effects [53]. There were already hints that BHs have a thermodynamic behavior. If one throws entropy S into the inside of the BH, this entropy disappears from our universe in direct violation of the second law of thermodynamics. Since there is a theorem [54], within classical general relativity, that states that in any process the area A of a BH never decreases, Bekenstein proposed that $S_{BH} \propto A$, such that the second law is not violated, $S + S_{BH} \geq 0$ always [55]. Since, to an entropy one can associate a temperature through the thermodynamic relation $S = \frac{Q}{T}$, the BH must have a temperature. Indeed, by complicated calculations of quantum field theory in a BH background, Hawking was able to find that the BH emits blackbody radiation at a temperature $T = \frac{\hbar c^3}{8\pi G k_B} \frac{1}{M} \simeq 6\text{x}10^{-8}(\frac{M_{\odot}}{M})K$. Since so many fundamental constants (section 1) enter this formula one can say that quantum mechanics, general relativity and thermodynamics must merge together in a unified theory. For $M \sim 1M_{\odot}$ one has $T \sim 10^{-7}$K. When $M \sim 10^{-19}M_{\odot}$ implies $T \sim 10^{12}$K. For a Planckian BH, $M \sim 10^{-5}$gm, therefore, $T \sim 10^{32}$K. Making the translation $E = k_B T$ one has that the energies involved in the evaporation of a Planckian size BH are $\sim 10^{19}$Gev $\sim$ 100watt-hour. This could do some damage in our body. The mechanism for evaporation can be explained in several ways, the most popular uses the idea that the vacuum is full of virtual particles which are created and annihilated without violation of the uncertainty relation $\Delta E \Delta t \gtrsim \hbar$. However near the event horizon it can happen that one particle enters the BH while the other escapes out to infinity. The net result is blackbody radiation at the Hawking temperature T. Now, the power emitted by a radiating BH is $4\pi R^2 \sigma T^4 = \frac{\lambda}{M^2}$, where σ is the Stefan-Boltzmann constant, and $\lambda = \frac{\hbar c^6}{15360\pi G^2}$, a value found through the equations given above. Then, one finds that the BH looses energy at a rate $\frac{dMc^2}{dt} = -\frac{\lambda}{M^2}$ which can be integrated to give $M = (M_o{}^3 - 3\frac{\lambda}{c^2}t)^{\frac{1}{3}}$. For an initial mass of $M_o \sim 1M_{\odot}$ one gets that the BH evaporates in 10^{67}years. If one puts $M_o \sim 10^{-19}M_{\odot}$ one finds $t \sim 10^{10}$ years, which means if created in the primeval Universe these BHs should be evaporating by now. This could happen in

a burst of final radiation after passing through the Planck scale. Some have speculated that the observed γ-ray bursts could come from these mini-BHs, but there are tight limits on their existence from gravitational lensing [56].

Thus, classically, BHs are stable, but quantum mechanically they are unstable, they slowly evaporate and shrink. One striking effect that arises immediately is the violation of baryon number. Baryon number conservation is a law in elementary particle physics. However, if, say, a totally isolated neutron star of 10^{57} neutrons (baryons) collapses onto a BH, it will evaporate in a baryon-antibarion manner, actually most of the radiation will be in photons which carry zero baryon number anyway. Thus, gravity and quantum field theory produce violation of baryon number.

One problem that Hawking radiation gives rise to is called the information paradox. To describe a star completely, one must specify a large ammount of information, such as, total mass M, total charge Q, total angular momentum J, temperature, pressure, gravitational multipole moments, other chemical potentials, and so on, including the quantum states of the 10^{57} protons and neutrons that constitute the star. When the star collapses to form a BH, the no-hair theorems say that the BH is described by only three parameters, M, Q and J. All the other information that was necessary to describe the original star is now hidden inside the event horizon. Hawking [57] found within his calculation, that the blackbody thermal spectrum of the emitted flux of particles would not carry the original information out to the exterior region. After the BH completely evaporates, the information that was trapped inside also vanishes with the BH. The information paradox for BHs is the problem of explaining what happens to the missing information. It is of great importance because, in usual quantum mechanics, the wavefunction ψ evolves in such a way that information contained in it is never lost. However, if the picture described here is correct, then gravitational collapse violates a fundamental principle of quantum mechanics.

Another important reason to study BH evaporation is that the final stages of the evaporation process involve physics near the Planck scale, where quantum gravity is expected to become important. Thus, BHs provide a theoretical laboratory where one can gain insight into the physics at this minimum scale.

All these issues are highly complicated in four spacetime dimensions. To understand better these problems one must resort to lower dimension theories. In two dimensions (one time plus one space dimension) general relativity is trivial, it has no dynamics. However, if one adds a dilaton scalar field the theory has many features similar to four dimensional general relativity (see, e.g. [58]). There are many different theories in two dimensions with interesting dynamics [59][60][61]. One that has been extensively studied [62] [63] [64] is related to string theory (a consistent theory of quantum gravity, although it has problems in delivering the other three fundamental interactions). In three dimensions general relativity has dynamics, although not much (the theory has no local degrees of freedom). Surprisingly, it has been found that a three dimensional black hole in a space with constant curvature exists [65] [66]. One can connect these three dimensional theories with four dimensional general relativity [67] [68] [69] [70]. The results obtained using two, three and four dimensional theories to solve the information paradox are still

controversial [71]. However, theoretical experiments, involving annihilation of a pair of BH-antiBH, have shown that information can indeed disappear altogether, inside an event horizon [72].

Extreme BHs also provide interesting results. A charged BH is called extreme when $Q = M$ (in geometrical units where $G = c = 1$, otherwise we can write $Q = \sqrt{G}M$). (If $Q > M$ then there is no horizon, instead one has a naked singularity, which if it exists complicates the thermodynamic picture. That is one reason why cosmic censorship [73], which forbidds the existence of naked singularities, is widely accepted). For extreme BHs the Hawking temperature is zero, they do not radiate. Thus they can be considered stable particles, that do not decay. If one of these BHs absorbs an infalling neutral particle, the BH's mass will be increased, the charge-to-mass ratio is then lowered raising the Hawking temperature above zero. The BH then emits particles by the evaporation process, and returns to its ground state. This appears as a scattering process, an incoming initial state of one particle is scattered into other particles as a final state. There are other processes that resemble particle physics or are connected to other physical branches, e.g., BH-BH scatering, and the statistics a BH gas should obey (are BHs fermions, bosons or neither? [74]).

Physicists believe that gravity becomes the dominant field at the quantum Planck scale 10^{-33}cm. It represents the minimum scale at which spacetime can be considered smooth. BHs are the objects to test this scale, through Hawking radiation, and related phenomena. Imagine the following futuristic experiment: two incoming particles in a huge accelerator are set to collide face-on, such that, a center of mass energy of $\sim 10^{19}$Gev is produced. Then, one might form a Planckian BH which will evaporate quickly in a burst, allowing us to study the physics at the Planck scale. One might think that by increasing the energy the study of sub-Planckian scales would follow. However, this is not the case. By increasing the energy one would produce a BH with larger mass, which would decay slowly, not allowing any test of Planckian physics.

5 Conclusions

BHs are used in many different phenomena, from high energy astrophysics to high energy elementary particle physics. The results brought from each area of study, either observational, theoretical or experimental, will serve to gain a better understanding of the physics of these beautiful objects. This review is a summary of some aspects of the nature of BHs.

Acknowledgements – I thank Horácio Dottori, Dalton Lopes and Vera Jatenco for inviting me to deliver the seminar to which this article corresponds, in the XXIth SAB meeting, 1995. I thank Verne Smith for his careful reading of the manuscript.

References

[1] C. Misner, Thorne, Wheeler, 1973, *Gravitation*, Freeman, S. Francisco.

[2] J. P. S. Lemos, 1994, *Ciência Hoje*, **97**, 42.

[3] D. Lynden-Bell e J. P. S. Lemos, 1988, *Mon. Not. R. astr. Soc.*, **233**, 197.

[4] J. P. S. Lemos e D. Lynden-Bell, 1989, *Mon. Not. R. astr. Soc.*, **240**, 317.

[5] J. P. S. Lemos, 1992, *Phys. Rev. Lett.*, **68**, 1447.

[6] C. E. Rhoades, R. Ruffini, 1978, *Phys. Rev. Lett.* **32**, 324.

[7] J. B. Hartle, 1978, *Phys. Rep.*, **46**, 201.

[8] G. Baym, C. Pethick, 1979, *Annu. Rev. Astron. Astroph.*, **17**, 415.

[9] S. Bachall, B. W. Lynn, S. B. Selipsky, 1990, *Ap. J.*, **362**, 251.

[10] E. Witten, 1984, *Phys. Rev. D*, **30**, 272.

[11] J. Michell, 1784, *Phil. Trans. R. Soc. (London)*, **74**, 35.

[12] J. H. Taylor, 1993, in *General Relativity and Gravitation 1992*, Proceedings of the Thirteenth International Conference on General Relativity and Gravitation held at Cordoba, Argentina, eds. R. J. Gleiser, C. N. Kozameh, O. M. Moreschi, IOP, Bristol, p. 287.

[13] S. L. Shapiro, S. A. Teukolski, 1983, *Black Holes, White Dwarfs and Neutron Stars, the Physics of Compact Objects*, Wiley and Sons, New York.

[14] J. P. Luminet, 1992, *Black Holes*, Cambridge University Press, Cambridge.

[15] M. Anderson, J. P. S. Lemos, 1988, *Mon. Not. R. astr. Soc.*, **233**, 489.

[16] A. F. Tennant, A. C. Fabian, R. A. Shafer, 1985, *Mon. Not. R. astr. Soc.*, **221**, 27P.

[17] E. V. P. Smith, K. C. Jacobs, 1973, *Introductory Astronomy and Astrophysics*, W. B. Saunders and Co., Philadelphia.

[18] R. M. Hjellming, A. M. Wade, 1971, *Ap. J. Lett.*, **168**, L21.

[19] E. P. Liang, P. L. Nolan, 1984, *Space Sci. Rev.*, **46**, 273.

[20] A. P. Cowley, et al., 1983, *Ap. J.*, **272**, 118.

[21] B. Paczyński, 1983, *Ap. J. Lett.*, **273**, L81.

[22] J. E. McClintock, R. A. Remillard, 1986, *Ap. J.*, **308**, 110.

[23] A. P. Cowley, P. C. Schmidtke, D. Crampton, J. B. Hutchings, 1990, *Ap. J.* **350**, 288.

[24] A. P. Cowley, 1992, *Annu. Rev. Astron. Astroph.*, **30**, 287.

[25] S. D'Odorico, T. Osterloo, T. Zwitter, M. Calvani, 1991, *Nature*, **353**, 329.

[26] A. C. Fabian, M. J. Rees, L. Stella, N. E. White, 1989, *Mon. Not. R. astr. Soc.*, **238**, 729.

[27] R. Sunyaev, et al., 1991, *Astr. Astroph.*, **247**, L29.

[28] J. Van Paradijs, J. E. McClintock, 1995, in *X-ray Binaries*, eds: W. H. G. Lewin, J. Van Paradijs, E. P. Van den Heuvel, (Cambridge University Press), in press.

[29] J. E. McClintock, 1987, in *Supermassive Black Holes*, Proceedings of the Third George Mason Astrophysics Workshop-1986, ed. M. Kafatos, Cambridge University Press, Cambridge.

[30] L. Stella, 1993, in *General Relativity and Gravitation 1992*, Proceedings of the Thirteenth International Conference on General Relativity and Gravitation held at Cordoba, Argentina, eds. R. J. Gleiser, C. N. Kozameh, O. M. Moreschi, IOP, Bristol, p. 263.

[31] D. Lynden-Bell, M. J. Rees, 1971, *Mon. Not. R. astr. Soc*, **152**, 461.

[32] K. Y. Lo et al, 1985, *Nature* **315**, 124.

[33] R. Genzel, C. H. Townes, 1987, *Annu. Rev. Astron. Astrophys.*, **25**, 377.

[34] R. Genzel, D. Hollenbach, C. H. Townes, 1994, *Rep. Prog. Phys.*, **57**, 417.

[35] A. Goldwurm, et al, 1994, *Nature* **371**, 589.

[36] R. Narayan, I. Yi, R. Mahadevan, 1995, *Nature*, **374**, 623.

[37] J. Kormendy, 1988, *Ap. J.*, **325**, 128.

[38] J. Kormendy, 1988, *Ap. J.*, **335**, 40.

[39] J. Kormendy, D. Richstone, 1992, *Ap. J.*, **393**, 559.

[40] M. J. Rees, 1984, *Annu. Rev. Astron. Astrophys.*, **22**, 471.

[41] M. C. Begelman, R. D. Blandford, M. J. Rees, 1980, *Nature*, **287**, 307.

[42] R. R. J. Antonucci, J. S. Miller, 1985, *Ap. J.*, **297**, 621.

[43] H. C. Ford, et al., 1994, *Ap. J. Lett.*, **435**, L27.

[44] M. Miyoshi, et al, 1995, *Nature* **373**, 127.

[45] L. J. Greenhill et al, 1995, *Ap. J.*, **440**, 619.

[46] D. Lynden-bell, 1969, *Nature*, **223**, 690.

[47] Kormendy, Richstone, 1995, *Annu. Rev. Astron. Astroph.*, **36**, in press.

[48] E. Maoz, 1995, *Ap. J.* **447**, L91.

[49] M. J. Rees, 1988, *Nature*, **333**, 523.

[50] B. J. Carr, S. W. Hawking, 1974, *Mon. Not. R. astr. Soc.*, **168**, 399.

[51] S. W. Hawking, 1979, in *General Relativity, an Einstein Centenary Survey*, eds. S. W. Hawking, W. Israel, Cambridge University Press, Cambridge, p. 746.

[52] J. A. Wheeler, 1963, in *Relativity, Groups and Topology*, eds. B. S. and C. M. De Witt, Gordon and Breach, New York, p. 317.

[53] S. W. Hawking, 1974, *Nature*, **248**, 30.

[54] S. W. Hawking, *Phys. Rev. Lett.*, **26**, 1344.

[55] J. D. Bekenstein, 1973, *Phys. Rev. D*, **7**, 2333.

[56] B. Carr, 1994, *Annu. Rev. Astron. Astroph.*, **35**, 531.

[57] S. W. Hawking, 1976, *Phys. Rev. D*, **13**, 191.

[58] J. P. S. Lemos, Paulo Sá, 1994, *Class. Quantum Gravity*, **11**, L11.

[59] J. P. S. Lemos, Paulo Sá, 1994, *Phys. Rev. D.*, **49**, 2897.

[60] J. P. S. Lemos, Paulo Sá, 1994, *Mod. Phys. Lett. A*, **9**, 771.

[61] J. P. S. Lemos, 1995, *Class. Quantum Gravity*, **12**, 1081.

[62] E. Witten, 1991, *Phys. Rev. D*, **44**, 314.

[63] C. G. Callan, S. B. Giddings, J. A. Harvey, A. Strominger, 1992, *Phys. Rev. D*, **45**, R1005.

[64] G. T. Horowitz, 1992, "The Dark Side of String Theory", hep-th/9210119.

[65] M. Bañados, C. Teitelboim, J. Zanelli, 1993, *Phys. Rev. Lett.* **69**, 1849.

[66] M. Bañados, M. Henneaux, C. Teitelboim, J. Zanelli, 1993, *Phys. Rev. D*, **48**, 1506.

[67] J. P. S. Lemos, 1995, *Phys. Lett. B*, **352**, 46.

[68] J. P. S. Lemos, 1994, "Cylindrical Black Hole in General Relativity", gr-qc/9404041.

[69] P. M. Sá, A. Kleber, J. P. S. Lemos, 1995, "Black Holes in Three-Dimensional Dilaton Gravity Theories", hep-th/9503089, to appear in *Class. Quantum Gravity*.

[70] J. P. S. Lemos, V. T. Zanchin, 1995, "Rotating Charged Black String and Three Dimensional Black Holes", submitted.

[71] G. 't Hooft, 1991, in *Proceedings of the 5th Seminar on Quantum Gravity*, eds. M. A. Markov, V. A. Berezin, V. P. Frolov, World Scientific, Singapore, p. 251.

[72] S. W. Hawking, G. T. Horowitz, S. F. Ross, 1994, "Entropy, Area, and Black Hole Pairs", gr-qc/9409013.

[73] R. Penrose, 1969, *Riv. Nuovo Cimento*, **1**, 252.

[74] A. Strominger, 1993, *Phys. Rev. Lett.*, **71**, 3397.

NEUTRINOS, DM AND THE RW UNIVERSE

Justin C. Huang[1]
Department of Physics and Astronomy,
University of Missouri, Columbia, MO 65211, USA

My topic in this talk will focus on the formal problem of neutrinos and the RW universe. The results of this discussion are based on work that I have done with N.O. Santos and A. Kleber (1995). Since neutrinos obey Dirac's equation and the RW universe is governed by Einstein's equation, the system of equations that I will be dealing with is the Einstein-Dirac system of equations. The problem is not just of academic interest, but can have important physical consequences with respect to our present day understanding of dark matter in the universe. There will also be some ambiguities which originate from assumptions made in the analysis.

Let me begin with the RW spacetime which describes a spatially homogeneous, isotopic universe. There are strong observational evidences for the spacetime described by this metric. The three major ones are:

1. Hubble expansion (1929)
2. Cosmic microwave background radiation (1965)
3. Nucleosynthesis involving the relative abundance of the light elements (1965-present)

The fundamental equation of gravity is the Einstein equation which has the form

$$R_{\mu\nu} - (1/2)g_{\mu\nu}R = 8\pi G T_{\mu\nu} \tag{1}$$

where $R_{\mu\nu}$ is the Ricci tensor and R is the scalar curvature. A cosmological term which is proportional to $g_{\mu\nu}$ can be added to the left hand side of the above equation, but we will ignore this possibility in this talk.

The RW metric has the form for the invariant distance ds

$$\begin{aligned} (ds)^2 &= g_{\mu\nu}dx^\mu dx^\nu \\ &= (dt)^2 - a^2[(dr)^2/(1-kr^2) + r^2(d\theta)^2 + r^2\sin^2\theta(d\phi)^2] \end{aligned} \tag{2}$$

where a is the cosmic scale factor which depends on the time t and $k = -1,0$, and$+1$ represents open, flat, and closed universes, respectively. For $k = 1$, r can only vary from 0 to 1. We can show that Eq. (1) in the RW metric reduces to

$$3[H^2 + k/a^2] = 8\pi G T_t^t \tag{3}$$

$$\delta_B^A[2\dot{H} + 3H^2 + k/a^2] = 8\pi G T_B^A \tag{4}$$

and

$$R_A^t = 8\pi G T_A^t = 0 \tag{5}$$

[1]Internet: physjch@mizzou1.missouri.edu

where the subscripts A and B can be r, θ, or ϕ, H is the Hubble variable which is represented in terms of a by

$$H = \dot{a}/a \tag{6}$$

and where the dot stands for differentiation with respect to t.

Using this spherical basis, we see that all the off diagonal elements of T^{μ}_{ν} are zero:

$$T^t_r = T^t_\theta = T^t_\phi = T^r_\theta = T^\phi_r = T^\phi_\theta = 0. \tag{7}$$

The spatial components are all equal,

$$T^r_r = T^\theta_\theta = T^\phi_\phi \tag{8}$$

and the time component T^t_t and the diagonal spatial components must only be functions of t since the cosmic scale factor a is only a function of the time t. The constraints on all the elements of T^{μ}_{ν} are rather severe and it is not at all obvious that all fundamental sources of nature have the necessary properties which can satisfy these constraints.

Let us next turn to the Dirac world. In flat spacetime, let us write down the equation for a field with a conserved current associated with charge conservation,

$$i\gamma^\alpha(\partial_\alpha - A_\alpha)\Psi = m\Psi \tag{9}$$

where A_α represents the electromagnetic 4-potential and for simplicity, a unit coupling has been chosen. In group theory language, this is the field equation for a system with U(1) gauge symmetry. The conserved 4-current associated with this equation has the form

$$J^\alpha = \bar{\Psi}\gamma^\alpha\Psi \tag{10}$$

where $\bar{\Psi}$ is the adjoint field. There are various possible interpretation of this equation in the literature. We can interpret the above equation as a single particle quantum mechanical equation. We can also normalize the field Ψ to represent N fermions and consider the equation as a N particle classical equation. It is of course not classical in the same sense as Maxwell's equation as we cannot form a continuum of states with fermions. We could also treat the above equation as an operator equation within the framework of a quantum field theory.

What happens when we transfer to curved spacetime? There are some straight forward modifications which must be performed. An easy way to understand the adjustments is to replace the local charge symmetries by the local Lorentz symmetries. The electromagnetic 4-potential A_α is then replaced by a gravity related quantity which we shall write as Γ_μ. The flat spacetime Dirac matrices γ^α are replaced by curved spacetime Dirac matrices e^μ. We use the Greek indices α and β to indicate flat spacetime quantities and the Greek indices μ and ν to indicate curved spacetime quantities. The curved spacetime Dirac equation can be written as

$$ie^\mu(\partial_\mu - \Gamma_\mu)\Psi = m\Psi. \tag{11}$$

In the group theory language, the U(1) gauge symmetry has now been replaced by the SL(2,C) gauge symmetry. The curved spacetime e^μ is defined by the equation

$$e^\mu e^\nu + e^\nu e^\mu = 2g^{\mu\nu}. \tag{12}$$

The curved and flat spacetime Dirac matrices are related by the tetrads

$$e^\mu = e^\mu_\alpha \gamma^\alpha. \tag{13}$$

In order to maintain the gauge symmetry or covariance of the equation, there must be a relationship between the tetrads e^μ_α and Γ_μ. It has the form

$$\Gamma_\mu = (i/4)\sigma^{\alpha\beta} e^\mu_\alpha e_{\beta\nu;\mu} \tag{14}$$

where

$$\sigma^{\alpha\beta} = (i/2)[\gamma^\alpha \gamma^\beta - \gamma^\beta \gamma^\alpha]. \tag{15}$$

The conserved current and energy-momentum tensor have the curved spacetime forms of

$$J^\mu = \bar{\Psi} e^\mu \Psi \tag{16}$$

and

$$\begin{aligned} T_{\mu\nu} = \quad & (i/4)[(\bar{\Psi} e_\mu \partial_\nu \Psi + \bar{\Psi} e_\nu \partial_\mu \Psi) - (\partial_\mu \bar{\Psi} e_\nu \Psi + \partial_\nu \bar{\Psi} e_\mu \Psi) \\ - \quad & \bar{\Psi}(e_\mu \Gamma_\nu + \Gamma_\nu e_\mu)\Psi - \bar{\Psi}(e_\nu \Gamma_\mu + \Gamma_\mu e_\nu)\Psi]. \end{aligned} \tag{17}$$

In the RW spacetime, we can write the tetrads as

$$e_{t\alpha} = (1, 0, 0, 0) \tag{18}$$

$$e_{r\alpha} = (0, -a/\sqrt{1 - kr^2}, 0, 0) \tag{19}$$

$$e_{\theta\alpha} = (0, 0, -ar, 0) \tag{20}$$

$$e_{\phi\alpha} = (0, 0, 0, -ar \sin\theta) \tag{21}$$

and the gauge quantity Γ_μ as

$$\Gamma_t = 0 \tag{22}$$

$$\Gamma_r = -(1/2)[\dot{a}/\sqrt{1 - kr^2}]\alpha^1 \tag{23}$$

$$\Gamma_\theta = -(1/2)[\dot{a}r\alpha^2 + \sqrt{1 - kr^2}\alpha^1\alpha^2] \tag{24}$$

$$\Gamma_\phi = -(1/2)[\dot{a}r \sin\theta\alpha^3 - \sqrt{1 - kr^2} \sin\theta\alpha^1\alpha^3 - \cos\theta\alpha^2\alpha^3]. \tag{25}$$

Let me return to Eq. (1) and the Einstein-Dirac system of equations. The left-hand side is a completely classical quantity. Therefore, the right-hand side must also be completely classical which it is not in an unambiguous way. In the literature, there are 2 ways to handle this delicate matter. If we are working with quantum fields with Ψ being a field operator, we must take some expectation value of $T_{\mu\nu}$ since in some sense, average values are classical quantities. A second method is to consider Ψ as a classical field with

again the understanding that it is not classical in the same sense as the Maxwell field. This seems to us to be the less ambiguous approach.

If we use Eqs (18) to (25), the energy-momentum tensor $T_{\mu\nu}$ for a Dirac source can be constructed in a completely consistent manner with the RW spacetime. Using the separation of variable method, we found a general solution for the mass m not zero which has the form

$$\begin{aligned}\Psi = \quad & \mathcal{T}\sqrt{\csc\theta}\sum_{n=-\infty}^{+\infty} G_n e^{in\phi}[(\tan\theta/2)^{in}(g_1U_1e^{imt}+g_2U_2e^{-imt}) \\ + \quad & (\tan\theta/2)^{-in}(g_3U_3e^{imt}+g_4U_4e^{-imt})]\end{aligned} \tag{26}$$

where

$$\mathcal{T} = \mathcal{T}_0\, e^{-3/2\int H\,dt}, \tag{27}$$

$$\begin{aligned} U_1 &= (v,v) & U_2 &= (v,-v) \\ U_3 &= (w,w) & U_4 &= (w,-w) \end{aligned} \tag{28}$$

with

$$v = (1,1) \qquad w = (1,-1). \tag{29}$$

We next tried both axially symmetric and non-axially symmetric boundary conditions for the solution to Ψ and searched for agreement with the conditions imposed by the RW spacetime on T^{μ}_{ν} as specified by Eqs (8), (9) and the time dependence of the diagonal elements. We found that the only class of solutions possible are solutions with zero energy-momentum tensor $T_{\mu\nu}$, but nonzero values for the current as determined from Eq. (16). These are known as ghost solutions and were also found by Davis and Ray (1974) for neutrinos in a plane symmetric universe. The ghost solutions represent a peculiar situation where a nonzero field cannot be distinguished from a vacuum situation gravitationally. However, in the RW case, they also correspond to the situation when the RW spacetime reduces to a flat spacetime.

For completeness, we studied also the massless case. As is well known, Dirac's equation decouples into two component equations with solutions which were straight forward to obtain. The results were more drastic for this case. Because of γ^5 terms appearing in $T_{\mu\nu}$, there were now no solutions which could satisfy the constraints imposed on T^{μ}_{ν} by the RW spacetime for both axially symmetric and non-axially symmetric solutions.

Finally, let me turn to a possible physical application of these results. We have seen that in a world of just neutrinos and gravity, the standard model of cosmology as embodied in the RW spacetime cannot be made consistent with each other. Can we have a world of predominantly neutrinos and gravity? Let me turn to the question of dark matter in the universe. From the search of mass using dynamical means, we find that there may be much missing mass in the universe. This is most obviously seen in spiral galaxies where instead of the damping curves of rotational velocity as a function of distance predicted from Kepler's third law applied to luminous matter, we have flat curves. The dynamical effects have been observed from rotational velocity curves at nearly all distance scales and

have also been reported in gravitational lensing observations. The ratio from these effects of luminous to missing mass is around one to ten. There have been a number of possible explanation for the dark matter question. Some have argued that the force laws are incorrect for large distances and that there is no missing mass. Most explanation involves missing mass of various forms. Let me mention four that are frequently mentioned. They are:(i) empty space contains mass in the form of a nonzero cosmological constant, (ii) massive neutrinos (hot dark matter), (iii) axions (cold dark matter), and (iv) machos (baryonic dark matter).

It is convenient to introduce an important parameter known as Ω which is a ratio of the mass density to the critical mass density (for a flat universe). Ω is greater than one for a closed universe, equal to one for a flat universe and less than one for an open universe. Let me quote some approximate values for Ω. For the luminous part of the universe, $\Omega_{lum} < .01$. From nucleosynthesis, the baryon contribution is given by $.01 < \Omega_{baryon} < .1$ with the uncertainty driven by the uncertainty in the value of the Hubble constant. The favored choice today for the total value of Ω is one since it is consistent with the inflationary models of the early universe. If we accept the $\Omega = 1$ value, then most of the universe must be composed of nonbaryonic, nonluminous matter. The approximate amount would be around 90 to 99%. If neutrinos are the answer to the dark matter dilemma, then the dominant equations governing the universe will be the Einstein-Dirac system of consistent equations. Using the classical field interpretation of the Dirac equation, our results indicate that these equations are inconsistent with the standard model of cosmology as represented by the RW spacetime. This suggest that a more likely answer to the missing mass problem will reside in other explanations. Recent detailed structural simulations of galactic formations seem to favor models of mixed cold and hot dark matter. These calculations are consistent with our results.

References

[1] J.C. Huang, N.O. Santos, and A. Kleber, Class. Quantum Grav. 12 (1995) 1245.

[2] T.M. Davis and J.R. Ray, Phys. Rev. D9 (1974) 331.

Section 2

Teaching of Astronomy

TEACHING OF ASTRONOMY IN BRAZIL

Rute Helena Trevisan
Departamento de Física, Universidade Estadual de Londrina
Campus Universitário, CEP 86.051-970,Londrina, Pr

1 Introduction

Astronomy, one of the most old science, has leaded the bases of all human knowledge. As the time pass, the man starts a blindly search for the general objective laws, renouncing to the philosophy and to the human being. Looking for a return to a science teaching where the historical necessities of looking for comprehension of the laws that move, make and govern the natural phenomena of the universe, the most of the curricula of the primary school of Brazil following the international tendency of the most schools of the world, are introducing Astronomy in the Science classes.

2 The professional astronomer in the basic teaching of astronomy

Feeling the necessity of the improvement of the primary schools teachers (Bisch, 1993; Lattari et al. ,1993; Lattari and Trevisan, 1993 a,b; Pereira, 1993; Trevisan et al. 1993a,b) and some professional astronomers who teach in universities, started a work in national level, having as principal objective, the teaching of astronomy in the primary and high schools, beginning with the teaching of astronomy to the teachers. Initially, it was created the *Astronomy Teaching Group* formed by some professional astronomers, during a double-annual Symposium of Physics Teaching (X National Symposium of Physics Teaching - SNEF) occurred in Londrina- Paraná, South of Brazil (1993) . It was the beginning of a large movement in the sense of teach astronomy to the children and to teach in a new way (Buso and Canalle, 1993; Crispin and Canalle, 1993; Daminelli, 1993; ; Espósito and Canalle, 1993; Nozawa, 1993; Oliveira, 1993; Souza, 1993).

The initial objectives of the Astronomy Teaching Group were :

01) developments of didactical equipment and procedures for astronomy teaching;
02) incentive to the editions of astronomy books;
03) to offer improvement courses for teachers;
04) to orientate students of graduation in Astronomy, at Scientific Initiation level;
05) to develop scientific divulgation activities;
06) to produce educative videos
07) to interact with other groups in Brazil and in the world.

Historically, we can say that the principal events and activities in teaching of astronomy, after the creation of this Group, occurred during the following events:

a) XIX ANNUAL MEETING OF BRAZILIAN ASTRONOMICAL SOCIETY - SAB

Caxambu, August, 1993

* Teaching of Astronomy Round Table; * Teaching of Astronomy Poster Section;* Assembly suggestion of Creation of the Commission of Astronomy Teaching

b) XX ANNUAL MEETING OF BRAZILIAN ASTRONOMICAL SOCIETY - SAB

Campos do Jordão, August, 1994

* Teaching of Astronomy Round Table

* Teaching of Astronomy Poster Section (Afonso, 1994; Araújo, 1994; Bisch, 1994; Canalle, 1994; Livi, 1994 ; Matsuura, 1994; Rocha, 1994; Trevisan, 1994a,b; Varella, 1994a,b,c.)

* Creation of the : **Commission of Astronomy Teaching** Brazilian Astronomical Society during the General Assembly of SAB.

The initial objectives of this commission were:

1) To make contacts with the Physics Teaching Secretary of the Brazilian Society of Physics, to change ideas about teaching;

2) To increment the activities of Astronomy Teaching(Courses, Hands on, Talks, etc.) in Brazilian Symposiums, in the next years,

3) to follow all the objectives initially proposed (listed above).

c) XI SNEF (National Symposium of Physics Teaching)

Niteroi, RJ, January, 1995 (see Atas do XI Simpósio Nacional de Ensino de Física 1995)

* Poster Section (Jafelice, 1995a; Lattari and Trevisan, 1995a; Makler, 1995; Nunes, 1995; Pereira,1995; Pereira and Barros, 1995, Trevisan et al., 1995a,b; Trevisan and Lattari, 1995)

* Courses and Hands-on for Teachers (Canalle, 1995a; Martins, 1995; Trevisan, 1995a)

* Videos Sections; * Show of Astronomy; * Theater; * Oral Communication (Araújo, 1995; Makler and Martins, 1995; Nascimento and Bittencourt, 1995; Nascimento, 1995; Neves and Pereira, 1995; Neves et al., 1995; Nunes and Zanon, 1995b; Tignanelli, 1995;); * Meeting on Teaching of Astronomy (Livi and Bisch, 1995)

d) ANNUAL MEETING OF BRAZILIAN SOCIETY TO THE PROGRESS OF SCIENCE (SBPC) : * Hands-On (Canalle, 1995b; Jafelice, 1995b)

e) INTERNATIONAL SCHOOL FOR YOUNGER ASTRONOMERS - ISYA - IAU

Belo Horizonte, MG, July, 1995

* Course of Teaching of Astronomy(Percy, 1995); * Talks of Teaching of Astronomy (Guerbaldi, 1995a; Livi, 1995; Trevisan, 1995b); * Teaching of Astronomy Round Table

f) XXI ANNUAL MEETING OF ASTRONOMICAL BRAZILIAN SOCIETY

Caxambu, MG, August, 1995

* Talks of Teaching of Astronomy (Guerbaldi, 1995; Trevisan, 1995c);

* Poster Section about Teaching of Astronomy (Afonso and Nadal, 1995; Canalle,1995b; Campos, 1995; Faraco et al., 1995; Souza et al., 1995 and Trevisan, 1995d);

* Courses for Primary School Teachers: the Teaching of Astronomy Commission programmed some activities to primary school teachers of the region of the Symposium:

Talks, Hands On and Shows in a Movable Planetarium.(Boczko, 1995; Canalle, 1995c; Jafelice, 1995b; Magalhães, 1995).

Besides these, some important projects of teaching of Astronomy occurred in Brazil. They are described below.

3 Some important projects of teaching of astronomy in Brazil

3.1 The Reformulation of the Curriculum in Elementary School

The most important project of Teaching of Astronomy in Brazil in the last years has been the reformulation of the curriculum of the Primary Schools, including big contents of Astronomy, generally, in Science, in the most states of the country.

The Teaching Astronomy Commission worked in this project together with the Government Education Technician , when it was possible.

The Teaching Astronomy Commission analyzed the curriculum of 15 Brazilian States (Trevisan et al. 1995c), including the Federal District (Brasília). It was made a survey of the extension where Astronomy appears in the curricular structure of the primary and high school. This study tried to identify the problems and the deficiency, to suggest the way to use astronomy as a manner to stimulate and to improve the Teaching of Astronomy.

This work detected that Astronomy is present in Elementary Schools (Children Ages: 6 to 13) in some of the eight years of school. In High School, Astronomy is absent of the most curricula, with only some topics suggested (Gravitation and Cosmological Concepts). We found the following problems: curricula deficient approaches; bad prepared teachers; serious mistakes in the books and no pedagogical material. There are only one exception where we have Astronomy in all the series of the Elementary Schools. This exception is the curricular reformulation occurred in Paraná State. They made a reformulation in the primary school, in the nine first years, with base in the contents of pedagogical ideas. It was a work that began in 1987 and evolved educators of all Teaching Governments Groups. This project has as a start point the implantation of a *BASIC ALPHABETIZATION CYCLE*, that permits the systematic progress of the child in the knowledge domain. This curriculum proposed three axes of knowledge: *Health, Matter/Energy and Astronomy*. A resume of this curriculum is below.

The Paraná Basic School Curriculum

The three axes proposed, must give an opportunity to appropriate of contents in a perspective of totality; they must develop the work with the fundamental concepts and their inter-connections.

The contents must enable the discovery of relations between an axis with the other axes, permitting to forme one link of contents, giving a total perspective of the reality. The content of the nature science must have the fundamental in the multiple relation of

interdependence of the elements that constitute the ecosystem and between the ecosystems. The objective is to give the opportunity of a clear idea of the dynamism of the various elements of the systems: physical, chemical and biological, having as a guide the transformer action of the man, interfering in nature.

The contents of Astronomy are included in science discipline, always in relation with the other axes, never isolated. To have an idea of the contends of astronomy, it is listed below.

Paraná Curriculum - Astronomy Contents

GRADE 7 - Sun: primary source of energy. Day and Night.

GRADE 8 - Sun: primary source of energy. Earth Movement: a) Referential; b) Rotation: day and night Orientation: a) Cardinal Points

GRADE 9 - Sun: primary source of energy: a) Heat source; b) Light - Solar Spectrum. Earth Movement: a) Referential; b) Translation; b) Rotation: Gravity. Another Celestial Bodies: a) Illuminated: moon/planets/asteroids; b) Illuminated: stars.

GRADE 10 - Sun: primary source of energy: a) energy types and transformations; b) IR/UV/Its influence on biosphere.

GRADE 11 - Astronomy: historical aspects. Matter and Energy: basic elements of Universe- General considerations. Solar System: Sun; Planets and satellites. Sun and Moon influence on living things. Translations Movements: a) differences of Sun/Moon trajectories (apparent movement); b) night and day: differences of duration.

GRADE 12 - Solar System: basic and general physical and chemical conditions for the analysis of the possible transformations of matter and energy. Physical and Chemical conditions of planets permitting or not the life.

GRADE 13 - Earth Planet. Earth position in Solar System. Inorganic Sphere: a) Hydrosphere; b) Lithosphere; c) Atmosphere. Tides.

GRADE 14 - Sun: source and heat and energy. Astronautic: development and applications.

3.2 The Divulgation Project of Total Solar Eclipse of November, 3, 1994

One of the most important projects of Teaching of Astronomy, in the last times, was the Project of Divulgation of the Total Solar Eclipse of November, 3, 1994, that occurred in the South of Brazil.

It was created by Astronomical Brazilian Society, under the recommendation of International Astronomical Union, a commission called "*Eclipse 94 Executive Commission* ", (Matsuura et al. 1994)to coordinate the assistance in arrangements for the observation of the total solar eclipse of 3rd of November, 1994, that in Brazil, was total in the South of Brazil.. Professional astronomers from Brazil and from several parts of the world were

mobilized in observing this eclipse. The general coordination was done by. Dr. Oscar Matsuura from the Astronomical and Geophysical Institute of University of São Paulo (IAG/USP), which worked with *State Coordinators*, each one of one state of the South and South-West States from Brazil.

Following the suggestion of the *Working Group on Eclipses of the International Astronomical Union*, this commission decided amplify their action, assuming the coordination of a large elucidation campaign about eclipses, close to the common people. Such campaign was aimed at giving technical and astronomical information and to prevent ophthalmological accidents in the people during the eclipse. Utilizing this fact, the *Executive Commission* decided to use this campaign to collaborate with the teachers, mainly in Elementary Schools, in science classes, motivating the students to observe the sky phenomena.

With the help of *Regional Supervisors* and *Special Monitors*, chosen between teachers from Universities, from High Schools and from Elementary Schools, education professionals from State Government Education Department, City Hall, Cultural Center, Second Grade Schools and Physics Students, Planetarium Technitian, and others, the Executive Commission, promoted: courses, talks, fairs, interviews in newspaper, radio, television, divulgations papers, posters, folders, elaborated and distributed didactic experiments and teaching instruments for children.

It's impossible to quantify the total population attended in the area of this campaign, but as indicated the quantification made in Paraná State, where all students of the Elementary and High Public Schools (1.207.832 students); all teachers too (2.040) ;the students of Primary Municipal Schools in all Cities of the State; journalists(60), Education Technician from Official Organisms(412) where attended, we suppose that 80 % of population from South of Brazil was reached by the *National Project Eclipse 94*. The Commission of Astronomy Teaching worked directly in this project, making the coordination in some states of Brazil.

3.3 Courses for Elementary Schools Teachers.

Several Universities, together with Education Technician of the City Hall, including some Planetariums, are working with teachers of Elementary and High Schools, teaching some basic concepts of Astronomy. In general, the courses focalize the content, considering the most practical way to teach it to the children, what is make with the help of simple experiments that show to the student the fundamental relations between the men and the space/time/energy of the ambience that involves him. The Universities that offers regular courses of Astronomy for teachers are: University of Londrina-Pr; Federal University of Espírito Santo- ES; Federal University of Rio Grande do Sul - RGS; Federal University of Viçosa- MG; Federal University of Minas Gerais - MG; Federal University of Rio Grande do Norte- RGN; State University of São Paulo- SP; University of Campinas- SP; Fluminense Federal University - RJ; State University of Rio de Janeiro - RJ, among others.

4 Conclusion

The Commission of Astronomy Teaching, worked hard in the three last years, presenting some good results, mainly of interest of the teachers of the Elementary and high school. As a matter of fact this work was an answer to the longing of the Elementary and High School teachers that have to teach before learning astronomy.

This work is not only a responsibility of a few astronomers. There is a lot of work to be done and it must be done by the community of astronomers, that can collaborate in many ways.

Our proposal is to chance the actual situation where we found students of physics graduation thinking that Venus is a star, the Earth orbits is a very eccentric ellipse and that the moon is illuminated in different ways in each phase, for example.

We are convinced that the level of popular ignorance about astronomy nowadays is, at least in part, responsibility of all that work with astronomy. The community of professional astronomers can change this situation. We noted also that, the initiative of Brazilian Astronomical Society to help the Elementary schools teacher is very well accepted by them, and they really hope that we carry on this work, because there are, as we said, a lot of work to be done.

The author would like to thank to the *Commission of Teaching of Astronomy of the Brazilian Astronomical Society* that make this good work. We also thank to *João Batista Canalle*(UERJ) for his comments on the manuscript and to *Cleiton Joni BenettiLattari*(UEL), for useful discussions.

5 References

- Afonso, G.B. 1994, Boletim da Sociedade Astronomica Brasileira Vol. 14, **1**,128
- Afonso, G.B.; Nadal, T.M. 1995,Boletim da Sociedade Astronomica Brasileira Vol. 15,**1**, 42
- Araújo, N.M.1994, Boletim da Sociedade Astronomica Brasileira Vol. 14, **1**, 129
- Araújo, N.M. 1995, Atas do XI Simpósio Nacional de Ensino de Física SBF, 397
- Bisch, S. 1993, Atas do X Simpósio Nacional de Ensino de Física SBF, 575
- Bisch, S. 1994, Boletim da Sociedade Astronomica Brasileira Vol. 14, **1**,131
- Boczko, R. 1995, XXI Reunião Anual da Sociedade Astronômica Brasileira
- Buso, S.J.; Canalle, J.B. 1993, Atas do X Simpósio Nacional de Ensino de Física SBF,
- Campos, J.A.S. 1995, Boletim da Sociedade Astronomica Brasileira Vol. 15, **1**,46
- Canalle, J.B.1994, Boletim da Sociedade Astronomica Brasileira Vol. 14, **1**, 131
- Canalle, J.B. and Jafelice, L.C 1995. 27ª Reunião Anual da SBPC,
- Canalle, J.B. 1995a, Atas do XI Simpósio Nacional de Ensino de Física SBF, 95
- Canalle,J.B. 1995b, Boletim da Sociedade Astronomica Brasileira Vol.15,**1**, 42
- Canalle, J.B. 1995c, XXI Reunião Anual da Sociedade Astronômica Brasileira

- Crispin, S.C.; Canalle, J.B. 1993, Atas do X Simpósio Nacional de Ensino de Física SBF,
- Daminelli Neto, A. 1993, Atas do X Simpósio Nacional de Ensino de Física SBF,
- Espósito, I.M.; Canalle, J.B. 1993, Atas do X Simpósio Nacional de Ensino de Física SBF,
- Faraco, S.A.; Trevisan, R.H.; Sanzovo, G. Boletim da Sociedade Astronomica Brasileira Vol.15,**1**,45
- Guerbaldi, M. 1995a, IAU International School for Young Astronomers in Brazil
- Guerbaldi, M. 1995b, XXI Reunião Anual da Sociedade Astronômica Brasileira
- Jafelice,L.C. 1995a Atas do XI Simpósio Nacional de Ensino de Física SBF, 179
- Jafelice,L.C. 1995b , XXI Reunião Anual da Sociedade Astronômica Brasileira
- Lattari, C.J.B; Trevisan, R.H.; Romano, E.B. 1993, Atas do X Simpósio Nacional de Ensino de Física SBF 584
- Lattari, C.J.B.; Trevisan, R.H. 1993a, Atas do X Simpósio Nacional de Ensino de Física SBF,487
- Lattari, C.J.B.; Trevisan, R.H. 1993b, Atas do X Simpósio Nacional de Ensino de Física SBF,501
- Lattari, C.J.B. and Trevisan, R.H. 1995a Atas do XI Simpósio Nacional de Ensino de Física SBF,164
- Lattari, C.J.B. and Trevisan, R.H. 1995b Atas do XI Simpósio Nacional de Ensino de Física,SBF,166
- Livi, S.H.B. 1994, Boletim da Sociedade Astronomica Brasileira Vol. 14, **1**, 132
- Livi, S.H.B. 1995, IAU International School for Young Astronomers in Brazil
- Livi, S.H.B. and Bisch, S. 1995, Atas do XI Simpósio Nacional de Ensino de Física SBF, 106
- Magalhães, A.M. 1995, XXI Reunião Anual da Sociedade Astronômica Brasileira
- Makler, M. e equipe, 1995 Atas do XI Simpósio Nacional de Ensino de Física SBF 177
- Makler, M. and Martins, R.A. 1995, Atas do XI Simpósio Nacional de Ensino de Física SBF,395
- Martins, R.A. 1995, Atas do XI Simpósio Nacional de Ensino de Física SBF, 94
- Matsuura, O.1994, Boletim da Sociedade Astronomica Brasileira Vol. 14, **1**, 130
- Matsuura, O. et al. , 1994, Apostila do Eclipse, Editora IAG/USP
- Nascimento, S.S. 1995, Atas do XI Simpósio Nacional de Ensino de Física SBF, 397
- Nascimento, S.S. and Bittencourt, M.K.C. 1995, Atas do XI Simpósio Nacional de Ensino de Física SBF, 396
- Neves, M.C.D. and Pereira, J.R.D. 1995, Atas do XI Simpósio Nacional de Ensino de Física SBF,403
- Neves, M.C.D.; Costa,L.G.; Ichiba, R.; Lima, S. 1995, Atas do XI Simpósio Nacional de Ensino de Física SBF, 403
- Nozawa, A. 1993, Atas do X Simpósio Nacional de Ensino de Física SBF,
- Nunes, M.R. 1995 Atas do XI Simpósio Nacional de Ensino de Física SBF, 158
- Nunes, M.R. and Zanon, R. 1995, Atas do XI Simpósio Nacional de Ensino de Física SBF, 403

Oliveira, I.A.G.; Canalle, J.B. 1993, Atas do X Simpósio Nacional de Ensino de Física SBF,
- Percy, J. 1995, IAU - International School for Young Astronomers in Brazil
- Pereira, O.S. 1993, Atas do X Simpósio Nacional de Ensino de Física SBF,
- Pereira, O.S. 1995, Atas do XI Simpósio Nacional de Ensino de Física SBF, 181
- Pereira, O.S. and Barros, M.P. 1995 Atas do XI Simpósio Nacional de Ensino de Física SBF,182
- Rocha, J.F.V.1994, Boletim da Sociedade Astronomica Brasileira Vol. 14, **1**,133
- Souza, M.O.;. 1993, Atas do X Simpósio Nacional de Ensino de Física SBF,
- Souza, E. ;Trevisan, R.H.; Nabarro, R. 1995, Boletim da Sociedade Astronomica Brasileira Vol. 1,**15**, 45.
- Tignanelli, H. Atas do XI Simpósio Nacional de Ensino de Física SBF, 394
- Trevisan, R.H; Romano, E.B.; Lattari,C.J.B.,. 1993a, Atas do X Simpósio Nacional de Ensino de Física SBF, 579
- Trevisan, R.H.; Dotta, E.; Pedron, I.; Machado; Richter, M.; Lattari, C.J.B. 1993b, Atas do X Simpósio Nacional de Ensino de Física SBF, 397
- Trevisan, R.H.1994a, Boletim da Sociedade Astronomica Brasileira Vol. 14, **1**,128
- Trevisan, R.H.1994b, Boletim da Sociedade Astronomica Brasileira Vol. 14, **1**,130
- Trevisan, R.H. 1995a, Atas do XI Simpósio Nacional de Ensino de Física SBF, 93
- Trevisan, R.H. 1995b, IAU International School for Young Astronomers in Brazil
- Trevisan, R.H. 1995c, XXI Reunião Anual da Sociedade Astronômica Brasileira
- Trevisan, R.H. 1995d, Boletim da Sociedade Astronomica Brasileira Vol.15, **1**, 43
- Trevisan, R.H.1995e, VIII Latin-American Regional Meeting of Astronomy
- Trevisan, R.H.; Lattari, C.J.B. 1995 Atas do XI Simpósio Nacional de Ensino de Física,SBF,170
- Trevisan, R. H.; Bruno, A.T.; Faraco, S.A.1995a Atas do XI Simpósio Nacional de Ensino de Física SBF,155
- Trevisan, R.H.; Souza, E. de; Nabarro, R.A. 1995b Atas do XI Simpósio Nacional de Ensino de Física SBF 174
- Trevisan, R.H.; Bisch, S.; De Campos, J.A.S.; Fonseca Rodrigues, O.P.; Jafelice, L.C. 1995c, VIII Latin-American Regional Meeting of Astronomy
- Varella, I.G.V.1994a, Boletim da Sociedade Astronomica Brasileira Vol. 14, **1**, 131
- Varella, I.G.V.1994b, Boletim da Sociedade Astronomica Brasileira Vol. 14, **1**, 131
- Varella, I.G.V.1994c, Boletim da Sociedade Astronomica Brasileira Vol. 14, **1**, 135

ASTRONOMY EDUCATION AND THE IAU

Michèle Gerbaldi
Institut d'Astrophysique, 98 bis Bd Arago, 75014 Paris France
and Université de Paris Sud XI

Introduction

The importance of Astronomy Education has been stressed many times (see for example the first Colloquium on Teaching Astronomy (IAU Colloquium 105 edited by Jay M. Pasachoff and John Percy, Cambridge University Press, 1988) or the Newsletters published by the Commission *Teaching of Astronomy.*

We shall point out here only some of the arguments developed.

Astronomy Education is important in two different domains :

- the quality of astronomy in the next century rely upon the quality of education given to-day to the undergraduate and graduated students.
- the degree of support of the public for astronomy rely upon the public's understanding and appreciation of our science. This one is coming partly from the teaching of astronomy in the schools, the colleges and the university specially to the non-scientific students and also through to the many channels to the public.

Why the non-scientific student ? very often the leaders of our countries are graduated in non-scientific domains.

There is also another reason to develop astronomy education: "math phobia" and fears of science are endemic everywhere and astronomy taught at basic level can be of great help because this science is very attractive to the youth. So, astronomy can inspire school children to study math and sciences, but it works only if the teacher is inspired first.

To fulfill this role for astronomy, very often, one first think of the activities developed by the amateur astronomers. In some domains they can play an important role, but as soon as we are dealing with astronomy education of the school teachers, professional astronomers must be present.

This is not a problem for the countries where astronomy is developed on a large scale through the universities, observatories or dedicated centers for research. So, we shall focus our attention on the countries with a "lone astronomer" that is the astronomer who facilitates astronomy at any level, being the only one in the country. For example the achievements of Mazlan Othman in Malaysia, Maria Luisa Aguilar in Peru or Alexis Torche Borgnigno in Paraguay are remarkable, just to take a few examples.

It exists another situation which is an extended country with few well developed astronomical centers as well as several small astronomical groups spread all over the country, often far from each other : India, Mexico, Brazil are such examples among others.

In these two situation : lone astronomer or small group of astronomers what are their needs ?

- to meet with other astronomers

- needs for books and journals : a small group must face to a competition with other larger departments in physics of the same university in order to buy the needed publications in astronomy.

- a good INTERNET link : to-day it is as important as a library.

- the training as astronomers, of their undergraduated students that is MSc and then PhD : collaborations with other institutions are needed because very often their university does not offer a degree in astronomy.

The main programmes developed by the IAU in these domains are presented below, but the efforts in those directions are not exclusively done by the IAU. Countries play also an important role in these domains, Brazil is one of them : at the universities of Sao Paulo or Rio de Janeiro, students coming from Uruguay, Argentina, Peru for example, are preparing their MSc or PhD.

The International Astronomical Union

The IAU is a non-governmental scientific union founded in 1919 to " provide a forum where astronomers from all over the world can develop astronomy in all aspects through international cooperation".

There are currently 60 countries adhering to the Union and 7839 individual members. Individual membership is by nomination, and no fees are to be paid to become a member. A global contribution is paid by each adhering country. The nomination is based on qualification - usually a Phd plus some years of experience. The nominations are proposed on a national basis, by each National Astronomical Committee which are ruled by the Sciences Academy. Individual membership can be applied directly to the Union.

The scientific activities of the Union are organized through the 40 Commissions which refer to all astronomical domains, one commission is concerned with education.

The headquarter is based at Paris. Most of the IAU funds are coming from adhering countries as well as some International Society such as UN. General Assemblies are held every 3 years and the IAU support symposia, colloquia. Many other meeting are co-sponsored with other international scientific Unions and Committee within the structure of the International Council of Scientific Unions (ICSU).

The IAU is governed by an Executive Committee , composed of a President, six vice-Presidents, a General Secretary and an Assistant General Secretary. The IAU publishes a semi-annual Information Bulletin which is send to each member as well as the libraries.

The IAU is the sole authority for assigning designations and names to celestial bodies and the surface features there on.

The IAU is primary an association of research astronomers and programmes are developed by the Union in order to promote international cooperation in various domains. In the framework of the international cooperation the isolated astronomers must not be forgotten : this is the role of the Commission 38 "Exchange of Astronomers"; there is also a Working Group for the World Wide development of astronomy.

The Commission 46 "Teaching of Astronomy" acts also in this line.

Commission 38 : Exchange of Astronomers

This Commission was created in order to help isolated astronomers to collaborate in various domains.

For example, in the period 1988-90, 35 travel grants were given for that purpose. For the period 1991-93, 38 were given which represent 10 percent of the budget allocated during the same period for the symposia and colloquia.

Commission 46 : The Teaching of Astronomy

This Commission was established recently in 1964, as a special Committee of the Executive Committee of the Union.

The main aim of this Commission is to act for the development of astronomy education at all levels. This Commission has about 100 members including representative from each country adhering to the IAU, consultants from countries not yet part of the IAU.

The most important membership of the Commission consists of national representatives approved by adhering organizations of respective countries. Their duties are to disseminate all the informations on the activities of the Commission in their countries, as well as to give to the other members of the Commission informations concerning the development of astronomy teaching in their countries.

This Commission as well as the others is governed by a President (currently J. Percy, Canada) a vice-President (currently Julieta Fierro, Mexico) and an Organizing Committee of individuals responsible for scientific projects and programmes.

A Newsletter is published. It is a link between all those interested by education in Astronomy. This Newsletter has been gradually transformed into an electronic one except for those for which the e-mail does not exist or is prohibitively expensive.

To receive the electronic version of the Newsletter contact Armando Arellano Ferro : armando@astroscu.unam.mx

In 1988, for the first time an international colloquium on Astronomy Education was organized. A second one will be helded at London in July 1996. During the IAU

General Assembly and the Regional Meetings, sessions dealing with different aspects of astronomy education are helded, as well as one-day workshop for local school teachers.

These sessions provide the opportunities to establish closer contacts between teachers and astronomers. The last such meeting helded in Utretch, Netherland, in August 1994, attracted more than 180 teachers.

Concerns is felt that many science teachers are not trained to deal with the introduction of astronomy at School. Obviously this is also the case with primary school teachers having a curricula in social sciences domain, more than in physics.

The organization of such meeting is not enough; teaching material and ideas debated at a meeting will only be used if there is a follow-up.

Such follow-up can be organized if a suitable connection is established between astronomers and school teachers. This can be done through the creation of a non-profit organization in order to establish and maintain such links.

The objectives and methods of such organization can be summarized as the following :

- to give access to theoretical knowledge through practical activities
- to increase the mood of observing and experimenting
- to push the teachers working at various level or on different subjects to exchange their experimentation and to dialogue in order to overcome the barriers between disciplines and teaching order
- to produce and distribute :

low cost and good quality educational material
easy to use
not extremely spenders of time
well tested from an educational point of view.

The driving idea in this domain is the following : to create a network of "resource persons" among the teachers, the starting point being the "training of the trainers" by astronomers. The feedback comes from the network of the Association's members.

In France, we have developed Astronomy among the school teachers with such methods, launching in 1977, the *CLEA : Comité de Liaison Enseignants Astronomes*; after several years it proved to be an efficient way.

Visiting Lecturer Programme (VLP)

The Visiting Lecturers Programme (VLP) was developed in order to provide a series of visiting lecturers to astronomically developing countries to establish on a longer term basis astronomy. The IAU provided the lecturer's travel and the host institution supported the lecturer while giving the courses.

The students attending these courses were receiving an academic credit. The coordinator of the VLP was Professor Donat G. Wentzel.

Why such a programme : simply because when the "lonely astronomer" disappears for any reason, astronomy disappears too.

Astronomy can exist only if there is at least a small but strong group of astronomers in a country.

The Visiting Lecturer Projects started in two countries where the universities agreed to a noticeable growth of astronomy. The countries were : Peru and Paraguay. In each case, there was already an astronomer teaching at the university.

The aim was to provide an astronomy course annually in each country during several years. Then in a second phase, students should be sent abroad for advanced studies and they would return. In such a way an astronomical community should be created.

In Peru,the programme started in 1984, and in Paraguay in 1988.

The lecturers had to speak Spanish and it has been extremely difficult to find Spanish speaking astronomers who can afford to spend about three months in Peru or Paraguay.

So, the courses have been delayed in time.

Nevertheless 9 lecturers went to Lima , and among them Prof. Horacio Dottori. Now, astronomy is very active at the Universidad Nacional Mayor de San Marcos : there is a Seminario de Astronomia y Astrofisica and young astronomers are studying in Bresil either for a MSc or a Phd.

The VLP in Paraguay at the University Nacional de Asuncion started in 1988 and ended in 1994. 6 visiting lecturers participated to it.

Several former students now teach astronomy in Paraguay schools. Two students are continuing their training abroad in Mexico and in Argentina.

The VLP has been cancelled and another project created : TAD " Teaching for Astronomy Development" more flexible. It should start at the end of 1995 and will be widely announced. In common with the VLP , the goal is to enhance astronomy at selected host institutions on a long-term basis. Requests for more informations on this new programme should be sent to : Dr. Donat G. Wentzel, Dpt of Astronomy, University of Maryland, College Park MD 20742, USA, e-mail : wentzel@astro.umd.edu, fax : 1 301 314 9067.

The International School for Young Astronomers (ISYA)

The ISYA is one of the most important project of the Commission 46. It started in 1967 with Josip Kleczek (Czechoslovakia) as the first secretary , now retired and followed by Donat G. Wentzel (USA) and Michèle Gerbaldi (France) as Assistant Secretary since 1991. The dominant goal of ISYA is to advance astronomy in astronomically developing countries. This is accomplished by increasing astronomy in the host institution.

An ISYA lasts 3 weeks and each school must have at least a third of its students from outside the host country, but very often it is half and half. Participants' background ranged from just-finished bachelor's degree to a PhD already started . They come usually from small universities with essentially no astronomy resources to establish research centers.
The School include lectures, starting for some of them at a level of undergraduate up to a graduate level including survey providing "research flavor".

The ISYA includes also as far as possible, observational work and data analysis.

The scope of the ISYA are :

- to broaden the academic experience of the participants
- to show the students the broaden aspect of astronomy
- to enlarge student's scientific perspectives

It is important to have faculty members able to stay if possible, for the whole duration of the ISYA in order to give to the participants the opportunity of many informal scientific individual discussions; another important factor is to always choose the school's participants from different countries, of different background, to get the discussion more lively. Most students give a brief seminar about their own university or observatory and they present their own research.

It is necessary to organize the ISYA in developed institutions with access to local libraries, computers. Observing facilities are useful even if it is a small telescope. For such purpose, when necessary the Traveling Telescope can be used. This Celestron-8 telescope has been funded by the Canadian Committee for UNESCO with some other institutions and is used in countries where astronomical research is developing. Currently the photometer of this telescope is used in Paraguay on a telescope located there.

An ISYA cannot take place in an university which are far away from astronomical centers. Travel cost of all faculty and participants are covered by the IAU, while the local costs, must be covered by the host institution. That is the reason that not all institut can apply for an ISYA, since they must have some local financial support.

The budget of the IAU for the ISYA is about 16 percent of the budget for Colloquia and Symposia.

There are about 2 ISYA every 3 years.

The faculty members are chosen by the host institution according to their dominant research line. Very often they are foreign astronomers having already well established collaboration or with the aim to develop it.

This year the ISYA was held at Belo Horizonte (Minas Gerai) July 9-29.

The Brazilian sponsors were the UFMG, CNPq (Centre Nacional da Pesquisa) and the Fapemig.

The local organizing Committee was chaired by Prof. Renato Las Casas. The members of the LOC were : Tulio Jorge dos Santos, Rodrigo Dias Tarsia, Domingo S. de Lima Soares, Luis Themystokliz Sanctos Mendes, Bernardo Reidel.

For the first time lectures on teaching astronomy has been organized as well as a panel discussion on the astronomy at university level.

The first two weeks, we met at the University Federal of Minas Gerais (UFMG), Belo Horizonte, the third week was at the Observatory Serra Piedade, runs by the Astronomical Group of the ICEx (Department of Phisics). The Observatory is located at some 50 km from Belo Horizonte, at an altitude of about 1800m.

The foreign faculty invited were :

Dr. Craig Gullixson (National Solar Observatory - USA) CCD Detectors
Dr. Jens Knude (Copenhagen University Observatory - Denmark) Interstellar Medium
Dr. Reynier Peletier (Kaptein Astronomical Institut - Netherlands) Galaxies
Dr. John Percy (Toronto University - Canada) Teaching of Astronomy - Variables stars. Dr. J. Percy is the President of Commission 46 "Teaching of Astronomy"
Dr. Bo Reipurt (ESO - Chile) Star Formation
Dr. Silvia Torres Peimbert (Observatorio Astronomico Nacional - Mexico) Practical Astronomy, Observations
Dr. Michèle Gerbaldi (Institut d'Astrophysique de Paris, Université de Paris Sud XI France) Teaching of Astronomy, Practical Observations.

The Brazilian faculty were :

Dr. Silvia Livi (Porto Alegre University) Teaching of Astronomy
Dr. Rute Trevisan (Londrina University) Teaching of Astronomy
Dr. Luis Paulo Vaz (UFMG Belo Horizonte) Stellar Evolution

Two seminars were given by the Brazilian faculty of Belo Horizonte University : Dr. Quiroga and Dr. Soares.

38 students participated to this ISYA, among them 19 came from Argentina, Bolivia, Colombia, Paraguay, Peru, Spain and Uruguay.

The feed back of these Schools are measured 2 years letters through a questionnaire sent to all the participants.

The result for the previous ISYA were :

- new scientific collaboration between the participants
- strong influence on the choice of the subject for a MSc or PhD
- broader view of science in general and how science can serve educational purpose
- spreading the friendship among young scientists

Conclusion

Many initiatives have been developed by the IAU but much more are needed and they could be achieved only if more professional astronomers are involved in it.

Acknowledgement. I greatly appreciated the invitation of the SAB to participate to this Annual Meeting

Section 3

Instrumentation

IMPROVING POLARIZATION-SENSITIVE VLBI IMAGES WITH MICROWAVE–LINKED DATA TRANSMISSION SYSTEMS

Everton Lüdke
eludke@nepae.ufsm.br
UFSM-LACESM, Centro de Tecnologia
97119-900, Santa Maria/RS, Brazil

Abstract

The MARK IIIa data recording system has become standard in VLBI acquisition systems for radioastronomy and geodetic measurements. Only recently the system has been used for interferometric circular polarization measurements which is a powerful tool to study magnetic fields in radio sources. In this talk, I review the recent advances in the field and and present recent results of an extensive investigation on a new technique which uses microwave radio links to improve the quality of radio maps by using joint observations with the available hardware of Multi-Element Radio-Linked Telescope Network (MERLIN) and the European VLBI Network.

1 Introduction

Circular polarization measurements of microwaves emitted by cosmic radio sources are a very powerful tool to study the dynamics of luminous radio sources in active galactic nuclei and the nature of magnetic fields in space.

The advent of long-baseline interferometry technique in which antenna separations can reach up to an Earth radius has made high sensitivity and resolution polarimetric observations possible. Technical limitations of previous digital data recording systems such as the now-extinct NRAO MARKII system (Clark, 1973) did not allow to record both hands of circular polarization (LCP, RCP) simultaneously. The MIT/NASA/NRAO MARKIIIa data acquisition system (Clark, 1985) has been introduced in 1980 with a faster data rate of 112 Mbits/s allowing a maximum 56 MHz bandwidth with several standard setups for data recording which are used in radioastronomical observations to obtain continuum and spectral line information. The mode C is normally used in polarization but with reduced bandwidth and tape usage and therefore, reducing the imaging sensitivity by $\sim 30\%$ from the full capability. A description of signal flow and frequency conversion in such system can be found elsewhere.

In this review paper, I present the results of an extensive investigation on a new observational technique which uses the longest and intermediate spacings of the MERLIN array (Thomasson, 1986) as an additional source of information to improve the polarization measurements accuracy and imaging fidelity. The method discussed here has been applied to data obtained with MARKIIIa recorders from the European VLBI Network since 1993 and the MERLIN array and is currently offered as standard joint MERLIN and EVN observations in polarization mode.

Figure 1: Telescope locations of the European VLBI Network (EVN) which are recommended for VLBI polarization measurements. The Cambridge telescope is added by microwave link networks to improve the polarization imaging quality.

The correlations and cross-correlations to obtain interferometric visibilities have been obtained after the observations with a MARK IIIa complex correlator such as the Max-Planck Institute für Radioastronomie, Germany (Alef, 1989) and in real-time with the MERLIN correlator, UK, allows to produce polarization maps which are good enough for most astrophysical purposes.

The main results from this paper are that microwave links from the MERLIN network are ideal to improve short-spacing coverage in the UV plane allowing polarized emission to be well detected at larger distances from the radio map phase centre.

2 The imaging problem

Radio interferometers employing VLBI techniques consist on an ensemble of antenna pairs with separations larger than ~ 10 Km which are used to make high-resolution measurements of brightness distribution and position of cosmic radio sources of strong astrophysical interest, radar imaging of planets and asteroids and tracking deep-space probes. In particular, the European VLBI Network (Figure 1) is a consortium of European radio observatories but with the eventual inclusion of Chinese (Shanghai), Japanese (Kashima) and South African (Hartbeestoek) antennas to increase the resolution and improve the synthesized beam shape for targets at low declinations. The current EVN data recording system are MARK IIIa and VLBA data recorders with the Bonn Correlator used in part-time to process the data to obtain the complex visibilities. In the correlator each

antenna output voltages ($E_{i,j}(u,v)$) are amplified, multiplied and integrated to obtain complex correlation coefficients, after digitally compensating the wave paths due to the earth surface geometry and electronic phase delays :

$$E_{ij}(u,v) = \int_{-\infty}^{\infty}\int_{-\infty}^{\infty} I(l,m)e^{-2\pi i(ul+vm)}dldm \qquad (1)$$

The radio image are the source brightness distribution $I(l,m)$ which is obtained by inverting the above Fourier transform from gridding and interpolating the data in both visibility plane (l,m) and the sky baseline projection plane (u,v). The Fourier transform of $E_{ij}(u,v)$ is a 'dirty' map which is contaminated by phase errors and spurious sidelobe response since it is a convolution of the true source brightness distribution and the interferometer difraction pattern. The true source image can then be recovered by using the non-linear complex CLEAN algorithm (Cornwell & Wilkinson 1991) which subtracts iteractively a beam pattern from the dirty map, obtaining the intensity at each pixel of the (l,m) plane. The final map is obtained by convolving the pixel values with a Gaussian function with same profile as the synthesized main beam. CLEAN convergence is guaranteed by the fact that radio sources are normally simple and that both beam and dirty map are obtained with the same locus in the (u,v) plane. The algorithm is not efficient in recovering extended, diffuse structure in the (l,m) plane but it works fine for compact and bright features in the dirty map, which are of astrophysical interest. CLEAN also converges with negative patterns so that the Stokes Parameters $Q(l,m)$ and $U(l,m)$ can be mapped with the same algorithm since they are related to the across correlations of LCP and RCP signals (Conway & Kronberg, 1969). The polarization position angles $\chi(l,m) = 1/2atan(U(l,m)/Q(l,m))$ and fractional polarization $m(l,m) = 100\sqrt{Q(l,m)^2 + U(l,m)^2}/I(l,m)$ are obtained from simple map arithmetics and are quantities which can be obtained by numerical simulations. It is out of the scope of this paper to make a detailed analysis of polarization imaging algorithms for VLBI (Conway & Kronberg, 1969; Cotton, 1993) but an important consequence is that the addition of long and intermediate spacings from MERLIN telescopes (10-212 Km) provides more constraints which helps in improving the definition of images with normal EVN capabilities.

The high-frequency part of VLBI data acquisition systems consist on Cassegrainian radiotelescopes of at least 20 m diameter, a corrugate horn antenna mounted in the secondary focus, a polarizer quadripole (septum, 1/4-wave plate or orthomode transducer) and a low–noise cryogenic receiver ($T_{sys} \sim 35$ K) (Rohlfs, 1990). Instrumental polarization occurs mainly due to wave reflections between the antenna surface and subreflector, leakage due to the cooling which can damage the electric shielding between polarization channels as well as imperfections in the polarizer and horns. Further electronic stages seldom contribute to crosstalk between LCP and RCP signals ($< 0.1\%$, Lüdke, 1994). The Linear approximation which considers a simple contamination of LCP and RCP channels by an arbitrary quadripole is employed to extract the receiver instrumental polarization and it works well for polarimetric observations with the Very Large Array and MERLIN. In both methods, the apparent source rotation due to alt-azimuthal telescope mountings

is used to calibrate the amplitude of instrumental polarization factors (D-terms, Conway & Kronberg, 1969) but it is unlikely to work when instrumental polarization is very strong since only the lowest-order contamination terms are used.

Another way of solving for instrumental polarization apart of this linear model is a more general scheme proposed by Fomalont and Wright (1974). The Ellipticity-Orientation Model (EOM) assumes an elliptical feed response which can be known *a priori* from feed measurements in a antenna testing range (Cotton, 1993). The EOM model has been built on more realistic and physical assumptions about the feed polarization response and take into account the electric characteristics of such systems which is the factorization of spatial responses based on parallactic angle variations. As suggested by Fomalont and Wright, the feed properties are represented by elliptical response functions with feed ellipticity and orientation as main variables. Lüdke (1994) has shown that both methods can be related by a simple transformation, if the instrumental contamination is less than about a dozen percent. This procedure has been recently implemented in the AIPS task PCAL by W.D. Cotton (1993), who was able to obtain a sensible polarization map of the jet in 3C138 with global VLBI (Cotton, private comm.) at 6 cm.

Further investigations in this field by myself and collaborators is that it is better to calibrate MERLIN and EVN data sets independently with the linear and EOM model and then to combine the data sets than to use a single phase calibration routine to be applied in the whole visibilities (Lüdke, 1994). The main restriction here is that there is a polarization position angle calibration for each telescope which is called AC phase offset, which is not stable for some EVN antennas while the phase stability is better for MERLIN telescopes.

3 The MERLIN hardware

The transport of information from a remote telescope by microwave links is a difficult task. At high frequencies, transmitter and receiver towers can vibrate due to the wind and variations in the troposphere refraction index can induce fast phase variations which can decorrelate the signal producing map noise levels larger than the theoretical Nyquist noise level which is determined by antenna system temperatures, number of telescopes, bandwidth and data averaging time. At 5 GHz the MERLIN telescopes are remarkably good but the polarization sensitivity of the Defford telescope is not so good as it is at L band due to surface errors.

The basic MERLIN signal flow architecture which is used in joint observations is summarized in figure 2. The 2-bit digital correlator gives the visibilities $E_{ij}(u,v)$ for all n MERLIN telescopes while the polarization data from Cambridge is also recorded in a VLBA-type tape, before the ϕ-rotators stages.

Phase variations due to the K-band microwave link paths are monitored by a pulse modulation scheme from which transmission and arrival times are measured by a logic unit and phase delays can be obtained and corrected on-line by phase rotator circuit boards before the data enters the correlator. The receivers are coherent since the phase

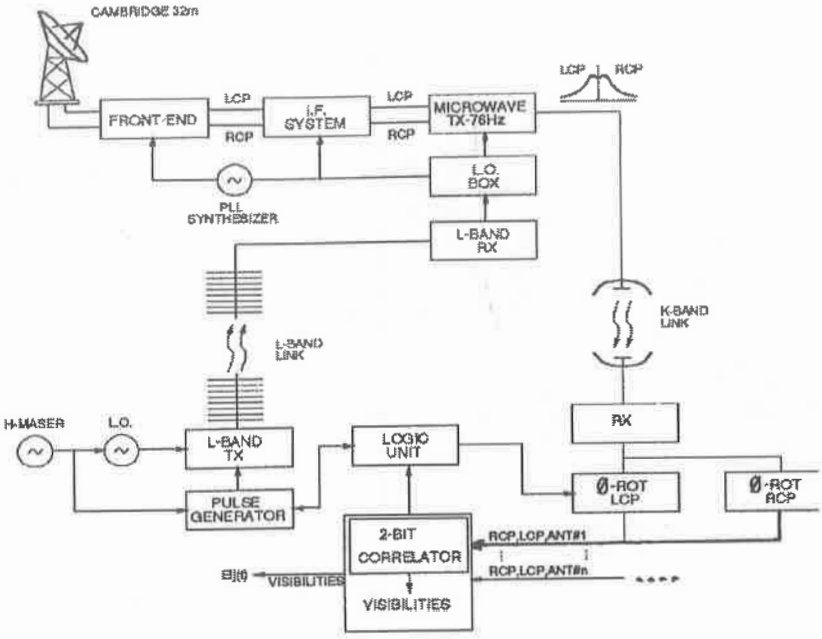

Figure 2: Summary of the MERLIN polarization architecture used when the Cambridge Telescope is included in the EVN network. The system is designed and maintained by the Nuffield Radio Astronomy Laboratories/UK.

of local oscillators in the front-end are phase-locked to the carrier of a secondary L-band link which transports the phase of a MASER clock to all telescopes. Similarly, all local oscillators from the microwave link network which are important to analog AM modulation and demodulation, are also phased-locked. Double-sideband AM modulation scheme send LCP and RCP over a $\sim$ 30 MHz bandwidth in a $\sim 7GHz$ carrier wave with no channel crosstalk, allowing a wider bandwidth (15 MHz) than the original architecture used in the late eighties. This automatically allows on-line polarization data recording which is a requisite of MARKIIIa and VLBA systems. Fortunately, these improvements were such that both hands of polarization from the Cambridge telescope can be recorded on-line by a VLBA data acquisition rack and making suitable to add the Cambridge 32-m telescope from the MERLIN array to the EVN network. In figure 1, this corresponds to (1-2) baseline which fills in the shortest EVN spacings adding more polarization sensitivity.

4 Defining the observing mode

The observations were planned in 1992 but started in 1993 due to delays in the hardware commissioning. They employed Mark III Mode A 28D, in which LCP is connected to the data acquisition rack IF1 input and RCP is connected to the IF2 input of the MARKIIIa system. In this mode, a larger bandwidth is available for polarization (28 MHz), which is almost twice the band allowed by the standard Mode C recording employed in Cotton's 3C138 observations. Within the data acquisition rack, the bandpass is split into several

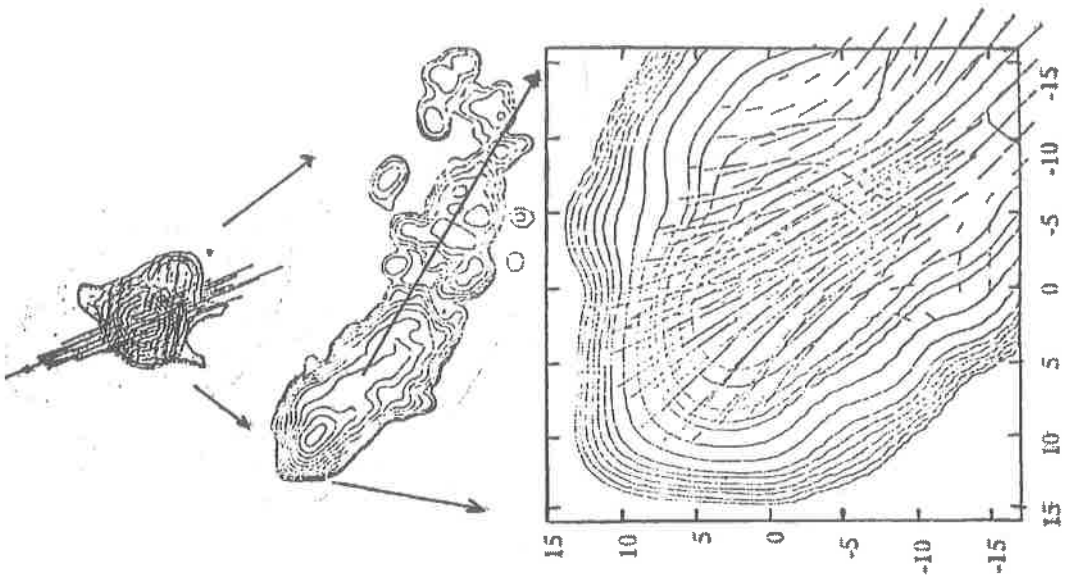

Figure 3: Polarization maps of the quasars 3C286. (TOP) is the MERLIN map at 5 GHz and 55 mas resolution; (MIDDLE) is the EVN+MERLIN radio map at 5 GHz showing flow details at 12 mas resolution; (BOTTOM) is the EVN polarization map at 5 GHz showing the polarization position angles which are related to the magnetic field direction.

sidebands of 2 MHz each. The signals are recorded in such a manner that LCP lies along even numbered videoconverters and the RCP is processed by odd videoconverters. No polarization crosstalk are expected from the tape recorder due to random longitudinal tape motions, since the tracks are more than 600 μm apart and the tape can run with enough mechanical accuracy.

The instrumental polarization can be obtained for the calibrators 0552+398 and OQ208 and the weighted average values of the baseline-based polarization contamination values are about 3% or less for MERLIN and 10 % or more for the EVN network showing high feed ellipticity for a large number of antennas.

The parallel (LL,RR), cross (LR,RL) and autocorrelations (LR per telescope) were obtained with the Bonn correlator. The autocorrelations have shown to be useful to measure directly the $\phi_R - \phi_L$ phases (AC phase offsets) which normally are assumed to be constant and corrected by a phase shift which depends on the polarization position angle calibrator. For MERLIN and at 5 GHz observing frequency, this quantity varies less than about four degrees per day since phase variations are compensated before the correlator by hardware. Since VLBI does not employ a phase monitoring scheme, such compensations have to be made by deriving phase corrections during calibrator scans with the AIPS powerful phase-correction task CLCOR prior to determining the EOM-model instrumental polarization solutions with the AIPS task PCAL.

Figure 3 shows the results of the first polarization experiment with the EVN and MERLIN held in 1993. The MERLIN polarization image of 3C286 at 5 GHz and 50 mas resolution shows the central component with the bulk of polarized emission and an extension to the southwest where the jet is seen. The combined MERLIN and EVN total intensity map ($I(l,m)$) shows fine details of the jet with 10 mas resolution. The central region is expanded showing the EVN-only polarization map with electric vectors which are perpendicular to the magnetic field vector direction. From this example one can see clearly the improvements in the image quality since the magnetic field lines can be tracers of fluid motion within the first few kiloparsecs from the central engine. The astrophysical implications of the data which suggests a connection between 3C286 and extended Fanaroff-Riley objects will be the subject of a forthcoming paper (Jiang et al, 1996).

5 Summary

In this talk, I have reviewed the techniques for polarization–sensitive VLBI and reported unpublished results from recent combined MERLIN and EVN observations of compact relativistic jets in compact quasars which are part of a major project to study the magnetic fields and Faraday rotation in relativistic jets within the narrow-line region.

The basic engineering strategy described here is the best to the moment to produce radio polarization maps at about 10 milliarcseconds resolution with the European VLBI Network at 5 GHz, which matches the VLBA at S-band and MERLIN at 22 GHz.

I am grateful to the EVN board of directors for making available their hardware to tests of polarization, the European VLBI friends for their support and the Max-Planck Institut für Radioastronomie for hospitality during my stay at the Bonn Correlator. It has been a pleasure to work with Drs. H. Sanghera, W.D. Cotton, M. Rioja and D. Dallacasa which are my collaborators in this project. In particular I wish to thanks the the director of MERLIN National Facility for support and encouragement. CAPES and CNPq partially funded this project and without their help, this paper could never be written.

References

Alef W., 1989, in *VLBI Techniques and applications*, eds. Felli M., Spencer R.E., NATO ASI Series, Kluwer, p.97

Conway R.G., Kronberg P.P., 1969, MNRAS, 142, 11

Cornwell T.J., Wilkinson P.N., 1981, MNRAS, 196, 1067

Cotton W.D., 1993, AJ, 106, 1241

Clark B.G., 1973, Proc. IEEE, 61, 1242

Clark T.A., 1985, IEEE Trans. Geodesy Rem. Sens., GE-23, 438

Fomalont E.B., Wright M.C.H., 1974, in *Galactic and Extragalactic Radio Astronomy*, Springer (Berlin)

Jiang D.R., Dallacasa D., Schilizzi R.T., Lüdke E., Sanghera H.S., Cotton W.D., 1996, A&A, in press
Lüdke E., 1994, PhD thesis, Victoria University of Manchester, UK
Rohlfs K., 1990, Tools of Radio Astronomy, P45, Springer-Verlag

ASTRONOMY IN SPACE: SATELLITES AT INPE

Thyrso Villela
Instituto Nacional de Pesquisas Espaciais – INPE
Divisão de Astrofísica
Caixa Postal 515
12210-970 - São José dos Campos, SP
e-mail: villela@das.inpe.br

Abstract

The ongoing scientific satellite programmes at INPE and the existing Brazilian satellite testing facility are described. The need for building space-based astronomical experiments is discussed as well as the chance for the Brazilian astronomical community to use the existing INPE's facility and acquired experience with the design, building and testing of scientific satellites to carry out astronomical experiments in space.

1 Introduction

Astronomy and Astrophysics in Brazil have reached such a level that are demanding new instruments, including space-based experiments. Many astrophysical queries can only be answered with data obtained by space-based instruments on board balloons, rockets and satellites. As balloons and rockets are, in general, dedicated instruments with not much observational time, satellite-based instruments seem to be a natural way to obtain these data. Although the majority of Brazilian scientists in the field is composed by individuals with little experimental background or expertise, the identification of the necesssary experiments to answer these questions does not depend on this as it is dictated only by the scientific driven goals. The Brazilian astronomical community has already proven itself capable of such identification. It is imperative for the Brazilian astronomical community to collect its own original data from space platforms and that these data are competitive and of good quality. But, in order to do that, it is necessary to have both human and technical capabilities. The technical capability is somewhat consolidated as far as spacecraft design, building and testing are concerned. The payload building capability is the one that needs to be strengthened as it involves both human and technical developments. Some actions have to be taken in order to achieve this goal, such as personnel training and laboratory upgrades.

Over the years, several countries have put in orbit experiments that drasticaly changed the way we view the cosmos. The examples are multiple and range from the small dedicated experiments to the so-called great observatories. The scientific knowledge obtained with such instruments was fabulous and the advancement in several astronomical fields was enormous. As the economical situation worldwide worsened lately, more and more scientific collaborations are expected in order to carry out experiments capable to fulfil the scientific needs. Any international cooperation must, despite the fact of inherent mutual

scientific interest, rely on the technical capabilities of the partners, and Brazil, nowadays, can join these collaborations as an equal in several aspects, namely the scientific insight and the spacecraft and payload design, building and testing know-how.

2 The present

It is possible at the moment, in Brazil, to design, test and operate a satellite, as the first Brazilian satellite SCD-1 (Satélite de Coleta de Dados - 1) has shown. The SCD-1 was launched in February 1993 and is still operating in orbit with no failures. The estimated lifetime was one year. This satellite was totally designed, built and tested at INPE. In order to inform the Brazilian Astronomical Society of the technical capabilities of INPE as far as satellite technology is concerned, it is described the available facilities at INPE in São José dos Campos, SP, and the ongoing satellite programmes. The descriptions below are reproductions of the available technical information about the existing testing facility at INPE and the SAC-B and SACI-1 projects, available from INPE and CONAE (see references), and can be obtained upon request from INPE and CONAE headquarters.

2.1 The Existing Facility in Brazil: LIT/INPE

INPE's Integration and Testing Laboratory (LIT) was specially designed and built to attend the necessities of the Brazilian Space Program. It represents one of the most sophisticated and powerful facilities in the qualification of industrial products which demand a high degree of reliability.

Environmental testing is conducted in a 100000 class clean area of 1600 square meters, with a useful overhead crane hook height of 10 meters. The types of tests performed include thermal vaccum, climatic, vibration and shock, eletromagnetic interference and compatibility. The 450 square meters integration area has a useful crane hook height of 6 meters and operates under a class 10000 cleanliness standard. Found in this part of the laboratory is a specially designed equipment for alignment measurement and three axis dynamic simulation. These activities, together with the measurement of mass, center of gravity, moment of inertia and product of inertia, form the basic nucleus of the functional testing and integration activities of space systems.

The satellite check-out station, designed to govern the functional tests of space hardware, as well as the other test control rooms, are adjacent to the clean areas with a full unobstructed view over all activities. With the intention of assuring the precision of all measurements, a sensor calibration laboratory for accelerometers, thermocouples, and pressure transducers was installed within LIT along with a global electrical calibration laboratory under rigid environmental conditions. To allow the widening of the scope of activities of LIT, a reliability laboratory is available for the reception, inspection, and qualification testing of electronic devices in accordance with specified norms. Complementing the environmental test facilities, there are special equipment installations which are designed to support the development of other space related activities. This is the

case, for example, of the explosion proof hydrazine compatible micropropulsion chamber and the 80 meter range antenna testing laboratory.

With a total constructed area of 10000 square meters, LIT contains a complete utility infrastructure which includes a filtered compressed air system, a closed circuit industrial water system, an electrical grounding system with less than 1 Ohm of resistance, a laboratory access control system, a fire detection and extinction system and a filtered stabilized electrical system complete with an uninterruptible power supply and emergency generators which help guarantee the quality, continuity, and security of all tests performed in the laboratory.

2.2 The satellites

2.2.1 SAC-B

The SAC-B (Satélite de Aplicaciones Cientificas) satellite is an example of what can be done in terms of international cooperation. It is carried out as an international cooperative project between the Argentina's National Commission of Space Activities (CONAE) and the U.S. National Aeronautics and Space Administration (NASA). The Secretariat of Science and Technology of Argentina participates in the financing of the project through the National Research Council (CONICET). CONAE is responsible for the design and construction of the SAC-B spacecraft, the HXRS instrument, the ground station operation, and the scientific data distribution; NASA will provide two scientific instruments, launch services on a Pegasus vehicle, and support for initial orbit monitoring and emergency backup throughout the mission life. By a separate agreement established Argentina, the Italian Space Agency (ASI) will provide the solar arrays plus a scientific instrument. The Brazilian National Institute for Space Research (INPE) is providing the facilities for the system qualification tests of SAC-B at LIT and a Brazilian co-investigator with the Argentine instrument (HXRS).

The HXRS science team is composed by H. Ghielmetti (Argentina), A. Hernandez (Argentina), M. Machado (Argentina), C. Mandrini (Argentina), P. Mauas (Argentina), M. Rovira (Argentina), B. Dennis (USA), U. Desai (USA) and T. Villela (Brazil). SAC-B is designed to advance the study of solar physics and astrophysics through the examination of solar flares, gamma ray bursts, diffuse X-ray cosmic background, and energetic neutral atoms. The scientific payload of SAC-B comprises an Argentine instrument (HXRS), developed by the Institute of Astronomy and Space Physics (IAFE), to measure the temporal evolution of X-ray emissions from solar flares and non-solar gamma ray bursts; a combination of detectors to measure soft X-ray emitted by solar flares and gamma ray bursts provided by NASA (Goddard X-Ray Experiment - GXRE); a diffuse X-ray background detector using CCD technology (CUBIC) from Penn State University; and an Italian instrument to measure energetic neutral atoms (ISENA).

Scientific objectives:

Solar Flares

Solar flares are the most dynamic and energetic phenomena in our Solar System. On time scales of a few minutes or even seconds, stored magnetic energy is suddenly released in these transient events, in the form of accelerated particles, radiation in the whole range of the electromagnetic spectrum, bulk heating and hydrodynamic shocks. Combined observations of the hard and soft X-ray emissions from solar flares, as those to be provided by the HXRS and the solar detector of GXRE, will help us to further our understanding of the interactions between accelerated particles and the ambient solar atmosphere.

Gamma ray Bursts

Intense transient emission of gamma radiation - the gamma ray bursts - does appear in some completely unpredictable regions of the sky. In spite of the enormous amount of energy involved in each of these events, the extensive investigations have not been able to explain them. To discriminate among different suggested models, new observations, such as those to be performed by the HXRS and GXRE, are needed.

Diffuse X-Ray Background

Below 1 keV the soft X-ray diffuse background is believed to be largely Galactic in origin. Thermal emission from hot gas is the likely source of this flux, and for this reason its spectrum is dominated by emission lines from highly ionized species. CUBIC should be able to distinguish between the strong line groups of oxygen, neon, iron, carbon, etc. In the X-ray band above 1 keV, the diffuse emission comes predominantly from sources of extragalactic origin. CUBIC studies will help to elucidate the origin of the diffuse X-ray background.

Energetic Neutral Atoms

Energetic neutral atoms are generated through charge exchange in the radiation belts and in the ring current region, where the trapped ion populations interact with the gas of the geocorona, and then travel down to the satellite's altitude. By the measurements of precipitating and escaping neutral atoms, ISENA will image those areas of the Earth's environment where the neutral atoms are coming from.

Mission:

SAC-B, a 181 kilograms class spacecraft, will be injected into orbit by a NASA provided Pegasus XL rocket. The Pegasus will carry SAC-B to an altitude of 550 km and a circular orbit inclined 38 degrees to the Earth's equator, which ensures an orbital lifetime of at least three years. A high-tech Argentine enterprise, INVAP S.E., is building the spacecraft and the Hard X-Ray Spectrometer (HXRS). It is expected to fly in 1996-97 depending upon Pegasus availability.

The SAC-B mission will be controlled from a ground station located in Argentina. This facility comprises the Telemetry, Tracking and Control (TT&C) Station and the Mission

Operations Control Center. The TT&C Station has a 3.6 m autotracking antenna, and it enables range and Doppler measurements and Master Clock Reception (GPS). The Control Center consists of two fully redundant Sun workstations linked to the receiving and transmitting equipment as well as PC terminals, which will control the satellite.

Spacecraft configuration:

The spacecraft body, built in Alluminum alloy, is a rectangular parallelepiped 62 cm by 62 cm wide by 80 cm high. Four deployable solar panels, covered by GaAs cells, generate 210 W to supply the electrical power to the different subsystems: Attitude Control, Thermal Control, Command and Data Handling, and RF Communications, as well as the instruments. The solar instruments (HXRS and GXRE solar detector) are mounted on the Sun-facing end of the spacecraft along with the Fine Sun Sensor, with fields of view looking toward the Sun. The GXRE gamma ray detectors are mounted on the solar platform, but they have fields of view on opposite sides of the spacecraft, set on normal to the Sun line. CUBIC and ISENA are mounted on the top, or the anti-Sun facing side of the spacecraft. CUBIC's field of view is normal to the Sun line.

Three-axis stabilization of the SAC-B will be accomplished by two momentum wheels in a "V" configuration for roll (Sun direction) and yaw axis (CUBIC boresight) control. Pitch axis control is effected with air core magnetic torquer coils. The two-axis Fine Sun Sensor and a three-axis magnetometer will allow attitude determination to an accuracy of 3 degrees in real time and 2 degrees by post-facto analysis. The temperature will be kept within the -10 degress Celsius to +40 degrees Celsius range by means of a semi-passive thermal control, using radiators and electrical heaters. Up to 100 Mbits per day of scientific data will be dumped to the ground station through the RF downlink on S-band (2255.5 MHz). Two quadrifilar helix antennae are mounted one at either end of the spacecraft, one right hand circular polarized, the other left hand circular polarized, yelding an omnidirectional pattern.

2.2.2 SACI- 1

Five experiments have been selected to be performed on board the first Brazilian scientific micro-satellite SACI-1 (Satélite de Aplicações Científicas):

a) Plasma Bubbles: to study plasma bubbles in the ionosphere;

b) Airglow Photometer: to measure the intensity of the terrestrial airglow emissions;

c) Geomagnetic Experiments: to study the Earth's magnetic field;

d) GPS: determination of the orbit and attitude of the SACI-1 using a GPS system;

e) ORCAS: to measure anomalous cosmic rays.

This latter experiment (ORCAS, which stands for **O**bservações de Raios **C**ósmicos **A**nômalos e **S**olares) is the only one related to astrophysics and it is the one that should be viewed here. The scientific motivation for this experiment is outlined below. The proposers of this experiment are Dr. A. Turtelli (UNICAMP) and Dr. U. B. Jayanthi (INPE) with collaborators from INPE (T. Villela), UNICAMP, NRL (USA) and RIKEN (Japan).

Scientific objectives:

In the interplanetary space, heavy nuclei of He and even Ne with energy below 50 MeV/amu, called Anomalous Cosmic Radiation (ACR), were discovered in 1970-73 by the space probes IMP and Pioneer 10 and 11. While the relation between the Carbon and Oxygen quantities (C/O) in the cosmic and solar radiation (GCR, SCR) is less than 0.5, in the ACR the C/O quantity is less than 0.1. The theoretical explanation for this is that the interstellar neutral atoms are captured by the Solar System in its movement, then are ionized and accelerated, and are transformed into ACR.

Starting with the discovery by the Skylab III in 1973, a series of experiments on board Spacelabs and Soviet satellites (in orbits of about 500 km), with recoverable passive plastic detectors, has detected particles with energy and composition similar to the ACR near the Earth. The presence of these particles, at these altitudes, despite the existence of the Earth magnetic field, is only possible if they are partially ionized and "trapped" by the magnetosphere.

For the first time, in 1993, a very sophisticated experience (MAST, in the satellite SAMPEX), using active solid state detectors, resulted in the measurement of these particles in the magnetosphere, as well as registering the time, position and direction of arrival of the particles. A new ion radiation belt was then found around Earth (L=2), composed of ACR, similar to those well-known Van Allen belts. This has a fundamental importance, as it allows the study of interstellar atom samples close to the Earth.

The telescope ORCAS, on board the Brazilian Scientific Satellite to be launched during the period of minimum salar activity, will have the capacity to measure fluxes, spectra and composition, temporal and spatial variations of ions from He to Ne, and protons and electrons with energy less than 50 MeV/amu. The main objective of the ORCAS telescope is to measure ACR fluxes, from C to Ne, "trapped" in the belt, using solid state detectors, identifying the time and direction of arrival of the particles. Although the ORCAS telescope is 3-4 times smaller in geometric factor, the flux to be measured will be better by a factor of 2 to 10 in comparison with MAST, as the intensity of the ACR trapped, expected for the period of 1996-98, will be at least 20 to 30 times greater than the measured by the SAMPEX in 1992-94.

Addtionally, the MAST experiment determined the ion belt of L=2.0 $\pm$ 0.2. Is this due to the fact that the SAMPEX-MAST have measured only 5 to 10% of the radiation population? In conditions of minimum solar activity with intense fluxes, the ORCAS telescope will allow studies of the space distribution and the dynamics associated of the population of the trapped particles.

The second important aspect is the presence of He ions, as it is not expected to find He in the population of ACR in this altitude. Only during solar eruptions the He was observed by the satellites INJUN and OHZORA. SAMPEX observed again a thin belt of He at L=1.8. The source of the He and the mechanisms of its entrance and trapping in the magnetosphere is an interesting problem. The ORCAS telescope as well as measuring the He flux will determine its source, as during the ORCAS experiment few solar eruptions are expected.

Mission:

The SACI spacecraft is a low orbit satellite for scientific purposes. The satellite will be put in a circular orbit inclined about 98 degrees to the Earth equatorial plane at an altitude near 750 km. It is scheduled to be launched, together with CBERS (China-Brazil Earth Resource Satellite), by a Chinese Long March rocket. It is expected to fly in 1997. During the passes visible either from the tracking stations or user's ground data collecting stations, scientific data will be transmitted to ground. The data can be produced in a longer time and stored in the on board computer. A communications system is responsible for sending to the ground the housekeeping telemetry, receiving the telecommand, and will also send scientific data to the ground. Dual cold redundant transmitters provides standard S-band (2255.5 MHz) telecommunication satellite to ground with BPSK modulation and 128, 256 or 512 kbits/s selected data transmission rate. The development of the microsatellite shall be done in less than 18 months. The total cost, including bus and scientific payloads, shall be less than US$ 4.6 million.

Spacecraft configuration:

The total satellite mass is less than 60 kg and the payload mass does not exceed 20 kg. The dimensions are 600 x 400 x 400 mm (parallelepiped). The conception is modular, with simple technical solutions. The thermal control shall be passive. The satellite expected lifetime is 18 months. The payload power requirement is 30 W and a solar array generator, which is composed of four deployable panels assembled on the solar side of the spacecraft structure, provides the necessary electrical power. The solar cells are made of GaAs/Ge with cover glass microsheet and silver plated invar interconnections and are expected to generate about 125 W.

The SACI-1 satellite attitude control system combines passive spin stabilization procedure with active spin rate and precession control. The actuators are three magnetic torque coils which interact with the Earth magnetic field to generate the necesary control torques. The pointing accuracy is 1 degree.

3 The future

3.1 The coming opportunities

It is expected in the forthcoming years that a large number of opportunities for launching a satellite become available. The newborn Brazilian Space Agency (AEB) is trying to stimulate international collaborations in order to broaden the space activities in Brazil, so the potential partners are Argentina, China, France, Russia, United States, and other countries as well, specially latin american countries. It is important to stress that international collaboration is the best way to conduct a satellite project, since it lowers the costs and adds technology to the country in a direct way, as simple technological transfer from developed countries, or indirectly, stimulating local industries to produce space qualified systems and components. The latter situation is also valid for a genuine Brazilian experiment.

3.2 Strategy for getting in space

In order to carry out experiments in space using the already existing Brazilian facilities and expertise in this area, it is imperative to coordinate actions that will lead to the design, building, testing and operation of the experiment. First of all, the science is, of course, the main factor to be considered. The mission technical constraints as mass limit and pointing accuracy are critical and very limiting points to be considered, since a dedicated launching will be very difficult for the first missions. After that, there is a need to search for funding. This is a crucial problem, since it does not make any sense to drain all the available resources from the financing agencies and stop other astronomical projects, namely the ground based experiments or other space-based experiments. So, it is important to obtain independent support from the funding agencies (e.g. CNPq, FINEP, FAPESP) and guarantee the continuity of the ongoing non-satellite based projects.

It is also important to bear in mind that one needs to use the available know-how to build both the spacecraft and payload in order to estimulate the training of individuals. This action will be extremely helpful for other missions or even non-space projects like new optical or radio telescopes. On the other hand, using the available human and technical resources helps to lower costs and development time. It became a tradition in the astronomical community to propose experiments in which the scientific instruments are built abroad with no (or almost none) interaction of Brazilian scientists and technicians. The reasons are obvious and reside mainly on the lack of human resources, but this needs to be changed. There is no tradition in the development of astronomical instrumentation in Brazil and most of the scientific work produced here is based on data analysis or theoretical approaches. A space-based scientific experiment has the merit to promote the advancement of the experimental astronomical activities in Brazil. It will be very difficult in the first missions to achieve this goal, but it is extremely important to stimulate such a change in our community.

4 Conclusion

It is necessary to start a long term program to capacitate Brazilian scientists, engineers and technicians to acquire space technology. The graduate programs should try as much as possible to involve the new students in experimental projects aiming satellite instruments. It seems that this is the only way to get a deep involvement with this new opportunity openned up to Astronomy and Astrophysics in the country. This program can no longer be delayed if the Brazilian scientists want to take a step forward to advance Astronomy and Astrophysics in Brazil.

The response for the Announcement of Opportunity for the first Brazilian scientific micro-satellite showed that the astronomical community in Brazil is not yet prepared to answer these calls. Apart from the ORCAS experiment and an X-ray polarimeter (which did not meet the mass limit requirement), no one else related to the astronomical community submitted a proposal. Several reasons lead to this situation, such as the very low mass allocated to the payload and the very short time for the preparation of

the proposals. A new Announcement of Opportunity, probably for a joint Brazil-France experiment, will be delivered late this year or early next year and we hope that several Brazilian proposals will be submitted in order to start the long term project proposed above.

Acknowledgement: I thank Alex Wuensche and João Braga for the reading of the manuscript and suggestions.

References

Laboratório de Integração e Testes - LIT, *folder*, INPE.

SAC-B - Satélite de Aplicaciones Científicas, *folder*, CONAE, 1993.

Satélite de Aplicações Científicas - SACI-1, *Technical Report 1*, INPE and AEB, 1995.

Section 4

Galactic Astronomy and Interstellar Medium

CHEMICAL COMPOSITION IN PHOTOIONIZED NEBULAE: THE PROBLEM OF THE TEMPERATURE DETERMINATION

Ruth Gruenwald
Instituto Astronômico e Geofísico, USP

Abstract

A good determination of the chemical composition in nebulae is important for an evolutionary study of a given class of objects, and for the knowledge of the chemical evolution of our, as well as of other galaxies. We describe here the methods generally used for the chemical abundance determination in photoionized nebulae. In particular, the methods for the calculation of the gas temperature, which is an important parameter for the determination of the abundances, are discussed.

1 Introduction

Basically, there are two methods for the abundance determination in gaseous nebulae. One method is the use of a detailed photoionization model, applied to a specific object, which fits a great number of observational data. This method requires a good set of observed data, from a great number of lines, for each particular object. When a great number of objects is treated, an empirical method is generally used. This method follows the schema proposed by Peimbert (1967) and Peimbert & Costero (1969). In this case, the abundance of an ion which produces an observed line λ can be calculated, relative to H^+, from the measured intensities of the line λ and of Hβ, knowing the gas density and temperature. Applying correction ionization factors in order to take into account ions which do not have observed lines, the corresponding elemental abundance can then be calculated. The abundance of an ion X^i, relative to the ion H^+ can be calculated from the equation

$$\frac{n(X^i)}{n(H^+)} = \frac{I_\lambda}{I_{H\beta}} \frac{\epsilon(T_{H\beta}, n_e)}{\epsilon(T_\lambda, n_e)} \tag{1}$$

where

$n(X^i)$ is the abundance of the element X in the ith ionization state;

$n(H^+)$ is the abundance of ionized hydrogen;

I_λ is the measured intensity of the line with wavelength λ, produced by the ion X^i;

$\epsilon(T_\lambda, n_e)$ is the emissivity of the line λ in a given temperature T_λ and a given electron density n_e. The temperature T_λ is the gas temperature in the region where the line is produced.

The electron density in a object with constant density is practically constant inside the ionized region, and generally do not present any problem. So, the empirical method is based in a good temperature determination.

There are several methods for the determination of the temperature in a gaseous region. For example, the temperature can be determined from the intensity ratio of auroral to nebular forbidden lines, from the ratio of the intensity of free-bound continuum to the intensity of a hydrogen line, or from the ratio of the free-free continuum intensity to the intensity of a hydrogen line. The problem is that, in general, different methods provide different values for the temperature. For example, in many cases the temperature given by the intensity of O^{++} forbidden lines ($T_{[OIII]}$) are higher than temperatures given by the Balmer discontinuity (T_{Bal}). This fact is generally explained by the presence of temperature fluctuations in the gas. Thus, if there are temperature fluctuations inside the gas the obtained value for the gas temperature from the observational data is strongly dependent of the method used and consequently the abundance will also depend on the method used for the determination of the temperature.

2 Temperature determination

Peimbert and Costero (1969) suggested a quantitative definition in order to caracterize the temperature fluctuation (t^2) and obtained also relationships between the different definitions for the temperature and t^2. If an average temperature is defined for the region where the ion X^i is present

$$T_o(X^i) = \frac{\int T_e(r) n(X^i, r) n_e(r) dV}{\int n(X^i, r) n_e(r) dV} \tag{2}$$

the temperature fluctuation for this ion is defined by

$$t^2(X^i) = \frac{\int \mid T_e^2(r) - T_o^2(X^i) \mid n(X^i, r) n_e(r) dV}{T_o^2(X^i) \int n(X^i, r) n_e(r) dV} \tag{3}$$

The integrals are calculated over the total volume of the ionized region, r corresponding to a given point inside the region.

A temperature obtained from the intensity ratio of two lines produced by a given ion can be written as a function of the average temperature T_o and of t^2 for the ion. For example, the following relationship is valid for the temperature obtained from the intensity ratio of forbidden lines produced by the ion O^{++}:

$$T_{[OIII]} = T_o [1 + (\frac{90800}{T_o} - 3) \frac{t^2}{2}] \tag{4}$$

valid for low values of t^2. In this equation, T_o and t^2 correspond to the ion O^{++}.

Peimbert and Costero (1969) also defined a characteristic value for the temperature (T_λ) of the region where a line with wavelength λ is produced by an ion X^i. This temperature can be written as a function of the average temperature T_o and of t^2 for the ion. The value of T_λ, called the "line temperature", would then be the most appropriated value to be used in the equation that determine the ionic abundance from the measured intensity of a line produced by this ion (Eq. 1). Briefly, for the determination of the

abundance of a given ion, the line temperature must be calculated. This temperature, in turn, can be obtained from the average temperature of the region where the ion exists, and from the temperature fluctuation of the ion.

Since it is not possible to determine t^2 and T_o for each ion from the observations, some approximations are usually done in the literature. In general, no temperature fluctuation is considered (t^2=0), e.g., the nebula is isothermal. In this case, the average temperature of the ions and, consequently the line temperatures, are taken equal to the temperature obtained from an observed forbidden line intensity ratio, generally $T_{[OIII]}$. When both $T_{[NII]}$ and $T_{[OIII]}$ are available, $T_{[NII]}$ is taken as the average temperature of the low ionization ions, while $T_{[OIII]}$ is considered to represent the average temperature of high ionization ions. These temperatures are then considered to represent the line temperatures. Using some appoximations, a value for t^2 can be obtained from the observations. In this case, it is assumed that T_o and t^2 are the same for all ions. The values for T_o and t^2 can then be obtained from two equations relating these parameters and observed temperatures. When more lines are observed, these parameteres can be obtained separately for the low and high ionization zones. These methods provide high values for t^2 (> 0.01) when applyed for some HII regions (Torres-Peimbert & Peimbert 1977), or when averages are obtained from HII regions and planetary nebulae (Peimbert & Torres-Peimbert 1971). In the literature, these values obtained for t^2 are applied in the determination of chemical abundances in HII regions as well in planetary nebulae.

In a detailed study for the planetary nebula NGC 7662, Harrington et al. (1982) obtained theoretical values for t^2 for this nebula; they argue that the values obtained for t^2 by Peimbert and collaborators are too large. However, in an observational study of several PNe, Liu & Danziger (1993) also find high values for t^2.

2.1 Temperature fluctuations in HII regions

Temperature fluctuations have been discussed in detail for HII regions (Gruenwald & Viegas 1992). Using a self-consistent photoionization code, they obtained theoretical values for the temperature fluctuation in a gas with typical physical conditions of HII regions. They also tested different hypotheses assumed in the empirical methods. The ionizing central source used in the calculations represent typical main sequence stars, with temperatures between 30900 K (B stars) and 50000 K (O4 stars). Models with black-body spectra as well as with different model atmospheres were also analysed. The gas density, also typical of HII regions, ranges between 1 and 10^3 cm^{-3}, while the abundances varies between three times the solar to $Z_\odot/100$. The results show that the value of t^2 obtained from theoretical models ranges from 0 to 0.21 for a central source emitting as a black-body, and its exact value depends on the considered ion, gas abundance, gas density, and stellar ionizing flux. In particular, t^2 decreases rapidly with increasing gas density. Ions of the same ionization degree do not have necessarily the same value of t^2. The stellar temperature is also an important parameter, but the t^2 dependence is not monotonic. Regions with higher abundances have higher temperature fluctuations. Different model atmospheres lead to different t^2 for a given ion. To illustrate the results of Gruenwald

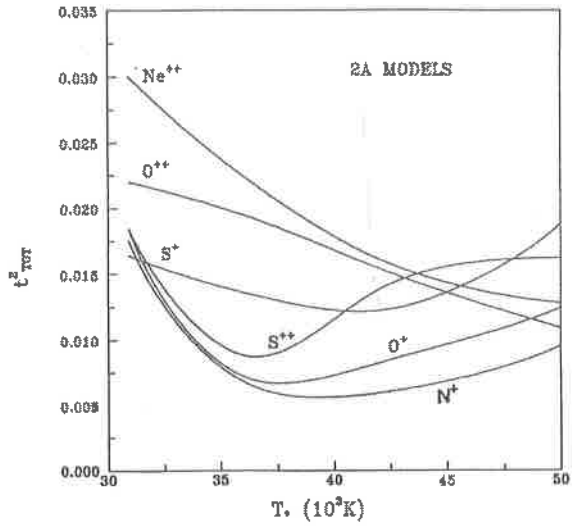

Figure 1: Temperature fluctuation versus black-body stellar temperature. Labels refer to the name of the corresponding ion. Models use typical parameters for HII regions and its ionizing star

& Viegas (1992), Fig. 1 shows the behaviour of t^2 with the stellar temperature for ions which produce observed lines in the spectrum of HII regions and which are commonly used for abundance determination. In the figure, the gas has a solar abundance and a density equal to 100 cm^{-3}. A comparison of the theoretical results with those obtained from the empirical relationships of Peimbert and collaborators showed that these relationships are better than 10% for t^2 less than 0.02; for greater values of t^2, the error increases steeply. Empirical ionizing correction factors were also analysed; a factor up to 3 is found between theoretical and empirical results for the elemental abundances (up to 10 for S). An estimate of the effect of t^2 in the calculation of the abundances is not straightfoward, since there is the effect of the temperature fluctuation of the ions (including H^+) on the ionic abundances and consequently on the ionization correction factors (even if their empirical formula are correct). Regarding the effect on the ionic abundances relative to H^+, the use of $t^2 = 0$ can lead to an error up to 3 (greater for oversolar abundances).

2.2 Temperature fluctuations in planetary nebulae

As said above, from a model obtained for the planetary nebula NGC 7662, Harrigton et al (1982) questioned the values obtained for t^2 from the observations. In their model for NGC 7662 they obtained values for t^2 much smaller then those provided by the observations. As also discussed above, these observed values are in general obtained for HII regions, or from an average for planetary nebulae (PNe) and HII regions. PNe have in general higher density, lower metalicity, and higher stellar temperature, when compared to HII regions. The results of Gruenwald & Viegas' (1992) analysis show that, for HII regions, t^2 is lower for high density objects. Although PNe are denser than HII regions, their central stars are usually hotter and t^2 may be significant.

Dinerstein *at al.* (1985) from $T_{[OIII]}$ obtained from two line intensity ratios produced by the ion O^{++} in the optical and in the infrared, obtained for 4 PNe high values for $t^2(O^{++})$, greater than 0.03.

Liu and Danziger (1993), in an observational study for several planetary nebulae, assumed that t^2 and T_o are the same for O^{++} and H^+. High values were obtained for t^2, of the order of 0.03; for some objects t^2 are greater than 0.10.

In order to analyse values for temperature fluctuations specific for planetary nebulae, Gruenwald & Viegas (1995) obtained theoretical values for t^2 in physical conditions typical of this kind of objects. The central ionizing source was represented by stars with temperature in the range 30000 K to 300000 K and luminosities variyng from 10 to 20000 $L_\odot$. The gas density ranges between 10^2 to 10^6 cm^{-3}. These values, following Pottasch (1984) are typical values for planetary nebulae and their central stars. The assumed abundances are those from Stasinska & Tylenda (1986).

The obtained values for t^2 range from $\simeq$0 to 0.50, and depend, as for HII regions, on the specific ion, and on the nebular as well as on the central star parameters. For the ions generally used for abundance determinations, t^2 ranges from $\simeq$ 0 to 0.15. Figs. 2 (a), (b), and (c) show t^2 versus the effective temperature of the central star with a luminosity of 3000 $L_\odot$. In these figures, the gas density is, respectively, 10^2, 10^4, and 10^6 cm^{-3}. The behaviour of t^2 for stellar temperatures less than 50000 K, for a given gas density, obtained for HII regions (Gruenwald & Viegas 1992) differs from those obtained for PNe due to differences in the central stellar luminosity between these two kind of objects. Part of the t^2 difference may be due to the adopted chemical abundance for PNe which are sligthly different from those typical of HII regions. As shown in the figures, ions of different elements in the same ionization stage can have different values of t^2. It can be also be notice that $t^2(S^+)$ is very sensitive to the stellar temperature. While $t^2(H^+)$ is strongly dependent on the stellar temperature for high densities, $t^2(O^{++})$ is not important. In the literature the temperature fluctuation for these two ions are generally assumed to be the same. From the figures it can be also noticed that t^2 generally increases with the stellar temperature, and for high stellar temperatures the temperature fluctuations can be important even for high densities. Low ionizations ions, like N^o, have high t^2 (up to 0.20). If these low ionization lines are used, misleading values of abundances can be obtained. Figs. 3 (a) and (b), show for densities of 10^2 and 10^6 cm^{-3}, respectively, the behaviour of T_{Bal}, $T_{[OIII]}$, and the line temperature for the [OIII]λ5007, T_{5007}, with the stellar temperature. Theses figures show the results for a stellar luminosity of 3000 $L_\odot$. It can be noticed from the figures that for high stellar temperatures and high gas densities the line temperature can not, for example, be taken to be equal to the temperature obtained from the forbidden intensity lines as it is usually done.

Comparing the results for t^2 of Gruenwald & Viegas (1995) with those from the literature, for NGC 7662 they agree with those obtained theoretically by Harrington *al* (1982) for the same nebula. Regarding the values obtained observationally by Liu & Danziger (1993), values for t^2 for 7 out of 11 objects, are in agreement. Notice, however, that these authors considered that the average temperature and the temperature fluctuation are the same for O^{++} and H^+ ions. A comparison with the values obtained from the observations

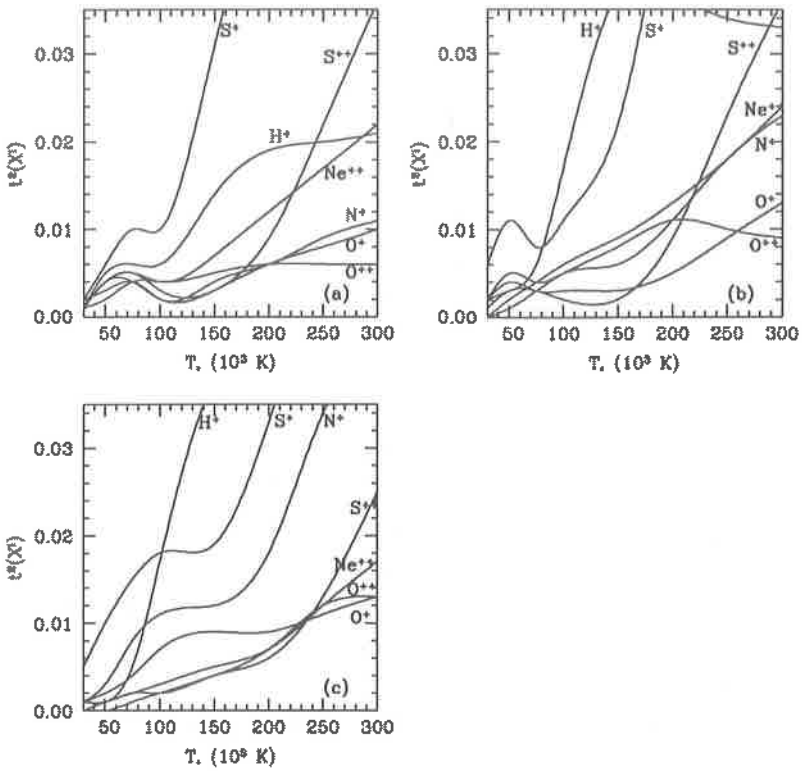

Figure 2: Temperature fluctuation versus stellar temperature for stellar luminosity $L/L_{\odot}$ = 3000. Figures (a), (b), and (c), correspond to densitues of 10^2, 10^4, and 10^6 cm^{-3}, respectively. The parameters are typical of PNe and their central ionizing star

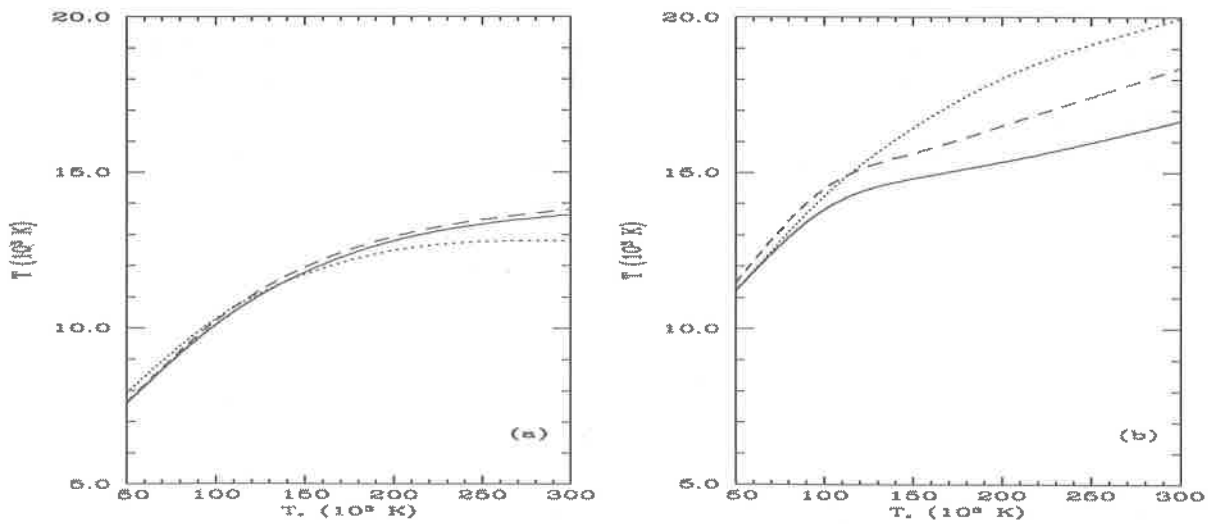

Figure 3: Values for the gas temperatures versus stellar temperature. Solid lines refer to T_{5007}, dotted lines to T_{Bal}, and dashed lines to $T_{[OIII]}$. densities for Fig. 3 (a) and (b) are, respectively, 10^2 and 10^6 cm^{-3}. The luminosity is 3000 $L_{\odot}$

Table 1. Parameters of the studied Planetary Nebulae

Object	T_*	$L_*/L_\odot$	n
NGC 650	150000	300	4780
NGC 2438	145000	120	500
NGC 2440	280000	*a*	5400
NGC 2452	121000	1300	2130
NGC 2818	210000	220	800
NGC 2867	130000	2500	4510
NGC 3211	150000	1900	900
NGC 3587	108000	44	4570
NGC 3918	141000	4200	6200
NGC 6302	224000	1780	25520
NGC 6309	100000	4300	2710
NGC 6439	147000	3600	4000
NGC 6445	191000	255	2470
NGC 6537	200000	745	15490
NGC 6565	130000	930	300
NGC 6720	134000	530	600
NGC 6741	175000	3180	11600
NGC 6818	191000	1820	2050
NGC 6853	147000	110	4540
NGC 6886	143000	6300	7180
NGC 6905	103500	1350	870
NGC 7027	174000	12700	82800
NGC 7293	110000	36	225
NGC 7662	112000	10700	3250
IC 2165	158000	5200	3930
Hu 1-2	130000	*b*	4100
J 900	129000	4700	3200

by Dinerstein *et al* (1985) show an agreement for 1 out of 4 objects. However, there are great incertantities in these infrared observations, and at least 2 of these 4 objects are clearly asymmetrical, while the theoretical models assume a spherical symmetrical geometry.

As discussed above, temperature fluctuations can be important for planetary nebulae whose central star has a high temperature ($\geq$ 100000 K). An application for planetary nebulae with a high temperature star was also done in Gruenwald & Viegas (1995). Planetary nebulae with high temperature were selected in the literature, and models were performed for those with known stellar luminosity and density. The selected objects are given in Table 1. In the table, the columns correspond to the name of the object, its central stellar temperature (in K degrees) and luminosity (in units of $L_{\odot}$), and gas density (in cm^{-3}). Using the model with the most similar input parameters, temperature fluctuations for each ion were then obtained. With these values for $t^2(X^i)$ and observed values for the line intensities obtained from the literature, ionic abundances were then calculated. When no temperature fluctuation is considered, lower values for the ionic abundances are obtained. However, for the analysed objects, the differences for the ionic abundances calculated with and without considering temperature fluctuations, are in general less than 10%. For nineteen out of 27 nebulae, one or more ions have a difference of up to 20%. The exception is S^+, with a difference of up to 40%.

3 Conclusions and perspectives

The results of the precedent sections show that the temperature fluctuation for a given ion can be important depending on the physical conditions of the nebula. A high temperature fluctuation can affect the determination of the abundances in a nebula. An analysis for some planetary nebulae with high stellar tempaerature, showed, however, that the combining effect of temperature fluctuations in the various parameters that enter in the calculation of ionic abundances affect the results in less than 40%.

The theoretical calculations up to now assume a spherical symmetrical geometry for the ionized gas and a homogeneous distribution for the density. However, in addition to the ionization distribution, some other factors can produce spatial fluctuation of the temperature. The effect of density variations on $T_{[OIII]}$ and T_{Bal} were studied by Viegas & Clegg (1994). Regions which present chemical abundance inhomogeneities as well as multiple interconnected HII regions can also present temperature fluctuations. For a more detailed study of asymmetrical and/or inhomogeneous regions, a 3-dimensional code was developed, and an aplication to bipolar planetary nebulae is under progress (Gruenwald & Viegas, in preparation).

References

[1] Dinerstein, H.L., Lester, D.F., Werner, M.W. 1985, ApJ 314, 551

[2] Gruenwald, R., Viegas, S.M. 1992, ApJS 78, 153

[3] Gruenwald, R., Viegas, S.M. 1995, A & A 303, 535

[4] Harrington, J.P., Seaton, M.J., Adams, S, and Lutz, J.H. 1982, MNRAS 199, 517

[5] Liu, X., Danziger, J. 1993, MNRAS 263, 256

[6] Peimbert, M. 1967, ApJ 150, 825

[7] Peimbert, M., Costero, R., 1969, Bol. Obs. Tonz. y Tac. 5,3

[8] Peimbert, M., Torres-Peimbert, S. 1971, ApJ 168, 413

[9] Pottasch, S. 1984, "Planetary nebulae", D.Reidel

[10] Torres-Peimbert, S., Peimbert, M. 1977, Rev. Mex. Astron. Astrofis. 2, 181

[11] Stasinska, G., Tylenda. R. 1986, A & A 155,137

[12] Viegas, S.M., Clegg, R.E.S. 1994, MNRAS 272, 993

THE INTERESTELLAR EXTINCTION CURVE AND THE POLYCYCLIC AROMATIC HYDROCARBON

Heloisa M. Boechat-Roberty (Observatório do Valongo - UFRJ)
Marcelo B. Fernandes (Observatório do Valongo - UFRJ)
Carlos A. Lucas (Instituto de Química - UFF)
M. Luiza Rocco (Instituto de Química - UFRJ)
G.Gerson B. de Souza (Instituto de Química - UFRJ)

Abstract

The interestellar extinction curve at ultraviolet region has a broad bump centered at 2175 Å(5.7 eV) with a width at about 480 Å. It has been sugested that the absorption peak is caused by small grains and by polycyclic aromatic hydocarbon molecules (PAHs). Electron energy-loss spetra were obtained in laboratory at vacuum ultraviolet region in several scattering angles for naphthalene and benzene molecules in order to determine cross section and oscillator strength of transitions in this region. Near zero scattering angle the incident electrons behavior like pseudophotons and the electron energy-loss spectra are considered as photoabsorption spectra. By comparision of the energy-loss spetrum with the interestellar extiction curve, a strong absorption at 5.9 eV (2138 Å) was observed that can be confirm the contribution of this molecules for the interestellar extinction.

1. INTRODUCTION

The interestellar extinction of starlight is due to the absorption and scattering processes by the interestellar matter. The extinction curve shows the behavior of the normalized color excess in magnitudes $E(\lambda-V)/E(B-V)$ as a function of $1/\lambda$ in μm^{-1}. Average normalized curve obtained from a number of determinations is illustrated in Figure 1 (Savage and Mathis 1979). At ultraviolet region a broad bump centered at 2175 Å (5.7 eV) with a width at about 480 Å has been sugested that is caused by small particles (Boulanger et al. 1994) and by polycyclic aromatic hydorcarbon molecules PAHs (Joblin et al 1992). The PHAs molecules have been found in several objects such as planetary nebulae, reflection nebulae. The infrared emission bands at 3.3, 6.2, 7.7, 8.6 and 11.3 μm known as the unidentified infrared band were interpreted as beeing due to PHAs. The aromatic structure of this molecules provides the stability necessary for a long life-times in the interestellar medium, and allows for the conversion ultraviolet energy into infrared emisson bands by the fluorescence mechanism (Leger and Puget 1984). Electron energy-loss spectroscopy has been used for determination of excitation energies, cross section and oscillator strengths of valence (Boechat-Roberty and de Souza 1992) and core-level excitations (Boechat-Roberty et al 1991). As part of a systematic study of the angular behavior of electron impact excitation, we present in this paper the generalized oscillator strength (GOS) for the $^1B_{1u} \leftarrow ^1A_g$ transition (5.9 eV) in the naphthalene molecule and the electron energy-loss spectra for the benzene molecule.

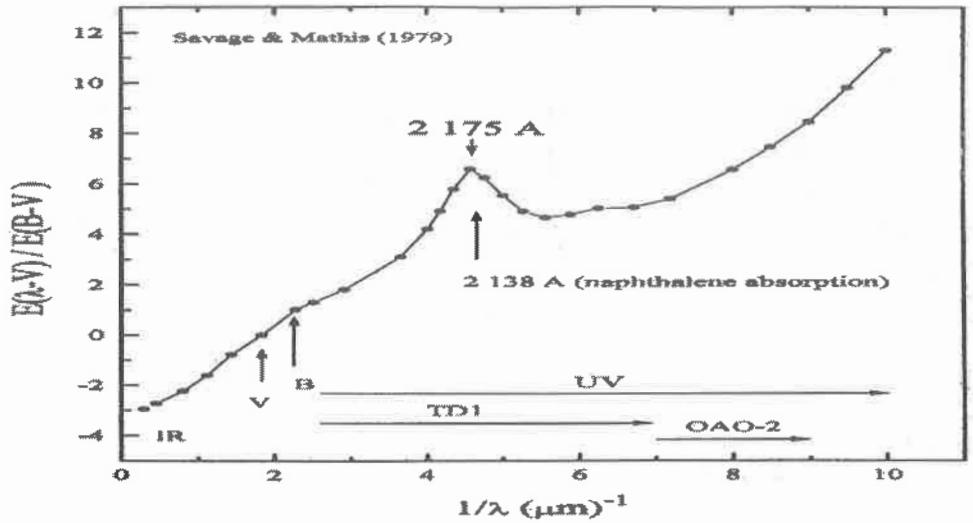

Figure 1: Interestellar extinction curve (Savage and Mathis 1979).

2. THEORY

The differential cross section, $(d\sigma/d\Omega)$, for the excitation of a molecule with N electrons and M nuclei by an electron with kinetic energy E is given by the following expression:

$$\left(\frac{d\sigma}{d\Omega}\right)_n = \frac{4}{|\mathbf{K}|^4}\,\frac{|\mathbf{k_f}|}{|\mathbf{k_i}|}\,|\epsilon_n(K)|^2 \tag{1}$$

Here n represents the final excited state, $\mathbf{K}$ is the momentum transfer, $\mathbf{K} = \mathbf{k_i} - \mathbf{k_f}$, and $\mathbf{k_i}$ and $\mathbf{k_f}$ are, respectively, the initial and the final momentum vectors for the scattered electron and $\epsilon(K)$ the scattering amplitude. A very useful quantity is the Generalized Oscillator Strength (GOS), $f_n(K)$, defined as

$$f_n(K) = \frac{2E}{|\mathbf{K}|^2}\,|\,\epsilon_n(K)|^2 \tag{2}$$

where E is the excitation energy and $|\mathbf{K}|^2$ is given by

$$|\mathbf{K}|^2 = |\mathbf{k_i}|^2 + |\mathbf{k_f}|^2 - 2\mathbf{k_i}\mathbf{k_f}\cos\theta \tag{3}$$

where θ is the scattering angle. Substituing $|\epsilon_n(K)|^2$ from equation (1) into equation (2) gives

$$f_n(K) = \frac{E}{2}\left(\frac{|\mathbf{k_i}|}{|\mathbf{k_f}|}\right)|\mathbf{K}|^2\left(\frac{\mathbf{d}\sigma}{\mathbf{d}\Omega}\right) \tag{4}$$

The GOS, useful in the electron-scattering theory, is independent of the incident energy at energies for which the First Born Approximation is valid and approaches

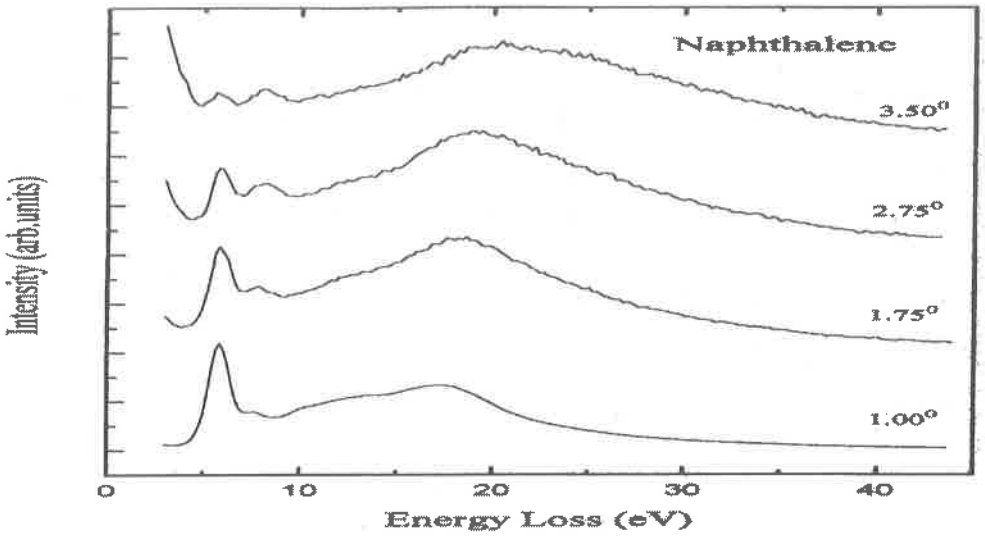

Figura 2: Electron energy-loss spectra for naphtalene molecule measured at scattering angles 1.00^0, 1.75^0, 2.75^0, 3.50^0.

the familiar Optical Oscillator Strength (OOS) as $K \to 0$. It means that, at small scattering angle or at higth impact energies the electron energy-loss spectra are similar to photoabsorption spectra. A very interesting review of the GOS properties can also be found in Inokuti (1971).

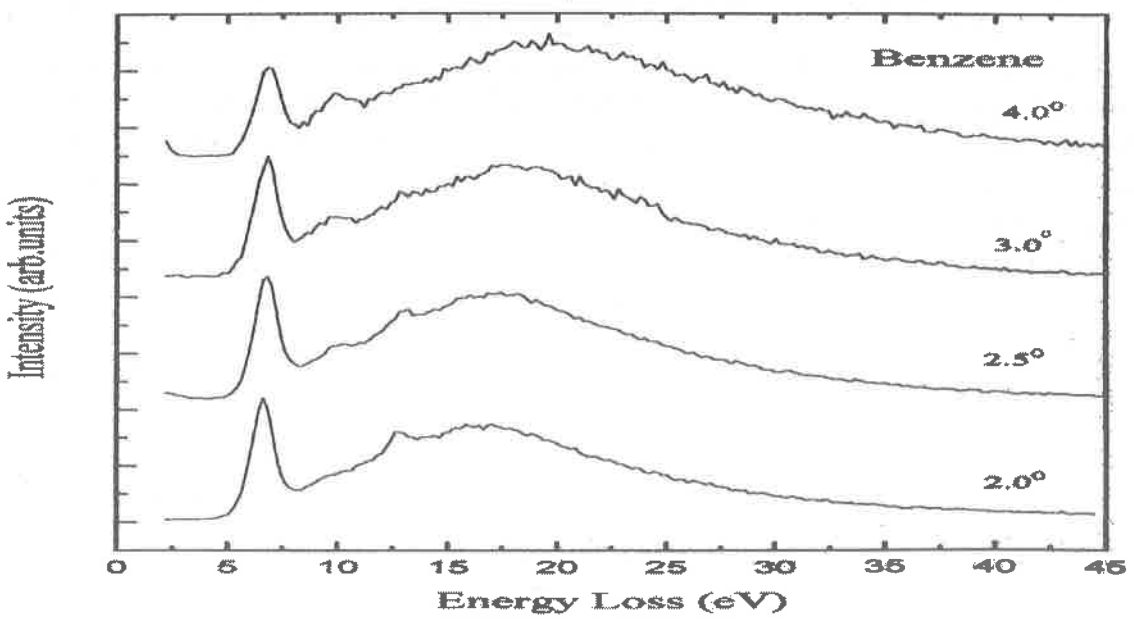

Figure 3: Electron energy-loss spectra for benzene molecule measured at different scattering angles.

3. EXPERIMENT

The same basic experimental procedure previously adopted in the determination of the oscillator strength for other excitation processes in different targets was used in the present work. Briefly, electron energy-loss spectra using a crossed-beam spectrometer were measured for a given set of scattering angles at a fixed impact energy. The crossed-beam spectrometer used in the present work has been described before (Boechat Roberty et al 1991). In order to obtain a higher luminosity and to work in a constant transmission mode, a newly developed Wien Filter type velocity analyzer was incorporated into the energy-loss spectrometer. The Wien Filter analyzer features two three-element zoom lenses. The first one brings the scattered electrons to a fixed pass-energy, for example 30 eV, resulting in an energy resolution of 0.8 eV, as determined by the full width at half maximum for the elastic peak, measured in the same conditions. The second zoom lens re-accelerates the electrons in order to increase the detection efficiency. The energy resolution of the apparatus is limited to 0.5 eV by the thermionically produced incident electrons. In the present case, though, a compromise was attained between resolution and count rate. The velocity-analyzed scattered electrons are detected by an electron multiplier (Spiraltron, Galileo Electro Optics). The pulses coming out of the detector are fed to a standard electronics (preamplifier, amplifier, discriminator) and are then then transferred to the memory of a 16-bits personal microcomputer which is also responsible for the scanning of the voltages in the zoom lenses. In the present measurements the incident electron energy was 1000 eV and the energy-loss spectra were obtained in the angular range of 1.0^0 - 4.0^0, with energy resolution of 0.8 eV. The scattering zero-degree angle was checked by measuring the elastic peak area over a 15^0 range on both the right hand and the left hand side with respect to the electron analyzer main geometrical axis. Although a precision mechanism allows the determination of the scattered angle with an accuracy of 0.02^0, our angle resolution, defined by the set of apertures in front of the electron analyzer, is limited to 0.23^0 in the present experiments. The area for the peak corresponding to transition was determined using a Gaussian fitting procedure previously discussed. The background contribution was determined by measuring the spectra at the same scattering angles, but allowing the gas to enter the scattering chamber trough a side flange, located far from the collision center. This contribution was then subtracted from the raw data. As the main interest consisted in the determination of the behavior of the area of the peak as a function of the scattering angle, great care was taken in order to make sure that all the spectra were obtained in the same experimental conditions. The experimental uncertainties are estimated in the following manner. The maximum statistical uncertainty was 3.5% as at least 2.300 counts were accumulated at the peak of interest for each scattering angle. Fluctuations in the primary beam current and on the sample pressure were of the order of 1% and 0.5% , respectively. The main source of error is the limited angular resolution (0.23^0) which depends on the scattering angle. The determination of the area of the peak is also subject to an error of 2%. The overall uncertainty, δ, defined as $\delta = (\sum \delta_i^2)^{1/2}$, is equal to approximately 6% for small angles, and 4% for large angles.

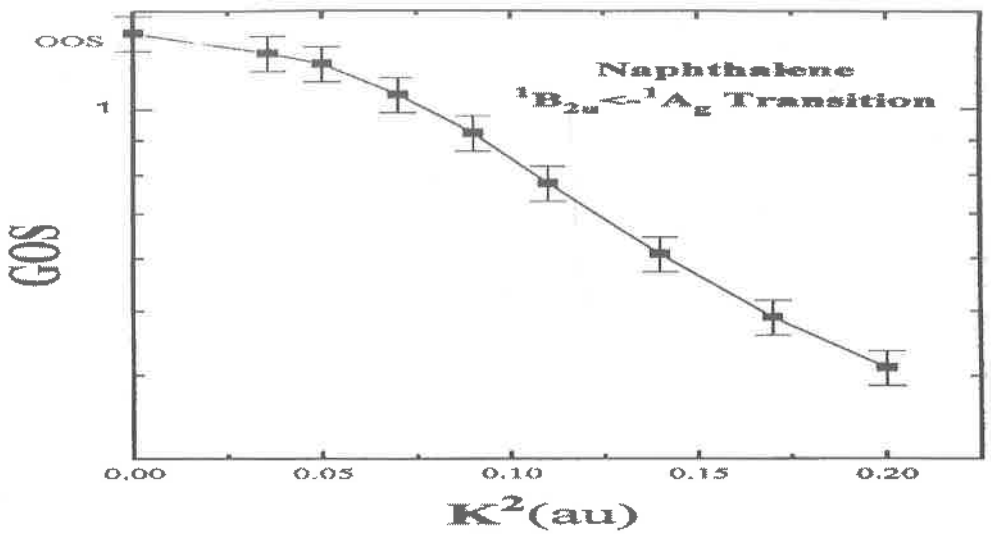

Figure 4: : Generalized oscillator strength (GOS) as a function of square momentum tranfer, K^2, for the $^1B_{1u} \leftarrow ^1A_g$ transition in the naphthalene molecule.

4. RESULTS AND DISCUSSION

The electron energy-loss spectra for naphthalene and benzene molecules measured at different scattering angle are shown in Figure 2 and Figure 3, respectively. The spectra, where the energy-loss corresponds to excitation energy, exhibit strong absorption in 5.9 eV (2138 Å) for the naphthalene and 6.8 eV (1823 Å) for the benzene molecule, both due to dipole-allowed transitions π and π^*. As a result the spetra obtained at small scattering angles resemble that measured by other absorption techniques. At highter electron scattering angles dipole-forbidden processes can also be observed, a major advantage of this technique over other conventional absorption techniques. The strong naphthalene absorption is near of the $\lambda = 2175\AA$ feature seen in the UV extinction curve. We determined the GOS as a function of K^2 for the $^1B_{1u} \leftarrow ^1A_g$ transition in the naphthalene molecule shown in Figure 4. The value of the optical oscillator strength (1.3) was obtained by the GOS curve extrapolation to zero scattering angle or $K^2 \rightarrow 0$.

5. CONCLUSION

We have obtained electron energy-loss spetra in laboratory at vacuum ultraviolet region in several scattering angles for naphthalene and benzene molecules and determined cross section and generalized oscillator strength (GOS) for the $^1B_{1u} \leftarrow ^1A_g$ transition in the naphthalene molecule. Near zero scattering angle the electron energy-loss spectra are considered as photoabsorption spectra. By comparision of the energy-loss spetrum with the interestellar extiction curve, we suggest that the strong naphthalene absorption at 5.9 eV (2138 Å) contributes to the UV bump and benzene molecule can contribute for the interestellar extinction.

6. REFERENCES

Boechat-Roberty H. M., Bielschowsky C.E., de Souza G.G.B.,1991, Phys. Rev. A **44**, 1694
Boechat-Roberty H. M., de Souza G.G.B 1992, J. Phys. B:At.Mol.Opt.Phys. **25**, 4641
Boulanger F., Prévot M.L., Gry C. 1994, Astron. Astrophys. **284**, 956
Inokuti M., 1971, Rev. Mod. Phys. **43**, 297
Léger A, Puget J.L., 1984, Astron. Astrophys. **137**, L5-L8
Savage B. D., Mathis J. 1979, Ann. Rev. Astron. Astrophys. **17**, 73

STRUCTURE OF INTERSTELLAR MEDIUM: A MULTIVARIATE APPROACH

Jorge R. Ducati
Jandyra M.G. Fachel

Institutos de Física e Matemática,
Universidade Federal do Rio Grande do Sul,
Porto Alegre, Brasil

Abstract

Some techniques from multivariate data analysis are presented. Applications to infrared data of stars show how the method helps to identify classes of stars and anomalous effects like circumstellar emission, and to detect observational errors.

Key words: statistical methods - interstellar medium - infrared

1 Introduction

New instruments and techniques to collect astronomical data have generated an increasing inflow of information available to investigators, to the point that presently only a small fraction of the stored information in all regions of the electromagnetic spectrum, or from cosmic rays, is effectively analyzed. Effects of observational bias are present not only from the persistent tendency of astronomers to observe objects which, in some way, are more conspicuous, but also from the analysis of vast amounts of digitized data. We can wonder about discoveries until now deeply buried (perhaps forever!) in shelves of stored data, after analysis which looked only for a precise phenomenon; but we have to recognize that it is impossible, from an human point of view (and even for computers ?) to face the asymptotic growth of available data. Projections were made on the geometrical increase of the number of volumes and pages of The Astrophysical Journal, from year to year, and the resulting rate of linear occupation of shelves in libraries. It turned out that this speed, in a foreseen future, will exceed the speed of the light ! To this predictions some critics retort, saying that there is no physical deadlock, since the Ap. J. carries no information... Nevertheless, the present trend to publish results on electronic support is already an option which will replace, to an unknown point, the ancient use of solidly printed information.

The problems of big, multiple data, and of the difficulty to handle and correlate multi-class information, are already set. An analysis in many wavelengths is cumbersome, even if only one object is studied; the problem is amplified when we are confronted with large lists, database-size. Facing these challenges, it is useful to turn to more powerful tools, brought from other sciences. We want in this article to provide an example of the use of statistical techniques colletively called multivariate data analysis, applied to an extensive set of stellar measurements, mainly in the infrared. For those more interested, an approach on applications of this method in astronomy may be found in Murtagh and Heck (1987). More comprehensive texts are Hair et al. (1987) or Chatfield and Collins (1980)

2 Applications

The catalogue of stars observations in the UBVRIJHKLMN colors (Ducati 1993) contains data for about 4000 stars. Besides the colors (U−V) to (N−V), other informations are provided, including coordinates and spectral types. Associated, derived lists, provide distances and color excesses. Those digitized files fill approximately 1.5 MB each; they allow either searches for particular objects, or a vast range of studies of many possible correlations. Such a large list contains many classes of objects; furthermore, the volume of space sampled by these observations covers different regions in the Galaxy, regarding stellar density, metalicity, or properties of the interstellar medium like reddening laws. The span of possible correlations, and the size of the data file, make an ordinary analysis by standard methods a tremendous task. Besides, one should allow for the probability of surprising, unexpected correlations (or non-correlations), to be uncovered by special methods.

The multivariate data analysis is a tool to deal with these problems, using techniques like :

- principal components analysis : where a set of variables is transformed in a much smaller set of factors; each factor is a linear combination of variables, weighted by coefficients, and contains the maximum of original information. Graphical representations of the transformed data are possible.

- cluster analysis : subdivides the data in groups or clusters, according to similarity criteria, which are specified by the user, who also sets the number of clusters.

- discriminant analysis : discriminates individual objects into predefined groups, according to a function which is a linear combination of several variables.

- multiple regression analysis : finds an equation or model that predicts the dependent variable, as a function of one or more independent variables.

We applied the cluster analysis to our file of infrared data, taking as variables the color excesses E(U−V), E(B−V), E(J−V) and E(K−V), for which data for more than 1300 stars exists. To cluster analysis it is crucial the choice of the number of clusters, so that the maximum information is preserved. A number too small will associate stars with only coarse similarities, while too many groups will put in different groups stars with subtle differences, possibly of the order of observational errors. For a sample of 1613 stars of all spectral types, an analysis generating ten clusters was a fair compromise. A good example of how stars are partitioned in groups is as follows : by ordinary sorting we selected the eight most distant stars in the catalogue, all at distances greater than 20 000 parsecs; this group was compared with one of the ten generated clusters, containing 18 stars. All those eight distant stars belong to this group created by cluster analysis, together with other four stars with distances bigger than 17 200 pc; the remaining five objects are main sequence stars, which are certainly in the solar neighborhood, even if the actual distance is a missing data in the catalogue. But from their spectral types we detect binarity, variability, emission or peculiar features. This illustrates how the method can either group similar stars, or reveal cases of anomalous observational data, from circumstellar emission or other physical reasons.

Regarding non-hierarchical cluster analysis, two points should be stressed. One, the concepts of centroid and distance to the centroid. In the method each cluster is computed, after the pivotal variables (for example, distance, E(B−V), E(K−V), E(L−V)). For each cluster defined under these constraints, there is a center of coordinates in the multi-dimensional space of the variables, called the centroid. Each star belonging to the group has a distance from the centroid. Examination of those stars loosely associated (with the larger distances) gives clues to either observational errors, peculiar stars or anomalous extinctions. So cluster analysis is a tool to search for outliers, when working with large lists. This leads to the second point. The partition of a catalogue in a number of clusters (ten, in our case) may generate one or two groups with quite a few stars. These in general are either objects with gross observational errors (like misidentifications), bias (like circumstellar matter), or are special cases of great interest.

We have also to refer to the multiple regression analysis capability to provide functional relationships between color excesses, either bi-dimensional (like E(B−V) vs. E(K−V)), or multi-dimensional (like E(B−V) as a combination of several infrared excesses). The important point is that not only this is possible for a whole list, like our complete catalogue, but this also can be done inside each cluster, which is a much smaller set. Clusters tend to associate similar stars, or stars under the same environmental conditions. Transformation equations for each cluster provide means to evaluate parameters for stars with incomplete (missing) data, with better accuracy than if relations derived from entire samples are used, since in this last case all kinds of stars have their data considered. Clearly, this is valid only if the number of stars inside a cluster is big enough to provide a good statistics.

TABLE I.

	E(U-V)	E(B-V)	E(J-V)	E(K-V)	E(L-V)	E(M-V)	E(N-V)
E(U-V)	1						
E(B-V)	0.9588 (1370)	1					
E(J-V)	-0.8029 (1250)	-0.8726 (1299)	1				
E(K-V)	-0.8186 (1366)	-0.8883 (1421)	0.9754 (1458)	1			
E(L-V)	-0.8001 (883)	-0.8795 (906)	0.9378 (942)	0.9818 (1042)	1		
E(M-V)	-0.5695 (198)	-0.6928 (213)	0.8349 (208)	0.9467 (226)	0.9763 (195)	1	
E(N-V)	-0.4402 (44)	-0.5536 (45)	0.5117 (45)	0.8703 (47)	0.9304 (44)	0.9708 (34)	1

Other interesting conclusions may be drawn from regression analysis. The table I shows the correlation coefficients between some selected color excesses (regressions performed for complete list of 1613 stars; number of common stars below coefficient):

This gives the level of reliability when infrared excesses are used to evaluate excesses in the blue region, for very red or very absorbed stars. We can see that observations of the N band at 10μ are prone to contain a larger scatter, frequently due to the difficulty of observing at those wavelengths, or to differences in filters from various observers. We see

also that correlations for E(L−V) are of the same order than for J or K, in spite of the circumstellar emission often associated with observations in L. This is due to the large amount of data involved; in fact, close examination shows that approximately 1% of the L data contains non-stellar emission.

3 Conclusions

Our concluding remarks point out to the need of using large databases; this allows subdivisions of the sample in spatial zones and star populations which are statistically meaningful, which in turn gives solid ground to apply multivariate analysis. It is clear that the space is not homogeneous with respect to the distribution of interstellar matter or its properties. Certain classes of stars have their own circumstellar contribution to observed photometric indices, which are usually supposed to provide information on interstellar processes only. To distinguish these effects in large amounts of data requires powerful techniques. Facing databases of astronomical size, multivariate analysis and other statistical methods are fundamental tools from now on.

4 References

Chatfield,C., Collins,A.J. 1980, Introduction to Multivariate Analysis, Chapman and Hall, London

Ducati,J.R. 1993, A Catalogue of 11-Color Observations of Stars, Wisconsin Astrophysics 504

Hair, J.F.,Jr., Anderson,R.E., Tatham,R.L. 1987, Multivariate Data Analysis, Macmillan, London

Murtagh,F., Heck,A. 1987, Multivariate Data Analysis, Reidel, Dordrecht

Section 5

Stellar Astrophysics

THE SOUTHERN HEMISPHERE YOUNG STARS SURVEY

C.A.O. Torres and G.R. Quast
Laboratório Nacional de Astrofísica/CNPq/MCT

Abstract

The discovery of isolated young stars has shown the need of reconsidering the spatial distribution of these objects traditionally characterized by their proximity to dense interstellar clouds, where they are frequently found in associations of similar objects. In order to investigate the subject we have carried out a survey selecting 4041 sources from the IRAS Point Source Catalog by their spectral indexes. The final sample of 502 optical objects south of 30°N to be observed was defined based on images from the Digitized Sky Survey. The nature of the possible optical associations with the IRAS sources has been tested using spectra at the Hα region. A star has been classified as T Tauri (TTS) when it has presented both Hα emission and the LiI λ6707 absorption line and as Herbig Ae/Be star (HAEBE) if hotter than F5 with Hα emission. The reduction of data is now ready for 95% of the survey. Until now there were discovery of 50 new TTS (plus 11 to be confirmed), 112 possible Herbig Ae/Be stars, 3 probable pos-fuori stars and, surprisingly, 14 lithium rich cool giants. During the preliminary stage of the survey 12 other TTS have been found (12 others awaiting confirmation), 3 possible HAEBE and 1 cool lithium rich giant star. Some young objects found in the survey are located far from star forming regions.

1 Introduction

During the pre-main sequence phase stars are usually placed in associations rich in gas and dust and this environment is used for the traditional definition of young stars. This is the case not only for TTS - young stars having masses around 1 $M_{\odot}$ and spectral types G, K, M - but also for HAEBE, stars whose masses are greater than 2 $M_{\odot}$ and earlier spectral types. The discovery of a young double-line spectroscopic binary star, V4046 Sgr (de la Reza et al., 1987), challenges this definition. The presence of LiI and strong Hα emission indicates this star to be in the pre-main sequence evolutionary stage. But in its spatial neighborhood there seem to be neither clouds nor stars of the same age, compelling it to be an "isolated TTS" (Torres et al. 1987a). Other isolated TTS were found (Torres et al. 1987b), but in a reduced number. It is important to find other examples in a systematic way in order to analyze the frequency of this occurrence. TTS surveys have been limited to dense interstellar clouds and generally used objective-prism plates in the Hα region. Even though the Hα emission is generally strong in TTS, an all-sky survey may not be cost effective.

An independent and potentially efficient selector has been presented by Gregório-Hetem et al.(1988). They noted that TTS in Chamaeleon Clouds have all similar infrared colors as measured by the *Infrared Astronomical Satellite* (IRAS). Analogous result was presented

by Emerson (1988) for TTS in general. From these results emerged the idea of making a young star survey without positional bias - the Pico dos Dias Survey (PDS) - using the selector based on IRAS colors. The infrared emission associated to TTS is supposed to originate from an accreting dust disk surrounding the central stellar object (e.g. Hartmann & Kenyon, 1988). The spectral distribution of this process will depend mainly on the temperature distribution in the disk, defining a box in the IRAS color-color diagrams. The use of IRAS emission to search for young stellar objects restricts the PDS to TTS having such disks. The TTS may be divided in classical T Tauri stars (CTTS) or weak T Tauri stars (WTTS) if the equivalent width of the Hα emission line is greater or smaller than 10Å, respectively. It has been proposed that only CTTS would have such disks. In this case the formation of intense Hα emission line would depend on these disks in some way and the geometry of the disk would be an important factor in the emission and detection of Hα. Depending on the line-of-sight, the disk itself may block the view of the Hα emitting region. Thus, genuine CTTS could be detected even though their Hα is in absorption or faintly in emission. A search based specifically on IRAS emission can also shed light on this question.

2 Observations

As the survey extended over several years, some changes in methodology have occurred. Even new results caused some feedback. Thus, the PDS may be divided in 4 stages which will be called "Eras" (besides another one called "pre-history"). In all of them the objects were selected from the IRAS Point Source Catalog (IPSC). The observations were made with the coudé spectrograph and 1.6m telescope of Observatório do Pico dos Dias (OPD) operated by Laboratório Nacional de Astrofísica (LNA). The spectra have resolution of 0.7Å and include the region of Hα and LiI λ6707 lines. Two different GEC CCDs were used, with 578 or 1152 pixels in the dispertion direction. This spectral region, near the maximum of the detector sensibility, and the coudé focus of the OPD, equipped with special high reflectivity mirrors, gives an efficient combination. The resolution allows the detection of spectroscopic binaries as well as discerning between dwarf and giant stars.

A star was considered a TTS if it presents both Hα emission and the LiI λ6707 absorption. This definition is practical, objective and can be used in any region of the sky, making the classification more reliable. Its main drawback is the limiting magnitude, not allowing the inclusion of extremely embedded objects presenting strong extinction and higher magnitudes. On F stars, where convection is not important, there is no efficient mixing between internal and external layers and, as a consequence, the photospheric Li abundance is not a good indicator for stellar ages. Although the proposed definition for TTS is used in the PDS for F stars, their classification must be accepted with caution and needs other evidences for confirmation. However, there are only a few cases in this situation.

The question of the HAEBE definition is more complex. There is no such a similar diagnosis. The time of evolution to the main sequence is very short, not only in comparison

to the dispersion of ages in the forming regions, but also with respect to the probable lifetime of the circumstellar disk. The star rapidly passes through distinct evolutionary stages, making it difficult to characterize the group according to spectral properties. Only a set of several criteria will produce a reliable classification. One of the strongest criteria proposed by Herbig (1960), their location in an obscured region, is useless for the purposes of the PDS. A discussion about difficulty can be found in Thé et al. (1994; hereafter TWP). Emission line stars earlier than about F5 with no lithium line were tentatively classified as possible HAEBE if their spectra are not very peculiar. So, at this stage of PDS, as a first approach, the possibly young stars were classified as TTS if they are later than F5, and as HAEBE if they are earlier.

For massive objects, the disk can survive the HAEBE phase. Among the selected stars one can find β Pic which does not have Hα emission and must be close to the main sequence. If in the PDS a β Pic-like object was observed, it would be taken for an optical-IRAS coincidence. Nevertheless, TWP have considered them possibly related to HAEBE. Anomalies on the Hα profile may indicate the presence of shells. There are other possible complications. Most of the objects thought to be in a pos-main sequence phase, such as classical Be, B[e], LBV, etc, have some HAEBE-like characteristics. TWP prefer to consider them as possible HAEBE. It is not only a confusion of spectral features, but there are also doubts about their evolutive phase. There are also ambiguities in distinguishing protoplanetary nebulae from HAEBE. Their spectral features are similar and PDS and surveys on protoplanetary objects have found the same stars due to the superposition of the IRAS color boxes. Other parameters are needed for the classification of early type emission line objects.

Another group of blue stars showed up in the survey: very bright stars, belonging to the *Bright Star Catalog* (BSC). Almost all of the 31 BSC stars observed in the PDS are hotter than A0 with 4 exceptions: one A3, one A5 (β Pic), one F0 and one G3. The histogram of the V-[12] color index shows a bimodal distribution and all "blue" V-[12] stars belong to to form an easily distinguishable class of objects.

3 The Eras

During the execution of the PDS the selection criteria and the observing procedures have changed depending on the available facilities. For instance, in order to observe a target object it is not enough to point the telescope at the IRAS coordinates due to the low positional uncertainty of the IRAS and to the telescope pointing errors. The procedures to overcome these limitations changed for each Era.

3.1 The Early Era

The selection of the target has followed the criteria below :

i - IRAS positions south of declination +30°

ii - fluxes in 12, 25 and 60μm above the detection limits in the IPSC

iii - absence of associations with galaxies or planetary nebulae in the IPSC

iv - infrared color box defined according to:

$$-0.02 < [12]-[25] < 0.53$$
$$-0.30 < [25]-[60] < 0.52$$

A list with 888 target sources was built using the IPSC version 1.0. The telescope was pointed to the coordinates of the targets and the field checked for an observable optical object nearby. The pointing of the 1.6m telescope was not very accurate and the available field at the coudé focus being very small forced a wandering around in the vicinity of the aimed position. Besides wasting time with sources without observable optical objects, one could not be sure if the objects found were inside the IRAS error ellipse, and stars far from the IPSC position with very low association probabilities could be observed. Anyway, there were interesting discoveries which can be classified as serendipities. At this Era the GEC P8603 385x578 pixels CCD was used (Gregório-Hetem et al. 1992). In the PDS pre-history, targets were selected with no restriction in the IRAS fluxes around TW Hya, a high galactic latitude TTS, to test its "isolated" status. Two new TTS were discovered, one of them being a visual binary, Hen 600 (de la Reza et al. 1989). Since the distance between optical and IRAS positions was not checked during observations, only Hen 600 was actually associated with an IRAS source and belongs to the list of 888 sources.

3.2 GSC Era

The use of the *Guide Star Catalog* (GSC) (through an optical disk kindly provided by NASA) allowed the correlation between target sources and optical objects, avoiding the blind search at the telescope. It was possible to know the relative positions of the optical objects and which ones were included in a chosen error ellipse. With the help of G.L. Vieira the 888 positions were checked in the *True Visual Magnitude Photographic Star Atlas* (Papadopoulos & Scovil, 1980), that has a similar limiting magnitude, being possible to show that the incompleteness of the GSC for this sample is less than 13% (Gregório-Hetem et al. 1992), which was considered acceptable by the gain in efficiency. The limiting magnitude is almost identical to the instrumental one used in the PDS. The missing bright stars can be obtained from catalogs as the SAO. Results of the Early and GSC Eras appear in Gregório-Hetem et al. (1992) and Torres et al. (1995).

3.3 Weintraub's Era

Weintraub (1990), making use of a larger number of young stars, mainly belonging to the *Third Catalog of Emission-Line Stars of the Orion Population* (Herbig & Bell 1988; HBC), has obtained more reliable limits for the color box. Although it represents an increase in the number of sources, and possibly also in the number of spurious associations, the use of GSC helped in keeping the work feasible. The IPSC version 2.0 was used leading to the exclusion of a few sources of the previous Eras. Conditions (ii) and (iii) from the Early Era were kept and the color box defined by:

$$-0.95 < [12]\text{-}[25] < 0.11$$
$$-0.95 < [25]\text{-}[60] < 0.32$$

The new list had 3540 sources all over the sky. An IRAS error ellipse of 3.3σ was used to include 99,9% of the associated optical objects. Through the use of GSC and SAO, 702 sources were selected, 540 of them south of $+30°$.
As much as possible the GEC P88200 1152x770 pixels CCD was used, resulting in doubling the previous spectral coverage. The reduction of these spectra was done with the IRAF software installed in the LNA workstations.

3.4 DSS Era

In 1995 it was possible to make use of the optical disks from the *Digitized Sky Survey* (DSS). Even though the quality and the type of plates used to produce the DSS vary through the sky, its use allowed better homogeneity, completeness and efficiency. A more consistent sample could be formed, making possible the verification of proposed associations to galaxies and planetary nebulae. The 4041 Weintraub all-sky IRAS sources prior to condition (iii) of the Early Era were examined on DSS images. The eventual optical objects inside the error ellipses were classified according to their magnitude, appearance and environment. For a more complete exclusion of quasars, active galactic nuclei and planetary nebulae, as they can have stellar-like appearance, the *A Catalogue of Quasars & Active Nuclei* (Véron-Cetty & Véron, 1993) and *The Strasbourg-ESO Catalogue of Galactic Planetary Nebulae* (Acker et al. 1992) were used. In this way, 551 sources were eliminated, 388 being galaxies and 163, planetary nebulae. The number of remaining positions, 3490, was somewhat smaller than that in Weintraub's Era. Elimihating the sources in the direction of the Magellanic Clouds (57) and those associated to HBC objects (147), the other 3286 optical images were examined for stellar objects inside the 3.3σ error ellipse. In this way, 689 sources were selected among objects of stellar appearance with magnitudes up to 14, stellar objects with magnitudes bellow 12 "near" to the ellipse and bright diffuse objects. The definition of "near" was somewhat personal and took into account the brightness of the star and the field density. Bright diffuse objects with saturated images were included for the possibility of a hiding star. The environment was also taken into account considering the presence of general nebulosity diffuse object. The sources south of $+30°$ are 502 (40 of them having bright stars "nearby") and define the final PDS sample.
There are 248 positions which were observed (or at least pointed at) in the previous Eras, although not belonging to the final sample. The DSS uses both visual and blue plates, not allowing consistent magnitude estimates. Worse, the observations of the PDS being in the red and since differences in color index may be important, the quality of sample completeness is poor. During the examination of the plates, star magnitudes were eye-calibrated by comparison with GSC fields. A more refined calibration would be time consuming without making the the sample any better. The selected DSS plate was the one in which the source was nearest to the center.
The higher quality of DSS maps compared to GSC resulted in a better reliability in the

Table 1: Results for sources not included in the final sample

Type of stars	Quantity	Visual binaries
"Normal" stars	18	
TTS	10	2
Probable TTS	11	
Possible HAEBE	03	
Cool Li-rich giant stars	01	
Other Hα emission stars	05	

identification of the associated objects. It was necessary to reobserve some positions in confused fields and in other ones having candidates fainter than those formerly measured.

4 Results

a) In all Eras, after each observation, the spectrum was displayed with the acquisition program, and as much as possible, classified according to its main characteristics (emissions, presence of Li line or TiO bands, etc) and a preliminary type was proposed for the object. When an object was suspected to be a TTS or other "interesting" star, more spectra were obtained. For TTS at least 3 spectra were taken in order to detect possible radial velocity variations. As the project was going on, new and unexpected types of stars showed up, like giant stars with strong lithium line, despite their rarity so far. Others are similar in the observed spectral range to old fuori stars.
During cloudy nights standard stars were observed for spectral classification. The chosen spectral region is not normally used for that purpose and the narrow range limits the number of useful lines. But anyway it seems possible to make a spectral classification in this region with a reasonable precision, mainly for advanced spectral types. That means that the TTS may be fairly well classified, unless strong veiling is present.
Frequently emission lines appear on the sky, mainly Hα, but also some forbidden ones, indicating the presence of an HII-region. The observed optical object may not have any relation to the HII-region. Probably in these cases the infrared emission is related to the HII-region, whose exciting source is not visible since it is very embedded. These regions are potentially very interesting. For this reason during reduction the sky spectrum was preserved and, whenever possible, the non-stellar emission was measured. These results are not presented here.

b) A more detailed analysis of the spatial distribution will be done later. A preliminary analysis shows that PDS young objects have a less concentrated distribution of distances to the nearest neighbor than those belonging to the HBC (Torres et al., 1992). Small groups of young stars have been discovered having no apparent connection with known

Table 2: Results of PDS

Type of stars	Quantity	Visual binaries
Faint objects/underexposed	018	
TTS	044	6
Probable TTS	009	2
Possible HAEBE	110	2
Possible old fuori	003	1
Shell stars	008	
Cool Li-rich giant stars	014	
Probable cool Li-rich stars	002	
Hot bright stars	026	2
Other Hα emission stars	028	2
"Normal" stars	240	
Sample size	502	

star forming regions, some of them at high galactic latitude, as the TW Hya group or the triple star HD141569, formed by one HAEBE and two TTS. However, for the goals which motivated the PDS, the results are rather frustrating, since few stars were found that can be considered isolated. If confirmed, isolated young stars would be statistically of little importance.

c) UBV(RI)$_C$ photometry being made for the PDS stars, using the FOTRAP (Jablonski et al., 1994) installed at the 60cm Zeiss telescope at OPD, is revealing some trends for HAEBE stars. With 60% of the possible HAEBE measured, broadly two conditions could be discussed: first, stars with low reddening which, when corrected, show typical colors of dwarf stars hotter than F5, consistent with their spectra; second, strongly reddened stars where correction is difficult because the standard reddening law cannot be applied and other alternatives, like an UV-excess in a cold photosphere, can not easily be discarded. Almost always the spectra present only the Hα line. If a standard reddening law is used, extinctions greater than 10 magnitudes are obtained. They may be strongly embedded stars with high intrinsic luminosity. Infrared observations could test this hypothesis.

d)After establishing the final sample in the DSS Era, it was found that 248 sources pointed at in previous Eras were no longer included, but for 111 of them no observable object was found. Other 30 sources have counterparts in HBC, one belongs to the objects were outside the error ellipse and showed no peculiar characteristic. Thus, for only 49 cases we have optical objects that actually could be examined. Table 1 summarizes the results for these sources.

In general these stars have magnitudes above 14 on the DSS, explaining the large number

of probable TTS. Actually this happens for all TTS and HAEBE (2 of them appear in TWP) in Table 1. The above-mentioned color differences between DSS plates and PDS have their nature defined. Further, young stars can show strong photometric variability and there may be magnitude differences between DSS and the PDS observations.

Although some young stars were found outside the error ellipse looking like casual discoveries, this is not as unpredictable as it seems. Several sources without apparent optical association may be very faint or embedded objects. As stars are generally formed in associations it is not surprising to find other young objects nearby.

e) Table 2 summarizes the results of the PDS final sample, with 95% of the spectra reduced. One of the difficulties in summarizing the results is the presence of more than one optical candidate inside the error ellipse. Several times just one of the objects is a presumed association. Whenever possible, even if all objects were observed, only the "best" candidate is displayed in

Many possible HAEBE are associated with clouds or star forming regions, strengthening their classification. Among the 113 possible HAEBE presented in Tables 1 and 2, 18 are classified by TWP as being "HAEBE members and candidate members" and 15 more ar

5 Conclusions

Although more definite conclusions must await the completion of the PDS, some of them may be advanced :

i - Young stars may be divided into two groups:
  a) distributed along the galactic plane without clustering
  b) clustered in star forming regions above or below the galactic plane.

ii - Truly isolated young stars are rare.

iii - There are many young stars in the periphery of associations, not detected yet.

A good alternative to explain these characteristics seems to be Lépine & Duvert's model (1994) relating stellar formation in the regions out of the galactic plane to the infall of high velocity clouds. The stars on the galactic plane could be formed according to more traditional ideas, as for instance, spiral waves.

6 Acknowledgements

The authors acknowledge the collaboration of the other members of the PDS group: Ramiro de la Reza, Jacques Lépine and Jane Gregório-Hetem and the helpful discussions with many other Brazilian astronomers who cannot be mentioned individually. The

References

[1] Acker, A., Marcout, J., Ochsenbein, F., Stenholm, B., Tylenda, R., Schon, C. 1992, *Strasbourg-ESO Catalogue of Galactic Planetary Nebulae*, European Southern Observatory

[2] de la Reza, R., Quast, G.R., Torres, C.A.O., Mayor, M., Meylan, G., Llorente de Andrés, F. 1987 in *New Insights in Astrophysics*, Proc. Joint NASA/ESA/SERC Conference, University College, London, 106

[3] de la Reza, R., Torres, C.A.O., Quast, G.R., Castilho, B.V., Vieira, G.V. 1989, ApJL, 341, L61

[4] Emerson, J.P. 1988, in *Formation and Evolution of Low Mass Stars*, Proceedings of the NATO-ASI, ed. A.K.Dupree & M.T.V.T. Lago, 193

[5] Gregório-Hetem, J., Lépine, J.R.D., Quast, G.R., Torres, C.A.O., de la Reza, R. 1992, AJ, 103, 549

[6] Gregório-Hetem, J., Sanzovo, G.C., Lépine, J.R.D. 1988, A&ASS, 76, 347

[7] Hartman, L., Kenyon, S. 1988 in *Formation and Evolution of Low Mass Stars*, Proceedings of the NATO-ASI, ed. A.K.Dupree & M.T.V.T. Lago, 163

[8] Herbig, G.H. 1960, ApJS, 4, 337

[9] Herbig, G.H., Bell, K.R. 1988, Lick Obs. Bull., 1111

[10] Jablonski, F., Baptista, R., Barroso Jr., J., Gneiding, C.D., Rodrigues, F., Campos, R.P. 1984, PASP, 106, 1172

[11] Lépine, J.R.D., Duvert, G. 1994, A&A, 286, 60

[12] Papadopoulos, C., Scovil, C. 1980, *True Visual Magnitude Photographic Star Atlas*, Pergamon Press

[13] Reipurth, B. 1990, IAU Symposium No.137 on *Flare Stars in Star Cluster, Associations and the Solar Vicinity*, eds L.V. Mirzoyan, B.R. Peterssen and M.K. Tsvetkov, 229

[14] Thé, P.S., de Winter, D., Pérez, M.R., 1994, A&ASS, 104, 315

[15] Torres, C.A.O., Quast, G.R., de la Reza, R., Lépine, J.R.D., Gregório-Hetem, J. 1995. AJ, 109, 2146

[16] Torres, C.A.O., Quast, G.R., de la Reza, R., Mello, G.F.P. 1987a, Rev. Mex. de Astron. y Astrof., 14, 360

[17] Torres, C.A.O., Quast, G.R., de la Reza, R., Mello, G.F.P. 1987b, Rev. Mex. de Astron. y Astrof., 14, 361

[18] Véron-Cetty, M.P., Véron, P. 1993, ESO Scientific Report No. 13

[19] Weintraub, D.A., 1990, ApJSS, 74, 575

DYNAMICS IN THE EQUATORIAL PLANE OF Be STARS

F.X. de Araújo
Observatório Nacional

Abstract

Accurate numerical solutions for the radial motion equation in the equatorial plane of rotating B-type stars are presented. We have considered an outflow driven mainly (or uniquely!) by optically thin lines. This is done by decreasing the value of the radiative parameter α in the domain $(0.5 \geq \alpha \geq 0.0)$. It was obtained a net shallowing of expansion with lower values of α. On the other hand reasonable mass fluxes require large values for the radiative parameter k. Our results give support to the idea that the dynamics in the equatorial region of Be star envelopes is dominated by a radiative force due to a great number of thin lines.

1 Introduction

Be stars are non supergiant B type stars which present (or have presented) Balmer lines in emission. Their other major observational characteristics are: a large broadening of the photospheric lines; an important infrared excess; the presence of asymmetric absorption lines from ionized species in the UV; a degree of linear polarization which may reach, in some cases, 1.0 – 1.5 % in the visible range.

The ad-hoc scenario most accepted nowadays for these objects is that of a fast rotator surrounded by a non-spherical circumstellar envelope. In a first approximation the envelope would be symmetric with respect to the rotation axis. According to this picture a weak (not dense) and fast wind is present in polar regions - where would be mainly formed the UV asymmetric lines. On the other hand the equatorial plane seems to be much more dense and slowly expanding (but with an important rotational velocity). The emission lines would originate in this last region. Such a scenario is generally summarized by assuming a two-component envelope: a "polar wind" and an "equatorial disc".

In the last decade some attempts have been made to understand Be envelopes in the context of the radiation-driven wind theory. Among other works the reader is referred to Poe & Friend (1986), Araújo & Freitas Pacheco (1989) and Koninx & Hearn (1992). More recently Bjorkmann & Cassinelli (1993) and Owocki et al. (1994) have concluded that a meridional current may be responsable for the concentration of matter towards the equator. However, the most important problem with all these models is that they produce too strong an equatorial expansion. Not only is the terminal velocity very high (about a thousand kms^{-1}) but also there is too rapid an increase to these velocities. Contrary to it the fitting of H_α line profile requires terminal velocities of about 200 kms^{-1}. (e.g. Poeckert & Marlbourough 1978). A detailed comparison between interferometric measurements of the star $\gamma\,Cas$ and theoretical visibility curves performed by Stee et al (in preparation) reinforces this conclusion.

Those attempts were based on Castor, Abbott & Klein (1975, hereafter CAK) theory. The radiative force in "CAK-type" models is essentially due to strong (optically thick)

lines. It describes an expansion which is able to reproduce many properties of hot star winds, and probably the "polar wind" of Be stars. But, as already said, it can not explain the properties of the equatorial plane of Be stars.

The possibility of an outflow driven mainly by thin lines was raised several years ago by Lamers (1986) in his study of P Cygni's wind. Subsequently Pauldrach & Puls (1990) and Lamers & Pauldrach (1991) concluded that the dominant driving lines may be optically thin lines in winds with large enough optical thickness. Boyd & Marlborough (1991) also suggested weak lines as a mechanism which could possibly act in the equatorial disc of B[e] supergiants. Very recently Araújo et al. (1994; see also Stee & Araújo 1994) have presented some results obtained with lower values of the radiative parameter α. (This parameter gives the importance of thick lines in driving the wind: $\alpha = 0$ corresponds to no thick lines at all whereas $\alpha = 1$ represents no thin lines). Although they obtained some encouraging results, technical difficulties prevented them from obtaining solutions for $\alpha < 0.4$. Chen & Marlborough (1994) have encountered analogous problems.

The aim of this paper is to present accurate numerical solutions for the expansion equation in the equatorial plane of rotating B-type stars, considering values of α in the range 0.5 to 0.0. This corresponds to an outflow driven mostly (or uniquely!) by optically thin lines. Whether or not this is the major mechanism acting in the equatorial plane of Be stars remains to be seen. Nevertheless the solutions clearly allow a wind with the desired properties: low terminal velocities and large mass fluxes.

In Sect. 2 the dynamical equations are presented and we discuss our method of solution. The special case $\alpha = 0$ is treated separately in Sect. 3. The method is applied in Sect. 4. We have considered two ensembles of parameters: one to represent a Be early-type (B0–B1 V–IV) and the other one a more late Be (B4–B5 IV–III). The results for a standard model are presented in sub-sections 4.1 and 4.2 and some conclusions are outlined in last section.

2 The expansion equation and it's solution

2.1 Assumptions and equations

Let us consider a spherical coordinate system in which the centre of the star is at $r = 0$ and the rotational axis coincides with the z axis. The equatorial plane is at $\theta = \pi/2$. By hypothesis our envelope is in a steady state situation. With these assumptions the radial motion equation in the equatorial plane is

$$v_r \frac{\partial v_r}{\partial r} - \frac{{v_\phi}^2}{r} + \frac{1}{\rho}\frac{\partial P}{\partial r} + \frac{GM(1-\Gamma)}{r^2} - \frac{1}{\rho}F^l = 0 \qquad (1)$$

Here P is the gas pressure, G is the gravitational constant, M is the stellar mass and Γ is the ratio between the radiative acceleration due to electron scattering and gravity. F^l is the radiative force due to line opacity. Following Friend & Abbott (1986) we may write

$$\frac{F^l}{\rho} = \frac{\sigma_e L}{4\pi c r^2} k t^{-\alpha} g(r, v_r, \frac{dv_r}{dr}) \tag{2}$$

The factor $g(r, v_r, \frac{dv_r}{dr})$ takes into account the size of the star ($g = 1$ for a dimensionless point source). t is an optical depth variable and k and α are the radiative parameters. k is related to the total number of contributing lines and α, as said previously, measures the relative importance of thin and thick lines. Other symbols have their usual meaning: L is star's luminosity, σ_e is the electron scattering coefficient and c is the velocity of light.

The mass conservation equation can be immediately integrated, leading to

$$\Phi = r^2 \rho v_r \tag{3}$$

where Φ is the mass flux per unit of solid angle.

Regarding the rotational velocity we have adopted the following expression:

$$v_\phi(r) = \chi \Big(\frac{GM(1-\Gamma)}{R}\Big)^{1/2} \Big(\frac{R}{r}\Big)^{\delta} \tag{4}$$

Here χ is the stellar rotation rate (given in terms of "break-up" speed) and R is the star radius. δ is an empirical viscosity parameter which may vary from -1 (solid body rotation) to $+1$ (angular momentum conservation).

In addition we have restricted our study to the case of an isothermal envelope and we have considered an ideal gas law

$$P = a^2 \rho \tag{5}$$

where a is the (isothermal) sound speed.

The equation which results for expansion (combining Eqs. (1) to (5)) is

$$\Big[v_r - \frac{a^2}{v_r}\Big] \frac{dv_r}{dr} + \frac{GM(1-\Gamma)}{r^2} \Big[1 - \chi^2 \Big(\frac{R}{r}\Big)^{2\delta - 1}\Big] =$$

$$= \frac{2a^2}{r} + \frac{C}{r^2} \Big(r^2 v_r \frac{dv_r}{dr}\Big)^{\alpha} g(r, v_r, \frac{dv_r}{dr}) \tag{6}$$

C is an eigenvalue of the solution. It is related to the mass flux by

$$C = \frac{\Gamma GMk}{(\sigma_e v_{th} \Phi)^{\alpha}} \tag{7}$$

2.2 The method of solution

The first step to obtain the numerical solution of this type of equation consists in computing the velocity and its derivative at a special point named critical radius. This point is defined by regularity and singularity conditions (see e.g. CAK, Araújo & Freitas Pacheco, 1989). From them we can perform the numerical integration in both directions (inward and outward) obtaining a whole solution. However, it is not straightforward to obtain accurate (and quick) estimates of $\frac{dv}{dr}$ at each step of integration.

We have re-written (6) in the form

$$H(x) = h_1(v)x + h_2(v,r)x^{\alpha} + h_3(r) = 0 \tag{8}$$

with $x \equiv \frac{dv}{dr}$.

As usual, only the r-dependence of $g(r, v_r, \frac{dv_r}{dr})$ is retained in a first iteration. In the subsequent ones a polynomial fitting of it is employed.

The problem consists now in finding the roots of $H(x)$. A simple analysis of this equation shows that if $h_1(v) \, . \, h_2(v,r) > 0$ then $H(x)$ is monotonically increasing (or decreasing). On the other hand if $h_1(v) \, . \, h_2(v,r) < 0$ the function has one (and only one!) point of maximum/minimum. In addition it must be kept in mind that $H(0) = h_3(r)$ and asymptotically $H(x) \propto h_1(v) \, . \, x$. It is easy to conclude that when $h_1(v) \, . \, h_3(r) < 0$ the function has one (and only one) root. Let us analyse now the case $h_1(v) \, . \, h_3(r) > 0$. In this case the function $H(x)$ may have roots if and only if it has a maximum or minimum. When this inflection point is of same sign of $h_1(v)$ or $h_3(r)$ there are no roots. When it is of the opposite sign it has two roots (in this last case one must be careful of trapping the good one: the greater for the outward integration and the smaller for the inward direction).

On the basis of the above analysis we have developed a code which determines numerically the derivative of the velocity in each step of the integration. Firstly is determined a range in which the function $H(x)$ changes sign. Secondly standard procedures (Press et al, 1992) are employed in order to obtain the root with the desired precision.

3 The case $\alpha = 0$.

In this case the line force is uniquely driven by optically thin lines. It has a simple r^{-2} dependence

$$\frac{F^l}{\rho} = \frac{k\sigma_e L}{4\pi c r^2} \tag{9}$$

The expansion equation in the equatorial plane is reduced to

$$\left[v_r - \frac{a^2}{v_r}\right] \frac{dv_r}{dr} + \frac{GM(1-\Gamma)}{r^2}\left[1 - \chi^2\left(\frac{R}{r}\right)^{2\delta-1}\right] =$$

$$= \frac{2a^2}{r} + \frac{C}{r^2} \tag{10}$$

Now, C is given by $C = \Gamma GMk$. So, Eq. (10) may be re-written as

$$\left[v_r - a^2\right] \frac{1}{v} \frac{dv_r}{dr} =$$

$$= \frac{2a^2}{r} - \frac{GM}{r^2}\left[(1-\Gamma)\left[1 - \chi^2\left(\frac{R}{r}\right)^{2\delta-1}\right] - k\Gamma\right] \tag{11}$$

This equation strongly resembles the solar wind equation (Parker, 1958; 1960). In this paper we will restrict our solution for $\alpha = 0$ to the case of Keplerian rotation i.e. $\delta = 0.5$ (see Eq. 4). Hence one obtains simply

$$\left[v_r - a^2\right]\frac{1}{v}\frac{dv_r}{dr} = 2\frac{a^2}{r} - \frac{GM}{r^2}\left[(1-\Gamma)(1-\chi^2) - k\Gamma\right] \quad (12)$$

This is a solar-type wind modified by rotation (χ), a continuum radiative force (Γ), and a thin line force ($k\Gamma$). Similar to solar expansion a transsonic wind must obey $v = a$ at the critical (sonic) point defined by

$$r_s = \frac{GM}{2a^2}\left[(1-\Gamma)(1-\chi^2) - k\Gamma\right] \quad (13)$$

4 Application to Be stars

In order to obtain the solutions of the equation we must choose several parameters. The stellar parameters are the mass, radius, luminosity (or effective temperature) and rotation rate. Concerning the envelope itself the eletron temperature must be assumed (since we do not consider the energy equation), also the rotational law and a boundary condition. The following strategy was adopted. Our "standard model" is defined by

$\chi = 0.66$
$T_{env} = 0.8\ T_{eff}$
$v_\phi(r) = v_{rot}(R/r)^{1/2}$ (keplerian rotation)

and a boundary condition given by the density at the basis of the wind ($r = R$)

$\rho_0 = 1.0$ x 10^{-11} gcm^{-3}

This last value is suggested by the work of Waters et al. (1991). The results obtained with these standard parameters, when the model is applied to stellar parameters typical of Be stars, are shown in next sub-sections 4.1 and 4.2.

4.1 A B0–B1 V–IV star

In this case it was assumed that M = 15 $M_\odot$, R = 10 $R_\odot$, L = 3.5 x 10^4 $L_\odot$ (and T_{eff} = 25000 K). These values were adopted following an analysis of several works in the literature: Poe & Friend (1986), Waters et al. (1991), Lamers & Pauldrach (1991), Waters & Marlbourough (1992), Koninx & Hearn (1992), Chen et al. (1992), Bjorkmann & Cassinelli (1993). They are not addressed to any specific object but it is supposed they are representative of a typical hot Be star.

Table 1 summarizes the main results. Columns 1 and 2 give the adopted radiative parameters α and k. Column 3 is the mass flux per unit of solid angle (given in solar masses per year-steradian) and column 4 is the velocity at 100 stellar radii (given in kms^{-1}). V_{100} is not the terminal velocity but it is close to V_∞. In order to justify it we show in column 5 the V_{100}/V_{300} ratio for some models. In almost all cases V_{100} is greater than 95% of V_{300}. The only exception is $\alpha = 0$. In this case we expect that an isothermal wind will expand without limit. So, the more important increase of $v(r)$ beyond V_{100} is not surprising. When $\alpha = 0.5$ (i.e. the driving contribution of thin and thick lines is of same importance) V_{100} is about 1200 kms^{-1}. As α is decreased there is a continous

Table 1: Results: B0-B1 star, standard model

α	k	$\Phi\,(M_\odot y^{-1} sr^{-1})$	$V_{100}(kms^{-1})$	V_{100}/V_{300}
0.5	0.3	3.610^{-9}	1184	99.5%
0.4	0.3	4.710^{-10}	853	
	0.5	1.710^{-9}	858	
	0.7	3.810^{-9}	861	99.4%
0.3	0.3	1.810^{-11}	618	
	0.7	2.910^{-10}	624	
	1.5	3.710^{-9}	630	99.3%
0.2	0.3	3.210^{-14}	427	
	1.5	9.510^{-11}	438	
	3.2	4.110^{-9}	445	99.1%
0.1	0.3	3.310^{-21}	217	
	3.2	5.810^{-12}	265	
	6.0	3.010^{-9}	272	98.2%
0.05	1.5	6.010^{-24}	159	
	6.0	6.110^{-12}	172	
	8.3	3.810^{-9}	178	97.0%
0.025	8.3	1.710^{-11}	119	
0.0	10.51	3.010^{-9}	68	

decrease of V_{100}, reaching $V_{100} \approx 150 - 250$ kms^{-1} for $\alpha \approx 0.05$–0.1. However, when α is small (≤ 0.2), reasonable mass fluxes require rather large values of k. This point will be discussed in the last section. Furthermore, for very small α there is no solution at all for k smaller than a certain value and in the case $\alpha = 0$ there is only a restricted range of k which leads to physical solutions (see Eq. (12)).

Figure 1 shows the expansion velocity profiles we have obtained for several values of α. In the models plotted here the mass flux is in the range $(3.0 \pm 1.0)\,10^{-9}\,M_\odot y^{-1} sr^{-1}$.

4.2 A B4–B5 IV–III star

In this second case we have assumed $M = 7.5 M_\odot$, $R = 6.0 R_\odot$, $L = 1.65\,10^3 L_\odot$ (and $T_{eff} = 15000K$). The remarks concerning stellar parameters made in the previous subsection are valid as well now.

Table 2 gives the results. The notation employed is the same as in Table 1. Again, the expansion velocity strongly decreases with α. V_{100} of about 200 kms^{-1} was obtained for α in the domain $0.05 - 0.1$. The model $\alpha = 0.5$ leads to a mass flux $\Phi = 2.0\,10^{-11}\,M_\odot y^{-1} sr^{-1}$. In order to have solutions with similar mass fluxes for decreasing α models we must admit high values for k. This requirement is even more strong than in the previous case (Sect. 4.1). For instance the model $\alpha = 0.1$ requires $k = 40.0$ to achieve $\Phi = 1.8\,10^{-11}\,M_\odot y^{-1} sr^{-1}$. The radial velocity profiles corresponding to such models are shown in Fig. 2.

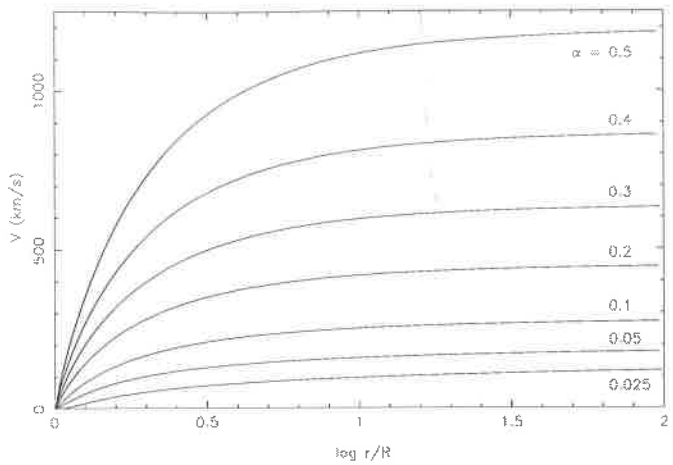

Figure 1: Expansion velocity (B0-B1 star) , for several values of α

Table 2: Results: B4-B5 star, standard model

α	k	$\Phi\,(M_\odot y^{-1} sr^{-1})$	$V_{100}(kms^{-1})$
0.5	0.3	2.010^{-11}	1121
0.4	0.3	7.910^{-13}	808
	0.5	2.810^{-12}	811
	1.0	1.610^{-11}	815
0.3	0.3	4.210^{-15}	585
	1.0	2.310^{-13}	595
	3.5	1.510^{-11}	597
0.2	0.3	1.510^{-19}	404
	1.0	6.010^{-17}	410
	3.5	3.110^{-14}	416
	13.0	2.110^{-11}	422
0.1	3.5	5.310^{-22}	245
	13.0	2.510^{-16}	252
	40.0	1.810^{-11}	259
0.05	40.0	3.910^{-16}	162
0.0	110.2	2.110^{-11}	46

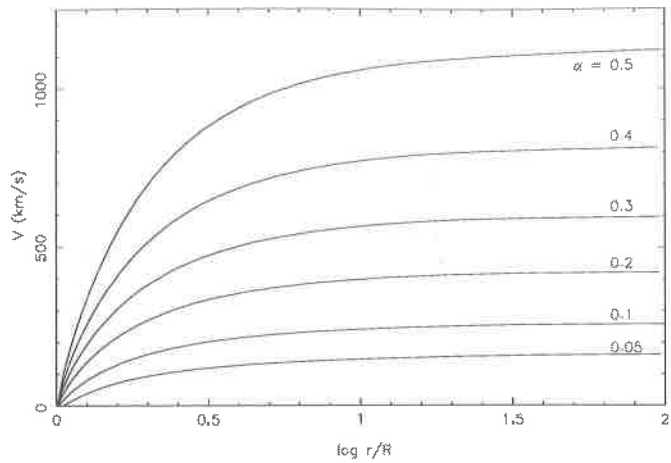

Figure 2: Expansion velocity (B4-B5 star) , for several values of α

5 The rotational profile $v_\phi(r)$

A consistent treatment of the conservation equations involves obtaining also a solution for $v_\phi(r)$. However, this demands some hypothesis on viscosity. Theoretical models often invoke conservation of specific angular momentum per unit of mass (Boyd & Marlborough, 1991; see also Chen & Marlborough, 1994). On the other hand Keplerian rotation has been widely employed in ad-hoc scenarios. Our treatment consists (see also Araújo & Freitas Pacheco, 1989; Araújo et al, 1994; Stee & Araújo, 1994) in adopting a viscosity parameter which may simulate different conditions, from solid body rotation to angular momentum conservation.

In Sect. 2 it was noted that this parameter (δ) should vary from -1 to +1. However, we managed to get solutions from our code only in the range $\delta = 0.0 - 1.0$. The results we could obtain with $\delta = 0.25$; 0.5; 0.75 and 1.0 are expressed in Table 3. Once again we have expansion decreasing with decreasing αs. But what must be emphasized now is that only for $\delta = 1/2$ (Keplerian rotation) are there solutions for very small values of α (0.05 - 0.025) and we are able to obtain $V_{100} \approx 100 - 200$ kms^{-1}! When $\delta = 0.25$ the model $\alpha = 0.1$ gives $V_{100} = 542$ kms^{-1} while for greater δs (i.e. approaching angular momentum conservation) it becames more and more difficulty to obtain numerical solutions. This result may possibly indicate that in Be envelopes the rotational profile must be close to a Keplerian law.

6 Conclusions

Our computations have shown that decreasing expansion velocities are obtained as decreasing values of the radiative parameter α are used. However, it seems that the rotational field $v_\phi(r)$ should not be very far from Keplerian rotation.

Table 3: The influence of $v_\phi(r)$

$v_\phi(r)$	$\alpha; k$	$V_{100}(kms^{-1})$	$\Phi\,(M_\odot y^{-1} sr^{-1})$	$\alpha; k$	$V_{100}(kms^{-1})$	$\Phi\,(M_\odot y^{-1} sr^{-1})$
$(R/r)^{0.25}$	0.5;0.3	1327	3.610^{-9}	0.5;0.3	1252	2.010^{-11}
	0.4;0.7	1026	3.910^{-9}	0.4;1.0	967	1.610^{-11}
	0.3;1.5	820	3.710^{-9}	0.3;3.5	773	1.510^{-11}
	0.2;3.2	667	4.410^{-9}	0.2;13.0	628	2.310^{-11}
	0.1;6.0	542	3.910^{-9}	0.1;40.0	508	2.410^{-11}
$(R/r)^{0.5}$	0.5;0.3	1184	3.610^{-9}	0.5;0.3	1121	2.010^{-11}
	0.4;0.7	861	3.810^{-9}	0.4;1.0	815	1.610^{-11}
	0.3;1.5	630	3.710^{-9}	0.3;3.5	597	1.510^{-11}
	0.2;3.2	445	4.110^{-9}	0.2;13.0	422	2.110^{-11}
	0.1;6.0	272	3.010^{-9}	0.1;40.0	259	1.810^{-11}
	0.05;8.3	178	3.810^{-9}	0.05;40.0	162	3.910^{-16}
	0.0;10.54	65	3.510^{-9}	0.0;110.2	46	2.110^{-11}
$(R/r)^{0.75}$	0.5;0.3	1165	3.510^{-9}	0.5;0.3	1057	2.010^{-11}
	0.4;0.7	765	3.710^{-9}	0.4;1.0	726	1.610^{-11}
$(R/r)^{1.0}$	0.5;0.3	1080	3.510^{-9}	0.5;0.3	1024	2.010^{-11}

On the other hand large values for the radiative parameter k are required if we want to obtain mass loss rates comparable to observational ones. Let us comment briefly on this point. When $\alpha = 0.0$ (no optically thick lines at all) k gives the ratio between the radiative acceleration due to the thin lines and the electron scattering force (see Eq. (9)). So, we should have a thin line force of about ten times stronger than the electron scattering one for the B0–B1 star. In the second case (B4–B5 star) this ratio should be even greater, of about two orders of magnitude.

The above discussion allows us to conclude that a radiative force due basically to optically thin lines may lead to an outflow with the desired properties - a shallow expansion and a large mass flux -, but indeed large number of these lines is required. Is this the main mechanism present in the equatorial plane of Be star envelopes? We cannot give a definitive answer to this question now. More sophisticated models should be developed: the radiative force must be calculated self-consistently rather than considering α and k as "free" parameters.

Despite the above remark a first sucessfull application of such a model is currently being done by Stee et al (in preparation). They have performed a detailed reproduction of the H_α line profile and the corresponding visibility curves of the star $\gamma\,Cas$. From this work they could infer the acceptable values of α: $\alpha = 0.05$ for the equatorial plane while $\alpha = 0.5$ for the polar axis of that star.

References

[1] Araújo, F.X., Freitas Pacheco, J.A. 1989, MNRAS, 241, 543

[2] Araújo, F.X., Freitas Pacheco, J.A., Petrini, D. 1994, MNRAS, 267, 501

[3] Bjorkman, J.E, Cassinelli, J.P. 1993, ApJ, 409, 429

[4] Boyd, C.J., Marlborough, J.M. 1991, ApJ, 369, 191

[5] Castor, J.I., Abbott, D.C., Klein, R.I. 1975, ApJ 195, 175 (CAK)

[6] Chen, H., Marlborough, J. M., 1994, ApJ, 427, 1005

[7] Chen, H., Marlborough, J. M., Waters, L.B.F.M. 1992, ApJ, 384, 605

[8] Drew, J.E., 1989, ApJS, 71, 267

[9] Friend, D.B., Abbott, D.C. 1986, ApJ, 311,701

[10] Kogure, T., Hirata, R., 1984, Bull. Astr. Soc. India, 10, 281

[11] Koninx, J.P.M., Hearn, A.G. 1992, A&A, 263, 208

[12] Lamers, H.J.G.L.M. 1986, A&A, 159, 90

[13] Lamers, H.J.G.L.M., Pauldrach, A.W.A. 1991, A&A, 244, L5

[14] Marlborough, J. M., Peters, G.J. 1986, ApJS, 62, 875

[15] Owocki, S.P., Cranmer, S.R., Blondin, J.M. 1994, ApJ, 424, 887

[16] Pauldrach, A.W.A., Puls, J. 1990, A&A, 237, 424

[17] Parker, E.N., 1958, ApJ, 128, 664

[18] Parker, E.N., 1960, ApJ, 132, 175

[19] Poe, C.H., Friend, D. 1986, ApJ, 311, 317

[20] Poeckert, R., Marlborough, J. M. 1978, ApJ 220, 940

[21] Press, W.H., Teukolsky, S.A., Vetterlin, W.T., Flannery, B.P., 1992, Numerical Recipes, Cambridge Univ. Press, Cambridge

[22] Stee, Ph., Araújo, F.X. 1994, A&A, in press

[23] Waters, L.B.F.M., Taylor, A.R., van den Hanvel, E.P.J., Taylor, A.R., Marlborough, J.M., Dougherty, S.M., 1991, A&A, 244, 120

[24] Waters, L.B.F.M., Marlborough, J. M. 1992, A&A, 253, L25

THE UPPER H-R DIAGRAM

Augusto Damineli Neto - IAG/USP

Abstract

We revise the status of massive stars knowledge. We describe the main families of stars in the upper H-R diagram and their interconnections. The LBV stage is focused in some detail, as it plays a crucial role in the mass loss and as a consequence, in the evolutionary tracks.

1 Massive stars in context

Many astronomers are not familiar with the upper part of the H-R diagram (UHRD). The blue part of the UHRD is yet imagined as populated by peculiar, extremely rare stars, not atractive to understand the the stellar phenomenon as a whole. This point of view has been drastically changed in recent times. For one hand, the observations revealled a large number of high mass stars in nearby galaxies, specially in starbursts. For another, theoretical simulations showed that they play an important role in the first stages of galaxy's life, by injecting energy, momentum and processed chemical elements (He and N) in the interestellar medium (ISM). Nowdays, models and evolutionary tracks of massive stars are able to explain the main features of the UHRD. Evolutionary synthesis calculations fits CIV, SiIV and HeII lines of the Wolf-Rayet (WR) galaxies. But the agreement is only qualitative. Some galaxies, like He2-10, are dominated by massive stars. A population of thousands of WR stars can be derived from the HeII 4686 emission line strenght in that and in other similar objects. Conti (1994) derived the masses of 9 knots in the nucleus of He2-10, containing the WR feature (HeII emission) and showed that they are compatible with young (10 Myear) globular clusters. This is a very interesting opportunity to study the evolution of these objects, that in our neighborhood are tousand times older.

The look back time for the galaxies with z=3-4 is such that we are seen them in a early stage of evolution, when they were plaintifull of massive stars. Massive stars are of great cosmological interest, in spite of being not completely understood. We refer as massive to a star of $M > 8M_{\odot}$, early than B5 on the main sequence (MS) and as supermassive to a star of $M > 15M_{\odot}$, O-type on the MS. The data of distant objects are interpreted by calibrations based in our Galaxy and in the Large Magellanic Cloud (LMC). At these distances, it is possible to study both the stellar and gaseous contents of the giant HII regions (GHIIR), to derive the Initial Mass Function (IMF), Star Fromation Rate (SFR), ages and to model the nebular spectrum. Some of them, as 30 Doradus in the LMC, have a high concentration of stars, $1.8\text{x}10^5 M_{\odot} pc^{-3}$. GHIIRs in starburst galaxies seems to be at least 10 times larger than 30 Dor. NGC3603, the largest young stellar cluster in our Galaxy, is much smaller than 30 Dor but has an even denser core (Hoffmann et al. 1995). It appears that larger clusters are located near the galactic center (GC), but we need a

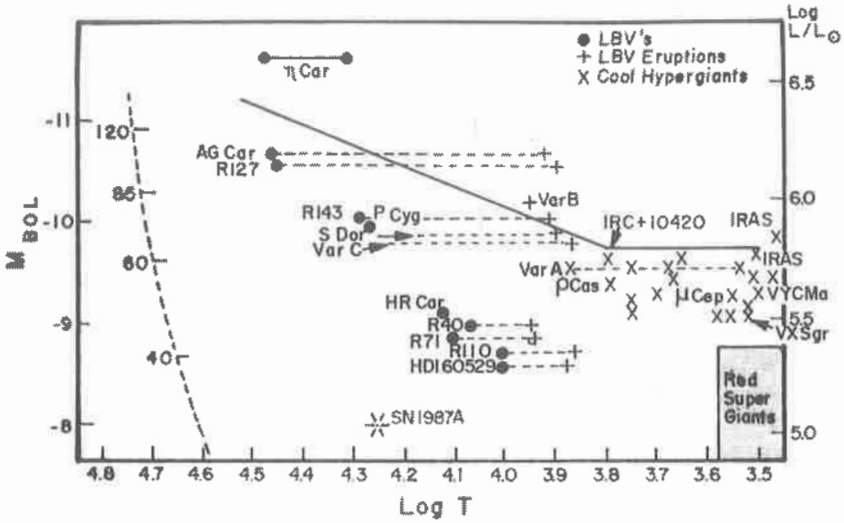

Figure 1: The UHRD (Humphreys, 1993)

new generation of large telescopes, optimized for the near infrared, to get observations in full details.

2 Main features of the UHRD

The main features of the UHRD, displayed in fig. 1 are:
a) Luminous hot stars are variable in several time-scales.
b) Mass loss rate grows towards higher luminosity, although the relation is not linear.
c) Luminous stars are evolved, the majority of them in the post Helium burning stage.
d) There is a well defined upper luminosity limit, above which no star is found. In the blue side it is known as Humphreys-Davidson's limit and in the red, as de Jager's limit.

Irregular and low amplitude variability of the α Cygni type is ubiquitous among hot luminous stars. The amplitude is ΔV=0.1-0.3 mag and the timescale 10-50 days. In longer timescales: years to tens of years, the LBVs (Luminous Blue Variables) show variations of the S Doradus type, whose amplitude is ΔV=0.5-2.0 mag, but at constant bolometric luminosity. In timescales of centuries or millenia the LBVs undergoes giant bursts, with $\Delta V > 2$ mag, releasing energy of the order of that of a supernova in a few decades. Wolf-Rayet and B[e] stars are not intrinsecally variables. There are some other types of stars that seems to be related to the evolved supermassives ones, as some highly luminous OH/IR and A hypergiants in nearby galaxies.

Stars with $L > 10^5 L_\odot$ do show line profile variabilty when its temperature is high enough: 40 000K $\geq$ T $\geq$ 20 000K. The amplitude of the line profile variations decreases towards the MS (Fullerton 1990, Fullerton et al. in preparation). Absorption components in the blue side of the line profile is an evidence that a star is undergoing mass loss, specially when the velocity is greather than the scape velocity. In many cases, this is

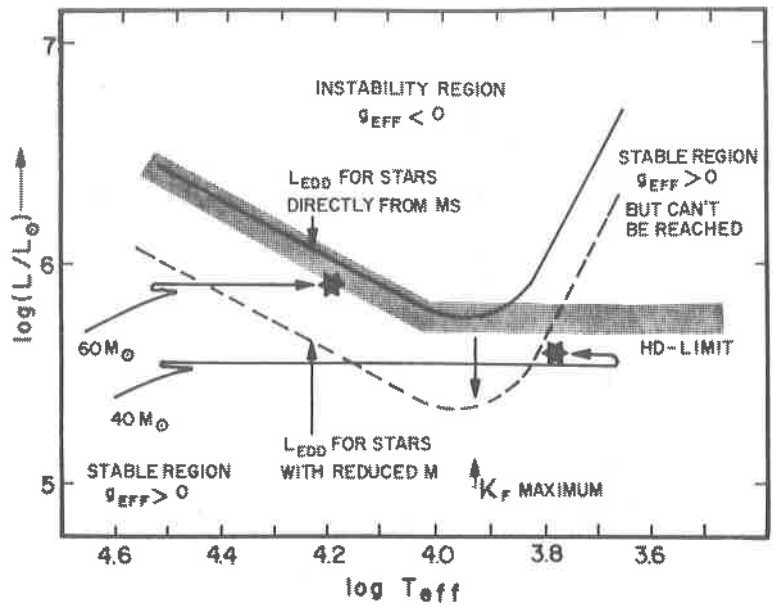

Figure 2: *The upper luminosity limit decreases a) towards lower surface temperatures and b) when the star evolves at constant luminosity and loose mass (Lamers 1995).*

corroborated by the presence of expanding nebulae surrounding the stars. In the UHRD, it is a common place to find overabundance of He and N and underabundance of O, as expected from CNO cycled material. The mass loss rate is a crucial parameter to calculate evolutionary tracks. But, in the UHRD, this parameter is up to now, introduced by hand in the models, on the basis of empirical determinations. Typical figures are: 10^{-7} to $10^{-9} M_\odot year^{-1}$ for classical Be stars, 10^{-5} to $10^{-6} M_\odot year^{-1}$ for O type, 10^{-4} to $10^{-5} M_\odot year^{-}1$ for WRs and 10^{-3} to $10^{-5} M_\odot year^{-1}$ for LBVs (Damineli and de Freitas Pacheco 1982, Crowter and Willis 1994, Leitherer and Lamers 1994). The proximity of the LBVs to the Eddington limit indicates that the low gravitacional force plays an important role in the mass loss. A generalized formula of the Eddington limit is given by:

$$Y = \frac{kL}{4\pi GM} \tag{1}$$

where Y is the ratio between the radiative and the gravitational forces and k is the opacity coefficient of the gas.

A star is unstable for $Y > 1$. Around 40 000K the gas is fully ionized in order that eletronic scattering is the main source of opacity. For lower temperatures, the degree of ionization decreases and the opacity increases, as it comes mainly from the metallic lines. The maximum opacity occurs around 10 000K. For cooler stars, the atmospheric turbulence also contributes to the pressure, reducing the Eddington limit for a given mass and luminosity (fig.2). In fact, there is an upper luminosity limit also for cool stars, known as de Jager's limit (Lamers 1995).

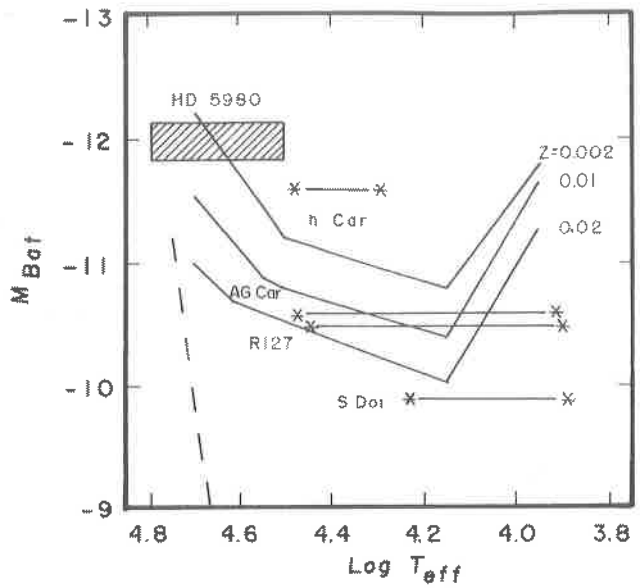

Figure 3: *Effect of metalicity on the Eddington limit (Barbá et al 1995)* .

Contrarely to the case of low mass stars, the massive ones evolve at constant luminosity. As they loose mass, the effective gravity becomes lower and lower, in order that a $M < 50M_{\odot}$ star, after becoming a red supergiant, reaches the Eddington limit and becomes unstable. This seems to be the case for the lower luminosity LBVs. For $M > 50M_{\odot}$, however, the star reaches the Eddington limit before the RSG branch. The evolutionary track bends towards the left, mantaining the star allways in the blue side of the HRD. As the opacity is a function of the chemical abundance, the Eddington limit is dependent also on the metal enrichment of the star, as can be seen in fig. 3 (Barbá et al. 1995). It is important to note that the majoriy of stars in the UHRD are near but not on the Eddington limit. A mass ejection méchanism is needed to put the gas outside the stellar gravity well. The radiative force is not powerfull enough to account for the mass loss rates in the LBV and some other phases in the UHRD.

3 LBV stars

LBV is a group of luminous, variable, evolved, generally blue stars, since before known as Huble-Sandage variables in M31 and M33 galaxies, S Doradus variables in LMC and P Cygni, η Car, AG Car, HR Car in our Galaxy, listed in Table I. Spectroscopically, they do not form a homogeneous class. The degree of excitation is generally low, with strong lines of H, FeII, HeI and seldom HeII in emission. Their P Cygni profiles shows moderate to low velocities (100-1000Km/s). In the eruptive phases the spectrum can show purely absorption lines.

The most characteristic photometric variability of LBVs are the S Doradus incoherent

cycles. During the low brightness phases, called "quiescence", the star is hotter, bluer and the higher excitated emission lines are stronger. During the photometric maxima, called "bursts", the star is redder and the line excitation degree is lower. The bolometric magnitude remains nearly constant, implying in a reprocessment of the energy from the UV towards the longer wavelengths (Caputo and Viotti 1970). The name "burst" is not appropriate to the S Dor cycle, as there is no real variation of the energy release. In the quiescent phase, the surface temperature of the most luminous S Dor reachs 30 000 K and that of less luminous 10 000 K. In the eruptive phase, however, all S Dor share the same limit around 8 000K. This is due to the fact that there is no way to the wind to cool below 7 000 K (Davidson 1978). The instability that drives the wind cannot be of photospheric origin, as the mass involved in the S Dor oscillation is high: 10^{-2} to $10^{-3} M\star$ (Lamers 1995). LBVs can show giant eruptions in timescale of centuries to millenia, in which there is a real variation of bolometric luminosity. Examples of this behavior are the bursts of SN1961V (that reaching Mbol=-17) that of P Cygni in the XVII century and that of η Carinae in the past century. These events are acompanied by huge mass ejection, contrarely to the S Dor cycles, where there seems to be no variation of the mass loss rate (Leitherer et al. 1994). The necessity of a phase of very high mass loss rate is deduced from the simple fact that an O type star loose mass at a rate of $10^{-6} M_{\odot} year^{-1}$, and at such rate it is able to eject only around $1 M_{\odot}$ during their lifetime (1 Myear). This is far below what is needed to expose the CNO cycled material and to transform an O type into a WR type star. There are indications that such phase corresponds to that of LBVs, that would be very short, due to the scarcity of this kind of stars. The time spent in this phase may be evaluated by comparing the number of LBVs with that of their progenitors, the WRs. In the LMC, there are 115 WR and 6 LBVs, giving a evolutionary time of :

$$t_{LBV} = t_{WR} \frac{N(LBV)}{N(WR)} = 25\ 000 years \tag{2}$$

4 Wolf-Rayet stars

WR are stars with strong emission lines of He, N and/or C. The equivalent width of HeII lines may reach 100 A and that of CIII up to 1000 A. The line profiles are top flated, with 1000 Km/s in the base. The HeI lines frequently show P Cygni profiles, indicative of dense winds. The N and C lines are indicative of CNO processed material. There are two sequences of WR stars, the WNs, dominated by Nitrogen lines and WCs, dominated by Carbon lines. The luminosity span the range $10^{4.5}$ to $10^{6} L_{\odot}$ for WNs and $10^{4.7}$ to $10^{5.5}$ for WCs (Hamman et al. 1983, Koesterke and Hamman 1995). The WR phase duration is estimated to be around 480 000 years, including both WN and WC phases. WRs are believed to be the ending products of the massive stars evolution, before to explode as SN. In this scenario, the WRs are very usefull to cense the massive star formation, as they

Table 1: Characteristics of known LBVs

Name	Mbol	Tmax(K)	Tmin(K)	M ($M_{\odot} year^{-1}$)	Galaxy
Eta Car	-11.6	30000	-	10^{-3}	Milk Way
P Cyg	-9.9	19000	-	$2x10^{-5}$	"
AG Car	-11.0	30000	9000	$3x10^{-5}$	"
HD160529	-8.9	11000	8000	-	"
HR Car	-8.9	14000	-	-	"
S Dor	-9.8	25000	8000	$5x10^{-5}$	LMC
R127	-10.5	30000	8500	$5x10^{-5}$	"
R71	-8.8	13500	9000	$6x10^{-5}$	"
R143	-10.0	20000	8500	-	"
R110	-8.9	10000	7500	$3x10^{-6}$	"
R40	-9.0	< 10000	8500	$8x10^{-6}$	SMC
HD5980	-12.8	< 35000	-	-	"
AE And	-10.0	30000	-	$2x10^{-5}$	M31
AF And	-11.4	< 30000	-		M31
Var B	-10.2	-	9000	$1x10^{-5}$	M33
Var C	-9.8	25000	8000	$5x10^{-5}$	M33

Other LBVs- Milk Way: He3-519, Wra 751, G79.29+0.46, g25.5+02, LMC:HDE269582, R84, R99, S61, S119, - M31: Var A-1, Var 15- M33: Var 2, Var 83, Romano's star - NGC2403: V12, V22, V35, V37, V38- M81: I1, I2, I3- M101: V1, V2, V10- NGC1058: SN 1961V.

are much easier to detect than their progenitors, the O type stars and their descendants, the SNs. They enable the determination of the slope of the IMF and of the M_{upper}. The number ratio WC/WN is indicative of the chemical enrichment of the ISM (Conti 1994). Higher metalicity produces higher opacity, resulting in stronger winds and increasing the range os masses to which a star ends it evolution as a WC. This is in accord to the fact that WC/WN is much lower in SMC and LMC than in the Milk Way. In our Galaxy, there is also a radial gradient fo this ratio. WC/WN=0.74 in external zones to the solar orbit and WC/WN=0.95 towards the galactic inner regions (Conti and Vacca 1990). These figures, however are not definitive, as the incompleteness of the sample is of the order of 50% in the solar neighborhood, due to the fact that Av=7 (van den Bergh 1991) for WR stars for the $D < 3Mpc$. Moreover, the O type stars are born in the inner core of the GMCs, and take 1 million years to escape from it, what is of the same order of its evolutionary time. The majority of them explode as SN before leaving the most obscured zones of the MC. It is possible that the sample of WR stars we know, are not representative of the massive stars, but only of the high speed members.

5 Evolutionary tracks in the UHRD

The most recent models of supermassive stars agree qualitatively with the observations (Maeder and Meynet 1987, Maeder 1991). One of the most striking feature is the prediction that a star with $M > 50M_{\odot}$ never reaches the RSG branch. However, for O stars, the predicted luminosity and He contents are higher than observed, for Of stars, the predicted mass loss rates is lower than observed and the LBV phase is not accounted for. The theory of radiation driven winds is able to explain the acceleration of the wind, but not to start it. The inclusion of Iglesias et al. (1992) opacities and of the violent coupling modes of oscillation of Kiriakidis et al. (1993), led to surprisingly better evolutionary models (Langer et al. 1994). This kind of instability is based in the annalisis of the stellar structure stability. The instability is originated near the Fe recombination zone and affects all massive stars. The prediction of the strange mode pulsations matches very well the observations (fig. 4). The strange, or violent mode pulsational theory predicts also instability of He cores, in accord with the observations that show a lower limit to the luminosity of WC stars.

This mechanism is also attractive due to the fact that it occurs in deep layers, as required by the S Dor oscillations. Fig. 5 shows the mass loss rates of a $60M_{\odot}$ star caculated by Langer et al. (1994), appropriate for P Cygni. Fig. 6 shows the evolutionary track calculated by Langer et al. (1994), for P Cygni.

The main conclusions of the Langer et al. model are:
a) H-rich WNL are in the phase of central core H-burning and their mass loss rates are explained by the violent coupling mode instability.
b) The high mass loss rate on the MS result in a lower ending mass in the WR phase, explaining the observed limit of luminosity of the H-free WN stars.

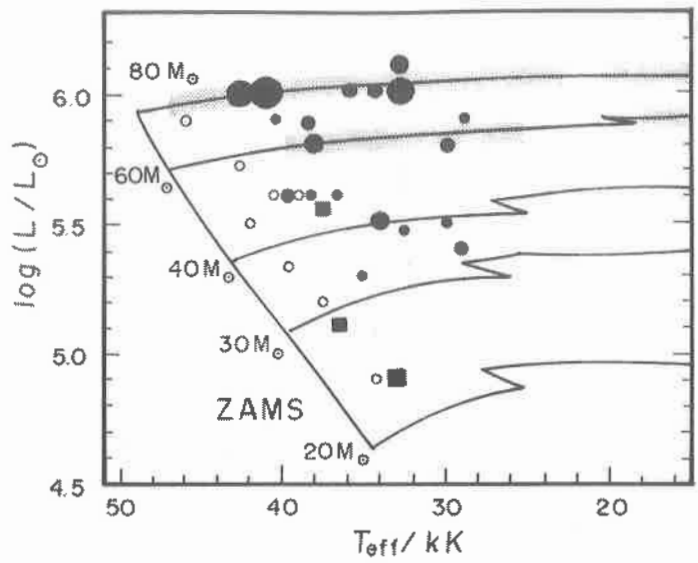

Figure 4: *shaded zones: phases in which instabilities are predicted by Kiriakidis et al. (1993) model. Circles and squares: measured amplitude of line profile variability by Fullerton (1990, 1991) and Fullerton et al. (in preparation).*

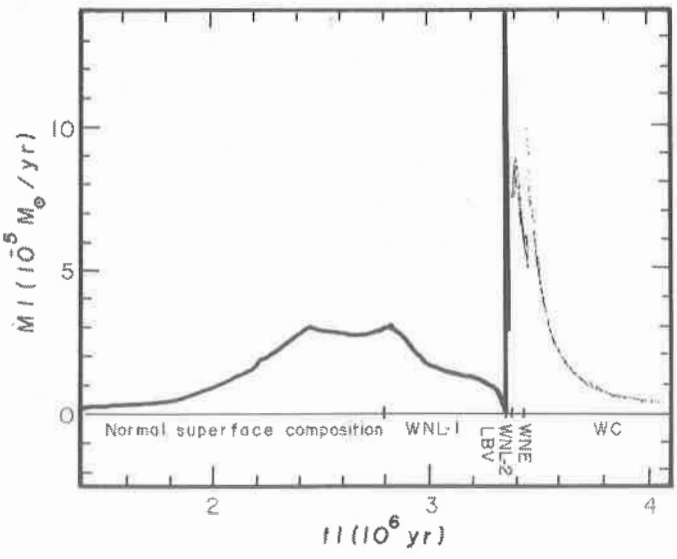

Figure 5: *Mass loss rate for a star of $60M_{\odot}$ (Langer et al. 1994). The peak in the LBV phase reaches $5x10^{-3}M_{\odot}year^{-1}$. The total mass loosed in the LBV phase is $6M_{\odot}$.*

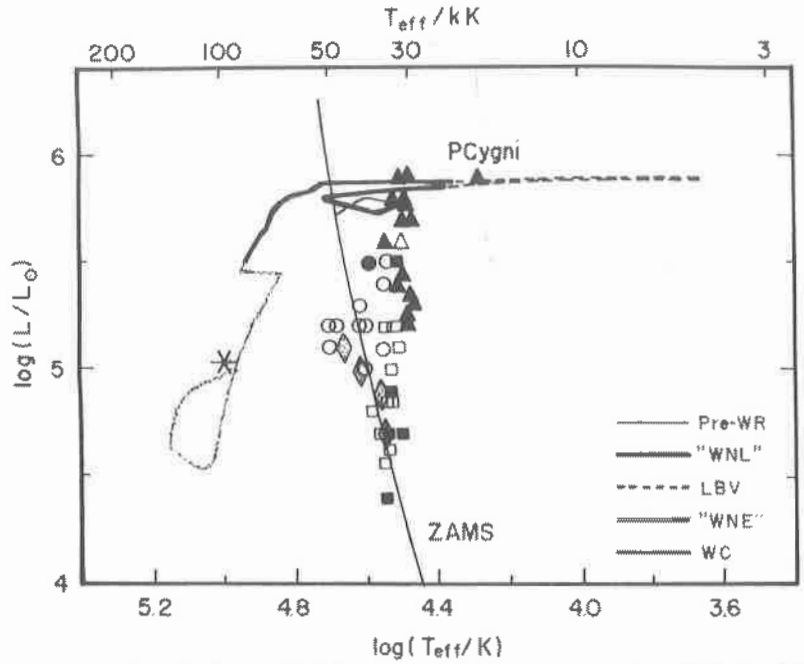

Figure 6: *Evolutionary track for a 60$M_\odot$ star by Langer et al. (1994). Triangles refer to mesured WNLs, circles to faint lined WNE, squares to strong lined WNE, diamonds to WC. Filled dots represent positive deteccion of H and unfilled, non detection of H.*

c) LBVs are He-rich, in accord with the observations, and are near their Eddington limit, due to the violent pulsations.
d) In the phase of core He burning, after the LBV phase, the star pass through a second WNL phase, but now, H-poor.

The detailed sequence of evolution of a $60M_\odot$ stars is, by this model is:
$O > H-richWN > LBV > H-poorWN > H-freeWN > WC > SN$

The general scheme presented previously by Maeder (1991) is:

$O > RSG > SN$	$35M_\odot > M > 15M_\odot$
$O > BSG > YSG > RSG > WR > SN$	$50M_\odot > M > 35M_\odot$
$O > Of > BSG > LBV > WR > SN$	$M > 50M_\odot$

The recent discover of Barbá et al. (1995), showing that the spectrum of HD 5980 changed from WN3.5+WN4.5 to that of an LBV, increasing by Δ V=2.3 mag, indicates that the evolution is not allways in the same sense. The star seems to perform incursions back and fort between the LBV and WR stages. Only long term observational programs of LBVs and WRs can provide the lacking of informations about the mechanism involved in this kind of behavior. We do not know if the giant eruptions are connected to the S Dor cycles, that have much smaller timescales: 5.5 years for η Car (Damineli 1996) and

up to 40 years for other stars. We do not expect to pick up a giant eruption by surveying a single star. A large sample, say 50 S Dor stars, including the Galactic Center and other galaxies up to the Virgo cluster, has a great probabilty of recording one great burst in a 10 year survey.

Aknowledgements: to FAPESP and CNPq for finnancial support.

References

[1] Barbá, R.H., Niemela, V.S., Baume, G., Vazquez, R.A.: 1995 (preprint).

[2] Caputo, F. & Viotti,R.: 1970 A&A 7, 266.

[3] Conti, P.S.: 1994 Sp. Sc. Rev. 66, 37.

[4] Conti, P.S. & Vacca, W.D.: 1990 AJ 100, 431.

[5] Crowter, P.A. & Willis, A.J.: 1994, Sp. Sc. Rev. 66,85.

[6] Damineli, A.: 1996 ApJL 460, L49.

[7] Damineli,A. & de Freitas-Pacheco, J.A.: 1982 MNRAS 198, 659.

[8] Fullerton, A.W.: 1990 Ph. D. Thesis Univ. Toronto

[9] Hammann,W-R., Koesterke, L.,& Wesselowsky, U.: 1993 A&A 274, 397.

[10] Hoffmann, K-H., Saeggewiss, W. & Weigelt, G.: 1995 (preprint)

[11] Iglesias, C.A., Rogers, F.J. & Wilson, B.G.: 1992 ApJ 397, 717.

[12] Kiriakidis, M., Fricke, K.J. & Glatzel W.: 1993 MNRAS 264, 50.

[13] Koesterke, L. & Hammann, W-R.: 1995 (preprint).

[14] Lamers, H.J.G.L.M.: 1995, IAU Coll 155 (em impressão).

[15] Langer, N.,Hammann, W-R., Lennon, M., Najarro, F., Pauldrach, A.W.A. & Puls, J.: 1994 A&A 290, 819.

[16] van den Bergh, S.: 1991 Phys. Rev. 204, 385.

Section 6

Solar System and Astrometry

NONGRAVITATIONAL EORCES IN PRESENT AND PAST SOLAR SYSTEM

Rodney S. Gomes

Observatório Nacional

Abstract

The association of nongravitational forces with resonant dynamics is a rich source of dynamical behavior. Some observed Solar System features are explained by this coupling phenomenon, like the Earth resonant dust ring, due to the lock of dust particles affected by Poynting-Robertson drag in external resonances with the Earth. Jupiter 1:1 resonant arcs are also supposed to exist by a similar process. Yarkovsky effect may be responsible to the delivery of asteroid fragments to the Earth's neighborhood, after these bodies goes through resonant regions with Jupiter. The evolution of the early Solar System must have been remarkably affected by mutual interaction of gas drag forces and resonances with protoplanets. This interaction must have had an important influence in the formation of Solar System bodies, including planets and asteroids.

I. Introduction

We aim at pointing out the important dynamical aspects of a trapping into a mean motion resonance when a nonconservative force is present. We divide this work into the following three sections. In section 2, we study Yarkovsky force and the consequences of its effect at mean motion resonances with Jupiter for a 1m diameter body, like an asteroid fragment. In section 3, the formation of dust clouds in the Solar System is presented, as a consequence of the interaction of Poynting-Robertson drag with resonant dynamics. Finally, in chapter 4, we show some relevant aspects of the action of gas drag in a primordial solar nebula associated with the gravitational effects of a protoplanet.

II. Yarkovsky effect

Suppose a rotating spherical 1m diameter body with its rotational axis normal to its orbital plane. Its rotational status implies in a hotter afternoon hemisphere, where from solar radiation will be mostly reradiated. This in turn yields a radiation force with a transverse component either in the direction of the body's velocity or opposite to it, depending on its rotation sense. In this case we may have either a dissipative or an antidissipative force acting on the body. The acceleration caused by this force at 1 AU onto that 1m diameter body, supposing that it has an uniform density equal to $2.5 g/cm^3$, is $0.65 \times 10^{-10} m/s^2$ (Afonso et al, 1995). This is a small force, but its effect may be important as it is nonconservative. The secular variation imposed on

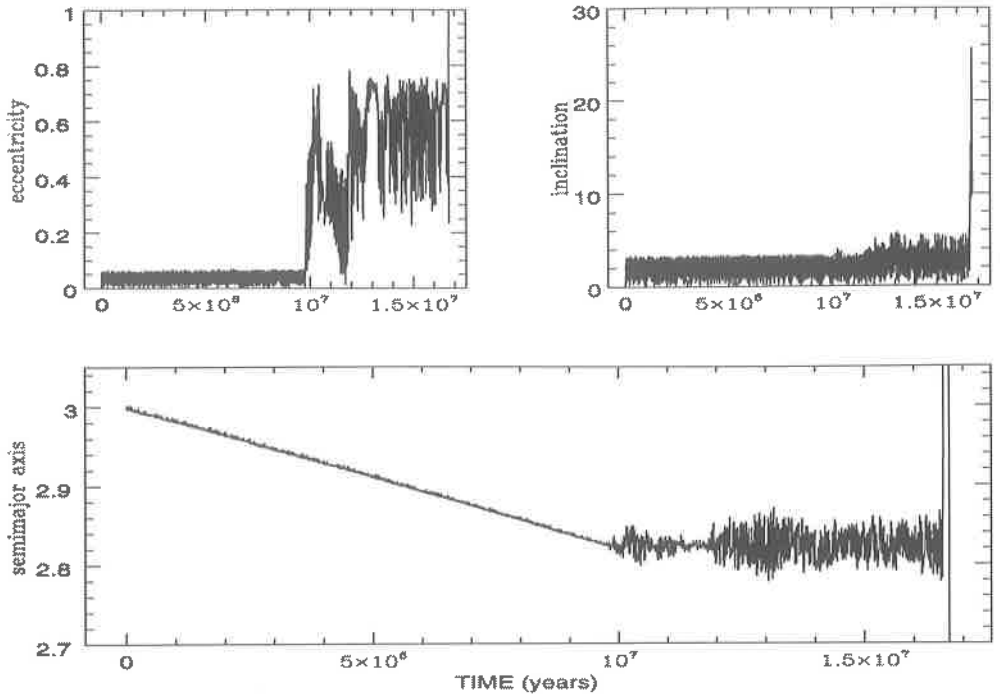

Figure 1: Evolution of orbital elements for a body affected by the Yarkovsky effect in the gravitational field of the Sun, Jupiter and Saturn.

the semimajor axis and eccentricity by the Yarkovsky effect up to second order in the eccentricities is given by (Gomes, 1995):

$$S_a/a = -\frac{K}{\sqrt{\mu a^3}}(2 + \frac{55}{8}e^2)$$

$$S_e/e = -\frac{K}{\sqrt{\mu a^3}}(2 + \frac{47}{6}e^2)$$

where a is the body's orbit semimajor axis, e its eccentricity, μ is a constant, and K is another constant related to the absolute value of Yarkovsky force, being positive or negative depending on its dissipative or antidissipative character.

Now suppose the body is in the gravitational field of Solar System planets. As its semimajor axis decays or increases through the above expressions, it will reach many resonant regions with the planets. In particular let us suppose that the body starts at $3AU$ in the gravitational field of the Sun and the perturbers Jupiter and Saturn, for the dissipative case. Figure 1 shows the evolution of 3 orbital elements, the semimajor axis, the eccentricity and the orbital inclination. At first, the semimajor axis starts decaying as expected from the Yarkovsky dissipative effect, but it eventually gets trapped in the 5:2 resonance with Jupiter. From this time, the semimajor axis stops its secular decay, although it gains a high amplitude variation around the resonant semimajor axis. The

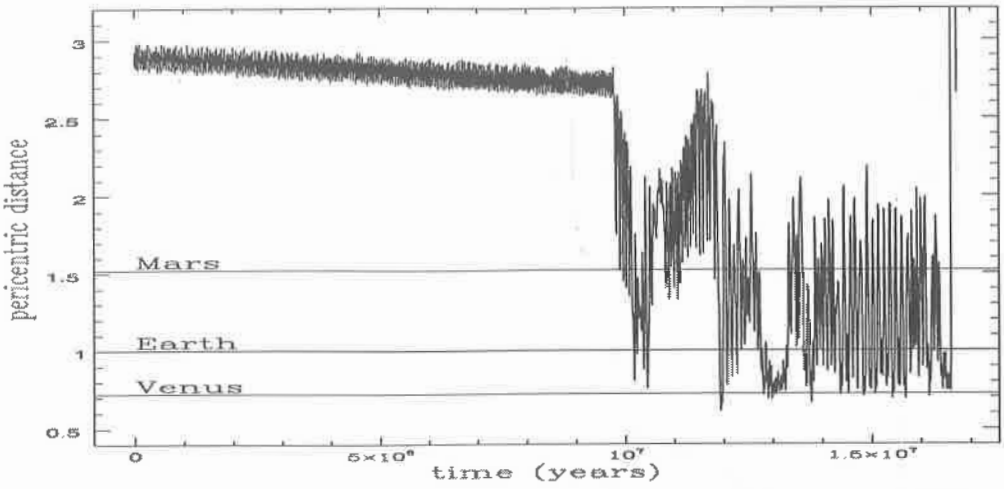

Figure 2: The same orbit as in figure 1, now showing the pericentric distance and the average distance of the inner planets to the Sun.

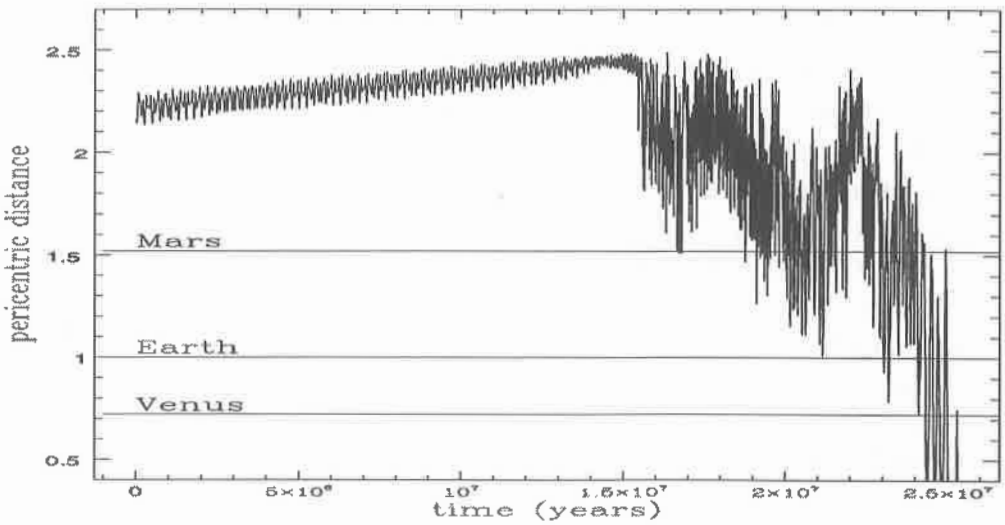

Figure 3: Pericentric distance or a body starting at 2.3 AU, with an antidissipative Yarkovsky effect. After capture into the 3:1 resonance with Jupiter, the body may get inside the inner planets' orbits.

eccentricity starts a somewhat chaotic variation after trapping, but in average it takes high values until the body gets into a hyperbolic orbit. The effect of this resonance on the pericentric distance is shown in figure 2. From this figure we notice that the body's orbit is Mars crossing, Earth crossing and even Venus crossing for a relatively long time during its trapped status. This phenomenon may cause the delivery of asteroids fragments into the Earth's atmosphere (Afonso et al, 1995).

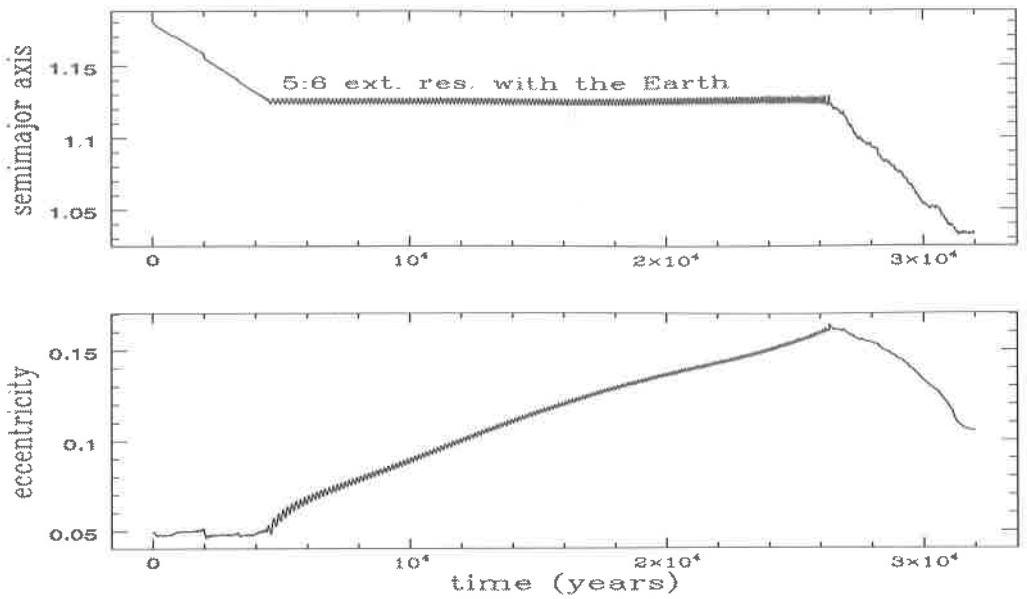

Figure 4: Evolution of a dust particle affected by Poynting-Robertson drag, showing a trapping in the 5:6 resonance with the Earth.

The capture into the 5:2 resonance with Jupiter shown in figure 1 does not necessarily occurs. Other examples of numerical integrations would show a very unstable trapping in the 4:1 resonance with Jupiter at $\sim 2AU$ which would place the body into a hyperbolic orbit in a relatively short time. Other examples would show a sharp increase of the eccentricity through the secular resonance also at about $2AU$, giving rise to inner planet's crossing orbits for a long time. A final example is shown in figure 3. The pericentric distance is plotted against time for a body starting at $2.3AU$ submitted to an antidissipative Yarkovsky effect. In this case, the body is trapped in the 3:1 resonance with Jupiter and its eccentricity increases until it takes a hyperbolic orbit. For a long time the body's orbit will be Mars crossing, Earth crossing and for a shorter time, but still non negligible, it will be Venus crossing.

III - Poynting-Robertson drag

The effect of radiation pressure on a micron sized particle induces an important dissipative effect onto the particle (Burns et al, 1979), the so called Poynting-Robertson drag. The secular variations in the semimajor axis and the eccentricity due to this dissipative effect are given by:

$$S_a = -\frac{C}{a}\frac{2+3e^2}{(1+e^2)^{\frac{3}{2}}}$$

$$S_e = -\frac{5}{2}C\frac{e}{a^2\sqrt{1-e^2}}$$

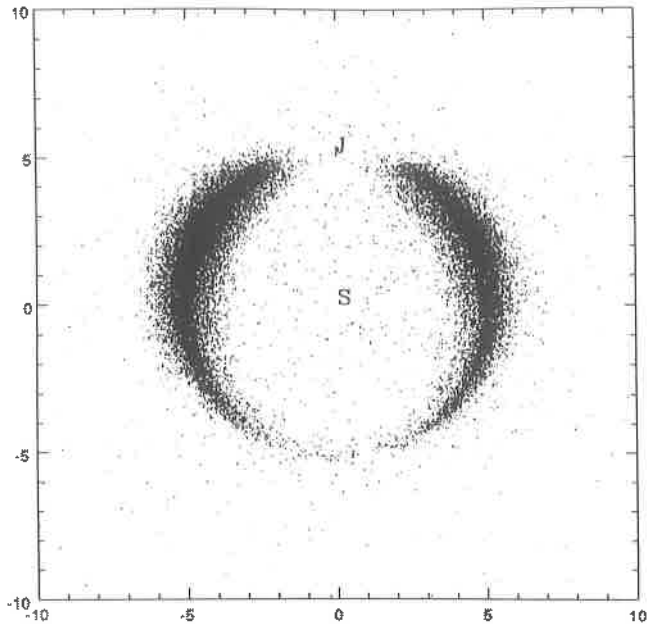

Figure 5: Numerical simulation showing dust arcs around Jupiter's orbit formed by dust particles coming from Trojan asteroids.

The decay in the semimajor axis may be couterbalanced by resonant effects coming from perturbing planets thus giving rise to resonance trappings. For this case of fast dissipative evolution (as compared to Yarkovsky effect), only external resonances are important. Here they are associated to converging orbits and trapping is a rather probable event (Henrard, 1982). Figure 4 shows a typical example of a trapping into the 5:6 resonance with the Earth. After trapping, the eccentricity will tend to increase to an equilibrium value (Gomes, 1995) if there is no close approach to the perturber that leads to resonance rupture, like this example. Trapping induced by Poynting-Robertson drag has always an unstable character, even when no close approach takes place (Gomes, 1995). This means that a particle will not stay 'for ever' in a resonance lock, just considering dynamical effects (of course it could be ejected from resonance by pure collision with another particle). Even so, the temporary lock of dust particles in external resonances with the Earth causes a denser number of particles just around the Earth's orbit (this must happen also with Venus and Mars, in a less effective way). This dust resonant ring, which was first proposed by Jackson and Zook (1989), has now observational evidence (Dermott et al, 1994).

Formation of dust rings may also occur at the 1:1 resonance with Jupiter (Liou and Zook, 1994). In this case particles may already start at the very resonant region. These would be particles released from the Trojan asteroids by continuous comminution. Figure 5 shows the results of a numerical simulation, where dust particles are released from the Trojan asteroids and their rectangular planar coordinates are plotted with respect to a referential frame rotating with Jupiter. This is the case with $\beta = 0.012$, where β is the ratio of the radiation pressure force to the gravitational force. For larger

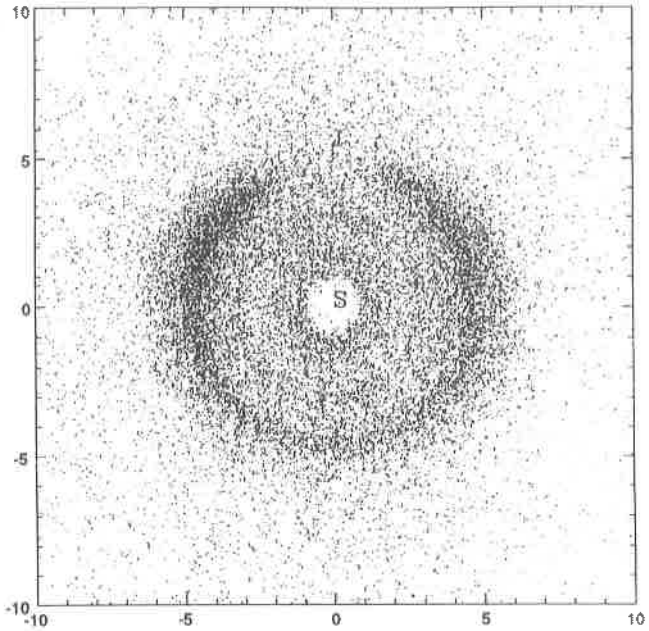

Figure 6: Numerical simulation showing dust arcs around jupiter's orbit formed by dust particles coming from the Eos asteroid family.

β (smaller particles), the radiation pressure on the just released particle will make it assume a larger orbit as it 'sees' the Sun with a smaller mass. In this case the particle may start out of the resonance region and posterior trapping is very difficult, so in respect with Trojan particles, the bigger ones are responsible for the formation of a possible cloud. On the other hand, due to the same radiation pressure effect, particles released in the main belt can be instantly placed in the Trojan region. This now will be possible for small particles (high β), as the gain in semimajor axis is higher for these particles. Figure 6 shows the possible formation of a dust ring in the (displaced) 1:1 resonant region with Jupiter, coming from particles that would be released from asteroids belonging to the Eos family. In this case we take $\beta = 0.25$. Although here the dust ring does not look so evident as that of figure 5, this is a more real case in the sense that dust is really formed in the main belt, whereas it is not sure that a significant amount of dust can be produced by the Trojan asteroids. In any case, there is not observational evidence of this Trojan ring. Particles are cold to be observed from the Earth, and surveyors sent to the outer Solar System always come near Jupiter and so not near the Trojan region. As a final comment, another promising candidate to have a dust ring around its orbit is Neptune. In this case dust would come from the Kuiper belt objects that seem to be numerous. The weak effect of Poynting-Robertson drag would also facilitate resonance trapping into external resonances with Neptune.

IV - Gas drag

Gas drag acted in the primordial Solar System nebula. The general expression for gas drag can be expressed as:

$$\vec{F}_g = -CV^{\mu}\vec{V}$$

where $\mu = 0$ or $\mu = 1$

$$\vec{V} = \vec{v} - \vec{v}_{gas}$$

$$\vec{v}_{gas} = 0.995\vec{v}_{kep}$$

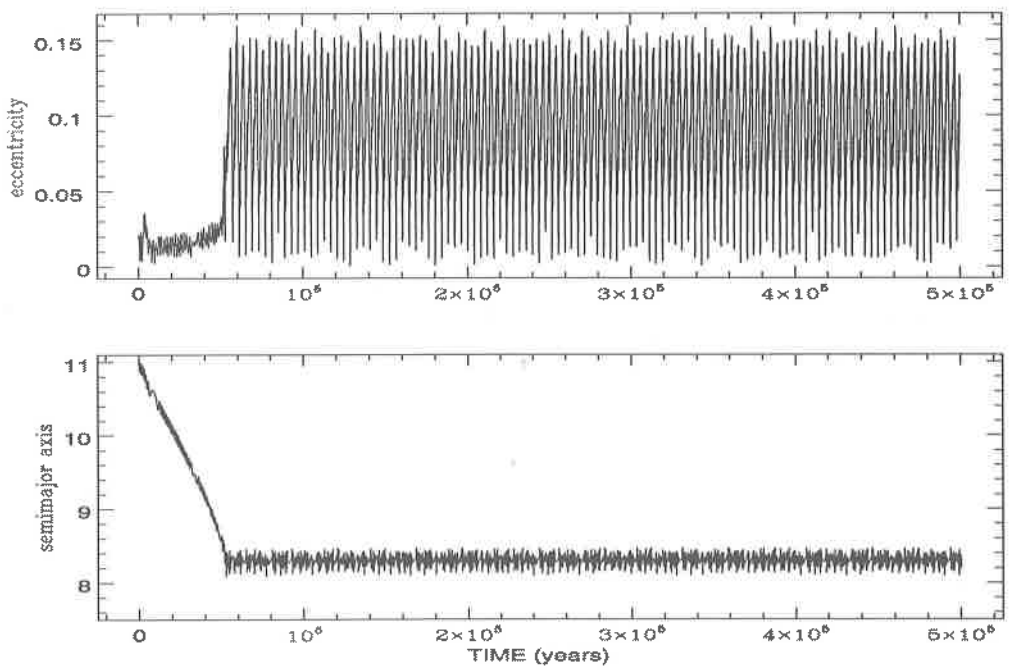

Figure 7: Trapping into the 1:2 resonance with Jupiter, for a body subject to gas drag, with $\mu = 1$

The case $\mu = 0$ is related to a less dense gas and smaller bodies, the opposite valid for the case $\mu = 1$. The interactive dynamics of both forms of drag with resonance are similar anyway. Figure 7 shows an example of resonance trapping for a body subject to gas drag (case $\mu = 1$), where Jupiter is the only perturber. Two interesting features are noticed here, differently from the Poynting-Robertson drag case. First the eccentricity stabilizes at a low value, thus preventing close approach with the perturber. Second, the semimajor axis oscillates with a constant amplitude, thus preventing resonance

rupture. Thus gas drag differs essentially from Poynting-Robertson drag (also from Yarkovsky effect and solar wind; see Gomes, 1995, for details) in the sense that trapping is stable under a dynamical point of view. Resonance rupture will be caused solely by intercollisions of planetesimals (Malhotra,1993). This stable aspect of resonance trapping induced by gas drag must have had an important contribution to Solar System formation. The planets themselves may have been formed in near resonance regions from one or two primordial ones (Patterson, 1987; Beaugé and Ferraz-Mello,1994). Gas drag may also have contributed to an early formation of the Trojan asteroids (Peale,1993).

IV - Conclusions

The interaction of nongravitational forces with resonant gravitational forces induces important phenomena in present and past Solar System. Due to Yarkovsky effect asteroids fragments may be trapped in resonances with Jupiter or pass by secular resonances induced by the pair Jupiter-Saturn. One of the effects of these resonances is the increase of orbital eccentricity, which can induce Earth-crossing orbits and possible delivery of these bodies into the Earth's atmosphere. For the case of Poynting-Robertson drag, resonance trappings of dust particles into exterior resonances with the inner planets are responsible for the formation of resonant rings around the inner planets orbits (the Earth's ring has been observationally proved to exist). Also a 1:1 resonant dust ring around Jupiter's orbit may exist. Finally, for the early Solar System, the association of gas drag forces with resonant gravitational effects coming from a protoplanet must have induced stable resonant locks of planetesimals, stability only broken by mutual collisions. Many aspects of today's Solar System may be a consequence of this early Solar System phenomenon, including the formation of trans-Jovian planets and the Trojan asteroids.

References

Afonso,G.B., Gomes,R.S. and Florkzac,M.A 1995. Asteroid fragments in Earth-crossing orbits. *Planetary and Space Science* **43:6** 787-795.

Beaugé,C., and S.Ferraz-Mello 1994. Resonance capture and the formation of the outer planets. *Mon. Not. R. Astron. Soc.* **270**, 21-34.

Burns,J.A., Lamy,P.L., Soter,S. 1979. Radiation Forces on Small Particles in the Solar System. *Icarus* **40** 1-48.

Dermott,S.F., Jayaraman,S., Xu,Y.L., Gustafson,B.A.S., Liou,J. C. 1994. A circumsolar ring of asteroidal dust in resonant lock with the Earth. *Nature* **369** 719-723.

Gomes,R.S. 1995. The effect of nonconservative forces on resonance lock: stability and instability. *Icarus* **115** 47-59.

Henrard,J. 1982. Capture into resonance: an extension of the use of adiabatic invariants. *Celestial Mechanics* **27**, 3-22.

Jackson,A.A. and H.A.Zook 1989. A Solar System dust ring with the Earth as its shepherd. *Nature* **337**, 629-631.

Liou,J.C. and Zook,H.A. and Jackson A.A. 1995. Radiation pressure, Poynting-Robertson drag, and solar wind drag in the restricted three-body problem. *Icarus* **116**, 186-201.

Malhotra,R. 1993. Orbital resonances in the Solar Nebula: strengths and weaknesses. *Icarus* **106**, 264-273.

Patterson,C.W. 1987. Resonance capture and the evolution of the planets. *Icarus* **70**, 319-333.

Peale,S.J. 1993. The effect of the Nebula on the Trojan precursors. *Icarus* **106**, 308-322.

VOYAGERS IMAGES REVEALING THE STRUCTURES OF THE PLANETARY RINGS

S. Giuliatti Winter

Grupo de Dinâmica Orbital e Planetologia
Campus de Guaratinguetá–UNESP

Abstract

The great tour of the Voyagers spacecraft revelead a large amount of information about the ring systems which encircle the four giants planets: Jupiter, Saturn, Uranus and Neptune. This paper describes the relevant structures discovered by the Voyager images.

1. INTRODUCTION

The rings of Saturn were first observed by Galileo in 1610 as an unusual phenomenon around the planet. Huygens in 1656 found the solution to this puzzle describing the ring as a thick, solid structure. In spite of many attempts in describing the ring as composed of small particles only in 1859 Maxwell proved that the stability of the ring required it to be formed by a large number of small moonlets. Later, this hypothesis was confirmed by Keeler's and Campbell's spectroscopic observations (Van Helden, 1984).

Andrew Common obtained the first photograph of Saturn in 1883. Since then a great expansion of observational capability in photometry, polarimetry and especially with the advent of spacecraft, revolutionized the field of planetary ring science.

Saturn presents the most complex planetary ring system in the Solar System. The main ring system is composed of two bright rings, A and B, the crepe C ring and the D ring. In 1966, during the ring plane crossing, the E ring was detected in photographs by Feibelman (1967). It is a faint ring which encompasses the orbits of the satellites Mimas, Enceladus, Tethys, and Dione. It has a brigth peak in the Enceladus orbit suggesting that this satellite could be the source for the ring particles. The F ring was discovered by Pioneer 11 in 1979. It is a narrow ring located about $\sim$ 4000 km from the main ring system.

The nine "classical" rings of Uranus were detected by Elliot *et al.* in 1977 during a star occultation through the Kuiper Airborne Observatory's 91-cm telescope. The rings were named in order of increasing distance from Uranus: 6, 5, 4, α, β, η, γ, δ and ϵ. The rings are very narrow varying between 2 and 12 km in width. There are two exceptions: the η ring ($W = 55$ km) and the ϵ ring ($W = 20$ to 96 km).

The ϵ ring shows a linear relation between its width and orbital radius, it has a width of 20 km at pericentre and 96 km at apocentre of its orbit. Nicholson *et al.* 1978 analysed the results obtained on April 11, 1978 observations and modeled the ring as a keplerian ellipse with different outer and inner eccentricities. Althought this model is in agreeement with the observations, differential apsidal precession due to the oblateness of

Uranus would change this configuration. Dermott and Murray (1980) have shown how self–gravity, collisions and differential precession can act together in order to stabilize the ϵ ring. The author is analysing this model by numerically simulating the ring particles using the tree code method developed by Richardson (1994).

After the discovery of Uranus rings many attempts have been made in order to detect rings around Neptune. During an occultation on July 22, 1984 observers led by A. Brahic and W. Hubbard found some evidence of material around Neptune. However, this material do not encircle the planet, implying the existence of "arcs" around Neptune. Because of these observations, Voyager 2 was reprogramed to collect more data about this recent discovery.

2. THE STRUCTURE OF THE RINGS

2.1 Voyagers Cameras

All the information described below has been extracted from the Voyager Imaging and Processing Userguide. The Voyager spacecraft are an advanced three–axis stabilized 'Mariner' class of spacecraft which have been designed for the exploration of the outer planets. They carried equipment for a total of eleven scientific investigations, including imaging science.

The cameras and the instruments necessary for imaging science are mounted on the scan platform, which incorporates sensors for the imaging, infra–red radiation (IRIS), UVS and PPS experiments. The scan platform can rotate about two angles, the azimuth and elevation angles, and the sensors are all 'boresighted' in order to point in a common direction.

There are three on–board computers, inter–connected, which control the orientation, instrument operation and scan platform movement of the spacecraft. One of these computers, the Flight Data System (FDS) is the one that supports the imaging science. It is responsible for the control of the Imaging Science Subsystem (ISS) throughout the mission. These instruments consist of:

- a narrow angle (NA) camera with a focal length of 1500 mm and a square field of view of 7.4 mrads or $0^{\circ}.42$.
- a wide angle (WA) camera with a focal length of 200 mm and a square field of view of 56 mrads or $3^{\circ}.21$.

The optical axes of the two cameras are 'boresighted' to be concentric and point in the same direction. Therefore, the image taken by the NA camera is contained in the centre of the image taken by the WA camera. All images were taken with the clear filter.

The duration of the exposure time is controlled by the shutter assembly controls, giving durations normally between 0.05 to 15 sec. The exposure time of each image depends on the feature that has to be analysed. The image formed by the camera lens is exposed onto the face plate called the vidicon tube. The output of each vidicon is a square array of picture elements (pixels), with 800 samples by 800 lines in a raw image. The light measured by the vidicon's photosensitive surface within each pixel is assigned a data number (DN) from 0 to 255.

These images can either be transmitted directly to Earth in real time, or they can be stored in digital form on the on–board spacecraft tape recorder to be transmitted in the future.

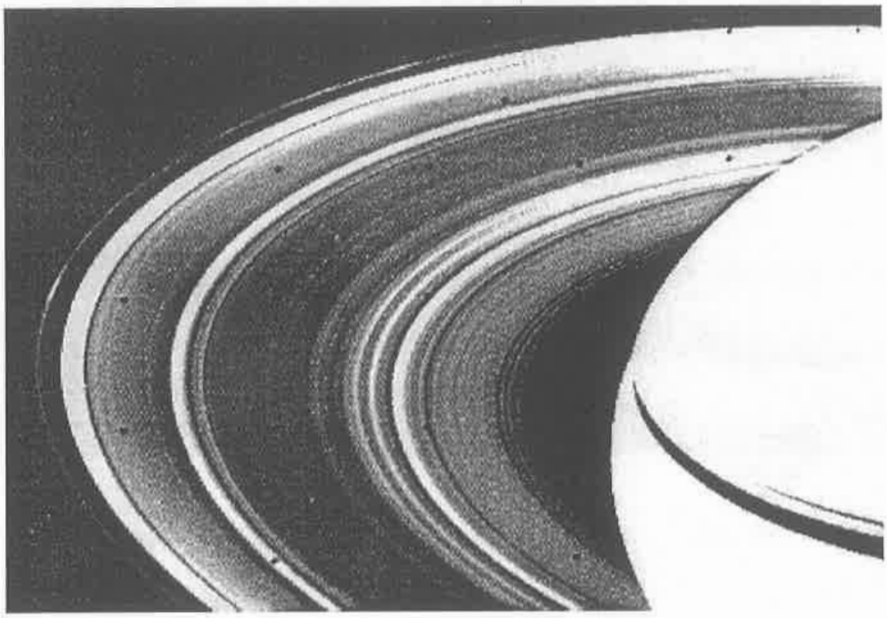

Figure 1. This Voyager 2 image (FDS 4410750) shows the main ring system of Saturn and the narrow F ring.

2.2 New Rings

Besides giving a detailed view of all the ring systems (for example, Figure 1) , Voyagers 1 and 2 also discovered new rings.

The G ring of Saturn is a faint ring visible in two Voyager images. It lies between the F and E rings. There was some evidence about this ring from the Pioneer 11 instruments before Voyagers encounter with Saturn. The G ring is mainly composed of dust ($\sigma = 10^{-6}$–10^{-7}) and has a width of 7000 km. Pioneer 11 instruments detected some signals which can be larger bodies, maybe the parent bodies of the G ring, of about 0.1–1 km. It has been proposed that the G ring could be the remanescent of a disrupted satellite.

Voyager 2 confirmed the existence of the nine rings of Uranus (Figure 2) and detected two new rings: the λ ring orbiting betweem the ϵ and δ rings and the 1986U2R ring orbiting interior to the 6 ring and extending to $\sim$ 3000 km in the direction of the planet. Due to the results from the radio and imaging observations the nine "classical" rings (Figure 2) are mainly composed of large particles of the order of meters.

In 1989 Voyager 2 revealed that Neptune has a ring system (Figure 3) composed of three rings named from the planet increasing distance: the Galle, Le Verrier and

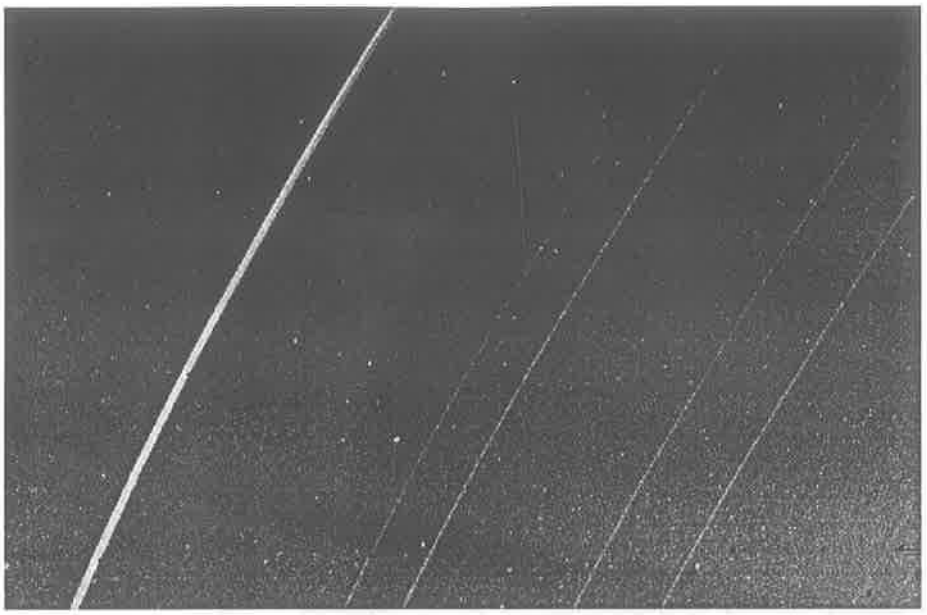

Figure 2. The nine classical rings of Uranus can be seen in this image (FDS 2681416)taken in back scattered light.

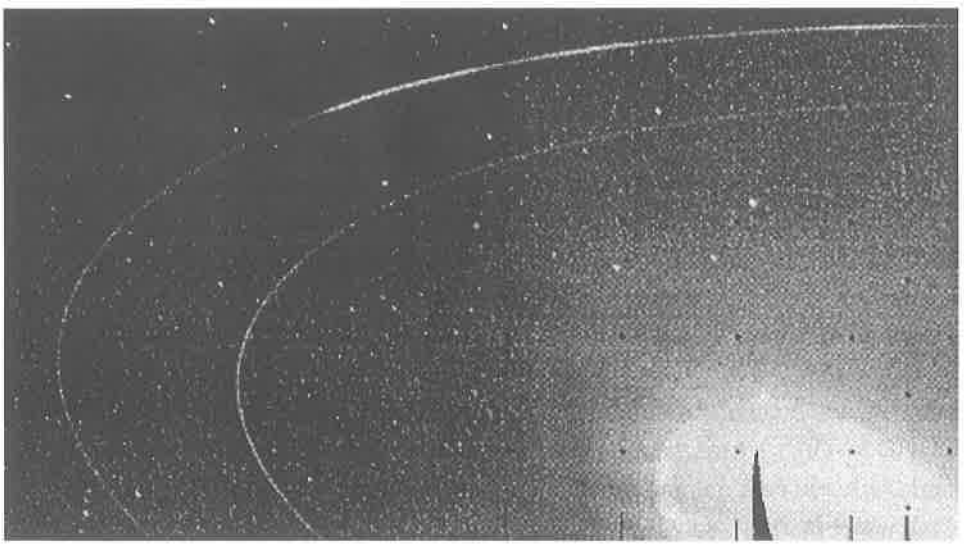

Figure 3. This image was taken by Voyager 2 (FDS 1141251) and the ring system of Neptune.

Adams rings. The four arcs, Courage, Liberté, Egalité and Fraternité, are the densest parts of the Adams ring. All these rings are brigther in forward–scattered ligth indicating a substantial population composed of dust.

The ring system of Jupiter was discovered by Voyager 1 in 1979 and additional

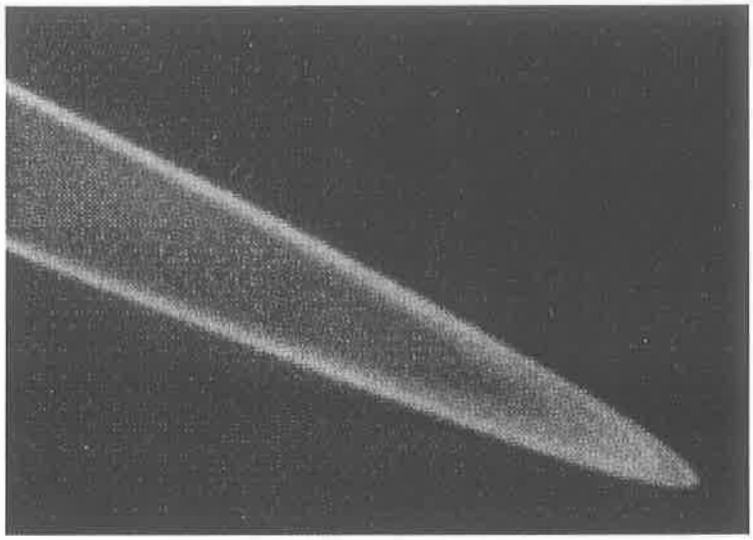

Figure 4. A Voyager 2 image (FDS 2069302) of the ring system of Jupiter.

images were obtained by Voyager 2. After analysing a sample of 25 Voyager 2 images Showalter (1985) concluded that the ring system is composed of three components (Figure 4):
- interior halo: $W = 30000$ km and vertical extension of 10000 km above and below to the equatorial plane of the ring;
- main ring: $W = 7000$ km, encircling the orbits of Adrastea and Metis;
- gossamer ring: $W = 81000$ km, near to Thebe's orbit.

The particles present in Jupiter ring system are brigther in forward–scattered light ($\sigma \sim 10^{-6}$) implying a population of dust. Lorentz resonance can explain the structure presented in the Jupiter ring system. A study by Schaffer and Burns (1987) showed that there are three locations of this kind of resonance: the limit between the halo and the main ring is in a 3:2 resonance, and the inner edge of the halo and the outer edge of the gossamer ring are in 2:1 and 2:3 Lorentz resonances, respectively.

2.3 Resonance

The resonant interaction between the ring particles and the satellite gives rise to density waves on the ring material. For the case of a satellite on an inclined orbit its resonant perturbation on the ring material will create a bending wave (Shu 1984).

There are density waves on the A and B rings caused by Janus, Prometheus and Pandora. Mimas causes density and bending waves on the A ring (Figure 5).

The shepherding mechanism proposed by Goldreich and Tremaine (1979), to avoid the spreading of a narrow ring due to dissipatives forces, was confirmed by the discovered of two satellites, Cordelia and Ophelia, by Voyager 2 encounter with Uranus. The narrow ϵ ring is shepherded by these two satellites. As studied by Porco and Goldreich (1987) Cordelia is in a 24:25 Lindblad resonance with the inner edge of the ring and Ophelia

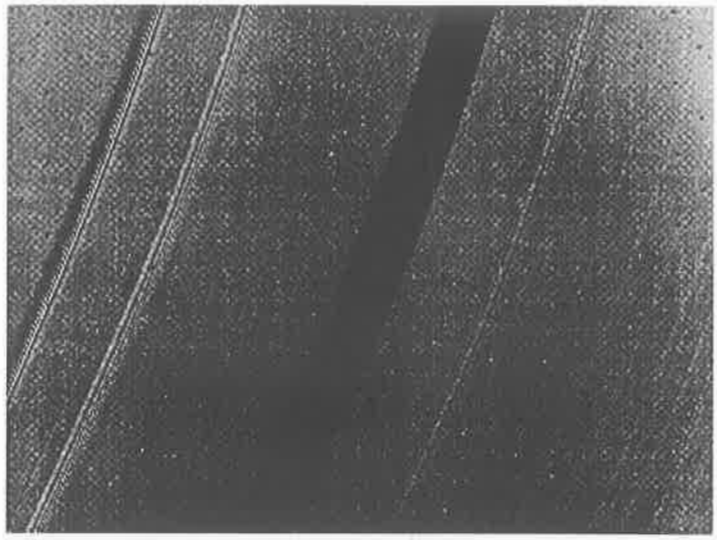

Figure 5. This imahe (FDS 4399350) shows he bending and the density waves on the A ring due to the resonant perturbations of the satellite Mimas.

in a 14:15 Lindblad resonance with the outer edge of the ring.

Galatea, the satellite discovered by Voyager 2, is the responsible for the radial and longitudinal stability of the arcs of Neptune. Galatea is about 900 km interior to the Adams ring and it is in a 42:43 Corotation resonance with the ring particles. This resonance induce the formation of sites of equilibrium with a maximum extension of 4° and a radial width of 0.6 km (Porco, 1991). These values are in good agreement with the observed from the Voyager 2 images.

2.4 New Satellites

Waves on the rings are the result of the satellite perturbation on the particles. A technique to find new satellites is to analyse waves on the ring.

Voyager 1 and 2 images of the Encke Division showed an azimuthal wave pattern on either or both inner and outer edges (Cuzzi and Scargle, 1985). The satellite Pan, responsible for the formation of the waves on the ring, was detected in some Voyager images by Showalter (1991). The Encke Division has also an incomplete ring in the same orbit of Pan suggesting that this satellite can be keeping the ring on a horseshoe orbit (Showalter, 1991).

The two close satellites of the F ring of Saturn, Prometheus and Pandora (discovered by Voyager 1), and hypothetical moonlets are claimed to be responsible for the strange morphology present in this ring such as the clumps, waves, kinks and braids. There are some evidence from the Voyager images that there are small moonlets orbiting in the neighbourhood of the F ring. Kolvoord *et al.* (1990) examined a series of Voyager images to look for periodicities in the azimuthal brightness that might be associated with nearby satellites. They detected the signature of Prometheus and provided some

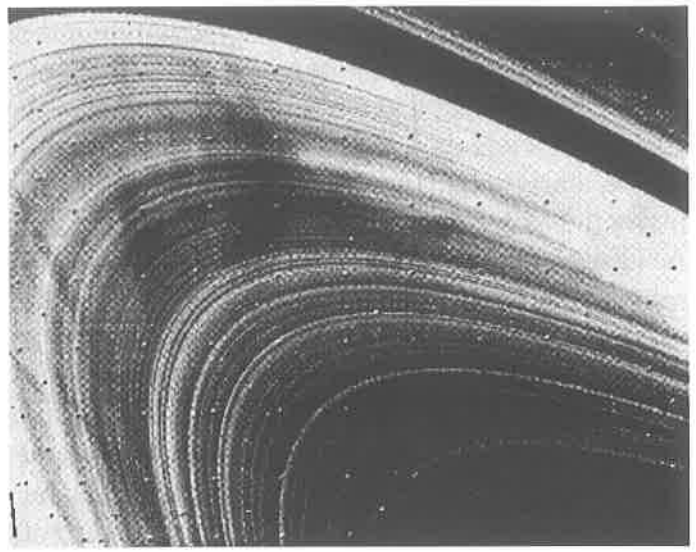

Figure 6. This image (FDS4390511) was taken in back scattered light. It shows the spokes on the B ring.

evidence for an undiscovered satellite at a separation in semi major axis of 1180 km from the F ring. By analysing a sequence of five Voyager 2 images which shows the ring divided into separate strands Giuliati-Winter *et al.* (1995) concluded that this structure can be preserved over $\sim 45°$ in longitude and it can be caused by small moonlets orbiting in the gap between the strands. However, these satellites with radii typically ~ 5 km are not ruled out on the basis of the limited Voyager spacecraft coverage of the F ring.

2.5 Dust

The B ring of Saturn presents a strange feature called spokes (Figure 6). They are located in the most optically thick region of the ring. Many studies revealed that the spokes are composed of microscopic particles and they are levitating above the orbital plane of the ring. The electromagnetic effects could be acting on these particles in order to make them charged and thus levitating off the ring (Burns, 1990).

A long exposure Voyager 2 image revealed a large number of dust rings around Uranus. The relation between this dust region and the rings are not clear yet. There is a model which suggest that the classical rings and some hypothetical satellites could be the source of this dust (Esposito and Cowell, 1989, Cowell and Esposito, 1990).

Neptune ring system also presents a dust region which extends from between the Adams and Le Verrie rings in the direction to the planet ($W = 38000$ km).

3. FUTURE PROSPECTS

During the period of 1995–96 the rings of Saturn will be seen on edge–on from Earth. At this time the faint rings of Saturn become visible, especially the E ring.

It has been organized an international campaign in order to improve the observations made during this period. The Planetology Group composed by members from the Observatório Nacional, UNESP-Campus Guaratinguetá and Universidade Federal de Curitiba is participating on this campaign, where our principal objectives are to analyse the radial distribution of the F, G and E rings, verify the temporal variations in radial distribution and the E–W variations, and the periodicity in the F ring structure. As has been analysed by Giuliatti-Winter and Murray (1995) there is the formation of a gap in the F ring during the closest approach between Prometheus and the ring particles each $\sim$ 18 years. The last closest approach was in May, 1993 and this event can span up to two years. This configuration can be observed during the ring plane crossing unless there is any kind of mechanism which can avoid the formation of the gap.

The Galileo spacecraft will improve the resolution on the rings of Jupiter and will allow to analyse the internal ring structure and possible additional moonlets. It will be important to know accurately the position of the known satellites, especially those one close to the ring system in order to verify their relevance to the ring structure. Because of the low inclination of the spacecraft's orbit it will not be possible to see the ring in three dimension, however the results from Galileo will be as good or better than the Voyager observations.

Cassini, a combined Saturn Orbiter and Titan Probe mission, will be launched in 1997 reaching its destination, Saturn, in 2004. Cassini will orbit Saturn during a four year mission. The primary objectives of the Cassini Imaging Science Subsystem (ISS) related to the ring system is to study the structure of the rings and the interactions between the rings and the satellites in an attempt to analyse the evolution of the Saturnian system.

The author is grateful to the Brazilian agency CNPq for providing financial support (Proc. 30110/94-9) and to Mitchell Gordon for kindly providing the Voyager images.

REFERENCES

Burns, J. A. (1990). Planetary Rings. In *The New Solar System* (J. Kelly Beatty and A. Chaikin, Eds.), 153–170. Cambridge University Press & Sky Publishing Corporation, Cambridge.

Colwell, J. E. and L. W. Esposito (1990). A numerical model of the Uranian dust rings. *Icarus* **86**, 530–560.

Cuzzi, J. N. and J. D. Scargle (1985). Wavy edges suggest moonlet in Saturn's Encke Gap. *Astrophys. J.* **292**, 276–290.

Dermott, S. F. and C. D. Murray (1980). Origin of the eccentricity gradient and apse alignment of the ϵ ring of Uranus. *Icarus* **43**, 338–349.

Elliot, J. L., Dunham, E. W., and R. L. Millis (1977). Discovering the rings of Uranus. *Sky Telescope.* **53**, 412–416, 430.

Esposito, L. W. and J. E. Colwell (1989). Creation of the Uranus rings and dust bands. *Nature* **340**, 322.

Feibelman, W. A. (1967). Concerning the "D" ring of Saturn. *Nature*, **214**, 793–794.

Giuliatti Winter, S. M., Gordon, M. K. and C. D. Murray (1995). Multiple strands in the F ring: Additional evidence for embedded moonlets? Submitted to Icarus.

Giuliatti Winter, and C. D. Murray (1995). The closest approach between Prometheus and Saturn's F ring. Submitted to Icarus.

Goldreich, P. and S. Tremaine (1979). Towards a theory for the Uranian rings. *Nature* **277**, 97–99.

Kolvoord, R. A., Burns, J. A. and M. R. Showalter (1990). Periodic features in Saturn's F-ring: Evidence for nearby moonlets. *Nature* **345**, 695–697.

Nicholson, P. *et al.* (1978). The rings of Uranus: Results of the 10 April 1978 Occultation. *Astron. J.*, **83**, 1240–1248.

Porco, C. C. and P. Goldreich (1987). Shepherding of the Uranian rings. I. Kinematics. *Astron. J.* **93**, 724–729.

Porco, C. C. (1991). An explanation for Neptune's rings arcs. *Science* **253**, 995–1001.

Richardson, D. C. (1994). Tree code simulations of planetary rings. *Mon. Not. R. Astron. Soc.*, **269**, 493–511.

Schaffer, L. E. and J. A. Burns (1987). The dynamics of weakly charged dust: Motion through Jupiter's gravitational and magnetic fields. *J. Geophys. Res.* **92**, 2264–2280.

Showalter, M. R. (1985). *Jupiter's ring system resolved: Physical properties inferred from the Voyager images.* Ph.D. Dissertation, Cornell University, Ithaca.

Showalter, M. R. (1991). Visual detection of 1981S13, Saturn's eighteenth satellite, and its role in the Encke gap. *Nature* **351**, 709–713.

Shu, F. H. (1984). Waves in planetary rings. In *Planetary Rings* (R. J. Greenberg and A. Brahic, Eds.), 513–561. Univ. of Arizona Press, Tucson.

Van Helden, A. (1984). Rings in astronomy and cosmology, 1600–1900. In *Planetary Rings* (R. J. Greenberg and A. Brahic, Eds.), 12–22. Univ. of Arizona Press, Tucson.

IS THE SOLAR DIAMETER VARIABLE?

N.V.Leister, M.Emilio, P.C.R.Poppe

Instituto Astronômico e Geofísico
Universidade de São Paulo

Abstract

We discuss the possible variations of the solar diameter, and its connection among other indices of activity or global parameters such as the irradiance or the neutrino production. The dependence of this variation with respect to the heliographic latitude is compatible with the non-radial pulsation with l=6.

key-words – Sun(the); oscillations of, Astrometry

1 Introduction

The solar radius has been measured more than three centuries, and displays considerable variation. The solar radius has been measured with an accuracy of a few parts in 10^{-4}. Traditional theory of stellar structure concerns itself with stars that are spherical symmetrical, nonrotating and devoid of magnetic fields. It expects for a star with the caracteristics of the Sun, a radius that increases by at most a few 10^{-11} of its own value per years.

The various methods that are in use for measuring the apparent solar semi-diameter, consists in directly measuring the angle between two opposite limbs, besides the other type of methods that consists in timing the duration between successive contacts of opposite limbs with fiducial lines on the sky.

Analysis of differents data sets including differents observational techniques made by Gilliland (Gilliland 1981) suggest of a cyclic variation of solar radius with periods between 10 and 120 years. Two of data sets are derived from independent meridian circle observations conducted at the Royal Observatory at Greenwich and the United States Naval Observatory at Washington D.C. (Eddy and Boornazioan 1979) was compiled by Shapiro (1980) and historical Mercury transit observations by Parkinson, Morrison, and Stephenson (1980) (Fig.1).

More recently, astrometrists have measured the apparent solar radius by means of a prismatic astrolabe (Laclare 1983, Leister 1989, Leister and Benevides-Soares 1990, Poppe 1994). Since 1974, a regular program is under way at Calern and A.Moraes Observatories. These series consists of 3,000 independent measurements distributed over all seasons and cover solar cycle 21 (Fig.2). The individual analysis of these data set show a variation of the apparent solar diameter with periods between 1 and 10 years. The most particulary signal occuring near 1,000 days, in phase in both set when independently analyse is made.

The Table 1 shows the individual values obtained in differents data sets with respectives epoch. The considerable variation display arises, in fact, because the various

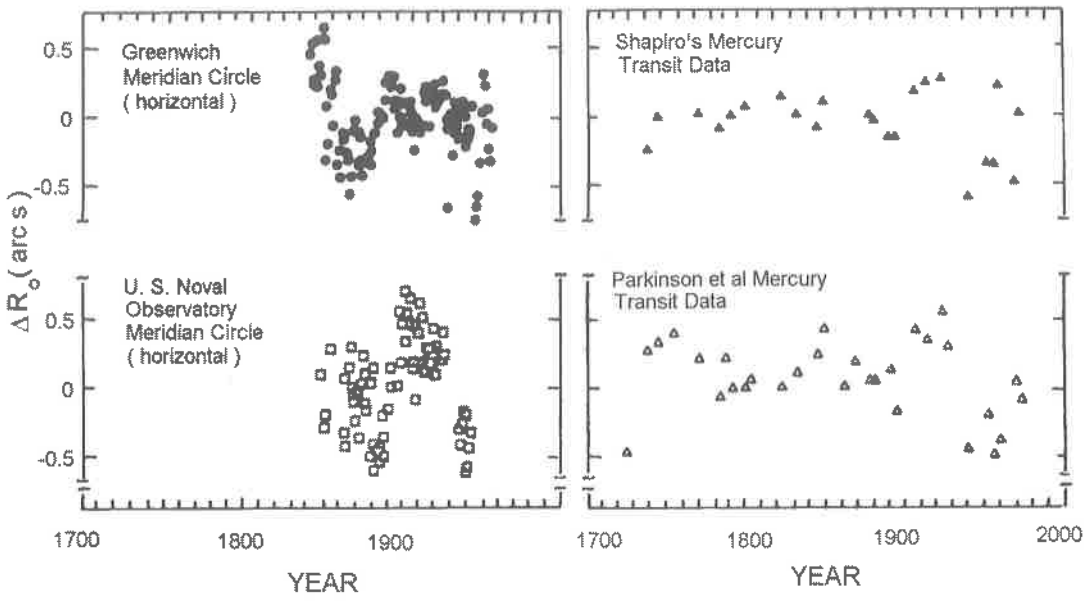

Figure 1. The data sets of solar radius measurements-arcsec deviations from mean (Gilliland 1981- modified).

Table 1: Values of the solar radius

Reference	Mean Epoch	Radius(arcsec)	Remarks
Lalande	1764	945.5	From Heliometer measurements
Delambre	1806	961.4	
Airy	1876	961.82	From Greenwich
Auwers	1895	959.63	From heliometer measurements
Sofia et al.	1978	959.77±0.06	From solar eclipses data
Leister et al.	1986	959.40±0.05	From prismatic astrolabe
Sofia et al.	1992	959.53±0.06	solar disk sextant on ballon flights
Laclare et al.	1985	959.42±0.02	From prismatic astrolabe

observation methods do not directly measure a true radius. The radius of a surface given optical depth. Rather, they measure properties of the Sun's limb darkening function, and are affected by many sources of degradation of the solar image.

However, the agreement among some values is evident, mainly long series of visual observations made with a same kind of instruments.

2 Solar Radius Variations

The real motivation for observing the solar radius is the suspicion that it might be variable. These investigation leave open the possibility that the apparent solar radius might vary by as much as a few tenths of an arcsecond.

The (anti)correlation between solar diameter and some indexes of solar activity has been noticed (Laclare 1996).

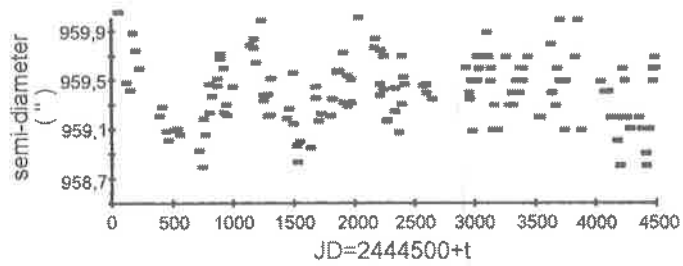

Figure 2. The date set of solar radius measure with prismatic astrolabe (Leister and Benevides-Soares 1990 - modified).

Table 2: Radius measurements spectral peack characteristic: peaks with amplitudes A

T(month)	ν(1/month)	A(arcsec)	Remarks
136.6	7.32E-03	0.10	Cerga
133.4	7.50E-03	0.09	Valinhos
61.6	1.62E-03	0.08	Cerga
33.3	3.00E-02	0.18	Valinhos
30.5	3.28E-02	0.13	Cerga
20.4	4.90E-02	0.07	Cerga
19.0	5.26E-02	0.04	Valinhos
10.4	9.61E-02	0.07	Valinhos
10.4	9.61E-02	0.06	Cerga
8.5	1.18E-01	0.09	Valinhos
8.3	1.21E-01	0.03	Cerga

We have examined two different data sets of solar radius measurements for evidence of cyclic behavior with periods between 1 and 11 years. These two data sets derived from independent prismatic astrolabe conducted at the CERGA and A.Moraes Observatories. The prismatic astrolabe measurements from A.Moraes have been discussed by the authors (Leister 1989, Leister and Benevides-Soares 1990) As plotted in Figure 2, the mean value of the radius over 1980 to 1994 is 949.40 $\pm$0.05 arcsec, and this value agree with CERGA mean value 959.42$\pm$0.02 see in Table 1.

The harmonic analysis over the CERGA and A.Moraes sets data reveals a aproximately 11 years periodic oscillation (anti)correlated with the Solar activity over the period to 1978-1994 (Fig.3). The Table 2 gives the radius spectral peak characteristic.

The anticorrelation between solar neutrino counting rate and some indexes of solar activity has been noticed long ago (Sakurai 1980, Subramanian 1979). Gavryusev (V.Gavryusev et al. 1994) evaluate and discuss correlation of radius data of the Sun with several combinations of harmonics obtained from neutrinos analysis.

In spite of a large dispersion there is some significant power close to frequency (1 year)$^{-1}$. Is not very easy decide whether this is due to the more or less regular winter interruption of the data, or it is due to real variations of the solar radius observations, but

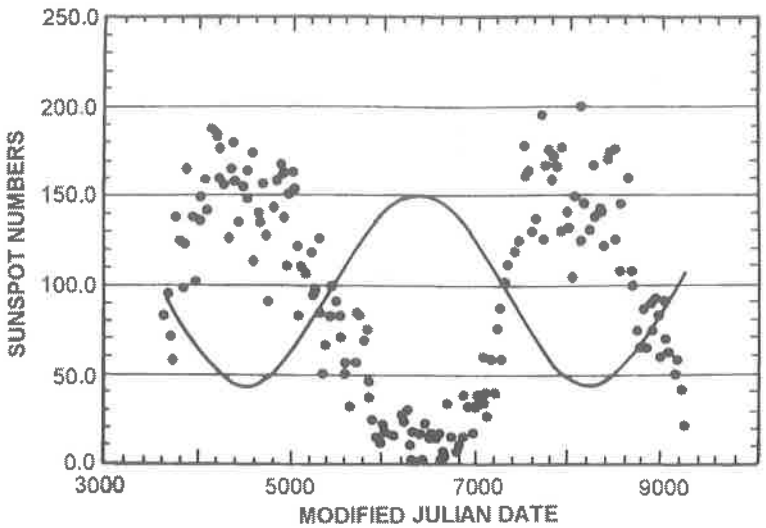

Figure 3. Solar semi-diameter an opposing phase relative to the solar activity given by the Sunspot Index Data Center (Laclare et al. 1996 - modified)

there are a significant peak in the neutrino flux power spectrum, close to these frequency computed by Gavryusev & Gavryuseva (1993). The Figure 4 shows the variations of the observed diameter with the neutrinos flux for the A.Moraes data set.

Finaly, the heliographic inclination of the observed diameter changes during the year and also with a given zenith distance. The measurements being sorted into classes of heliographic latitude. The results are shown in Figure 5, which seems to indicate that the solar radius varies with period 1 year and semi-amplitude 0.04 arcsecond. The exact forms of these dependencies are difficult to calculate, especially for visual observations; those uncertainties make interpretation of such observations difficult, but these results suggest that this variation is compatible with non-radial pulsation with $l = 6$.

3 Conclusion

The observation of *p-mode* frequency changes over a solar cycle time scale (Woodard and Noyes 1985) Using the ACRIM satellite solar irradiance data, these authors argued that the low degree ($l<2$) *p-mode* frequency decrease by about 0.4nHz between 1980 and 1984. Subsequent observations by Fossat et al. (1987) using velocity data provided consistent evidence for *p-mode* frequency variability. Although there are conflicting report concerning the evidence for this variability, we consider that the variability is a solar fenomenon.

The possibility that the Earth's atmosphere is also responsible for some long-term variations still remains. An intriguing correlation between the stratospheric circulation reversal with the 1,000 day oscillation of the apparent radius has been noted by Ribes et al. (1988). Since the Quasi-biennial Oscillation (QBO) are located within the tropics, it would be surprising that they affect astrometric station at different latitudes at the same time. The 1000-day periodicity is roughly in phase for observational station such as CERGA 43.5°N, Belgrade 43.5°N, and Sao Paulo 23.0°S and cannot easily be explained

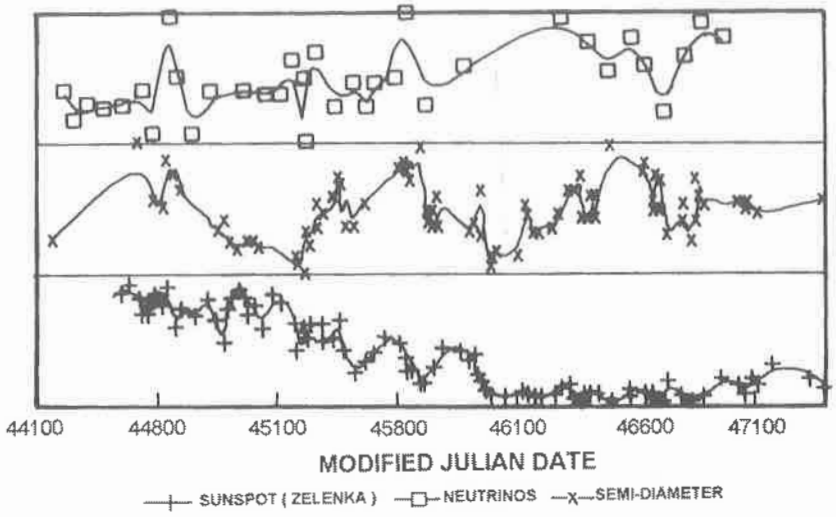

Figure 4. Semi-diameter variations and neutrinos flux.

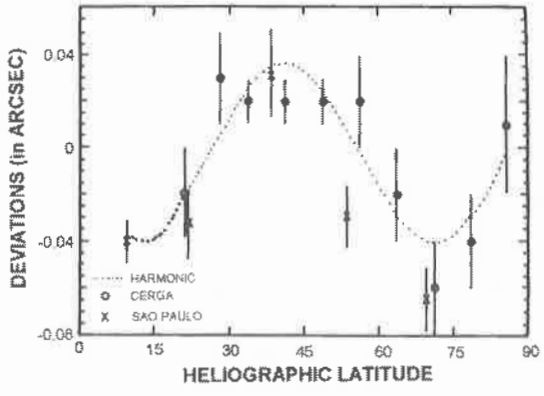

Figure 5. Correction to semi-diameter and heliographic latitude

as an atmospheric effect.

References

[1] Gilliland, R.L., 1981, *The Astroph. Journal* **248**, 1144

[2] Eddy, J.A.,and Boornazion, A.A., 1979, *Bull. A.A.S.* **1**, 437

[3] Shapiro, I.I., 1980, *Science* **208**, 51

[4] Parkinson, J.H., Morrison, L.V., and Stephenson, F.R., 1980, *Nature* **288**, 548

[5] Laclare, F., 1983, *Astron.Astrophys* **125**, 200

[6] Leister, N.V., and Benevides-Soares, P., 1990, *C.R.Acad.Sci. Paris* **313 SII**, 399

[7] Poppe, P.C.R., 1994, *Msc* **Mestrado**, 110 pages

[8] Leister, N.V., 1989, *PhD* **Doutorado**, 150 pages

[9] Auwers, A.A.,1891, *Astron.Nachr* **128**, 361

[10] Sofia, S.,Heaps, W.,and Twigg, L.W., 1994, *Astrophys.J.* **427**, 1048

[11] F.Laclare, C.Delmas, J.P.Coin, and A.Irbah, 1996 *Solar Physics* **in press**, 0

[12] Sakurai, K., 1980, *Pub.Astron.Soc.Japan* **32**, 547

[13] Subramanian, A., 1979, *Curr. Sci.* **48**, 705

[14] V.Gavryusev, E.Gavryuseva, Ph.Delache, and F.Laclare, 1994, *Astron.Astrophys.* **286**, 305

[15] V.Gavryusev, E.Gavryuseva, 1993, *Astron.Astrophys.* **accepted**

[16] Woodard, M.F., and Noyes, R.C., 1985, *Nature* **318**, 449

[17] Fossat, E., Gelly, B., Grec, G., and Pomerantz, M., 1987, *Astron.Astrophys.* **177**, L47

[18] Ribes, E., Ribes,J J.C., 1988, *Nature* **332**, 689

Impressão e Acabamento:

WinnerGraph

5584-6023